The cellular and molecular landscape of human trigeminal nerves and lingual neuromas linked with neuropathic pain

Martina Morchio

A thesis submitted in partial fulfilment of the requirements for the degree of Doctor of Philosophy

The University of Sheffield
Faculty of Health
School of Clinical Dentistry

February 2024

Acknowledgements

I would like to thank my supervisors, Professor Fiona Boissonade for her invaluable knowledge and unwavering support and Professor Dan Lambert for his enthusiasm and optimism. Their encouragement to apply for further funding and help with crafting the applications resulted in an extremely enriching and stimulating PhD experience, which would not have been possible without their mentorship.

I'm extremely grateful to Dr Ted Price and the Neurobiology of Pain research group at UTD for welcoming me to Dallas for six months and introducing me to the wonderful world of human DRGs. Special thanks to Dr Diana Tavares Ferreira for being an inspiring role model and to Dr Ishwarya Sankaranarayanan for her kind help and expertise with single nuclei RNA sequencing.

I would like to thank my secondary supervisors from Eli Lilly, Dr Emanuele Sher, for the support and advice, and Dr Achim Kless, for sharing his genomics expertise with me and welcoming me to Lilly's UK Neuroscience Hub during my industrial placement.

Importantly, I would like to thank the patients who consented to take part in this research and Dr Simon Atkins who performed the surgeries, without whom this project could not have happened, as well as the donors from the Netherland Brain Bank and Dr Stephanie Shiers and Dr Ted Price for letting us use their samples. I would also like to acknowledge Eli Lilly, BBSRC and Battelle for their financial contribution to this project.

Thanks to the Neuroscience group in Sheffield for the moral support, particularly to Dr Sara Memarpour Hobbi for the laughs and the sass and Dr Natalie Wong for the advice and the wisdom. Thanks to all the students I have had the pleasure to work with, particularly to Evgeniya Anisimova for her help with the immuno work. Finally, thanks to all the friends that have crossed my path throughout all these years in Sheffield and to my family for their encouragement and support.

"Anything is possible if you've got enough nerve".

- Ginny Weasley

Abstract

Neuropathic pain – defined as pain arising from damage to the somatosensory system – affects 7-10% of the population, causing patients to experience burning or stabbing sensations even in the absence of any external stimuli. Injuries to the trigeminal nerve, responsible for sensory innervation to the face, may occur during routine dental procedures, resulting in the formation of a neuroma accompanied by loss of sensation and/or symptoms of pain.

Here, the cellular and transcriptional landscape of healthy and injured human trigeminal nerves was characterised at single-cell resolution and the cell-cell communication between non-neuronal cells and trigeminal neurons was computationally inferred. The transcriptional landscape of painful and non-painful human neuromas within the tissue architecture was profiled using spatial transcriptomics and several differentially expressed genes were identified. Finally, RNAscope and immunohistochemistry were utilised to validate single nuclei RNA sequencing and spatial transcriptomics experiments.

This study characterises human trigeminal nerves at single-cell level, before and after injury, highlighting transcriptomic changes in Schwann cells and immune cells associated with injury. Differential expression analysis between painful and non-painful neuromas highlighted the role of inflammatory mediators in neuropathic pain: in particular, CXCL2, CXCL8 and HLA-A were upregulated in painful samples. Cell-cell communication inference indicates that macrophage-derived CXCL8 may underpin neuronal sensitization through the atypical chemokine receptor 1. RNAscope and immunohistochemistry confirmed the expression of several injury- and pain-relevant molecules in the predicted cell-types, including Peptidase Inhibitor 16 expression in endoneurial fibroblasts and the p75 neurotrophin receptor and prostaglandin D2 synthase in perineurial fibroblast.

The cellular atlas generated in this study will be of significant interest to the wider research community, reporting the expression of thousands of genes at single-cell resolution in clinically relevant human tissue in health and associated with nerve injury and pain, providing a precious resource for the development of novel pain treatments.

Table of Contents

List of Figures

List of Tables

List of Abbreviations

5-HT	Serotonin (5-hydroxytryptamine)
AATK	Apoptosis-associated tyrosine kinase
ABC	ATB-binding cassettte
ACD	Advanced Cell Diagnostics
ALPL	Alkaline Phosphatase
ALS	Amyotrophic lateral sclerosis
AMPA	α-amino-3-hydroxy-5-methyl-4-isoxazolepropionic acid
AP	Action Potential
APOD	Apolipoprotein D
AR	Antigen Retrieval
ASIC	Acid Sensing Ion Channel
ATP	Adenosine Tri-phosphate
BDNF	Brain-Derived Neutrophic Factor
BNB	Nlood-Nerve Barrier
BNI	Blood-Nerve Interface
BSA	Bovine Serum Albumin
CALCA	Calcitonin Related Polypeptide Alpha
CC	C-C motif
CCA	Canonical correlation analysis
CCI	Chronic Constriction Injury
CCL	C-C motif ligand
CFA	Complete Freund's Adjuvant
CGRP	Calcitonin Gene-related peptide
CIP	Congenital insensititvity to pain
CIPD	Chronic inflammatory demyelinating polyneuropathy
CKM	Creatine kinase, muscle
CLU	Clusterin
CNP	2',3'-Cyclic Nucleotide 3' Phosphodiesterase
CNS	Central Nervous System
CRYAB	Crystallin Alpha B
CXC	C-X-C motif
CXCL	C-X-C motif ligand
CYTIP	Cytohesin 1 Interacting Protein
DAPI	4′,6-diamidino-2-phenylindole
DARC	Duffy antigen receptor for chemokine
DCN	Decorin
DE	Differentially expressed
DHH	Desert Hedgehog
DNA	Deoxyribonucleic Acid
DRG	Dorsal Root Ganglia
DSP	Desmoplakin

DTT	D-Dopachrome Decarboxylase
DWLS	Dampened weighted least squares
ECM	Extracellular Matrix
ECSCR	Endothelial Cell Surface Expressed Chemotaxis And Apoptosis Regulator
EGR	Early Growth Response
EMCN	Endomucin
ERK	Extracellular signal-regulated kinase
FDR	False Discovery Rate
FFPE	Formalin-fixed Paraffin-embedded
FGF	Fibroblast Growth Factor
FITC	Fluorescein isothiocyanate
FLT	Fms Related Receptor Tyrosine Kinase
GABA	Gamma-aminobutyric acid
GDNF	Glial-derived neurotrophic factor
GEM	Gel Bead-In-EMulsion
GEX	Gene Expression
GFAP	Glial Fibrillary Acidic Protein
GFP	Green Fluorescent Protein
GFRA	GDNF family receptor alpha
GLUL	Glutamate-ammonia ligase
GLUT	Glucose Transporter Protein Type
GPCR	G-protein Coupled Receptor
GPU	Graphic Processing Unit
GSN	Gelsolin
HLA	Human Leukocyte Antigens
HRA	Human Right Act
HRP	Horseradish Peroxidase
IAN	Inferior Alveolar Nerve
IASP	International Association for the Study of Pain
ICAM	Intercellular Adhesion Molecule
ICD-11	11th International Classification of Disease
ID	Identity
IFN-γ	Interferon Gamma
IG	Immunoglobulin
IGF	Insulin Growth Factor
IGKC	Immunoglobulin Kappa Constant
IHC	Immunohistochemistry
IL	Interleukin
ISH	In Situ Hybridisation
ITGAM	Integrin alpha M
JMJD	Jumonji Domain
KCNA	Potassium voltage-gated channel subfamily A
KEGG	Kyoto Encyclopedia of Genes and Genomes

KOH	Potassium Hydroxide
LAS	Leica Associated Suite
LBP	Low Back Pain
LED	Light Emitting Diode
LFC	Log Fold Change
LIF	Leukemia Inhibitory Factor
LTMR	Low Threshold Mechanoreceptor
LYZ	Lyzozyme
MAPK	Mitogen-activated protein kinase
MAST	Model-based Analysis of Single-cell Transcriptomics.
MB	Myoglobin
MBP	Myelin Basic Protein
MCP	Membrane Cofactor Protein
C-MH	Mechanical and thermal sensitive C-fibre
MHC	Major Histocompatibility Complex
MLIP	Muscular LMNA Interacting Protein
MOBP	Myelin Associated Oligodendrocyte Basic Protein
MOG	Myelin Oligodendrocyte Glycoprotein
MPZ	Myelin Protein Zero
MRGPRD	MAS-related GPR, member D
MSC	Myelinating Schwann Cells
MYLK	Myosin light chain kinase
NA	Not Applicable
NBB	Netherland Brain Bank
NBF	Neural Buffered Formalin
NCMAP	Non-Compact Myelin Associated Protein
NDS	Normal Donkey Serum
NEFH	Neurofilament heavy chain
NF-kB	Nuclear factor kappa B
NGF	Nerve Growth Factor
NGFR	Nerve Growth Factor Receptor
NGS	Normal Goat Serum
NHS	National Health Service
NK	Neurokinin
NLR	Nucleotide-binding and Leucine-rich repeat immune Receptors
NMDA	N-methyl-D-aspartate
NMSC	Non-myelinating Schwann cells
NOTCH	Neurogenic locus notch homolog protein 2
NP	Non Peptidergic
NPPB	Natriuretic Peptide B
NT	Neurotrophin
OCT	Octamer-binding transcription factor
OGN	Osteoglycin

OSM	Oncostatin M
PAGE	Parametric Analysis of Gene Set Enrichment
PAINSTORM	Partnership for Assessment and Investigation of Neuropathic Pain: Studies Tracking Outcomes
PB	Phophate Buffer
PBS	Phosphate Buffered Saline
PCA	Principal Component Analysis
PCR	Polymerase Chain Reaction
PDGFR	Platelet-derived growth factor family
PEP	Peptidergic
PKA	Protein Kinase A
PKC	Protein Kinase C
PKD	Protein Kinase D
PN	Product Number
PNI	Peripheral Nerve Injury
PPIB	Peptidylprolyl Isomerase B
PRX	Periaxin
PTDGS	Prostaglandin D synthase
PTPRC	Protein tyrosine phosphatase, receptor type, C
PTPRT	Protein tyrosine phosphatase, receptor type, T
PVALB	Parvalbumin
RA	Rapidly Adapting
RBC	Red Blood Cell
RNA	Ribonucleic Acid
RTK	Receptor Tyrosine Kinase
SA	Spontaneously Activated
SC	Schwann Cell
SCT	Single cell transform
SELE	Selenin
SGC	Salivary Gland Cell
SMA	Smooth Muscle Actin
SNARE	Soluble N-ethylmaleimide-Sensitive Factor Attachment Proteins Receptor
SNI	Sciatic Nerve Injury
SNP	Single Nucleotide Polymorphism
SOX	Sry-related Homeobox Genes
SP	Substance P
SRY	Sex-determining Region Y
SSC	Saline Sodium Citrate
SST	Somatostatin
ST	Spatial Transcriptomics
STH	Sheffield Teaching Hospitals
TCAP	Telethonin
TE	Tris EDTA buffer

TF	Transcritpion Factor
TG	Trigeminal Ganglia
THEMIS	Thymocyte Selection Associated
THSB	Thrombospondin
TMJ	Temporomandibular Joint
TNF	Tumour Necrosis Factor
TRAC	T Cell Receptor Alpha Constant
TRAP	Ribosome affinity purification
TRP	Transient Receptor Potential
TSA	Tyramide Signal Amplification
TTN	Titin
UMAP	Uniform Manifold Approximation and Projection
UMI	Unique Molecular Identifier
UTR	Untranslated Region
VAS	Visual Analogue Scale
VCAM	Vascular Cell Adhesion Molecule
VEGF	Vascular Endothelial Growth Factor
VIM	Vimentin
VWF	Von Willebrand Factor
WDR	Wide Dynamic Range

Chapter 1. General Introduction

1.1 Introduction on pain

The perception of pain serves as an evolutionary advantage, allowing organisms to learn from noxious experiences and avoid harmful stimuli. However, when acute pain transitions to chronic pain, it becomes a burden that influences every facet of life, severely impacting quality of life.

The IASP defines pain as “an unpleasant sensory and emotional experience associated with, or resembling that associated with, actual or potential tissue damage” (Raja et al., 2020). By alerting us of actual or potential tissue damage, pain enables us to avoid harm and increase our chances of survival. The importance of pain is evident in patients affected by congenital insensitivity to pain (CIP), where genetic mutations prevent the appropriate development and functioning of nociceptive pain pathways, resulting in the inability to perceive pain. CIP patients suffer from a shortened life span due to self-mutilations, fractures, joint injuries and infections (Drissi et al., 2020).

The nociceptive system relies on primary sensory neurons that transduce noxious mechanical, thermal or chemical stimuli from the periphery and transmit this information to the central nervous system. Primary sensory neurons express a wide variety of sensory receptors that enable the detection of mechanical, thermal and chemical stimuli at low innocuous or high noxious thresholds. One example of this is a prominent family of sensory receptors known as the transient receptor potential (TRP) ion channels, whose members can detect various ranges of noxious and non-noxious thermal and chemical stimuli. For example, TRPV1 can detect heat (>43°C), capsaicin, protons and various lipids (Tominaga and Tominaga, 2005), while TRPM8 is activated by cold (<30°C) and menthol, and TRPA1 is sensitive to noxious cold (<17°C) and irritants such as mustard and heat (Dhaka et al., 2006, Moparthi et al., 2016). The signal detected by sensory receptors is then conducted from the periphery to the central terminal of primary sensory afferents via action potentials, generated by ion channels such as voltage-gated sodium channels (Bennett et al., 2019).

When the harmful stimulus is recurrent and persistent, acute nociceptive pain can transition to chronic nociceptive pain, as in osteoarthritis patients, where normal weight bearing on deformed joints may produce persistent activation of the synovial mechanoreceptors (Neogi, 2013, Costigan et al., 2009).

A lesion of the tissue is followed by an inflammatory response, mediated by pro-inflammatory mediators including cytokines, chemokines, prostaglandins and nerve growth factors, which, in order to protect the injured tissue, enhances the nociceptive responses associated to noxious stimuli (hyperalgesia) and produces a noxious response from innocuous stimuli (allodynia). This mechanism, known as peripheral sensitisation, serves to alert the organism to protect the affected area from further injury and allow healing (Chen et al., 2013). Typically, the pain disappears after the resolution of tissue injury; however, chronic inflammatory disorders such as rheumatoid arthritis result in persistent inflammatory pain characterised by chronic inflammation of the joints (Walsh and McWilliams, 2012). In several chronic painful conditions, the pain can persist even when peripheral inflammation is treated pharmacologically, sustained by central sensitisation (McWilliams and Walsh, 2017), where nociceptive neurons in the central nervous system are increasingly responsive to sub-threshold stimuli due to synaptic plasticity caused by prolonged peripheral hyperexcitability (Woolf, 2011).

When the lesion or disease that causes pain involves the somatosensory nervous system, the pain is classified as neuropathic, which persists even after the resolution of injury due to maladaptive plasticity in the process of neural tissue healing (Costigan et al., 2009). Neuropathic pain is generated through several biological processes, including changes in receptors and ion channels expression in primary sensory afferents, resulting in altered excitability and spontaneous firing, activation of immune cells and central amplification triggered by altered synaptic connectivity (Costigan et al., 2009, Finnerup et al., 2021).

1.1.1 Impact of Neuropathic Pain

Neuropathic pain has recently been included in the 11th revision of the international classification of disease (ICD-11) (Nicholas et al., 2019, Scholz et al., 2019), in response to the need of a better classification system to improve diagnosis

and treatment of patients affected by persistent pain. Neuropathic pain affects roughly 7-10% of the general population (van Hecke et al., 2014, Fayaz et al., 2016) and includes a wide variety of conditions with different aetiologies (Figure 1.1), further classified into peripheral neuropathic pain, which includes nerve injury-induced neuropathic pain, trigeminal neuralgia, postherpetic neuralgia, painful polyneuropathy, postherpetic neuralgia and painful radiculopathy; and central neuropathic pain, associated with spinal cord or brain injury, stroke and multiple sclerosis (Scholz et al., 2019). Neuropathic pain is often reported by patients as ongoing or intermittent and described as burning, searing, shooting, pricking, pins and needles, squeezing, crushing or freezing. It can be accompanied by non-painful abnormal sensations that can be unpleasant, generating discomfort (dysesthesia). The pain can also be evoked by mechanical or thermal stimuli, with both allodynic and hyperalgesic characteristics, which can be reported in addition to loss of sensation (Finnerup et al., 2021).

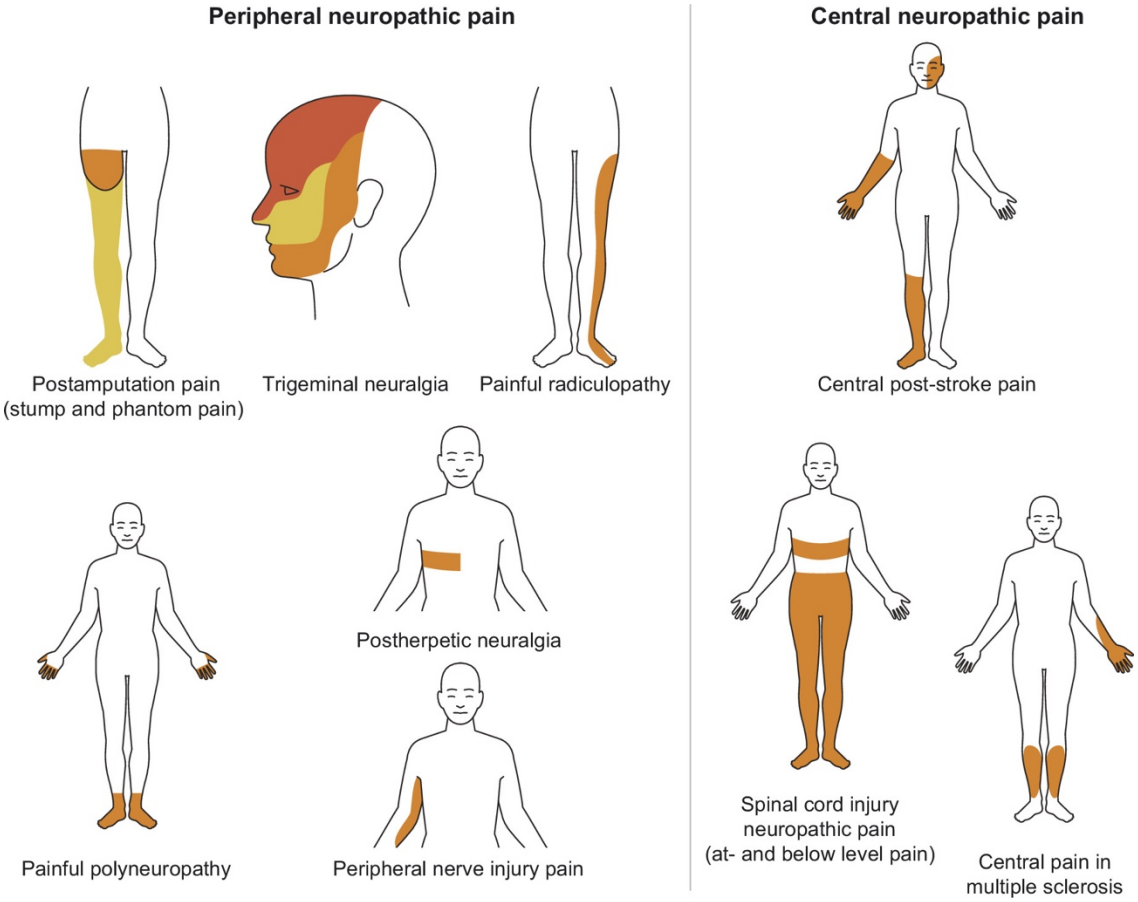

Figure 1.1 Classification of neuropathic pain conditions.
Classification of neuropathic pain conditions and examples of the anatomical distribution of pain and sensory abnormalities. Obtained with permission from Finnerup et al. (2021).

Current first-line treatments for most neuropathic pain conditions include gabapentinoids (gabapentin and pregabalin), which act on voltage-gated calcium channels and, while according to some meta-analyses they are effective in some neuropathic pain indications, particularly post-herpetic neuralgia and diabetic neuropathy (Cavalli et al., 2019, Wiffen et al., 2017, Derry et al., 2019, Finnerup et al., 2015), in other reports the effects seem to be moderate and are often outweighed by the risks of addiction and adverse effects (Williams et al., 2023, Chincholkar, 2020). Their mechanism of action involves the decrease of neuronal hyperexcitability and excitatory transmitter release through the reduction of activity-dependent calcium signalling (Kremer et al., 2016). Other first line treatment include tricyclic antidepressants (TCAs) and serotonin-norepinephrine reuptake inhibitors (SNRIs), which also show high efficacy for some indications, but come with substantial side effects (Finnerup et al., 2015, Ferreira et al., 2023, Cavalli et al., 2019). They act on the pre-synaptic reuptake of serotonin and noradrenalin and are thought to achieve analgesia via the activation of descending pathways at spinal and supraspinal levels, as well as modulating neuroimmune interactions (Kremer et al., 2016).

Drugs with a weak indication include capsaicin and lidocaine patches and botulinum toxin type A injections (Finnerup et al., 2015). Tramadol and opioids are effective analgesics, but not recommended for chronic non-cancer pain patients due to tolerance and addiction (Finnerup et al., 2015). Sodium channel blockers such as carbamazepine and oxcarbazepine are recommended for trigeminal neuralgia patients (Lambru et al., 2021), but inconclusive for other types of neuropathic pain (Wiffen et al., 2011).

A survey on chronic pain attitudes in European countries identified that 64% of chronic pain patients taking pain medications report that the medication is inadequate at times at managing the pain, while 63% of respondents are concerned about the medications' side effects (Breivik et al., 2006). This survey was conducted on patients suffering from various chronic pain conditions who primarily used NSAIDs and opioids for pain management, which are ineffective for neuropathic pain. As highlighted by Finnerup et al. (2021), few treatments have been introduced in the past 120 years for neuropathic pain, which have been developed primarily

from clinical observation rather than translational approaches. In the meantime, neuropathic pain is still insufficiently managed by drugs associated with substantial side effects. The development of new therapies is challenging due to the heterogeneity of neuropathic pain conditions and mechanisms of chronic pain development, therefore, methods to stratify patients based on the symptoms and signs reported have been suggested, which might indicate the mechanism underlying the symptoms of neuropathic pain and point to the best strategy for pain relief (Bouhassira and Attal, 2016, Finnerup et al., 2021).

1.2 Nociceptive pain pathways

The anatomical and cellular structures that compose nociceptive pain pathways are summarised in the following sections to provide a basic overview of the steps involved in nociception and pain processing, as a basis to understand how chronic neuropathic pain may arise following lesion or disease to the somatosensory system.

1.2.1 Primary sensory afferents

Noxious stimuli are detected at the periphery and transmitted to the central nervous system by nociceptors, a subset of primary sensory afferents that respond to high threshold stimuli, forming the first step in the pain pathway (Basbaum et al., 2009).

Since the work of Rivers and Head (1908), which identified “protopathic” and “epicritic” sensations, where the first corresponds to a dull poorly localised sensation of pain and the second to well-localised thermal and touch stimuli detection system; there has been considerable refinement on the characterisation of sensory primary afferents.

Nociceptive afferents have a pseudo-unipolar morphology where both peripheral and central axons arise from a single axon that splits into two branches shortly after leaving the cell body. They have free nerve endings characterised by unencapsulated peripheral terminals (Basbaum et al., 2009). Historically, primary sensory afferents have been classified based on their size and myelination status in Aβ-nerve fibres, Aδ-nerve fibres and C-fibres. Myelinated large diameter Aβ-fibres

detect low-threshold mechanical stimuli such as a light touch, but a proportion can also respond to high-threshold noxious stimuli (Djouhri and Lawson, 2004, Nagi et al., 2019). Aδ-fibres are lightly myelinated and together with unmyelinated small diameter C-fibres respond to high-threshold stimuli, transducing nociceptive pain (Basbaum et al., 2009).

Aδ-fibres can be further divided into type I and type II. Type I Aδ-fibres respond to mechanical and chemical stimuli, with a high-threshold for heat stimuli (>52ºC). Type II Aδ-fibres respond to thermal and chemical stimuli, and are mostly mechanically insensitive (Scholz and Woolf, 2007).

C-fibres are mostly polymodal, responding to mechanical, thermal and chemical stimuli (Basbaum et al., 2009) and are furtherly classified by their molecular characteristics. Peptidergic C-fibres release neuropeptides such as substance P (SP) and calcitonin gene-related protein (CGRP) and express the tyrosine kinase receptor A (TrkA) for nerve growth factor (NGF). In contrast, non-peptidergic C-fibres express G protein-coupled receptors (GPCR) of the Mas-related genes family (MRGPRD) and the purinergic receptor P2X3 (Basbaum et al., 2009).

Due to their smaller diameter and lack of myelination, C-fibres convey pain sensation slower than Aδ-fibres, providing the dull and aching sensation of pain, also known as “second pain”, equivalent to Head’s “protopathic pain”. This “second pain” follows the acute and localised sensation of pain transduced by Aδ-fibres, or “first pain”, equivalent to Head’s “epicritic pain” (Price and Dubner, 1977, Basbaum et al., 2009).

In recent years, advances in electrophysiology, calcium imaging and transcriptomics have enabled to further classify and characterise the subtypes of sensory neurons and their functionality, by identifying subtype-specific molecular profiles and responses to different stimuli modality and intensity (St. John Smith, 2018).

1.2.1.1 Recent advances in primary afferents classification

Technical advances, including single-cell and spatial transcriptomics as well as genetic manipulations in animal models, have led to the refinement of molecular and functional classifications of primary sensory neurons, a field which is rapidly

evolving (Middleton et al., 2021). Additionally, while the majority of functional and transcriptional studies characterizing sensory neurons has been performed in animal models, several studies published in recent years have focused on human sensory neurons, often performing cross-species comparisons to establish the validity of animal models, from rodents to non-human primates, as well as non-canonical models for pain research such as the axolotl and drosophila (Tavares-Ferreira et al., 2022, Yang et al., 2022, Nguyen et al., 2021, Huasheng et al., 2023, Jung et al., 2023, Bhuiyan et al., 2023). Bhuiyan et al. (2023) performed a cross-species comparison integrating several single-cell studies of DRG and TG and identified species-specific molecular markers to identify neuronal subtypes. Markers identified for human DRG and TG neuronal subtypes are summarised in Table 1.1.

Tavares-Ferreira et al. (2022b) used 10X Visium technology to profile human DRG neurons identifying a total of 12 neuronal subtypes, classified using a mixture of transcriptional, morphological and putative functional characteristics. Among the large fibre neurons, proprioceptors (PVALB+/KCNS1+/ASIC1+), Aβ slowly adapting low-threshold mechanoreceptors (Aβ-SA LTMR2, PVALB+/NTRK3+), Aβ rapidly adapting low-threshold mechanoreceptors (Aβ-RA LTMRs, $NTRK3^{high}$+$NTRK2^{low}$), Aβ nociceptors (SCN10A+/NTRK3+), Aδ low-threshold mechanoreceptors (Aδ-LTMR, $NTRK2^{high}$) and Aδ high-threshold mechanoreceptors (Aδ-HTMRs, SCN10A+/CPNE6+) were identified. Among the small fibre neurons, TRPM8+ cold nociceptors, TRPA1+ nociceptors, putative silent nociceptors (CHRNA3+), pruritogen receptor enriched (NPPB+) and putative C-LTMRs (GFRA2+) were identified.

In a cross-species harmonisation which includes human, non-human primates and rodent DRG and TG cells, Bhuiyan et al. (2023) identifies similar subtypes among the A-type fibres, with the further subdivision of Aδ-HTMRs into CALCA+ CHRNA7+ neurons, representing putative polymodal A-fibres (A-MH/C), and CALCA+ KIT+ neurons, representing putative mechanically sensitive A fibres (A-M). Among the C-fibres population, there is more discrepancy in the nomenclature used. Tavares-Ferreira et al. (2022b) avoids the classical peptidergic/non-peptidergic nomenclature due to the increasing body of evidence that in human nociceptors, classical peptidergic markers, such as TRPV1, CALCA, SCN10A and

the P2X3 receptor, are widely expressed in most sensory neurons (Shiers et al., 2021, Shiers et al., 2020). Instead, Bhuiyan et al. (2023), using a cross-species harmonisation approach, aims to identify corresponding subtypes across different species based on overall transcriptional profiling rather the expression of specific markers at individual gene level. With this classification approach, Bhuiyan et al. (2023) identifies the following markers to distinguish between C-fibres neurons in the human datasets: CALCA+PTPRT and CALCA+ADRA2A, which can be mapped back to peptidergic fibres in rodents, and SCN11A+GFRA1, which can be mapped back to non-peptidergic populations in rodents, as well as a TRPM8 for cold nociceptors, Th for C-LTMRs and SST for silent nociceptors.

A different approach was used by Huasheng et al. (2023), who performed laser capture microdissection to deeply sequence neuronal soma from human DRG, avoiding the loss of cytoplasmic RNA encountered in single nuclei datasets but retaining single-cell identity, instead of the near-single cell resolution obtained with Visium by Tavares-Ferreira et al. (2022b). The resulting deeply sequenced dataset includes 16 subtypes characterised by cell size and gene expression, which was classified using the classical peptidergic/non-peptidergic nomenclature (Huasheng et al., 2023).

Overall, sensory neuron subtypes can be consistently identified across studies in humans, with differences often related to technical factors and nomenclature choices. Across different species, sensory neurons can mostly be mapped back to common subtypes, but the proportion of certain neuronal populations and the level of expression of specific genes diverges, possibly as a result of evolutionary adaptations (Bhuiyan et al., 2023). Whereas the debate on sensory neuron classification might be often semantic, identifying the differences across species and the most suitable markers in each organism is essential to translate studies from animal models to humans and is an active and rapidly advancing area of research.

This classification effort doesn’t end here, as a specific transcriptional profile doesn’t itself determine a functional role. Instead, functionality is often determined by the innervation target and considerable advance is underway using transgenic reporter mouse lines to label and transcriptionally characterise sensory neurons

innervating a specific organ, such as the tongue, teeth or adipose tissue (Ibrahim et al., 2023, Wu et al., 2018, Lee et al., 2023, Wang et al., 2022a). Novel technologies such as patch-seq are helpful to bridge the classification between electrophysiological and molecular profiling (Parpaite et al., 2021), whereas genetic manipulations in animal models, including chemogenetic systems, are helpful to recapitulate the physiological and behavioural function of molecularly-defined subtypes (Perez-Sanchez et al., 2023).

Table 1.1 Classification and gene markers of human primary afferents.
The table summarises the proposed afferent subtypes based on transcriptional profiling from a cross-species atlas, adapted from Bhuiyan et al. (2023). Abbreviations: Aβ-SA-LTMR= Aβ slowly adapting low threshold mechanoreceptors, Aβ-RA-LTMR= Aβ rapidly adapting low threshold mechanoreceptors, Aδ-LTMR = Aδ low threshold mechanoreceptor, A-MH/C = responsive to mechanical, heat and cold stimuli, A-M= A fibre responsive to mechanical stimuli, C-LTMRs = C fibre low threshold mechanoreceptor, C-MH = C fibre responsive to mechanical and heat stimuli, C-H = C fibre responsive to heat stimuli, C-C = C fibre responsive to cold stimuli.

Fibre type	Axon diameter	Myelination	Conduction velocity	Genetic markers in humans	Cutaneous physiology
Aβ	Large	High	> 40 ms^{-1}	PVALB	Proprioceptors
				$NTRK3^{high}$ + GRM8	Aβ-SA-LTMR
				$NTRK3^{high}$ +NTRK2	Aβ-RA-LTMR
Aδ	Medium	Lightly	> 2 ms^{-1}	$NTRK3^{low}$ +NTRK2	Aδ-LTMR
				CALCA+CHRNA7	A-MH/C
				CALCA+KIT	A-M
C	Small	None	< 2 ms^{-1}	CDH9	C-LTMR
				SCN11A+GFRA1	C-MH
				CALCA+PTPRT	C-H
				CALCA+ADRA2A	?
				TRPM8	C-C
				SST	C-MH

1.2.2 Central projections of primary afferents

Primary afferents from the periphery project to the dorsal horn of the spinal cord, which is organised in different laminae as first proposed by Rexed (1954) (Figure

1.2). Generally, Aβ myelinated low-threshold mechanoreceptors project to lamina II-V, while Aδ and C-fibres project mainly to lamina I and II (Todd, 2010). More specifically, Aδ nociceptors mostly terminate in lamina I, whilst a subset of Aδ-fibres terminates deeper in lamina III-V. Classically defined peptidergic C-fibres terminate in lamina I while non-peptidergic C-fibres terminate in lamina II (Todd, 2010, Basbaum et al., 2009). Within the dorsal horn, post-synaptic neurons which carry the signal to the brain can be specific to each type of fibres input or receive inputs from all three, in which case the neurons are known as wide dynamic range (WDR) neurons (Sessle, 2005, Basbaum et al., 2009).

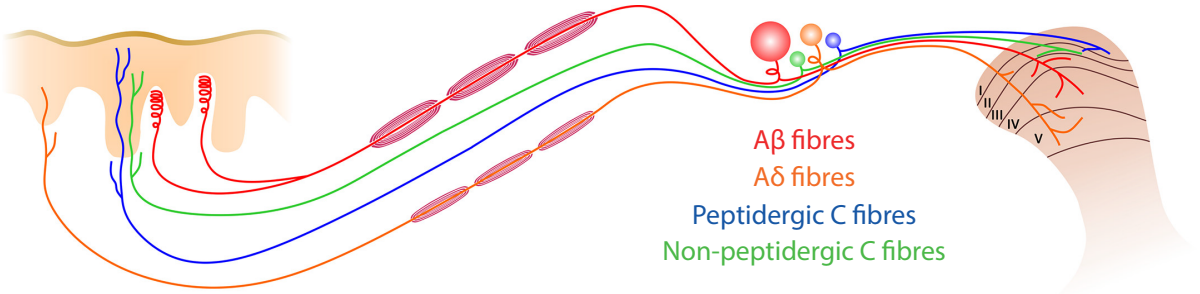

Figure 1.2 Central projections of primary sensory afferents in the spinal cord.
Diagram displaying the organisation of the spinal dorsal horn and the central projections of different types of primary afferents. Aβ fibres project to lamina II-V, Aδ and fibres project to lamina I, whilst a subset projects to deeper lamina. Peptidergic C fibres project to lamina I, while non-peptidergic C fibres project to lamina II. Image adapted with permission from Bennett et al. (2019).

1.2.3 Spinal circuits involved in nociceptive processing.

Melzack and Wall (1965) postulated the gate-control theory where they theorised that nociceptive inputs are modulated by low-threshold afferents in the substantia gelatinosa before being transmitted to the brain to elicit pain perception and behavioural responses. This was in contrast to the specificity theory which theorised the existence of a specialised circuit to transmit nociceptive information, supported by the evidence of the selective activation of a subset of central projection neurons by high threshold mechanical and thermal stimuli (Christensen and Perl, 1970). These theories have been tested in the past 60 years to define the circuitries that underlie nociceptive perception, leading to the identification of

several different classes of spinal neurons that contribute to and modulate nociceptive processing.

In the dorsal horn, projection neurons, which relay the primary afferent inputs to the brain, are concentrated in lamina I (Todd, 2010). Projection neurons cross the midline, travel rostrally in the contralateral white matter and terminate in various brainstem and thalamic nuclei, including the caudal ventrolateral medulla, the nucleus of the solitary tract, the lateral parabrachial area, the periaqueductal grey matter and several nuclei in the thalamus (Todd, 2010). Most projection neurons express the neurokinin 1 receptor (NK1R), targeted by substance P and are required for the development of hyperalgesia in neuropathic and inflammatory pain, receiving inputs from peptidergic primary afferents (Mantyh et al., 1997, Todd et al., 2002).

Interneurons make up the vast majority of neurons in laminae I-III and are extremely heterogeneous: they arborise locally and include both inhibitory and excitatory neurons, receiving inputs from primary afferent neurons (Todd, 2010). Indeed, these neurons embody the gate-control system theorised by Melzack and Wall (1965), providing excitatory and inhibitory controls dependent on both low-threshold mechanical and nociceptive polymodal inputs (Duan et al., 2014)

Finally, descending inputs from the brain project to the dorsal horn, including the serotonergic system originating from the nucleus raphe and the noradrenergic pathway, originating from the locus coeruleus (Todd, 2010), which are thought to mediate pain relief through the action of SNRIs and TCAs (Kremer et al., 2016). GABAergic axons also descend from the rostral ventromedial medulla and form axoaxonic synapses with primary afferents to modulate nociceptive inputs (Todd, 2010, Kato et al., 2006, Zhang et al., 2015b).

Overall, uncovering the complexity of spinal circuitries involved in nociceptive processing is fundamental to identify how synaptic plasticity may result in persistent pain perception and how it can be harnessed to treat neuropathic pain (Woolf, 2011, Todd, 2010).

1.3 Nerve injury, regeneration and neuropathic pain development

Neuropathic pain arises as a direct consequence of lesion or diseases affecting the somatosensory system (Scholz et al., 2019). Traumatic nerve injuries are a common cause of neuropathic pain development, where the changes underpinning nerve regeneration may result in ectopic activity and maladaptive plasticity leading to persistent pain.

In the following paragraphs, the mechanisms that underlie the generation of neuropathic pain will be elucidated, starting from an overview of the types of peripheral nerve injuries and mechanisms underlying nerve regeneration, leading to the neurobiology of neuropathic pain development, including mechanisms of peripheral and central sensitisation.

1.3.1 Peripheral nerve injury

Peripheral nerves enable the transmission of information from the periphery to the central nervous system and vice-versa. They contain the axons of sensory, motor and autonomic neurons, myelinated by Schwann cells or sheathed by non-myelinating Schwann cells in Remak bundles (Zochodne, 2008). They are grouped in bundles, also known as nerve fascicles, where several myelinated and non-myelinated axons, as well as endoneurial fibroblasts and blood vessels, are enwrapped by a perineurial sheath. Several nerve fascicles are grouped together within the epineurium, composed of fibroblasts and epineurial blood vessels (Zochodne, 2008). A more in-depth description of the organisation and the cell-types that populate peripheral nerves will be introduced in Chapter 2.

1.3.1.1 Peripheral nerve injury classification

The structure of peripheral nerves serves to protect the axons from changes in ionic composition, pathogens, toxins and trauma (Iwanaga et al., 2022). Traumatic nerve injury can affect the integrity of peripheral nerves to several degrees. Seddon (1943) classified nerve injury types into neuropraxia, axonotmesis and neurotmesis, while Sunderland (1951) used a grading system ranging from type 1 to type 5, from least to most severe, respectively.

Neuropraxia (Sunderland's type 1) refers to a transient lesion of the nerve where the myelin sheath is affected but the axon is intact, although compressed, and may display a conduction block due to focal demyelination or ischaemia (Robinson, 2000). Axonotmesis is commonly seen in crush injuries, nerve stretch injuries or percussion injuries (such as motor vehicle accidents, falls or gunshot wounds) and involves damage to the axons (Robinson, 2000). It's furtherly classified by Sunderland (1951) based on the extent of the damage affecting exclusively the axon (type 2), the endoneurium (type 3) and the perineurium (type 4). In these instances, the epineurium of the nerve is still present, which enables functional recovery. Finally, neurotmesis (Sunderland's type 5) refers to the complete transection of the nerve with poor likelihood of recovery without surgical intervention.

1.3.1.2 Wallerian degeneration

Following axonal damage, a process known as Wallerian degeneration occurs (Figure 1.3), which involves the degradation of the axons and myelin distal to the site of injury and the reinnervation of their end-targets. This process is accompanied by the breakdown of the blood-nerve barrier formed by perineurial cells which aids the infiltration of immune cells, particularly macrophages, as well as neutrophils (transiently after injury) and fibroblasts (Stoll and Müller, 1999, Gaudet et al., 2011).

Upon loss of axonal contact, Schwann cells de-differentiate from their mature myelinating or non-myelinating state to a proliferative repair state, expressing markers common to the immature phenotype, including Sox2, Oct6, Pax3, but also repair-specific TFs, such as c-Jun and Merlin (Stoll and Müller, 1999, Balakrishnan et al., 2021, Jessen and Arthur-Farraj, 2019). This results in the downregulation of myelin-related genes (Mbp, Mag, P0, Pmp22 and Prx) and upregulation of Ngfr, Gfap, L1cam and Ncam (Balakrishnan et al., 2021). In order to support repair, Schwann cells produce growth factors and ECM components (GDNF, artemin, BDNF, NT3, NGF, VEGF, erythropoietin, pleiotrophin, laminin and N-cadherin) and acquire an elongated shape, arranging themselves into tubular structures known as bands of Büngner to provide a guide for regenerating nerve fibres (Jessen and Arthur-Farraj, 2019). Following toll-like receptors (TLRs) activation, Schwann cells also produce cytokines (TNFα, iNOS, LIF, IL-1β, MCP-1) to recruit macrophages to

the site of injury, which will clear the majority of debris (Martini et al., 2008, Gaudet et al., 2011).

Shortly following injury, axonal and myelin debris form lipid droplets, named ovoids, which are initially phagocytosed by Schwann cells and resident macrophages. At day 2 following injury, circulating monocytes-derived macrophages enter the distal stump guided by the ICAM-1 and VCAM-1 receptors on endothelial cells, upregulated by cytokine production at the site of injury (Stoll and Müller, 1999, Brück, 1997). Myelin ovoids are recognised by macrophages through the complement receptor type 3 and complement component C3 interaction (Brück, 1997). Following clearance of debris and axonal regeneration, Schwann cells re-differentiate in a proximal-to-distal fashion from the site of injury, losing the de-differentiation markers and bands of Büngner morphology and re-acquiring mature myelinating or non-myelinating gene expression (Stoll and Müller, 1999). Reinnervation of the appropriate end-target is guided by molecular clues: for example, Schwann cells that were previously innervating motor fibres retain the ability to express the carbohydrate epitope L2/HNK-1 when contacted by motor axons during regeneration, which promotes the preferential myelination and guidance of motor axons to their appropriate muscle pathways (Martini et al., 1994).

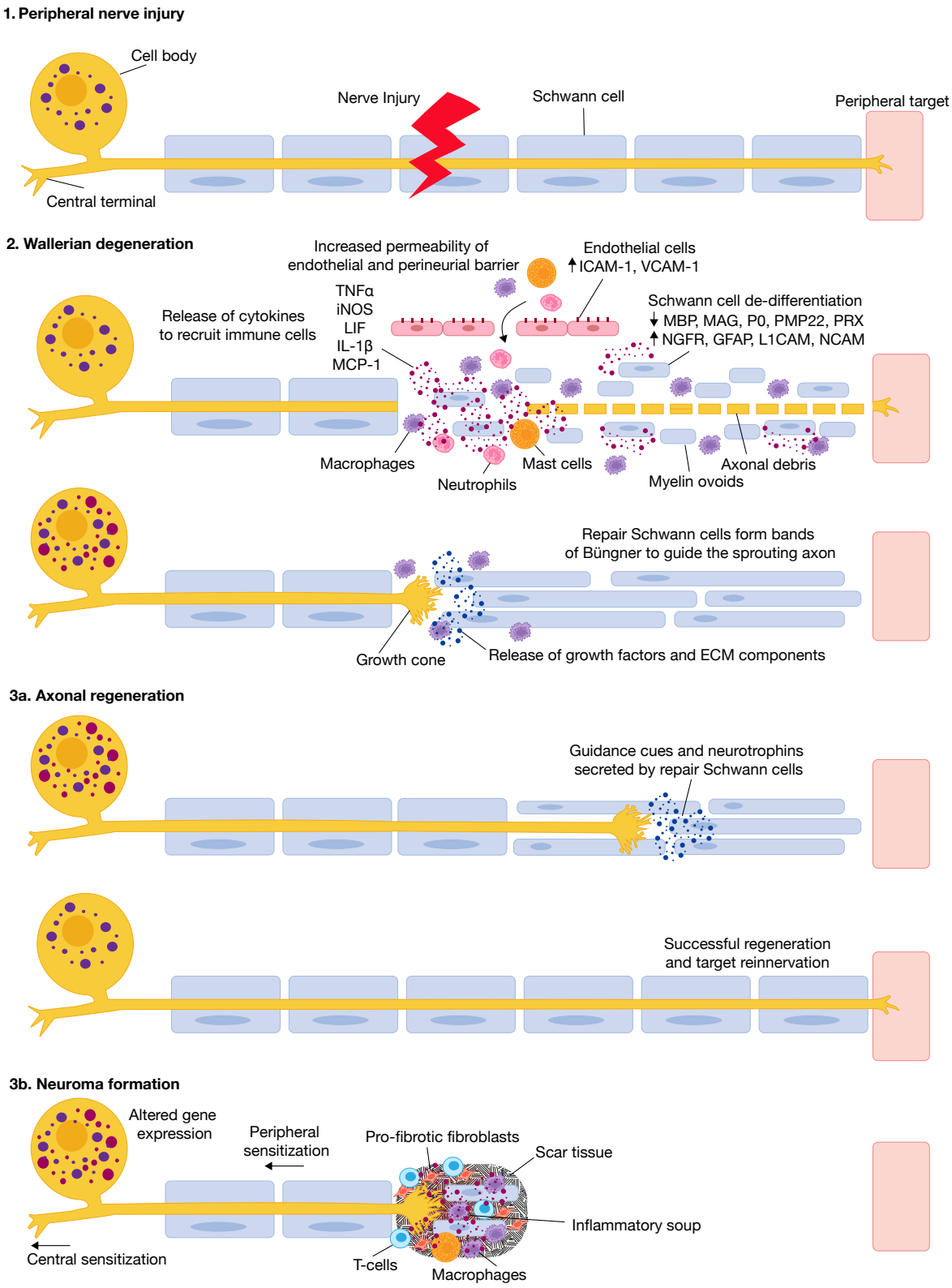

Figure 1.3 Nerve injury and neuroma formation.
Diagram describing the mechanisms that follow nerve injury leading to nerve regeneration or neuroma formation. Peripheral nerve injury (1) induces Wallerian degeneration (2), where axons and myelin degenerate forming lipid ovoids. Schwann cells de-differentiate and release cytokines that lead to the increased permeabilization of the endothelial and perineurial barrier and the infiltration of immune cells (neutrophils, macrophages, mast cells) to clear axonal and myelin debris. Repair Schwann cells form bands of Büngner to guide the sprouting axons (3a), releasing growth factors,

ECM components and guidance cues, promoting the regeneration of the axons to the innervation target. The presence of scar tissue deposited by pro-fibrotic fibroblasts may entrap the sprouting axons (3b), preventing their crossing to the distal stump and target reinnervation. Immune cells (macrophages, T-cells) entrapped in the scar tissue release pro-inflammatory mediators that may lead to peripheral and central sensitisation.

1.3.1.3 Neuroma formation

Following nerve injuries, tissue damage might result in the formation of scar tissue that prevents axons to cross the injury gap, resulting in the formation of a swollen mass where axons become entrapped and are prevented from reaching their innervation target. The swellings observed at the distal ends of the proximal segments of injured peripheral nerves have been first described by Odier (1811) but were named as neuromas by Wood (1829). Throughout the 19th and 20th century, the mechanisms of neuroma formation and their clinical presentations was furtherly elucidated (Swanson, 1961). Neuromas are non-neoplastic proliferation of cell types in an injured nerve, usually resulting from trauma due to surgical procedures such as amputations and dental treatment, or chronic inflammatory irritation, such as in Morton's neuroma, caused by chronic irritation of the foot (Yang et al., 2023). Depending on the degree of nerve injury, they can be subdivided in nerve-end-neuromas, where the nerve is completely transected, or nerve-in-continuity, where the distal and proximal end of the nerve are at least partially connected. The most common symptoms in patients with neuromas are paraesthesia and pain, which can be described as burning, stabbing, raw or gnawing (Yang et al., 2023).

Neuroma formation is thought to be caused by signalling that promotes nerve regeneration following injury and its interaction with wound-healing cells that are activated as a result of tissue damage: the proliferation of Schwann cells and profibrotic fibroblasts, as well as the disorganised sprouting of axons, lead to an entangled swollen mass of connective tissue and nerve fibres (Yang et al., 2023).

An important feature characteristic of nerve injury and neuromas is the presence of ectopic activity in the injured nerve fibres. Following nerve lesion, an accumulation of ion channels at the site of injury is observed, which might be caused by impaired anterograde transport or changes in gene expression and lead to ectopic activity and increased excitability (Grossmann et al., 2009). In experimental models of neuromas, local ectopic activity from both the axotomized

and non-injured fibres can be blocked by ion channel modulators (Bernal et al., 2016, Burchiel, 1988). Altered expression of ion channels at the site of injury are thought to mediate changes in excitability and hypersensitivity to mechanical and thermal stimuli (Gold et al., 2003, Vilceanu et al., 2010, Devor et al., 1993). Upregulation of several ion channels has also been reported in human painful neuromas compared to control tissue from the same patients or to non-painful controls (Black et al., 2008, Bird et al., 2013).

Ectopic excitability is enhanced by local inflammation at the site of injury (Grossmann et al., 2009), while genetic impairment of interleukin-1 signalling attenuates ectopic activity following nerve injury (Wolf et al., 2006). The accumulation of immune cells and pro-inflammatory cytokines at the site of injury (Vora et al., 2007, Khan et al., 2017) during nerve regeneration may contribute to the establishment of ectopic activity and lead to peripheral sensitisation, generating symptoms of neuropathic pain, as well as central sensitisation of the nociceptive pathways, contributing to the maintenance of persistent pain. These mechanisms are broadly summarised in Figure 1.4.

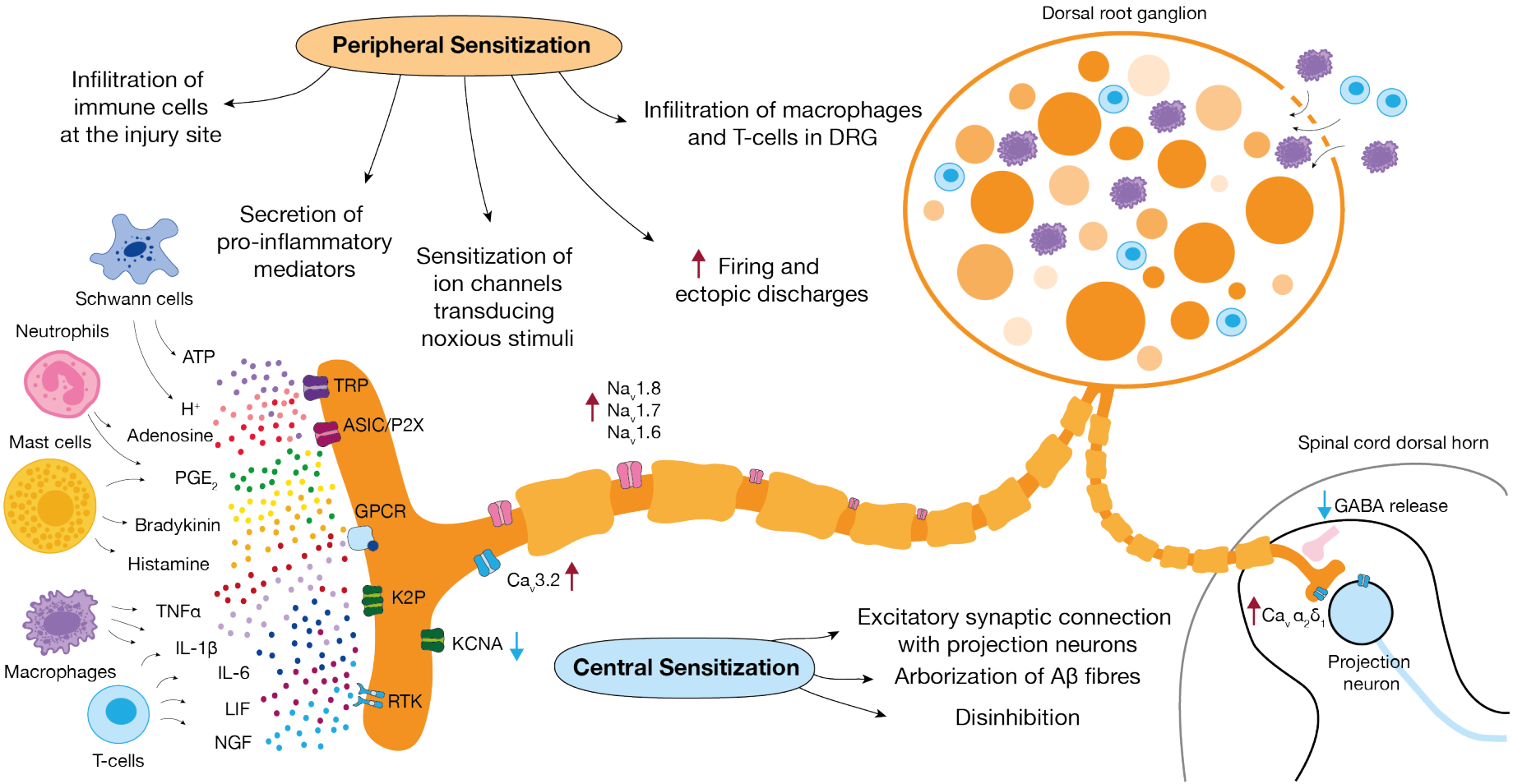

Figure 1.4 Mechanisms of peripheral and central sensitisation in neuropathic pain.
Nerve injury leads to the secretion of pro-inflammatory mediators by damaged cells and the recruitment of immune cells to the injury site. The inflammatory milieu sensitises or activates receptors on the nerve endings: transient receptor potential (TRP) channels, such as TRPV1 and TRPA1, are modulated by ATP, protons, NGF, bradykinin, acid-sensing ion channels (ASICs) are activated by protons that lead to acidification, while P2X receptors are activated by ATP, leading to depolarisation; G-protein coupled receptors (GPCR) include receptors for prostaglandins, bradykinin and histamine and when activated lead to depolarisation through the activation of intracellular signalling cascades; two-pore-domain potassium (K2P) channels are modulated by pH, phospholipids and intracellular signalling, giving rise to leaky potassium currents which alter the membrane's excitability and receptor tyrosine kinases (RTK) are activated by neurotrophins resulting in sensitisation. Overall, the activation and modulation of these receptors by inflammatory mediators results in hyperexcitability and increased firing of action potentials. Persistent activation of sensory neurons causes dysregulation of ion channels expression (e.g. $Na_v1.6$, $Na_v1.7$, $Na_v1.8$, KCNA, $Ca_v3.2$ and Ca_vs accessory subunits) as well as infiltration of immune cells in the DRG (e.g. Csf1 expression in sensory neurons stimulating macrophages infiltration). At the central terminals, the increase of calcium currents leads to potentiation of synaptic connections with projection neurons, while the decrease of GABA neurotransmission leads to disinhibition. Image adapted with permission from Basbaum et al. (2009) and Finnerup et al. (2021).

1.3.2 Peripheral sensitisation

Peripheral sensitisation refers to the increased responsiveness and reduced threshold of nociceptive neurons in the periphery to the stimulation of their receptive fields, as defined by the IASP (Loeser and Treede, 2008). Nerve injury leads to the secretion of pro-inflammatory mediators that promote nerve regeneration but might also lead to the reduction of excitability thresholds and ectopic activity in neurons.

Both nociceptors and non-neuronal cells, including mast cells, basophils, platelets, macrophages, neutrophils, endothelial cells, keratinocytes and fibroblasts, contribute to the secretion of pro-inflammatory mediators at the site of injury, creating an “inflammatory soup” made up of neurotransmitters, peptides (substance P, CGRP, bradykinin), eicosanoids and other lipids (prostaglandins, thromboxanes, leukotrienes, endocannabinoids), neurotrophins (NGF, BDNF, NT-3, NT-4), cytokines (IL-1β, IL-6, TNFα), chemokines, extracellular proteases and protons (Basbaum et al., 2009). Receptors present on the surface of nociceptors can recognise these inflammatory mediators (Figure 1.4), leading to the activation of intracellular cascades which result in increased excitability, through alterations in ion channels and receptor expression that promote signal transduction (alterations in TRP and ASICs channels and P2X receptors), signal amplification (changes in voltage gated sodium and potassium channels’ expression and kinetics) and synaptic transmission (alterations in voltage gated calcium channels and SNARE-mediated vesicle fusion) (Finnerup et al., 2021).

Several other mechanisms have been implicated in peripheral sensitisation, such as the involvement of fibroblasts in neuropathic pain generation (Singhmar et al., 2020), or the activation of a subset of ‘silent’ nociceptors by NGF which become responsive of mechanical stimuli (Prato et al., 2017).

1.3.2.1 Alterations in ion channels

Primary afferents are the first point of contact between external environmental stimuli and the nervous system and require mechanisms to transduce a variety of chemical, mechanical and thermal stimuli into electrical signals that can be relayed to and processed by higher brain centres. Several families of ion channels are

encoded in our genome to transduce, amplify and transmit noxious stimuli, and the alteration of their expression and kinetics by transcriptional, translational and post-translation regulation may result in peripheral sensitisation (Finnerup et al., 2021).

The transient receptor potential (TRP) family, the acid-sensing ion channels (ASIC) and the ATP-gated purinergic channels (P2X) are some of the most important ion channel families involved in signal transduction (Finnerup et al., 2021, Gu and Lee, 2010, Basso and Altier, 2017, Bernier et al., 2018). The TRP family includes the thermosensitive channels TRPV1, TRPA1, TRPV4 and TRPM8, which have been implicated in peripheral sensitisation in neuropathic pain (Basso and Altier, 2017). For example, TRPV1, which is activated by capsaicin, protons and heat (> 43°C) and is essential for pain perception (Caterina et al., 2000), can be sensitised by prostaglandin signalling leading to altered gating properties and its activation to lower temperatures (< 35°C) in the presence of PGE_2 and PGI_2 in a PKC-dependent manner (Moriyama et al., 2005). NGF was also shown to drive peripheral sensitisation by rapidly increasing TRPV1 insertion in the membrane, leading to increased currents (Zhang et al., 2005). Indeed, desensitisation of TRPV1 by capsaicin topical application has shown efficacy in post-herpetic neuralgia and diabetic polyneuropathy, specifically in patients with high TRPV1 peripheral expression (Bonezzi et al., 2020).

The transduction of the initial sensory stimuli involves a transient change in the membrane's potential, which, when a certain threshold is reached, is amplified and conducted as action potentials to relay the signal to the spinal cord (Bennett et al., 2019). Sodium channels, particularly $Na_v1.1$, $Na_v1.6$, $Na_v1.7$, $Na_v1.8$ and $Na_v1.9$, are the major sodium channels expressed in the peripheral nervous system and are crucial in the conduction of action potentials in sensory neurons (Bennett et al., 2019). Several mutations within these ion channels have been linked to congenital pain disorders or insensitivity to pain (Drissi et al., 2020). Alterations in sodium channels expression have been reported in clinical samples of several neuropathic pain conditions, including lingual nerve neuromas (Bird et al., 2007, Bird et al., 2013) and trigeminal neuralgia (Siqueira et al., 2009). Additionally, carbamazepine and lamotrigine, drugs effective in neuropathic pain conditions, particularly in trigeminal neuralgia, are sodium channel blockers (Wiffen et al., 2011). The role of sodium

channels in peripheral sensitisation is driven by several alterations in epigenetic (Luo et al., 2021, Morchio et al., 2023) and post-translational mechanisms which lead to their increased insertion in the membrane or altered gating properties (Laedermann et al., 2015).

On the other hand, potassium channels are crucial to establish and maintain the resting membrane potential, repolarising the membrane potential following an action potential. Their activation leads to the hyperpolarisation and inhibition of AP generation in sensory neurons. Several chronic pain conditions display a reduction in potassium channels' expression leading to an increased firing rate and excitability in sensory neurons (Tsantoulas and McMahon, 2014).

Finally, calcium channels are involved in both the initiation of action potentials and in synaptic transmission at the central terminals of primary afferents and their inhibition leads to analgesia in animal models (Zamponi et al., 2009). Indeed, commonly used drugs for neuropathic pain such as gabapentin and pregabalin act by blocking the accessory $\alpha_2\delta_1$ subunit of voltage gated calcium channels on DRG neurons, thereby reducing trafficking of the pore-forming α_1 subunit to the plasma membrane, reducing Ca^{2+} currents (Kukkar et al., 2013).

1.3.2.2 Role of immune cells in neuropathic pain

Neuro-immune interactions have been implicated in countless studies in neuropathic pain generation. Particularly, mast cells, neutrophils, macrophages, T cells and dendritic cells have been implicated both at the injury site and in DRG and TG in peripheral sensitisation (Finnerup et al., 2021). Their interaction with sensory neurons often occurs through the secretion of pro-inflammatory mediators, including TNF-α, interleukins (IL-10, IL-1β, IL-4, IL-17) and IFN-δ (Finnerup et al., 2021).

Macrophages are crucial for Wallerian degeneration and axonal regeneration. Nerve resident macrophages populations, including endoneurial and epineurial subtypes, have been identified as distinct from circulating monocytes and CNS-specific microglia (Ydens et al., 2020). Endoneurial nerve-resident macrophages produce monocyte chemoattractants following injury, leading to further macrophage infiltration to aid in the repair process (Ydens et al., 2020). Following spared nerve

injury, proliferation and infiltration of macrophages in the DRG and in the sciatic nerve leads to mechanical allodynia (Yu et al., 2020, Shepherd et al., 2018). Shepherd et al. (2018) have shown that macrophages' role in neuropathic pain is mediated by the angiotensin pathway activation in AT2R-expressing macrophages at the site of injury, as peri-sciatic but not intrathecal delivery of AT2R inhibitor dose-dependently attenuates mechanical hypersensitivity following SNI. On the other hand, Yu et al. (2020) argue that macrophages expansion in the DRG, rather than at the injury site, initiates neuropathic pain. Macrophage proliferation in the DRG is driven by CSF1 expression in axotomised sensory neurons and leads to the increase in IL-1β in the DRG and BDNF expression in sensory neurons, resulting in peripheral sensitisation (Yu et al., 2020)

T-cells have also been implicated in peripheral sensitisation. Infiltrating the site of injury and the DRG weeks to month following nerve injury, T-cell depletion results in the reduction of nerve-injury induced mechanical allodynia (Laumet et al., 2019). T-cells have been shown to induce the transition from acute to chronic pain following nerve injury via their infiltration in the leptomeninges of the DRG (Du et al., 2018).

1.3.3 Central sensitisation

The concept of central sensitisation was proposed by Woolf (1983) and refers to the process through which a state of hyperexcitability is established in the CNS, leading to enhanced processing of nociceptive stimuli. Several mechanisms have been identified to contribute to central sensitisation, including alteration in glutamatergic neurotransmission of nociceptive inputs, structural changes in the dorsal horn neurons leading to non-nociceptive inputs engaging in pain transmission circuits, loss of inhibitory controls (disinhibition), and glial-neuronal interactions (Todd, 2010, Basbaum et al., 2009).

The synaptic release of glutamate from central terminals of nociceptors to second order dorsal horn projection neurons underpins the transmission of acute pain sensations, driven by the activation of post-synaptic AMPA and other glutamate receptors (Basbaum et al., 2009). Following nerve injury, the increased neurotransmitter release can activate NMDA receptors, leading to increased calcium channel influx which strengthen the synaptic connection, in a process

similar to hippocampal long-term potentiation (Basbaum et al., 2009). Particularly, long-term potentiation in NK1R+ lamina I projection neurons has been reported following peptidergic C-fibre stimulation through calcium-dependent postsynaptic mechanisms (Ikeda et al., 2003). Downstream activation of signalling pathways by kinases such as MAPK, PKA, PKC, PI3K and Src, further increase excitability in these neurons (Basbaum et al., 2009). For example, Kv4.2-mediated A-type potassium currents, important in establishing membrane potential and neuronal excitability, is modulated by ERK, which is activated following noxious stimuli (Hu et al., 2006, Ji et al., 1999).

In addition to homosynaptic potentiation, structural changes in the projections of primary afferents in the dorsal horn following nerve injury contribute to central sensitisation through heterosynaptic plasticity. For example, following inflammation and nerve injury, Aβ-fibres are reported to sprout into lamina II, underlying symptoms of allodynia (Woolf et al., 1992, Bester et al., 2000).

A loss of inhibitory GABAergic and glycinergic neurotransmission in spinal and supraspinal circuits has also been observed, also known as disinhibition (Basbaum et al., 2009). Loss of inhibitory postsynaptic currents and a decrease in GABA signalling in the dorsal horn has been reported in several nerve injury models (Moore et al., 2002), but no significant neuronal cell death has been reported (Polgár et al., 2004), indicating that disinhibition might be caused by an alteration of neuronal membrane potential, alteration in the inputs or intrinsic properties of the interneurons, rather than a loss of inhibitory neurons itself (Todd, 2010).

While it's well-established that spinal circuits are modulated by non-nociceptive inputs and a loss of balance in these modulatory inhibitory and excitatory circuits leads to the establishment of allodynia, the precise organisation of these circuits across species is still poorly characterised (Woolf, 2011). Advances in chemogenic and optogenetic techniques have improved the functional characterisation of spinal neuron subpopulations in rodents (Guo et al., 2022). Understanding whether these findings can be translated to humans is paramount to identify mechanisms of chronic pain establishment that can be harnessed for pain relief.

Controversy regarding the importance of central sensitisation to the maintenance of chronic pain has been raised (Cervero and Wood, 2020): for example, whilst in animal models the deletion or pharmacological blockade of NK1R+ projection neurons abolishes central sensitisation along with a loss of pain behaviour (Mantyh et al., 1997), NK1R antagonists have failed as analgesics in the clinic (Hill, 2000). Central sensitisation contributes to the initiation and maintenance of chronic pain states (Woolf, 2011), however, spontaneous peripheral input is required to sustain neuropathic pain, evidenced by the abolition of pain sensation following nerve block, while no evidence has shown that central sensitisation mechanisms can independently sustain neuropathic pain (Meacham et al., 2017).

1.3.4 Glial cell activation

In the CNS, glial cells, including oligodendrocytes, astrocytes and microglia, support neurons, providing protection and nutrition. Following nerve injury, they also play a role in the generation and maintenance of neuropathic pain.

Microglia (5-20% of glial cells) are resident immune cells of myeloid origin which colonise the CNS during foetal development, where they regulate homeostasis by removing cellular debris and secreting trophic factors, as well as responding to insult or tissue injury (Tay et al., 2017). Following injury, microglia proliferate and display an activated phenotype, characterized by MHC Class II antigen presentation, the activation of p38-MAP kinase and the release of pro-inflammatory mediators including cytokines (e.g. TNF and IL-1β), chemokines (e.g. CCL2), reactive oxygen species and nitric oxide (Scholz and Woolf, 2007, Old et al., 2015). Spinal microglial activation peaks one week after injury, followed by a slow decline over several weeks (Scholz and Woolf, 2007).

Astrocytes account for 20-40% of glial cells in the CNS and maintain homeostasis by sustaining the metabolic levels of potassium ions, glutamate and water (Cheng et al., 2022). Following injury, astrocytes adopt a reactive phenotype characterised by hypertrophy and the increased expression of GFAB, S100β and vimentin (Old et al., 2015). Astrocytes contribute to neuropathic pain development through the secretion of inflammatory mediators (e.g. TNF-α, IL-1β, CCL2, CXCL1, BDNF, MMPA-2) as well as a reduction in glutamate uptake, leading to

hyperexcitability of post-synaptic neurons (Cheng et al., 2022). Compared with the microglial response, astrocyte proliferation begins relatively late and progresses slowly, but is sustained for a longer period of over 5 months (Scholz and Woolf, 2007).

One of the major signalling pathways underpinning neuropathic pain development from neuro-glial interactions include fractalkine-mediated signalling. Fractalkine (CX3CL1) is a chemokine that can be tethered to the membrane of dorsal horn neurons or solubilised by metalloproteases or Cathepsin S-mediated cleavage, leading to CX3CR1 activation in microglia (Old et al., 2015). This results in the release of pro-inflammatory mediators which sensitise dorsal horn neurons, leading to mechanical allodynia and thermal hyperalgesia in animal models of neuropathic pain (Silva and Malcangio, 2021). Other signalling pathways involved in glial activation leading to neuropathic pain include Toll-Like Receptor (TLR) activation, resulting in NF-kB-mediated upregulation of interferons and pro-inflammatory cytokines, and ATP binding to P2X receptors expressed in microglia, which results in BDNF release, interfering with GABA signalling (Scholz and Woolf, 2007).

1.4 “Omics” approaches in the study of human pain conditions

In recent years, we have seen the development and increased accessibility of unbiased high-throughput molecular screening technologies that have led to an explosion of data in the field of genomics, epigenetics, transcriptomics, translatomics, proteomics and metabolomics, providing a vastity of information on cell states in health and disease. Additionally, the creation of large-scale databases for human data (UKBioBank, GTEx), tissue banks (Netherland Brain Bank) and consortia (DOLORisk, PAINSTORM) have fuelled data generation from human tissues and analysis of population-wide information (Hébert et al., 2023).

At the level of DNA, whole-genome, exome sequencing, genotyping and DNA methylation assays have been rapidly developing, and several large-scale population studies have emerged linking genetic variations with an increased risk to

develop certain pain conditions (Veluchamy et al., 2018, Meloto et al., 2018, Diatchenko et al., 2022).

Technologies to measure gene expression at transcriptome-wide level are improving and evolving, becoming cheaper and more flexible and are now routinely applied to single cells or tissue sections retaining information on the histological context (Stark et al., 2019, Hwang et al., 2018). Spatial and single cell transcriptomics have been used to molecularly classify human sensory neurons (Tavares-Ferreira et al., 2022b, Yang et al., 2022), as well as human spinal cord neurons (Yadav et al., 2023a), regions of the human brain (Siletti et al., 2023) and whole brain in rodents (Yao et al., 2023).

The decreasing cost per sample of bulk RNA sequencing has allowed unbiased gene expression analysis in clinical samples linked with symptoms of pain and identify sex-dependent mechanisms linked with neuropathic pain (Ray et al., 2023, North et al., 2019), as well as shedding light on neuroimmune interactions (Parisien et al., 2022). North et al. (2019) used the DRG of 26 patients undergoing surgery for tumour resection or spinal reconstruction, with and without dermatome-associated neuropathic pain, for electrophysiological and transcriptional characterisation. The study identified sex-dependent mechanisms linked with neuropathic pain, such as the enrichment in gp-130 receptor signalling in painful male samples, particularly in OSM signalling (North et al., 2019). This work was repeated with an increased sample size of 50 DRGs in Ray et al. (2023), confirming previously identified differences as well as identifying interferon-induced signalling to be upregulated in female samples with neuropathic pain. In other work, Parisien et al. (2022) sequenced peripheral immune cells from patients with low back pain (LBP) to characterise the pathophysiological mechanisms underlying the acute to chronic transition of chronic LBP, identifying an increased neutrophil signature in patients that had resolved LBP. Experiments in animal models confirmed that early suppression of acute inflammation delays the recovery to baseline in neuropathic and inflammatory pain models, while data from the UKBioBank confirmed that the use of NSAIDs increased the risk of back pain 2 to 6 years following initial assessment (Parisien et al., 2022).

Obtaining clinically relevant samples for the study of neuropathic pain is challenging, evidenced by the scarcity of studies using such samples in the literature. In this thesis, transcriptional analysis on samples of injured lingual nerves linked with clinical information on the symptoms of pain is presented, exploring the cellular and transcriptional changes linked with nerve injury and neuropathic pain.

1.5 Lingual nerve injury and the trigeminal system

The project described in this thesis focuses on the unbiased and high-throughput characterisation of the cellular and transcriptional landscape within human samples of painful and non-painful lingual neuromas and healthy trigeminal nerves using spatial and single nuclei transcriptomics. Human lingual neuromas develop as a result of lingual nerve injuries, often caused by routine dental treatment such as third molar removal. The lingual nerve is a branch of the fifth cranial nerve, the trigeminal nerve. In order to provide an overview of the context of lingual nerve injuries, the following paragraphs will describe the anatomy and the clinical relevance of the trigeminal pathways for somatosensation and nociception and highlight some differences that have been reported between the trigeminal nociceptive system and the spinal system. The incidence, causes and surgical management of lingual nerve injury will also be described.

1.5.1 Anatomy of the trigeminal nerve

The trigeminal nerve is the largest cranial nerve, originating from the brainstem at the mid-lateral surface of the pons, with both a smaller motor and a larger sensory root. The afferent fibres transmit information from the face, oral and nasal mucosa, the scalp and the cranial tissues, including the meninges, with cell bodies located in the trigeminal ganglia. The trigeminal nerve also contains visceral efferent fibres supplying the lacrimal, salivary and nasal mucosa glands, these fibres originate from the facial or glossopharyngeal nerves. The somatic efferent fibres of the trigeminal nerve innervate the masticatory muscles (Rodella et al., 2012).

The trigeminal nerve divides into three branches distal to the trigeminal ganglion: the ophtalamic (V_1), maxillary (V_2) and mandibular (V_3) division. The ophthalmic division (V_1) provides sensation to the eyeball, conjunctiva, lacrimal glands, nasal

mucosa, skin of the nose, eyelid, forehead and dura mater. The maxillary division (V_2) innervates the dura, the maxillary teeth and associated gingiva, the maxillary sinus, the upper lip, the lateral surface of the nose, the lower eyelid and conjunctiva, the skin of the cheek and of the side of the forehead, the nasal cavity and the mucosa of the hard and soft palate. Finally, the mandibular division (V_3) provides innervation to the dura, the temporomandibular joint, the skin over the side of the head above the ears, the tongue and its adjacent gingiva, the muscle of the floor of the mouth, the mandibular teeth and associated gingiva, the mucosa and skin of the cheek, the lower lip, the chin and the muscles of mastication (Rodella et al., 2012).

Trigeminal sensory afferents project to the trigeminal sensory nuclei, located in the brainstem and displayed in Figure 1.5. The trigeminal sensory nuclei include a principal nucleus for discriminative and tactile information and a spinal nucleus, located in the medulla, which receives nociceptive information and is continuous with the cervical dorsal horn at the caudal end, displaying the same laminated structure. The spinal nucleus is furtherly divided into three subnuclei: oralis, interpolaris and caudalis (Terrier et al., 2022). Fibres that provide intraoral and dental sensation, including pain, project to the spinal nucleus oralis and caudalis. Nociceptive and thermoreceptive fibres that provide cutaneous innervation of face and cranial tissues mainly terminate in the spinal nucleus caudalis. The spinal nucleus interpolaris receives inputs from fibres that carry cutaneous nociceptive or low-threshold mechanical inputs (Terrier et al., 2022). Second-order neurons relay nociceptive information from the spinal nuclei to the contralateral thalamus through the trigeminothalamic tract (Henssen et al., 2016).

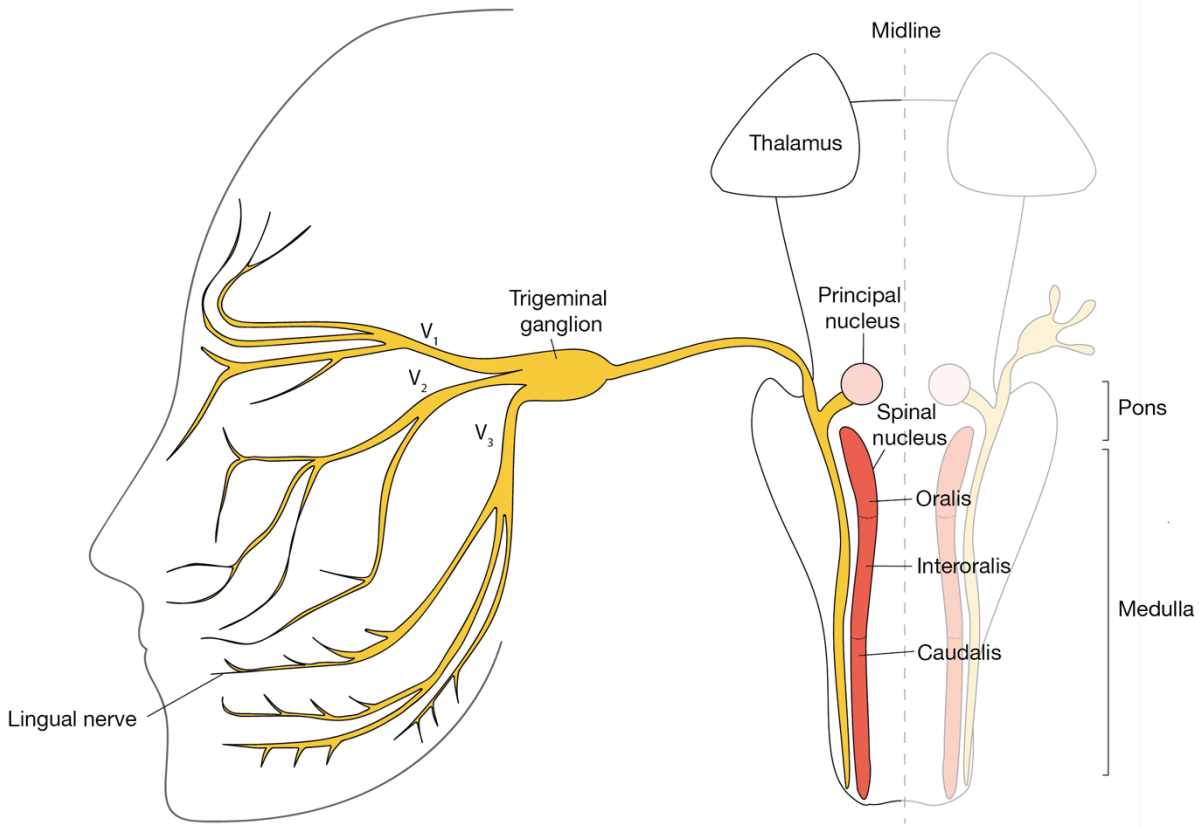

Figure 1.5 Anatomical structure of the trigeminal nerve and sensory nuclei
The diagram displays the trigeminal nerve and its divisions, with the lingual nerve labelled as one of the branches of the mandibular division (V_3). The trigeminal nerve enters the brainstem at the pons and projects to its nuclei, including the principal nucleus for discriminative and tactile information and the spinal nuclei, for nociceptive and thermoreceptive afferents. The spinal nucleus is furtherly divided in subnucleus oralis, interpolaris and caudalis. Second-order neurons project to the thalamus. Image of the brainstem adapted with permission from Henssen et al. (2016).

1.5.2 Trigeminal chronic pain

Orofacial pain disorders were recently classified in the International Classification of Orofacial Pain (2020), with distinctions involving pain arising from dentoalveolar structures, myofascial pain, temporomandibular joint disorders, lesions or disease of the cranial nerves, pain resembling primary headaches and idiopathic orofacial pain. The trigeminal nerve is susceptible to several of these chronic pain conditions, particularly of neuropathic nature. Dental procedures, including tooth extraction, local anaesthetic injection, neoplastic resections and implant placement, may lead to peripheral nerve injury-induced neuropathic pain, most often affecting the lingual and inferior alveolar nerves (Jones, 2010). Trigeminal neuralgia may arise as a result of the compression of the trigeminal root by a blood vessel, a tumour or due to

demyelination induced by multiple sclerosis, leading to short recurrent episodes of intense electric shock-like pain affecting an area of the face (Lambru et al., 2021). Trigeminal nerve fibres also innervate the majority of the dura mater and are implicated in headache and migraine pain (Edvinsson et al., 2020). The trigeminal nerve is also susceptible to infection by the varicella zoster infections, which commonly affects the oral mucosa and may lead to the development of postherpetic neuralgia, a painful condition characterised by unilateral acute and stabbing pain which persists months after the initial infection (Feller et al., 2017). As the nerve innervating the temporomandibular joint, the trigeminal nerve has also been implicated in TMJ disorder (Moayedi et al., 2012).

1.5.3 Differences between trigeminal and spinal nociception

The somatotopic representation of trigeminal-innervated areas, particularly the lips, tongue, perioral and intraoral regions, occupies a large proportion in the primary sensory cortex, reflecting the importance of these areas for survival (Moulton et al., 2009). Despite the multitude and variety of clinical presentations of neuropathic pain affecting the trigeminal nerve, its molecular and cellular composition is much less studied than that of spinal nerves in humans, evidenced by the lower number of single cell studies performed on TG compared to DRG (Bhuiyan et al., 2023).

Studies on human participants have shown that noxious heat stimulation elicited higher sensitisation when applied to the head than to the limbs of participants (Schmidt et al., 2015). The susceptibility of the trigeminal system to sensitisation might be caused by differences in the central nociceptive pathways: an fMRI study has shown that noxious stimulation to trigeminal areas results in the increased activation of areas of the brain linked with fear (Schmidt et al., 2016). These observations might be explained by the importance of the face and head to preserve vital functions which might have led to evolutionary adaptations that stimulate the avoidance of potentially harmful stimuli directed at these areas (Schmidt et al., 2016).

The differences in the sensitizing capabilities between the spinal and trigeminal system might be underpinned by changes in the central pathways transmitting

nociceptive information, as it was demonstrated that trigeminal neurons can directly project to the parabrachial (PB) nucleus skipping the synapsis with second-order neurons, leading to increased activation of the PB following noxious stimulation to the face (Rodriguez et al., 2017). However, there may also be differences in the cellular composition of the trigeminal and dorsal root ganglia, as well as differences in their transcriptional profile. For example, studies have reported a lower unmyelinated to myelinated fibre proportion, as well as fewer sympathetic fibres, in the trigeminal nerves compared to spinal nerves (Sessle, 2000).

The neuronal composition of human trigeminal nerve was first investigated in un unbiased matter by Yang et al. (2022) using single nuclei RNA sequencing. A comparison of TG and DRG single nuclei datasets identifies the absence of proprioceptors (Pvalb+), as well as functionally uncharacterised Calca+/Dcn+ and Rxfp1+ clusters, in the TG; however, the clusters common to both DRG and TG exhibit a high correlation in terms of cell-type specific gene expression (Bhuiyan et al., 2023). This observation was in agreement with a previous transcriptome-wide study on mice, which identified only 24 differentially expressed genes between TG and DRG neurons (Lopes et al., 2017).

However, changes in translational regulation might result in more significant differences in the translatome and proteome of TG and DRG neurons that might underlie the differences in sensitisation susceptibility. Using translating ribosome affinity purification (TRAP) to compare the mRNA translation in Scn10a+ nociceptors in male and female mice, Megat et al. (2019) identified more differences in the translatome of nociceptors in DRG and TG than by using transcriptomic information only. Several pathways were differentially translated between the TG and DRG, including genes involved in mTOR, VEGF and FGF signalling (Megat et al., 2019).

Differences in the response to nerve injury of trigeminal afferents compared to spinal afferents have been identified (Robinson et al., 2004). Studies in the ferret have highlighted differences in the time-course of ectopic activity generation in injured trigeminal fibres, where damage to the inferior alveolar nerve result in an earlier peak of spontaneous activity, followed by a more accelerated decline in comparison to injuries to spinal nerves (Bongenhielm and Robinson, 1996), while

injury to the lingual nerve presented a late rise in spontaneous activity (Yates et al., 2000). Instead, following chronic constriction of the infraorbital nerve in the rat, trigeminal afferents were less likely to display spontaneous ectopic activity compared to spinal nerve constriction, attributed to the short distance between the site of injury and the trigeminal ganglion and the different embryological origin of trigeminal neurons (Tal and Devor, 1992). Additionally, differences in ion channel dysregulation were identified following injury to branches of the trigeminal nerve compared to the spinal system, particularly in the case of $Na_v1.3$ expression (Robinson et al., 2004, Davies et al., 2006).

Understanding the molecular and cellular features underlying the increased susceptibility to sensitisation of the trigeminal pathways to noxious stimulation might lead to the development of therapies that are particularly effective for orofacial pain. While studies have highlighted differences and similarities at the level of central projections, primary afferents subtypes' RNA and protein expression and response to nerve injury; differences in the transcriptional composition of the cells that support the axons at the periphery haven't been investigated yet. In Chapter 2, single nuclei RNA sequencing data of healthy and injured trigeminal nerves from human samples will be described, aiming to characterise the cellular composition of the structures that support trigeminal axons in human.

1.5.4 Lingual nerve injury

Lingual nerve injury may occur as a result of routine dental procedures including third molar removal, potentially leading to neuroma formation, loss of sensation and neuropathic pain (Atkins and Kyriakidou, 2021). The trigeminal nerve injury clinic at the Charles Clifford Dental Hospital in Sheffield, UK is a national NHS referral centre for patients with trigeminal nerve damage (Figure 1.6), primarily treating lingual and inferior alveolar nerve injuries. During lingual nerve repair surgery, the injured part of the nerve – the neuroma – is removed and processed for molecular and histological examination. The aim of this PhD project was to characterise the cellular and molecular landscape of lingual neuromas and identify changes linked with symptoms of pain. In the following paragraphs, an overview of the nature of the

lingual neuroma samples and the clinical outcomes of surgical nerve repair will be described.

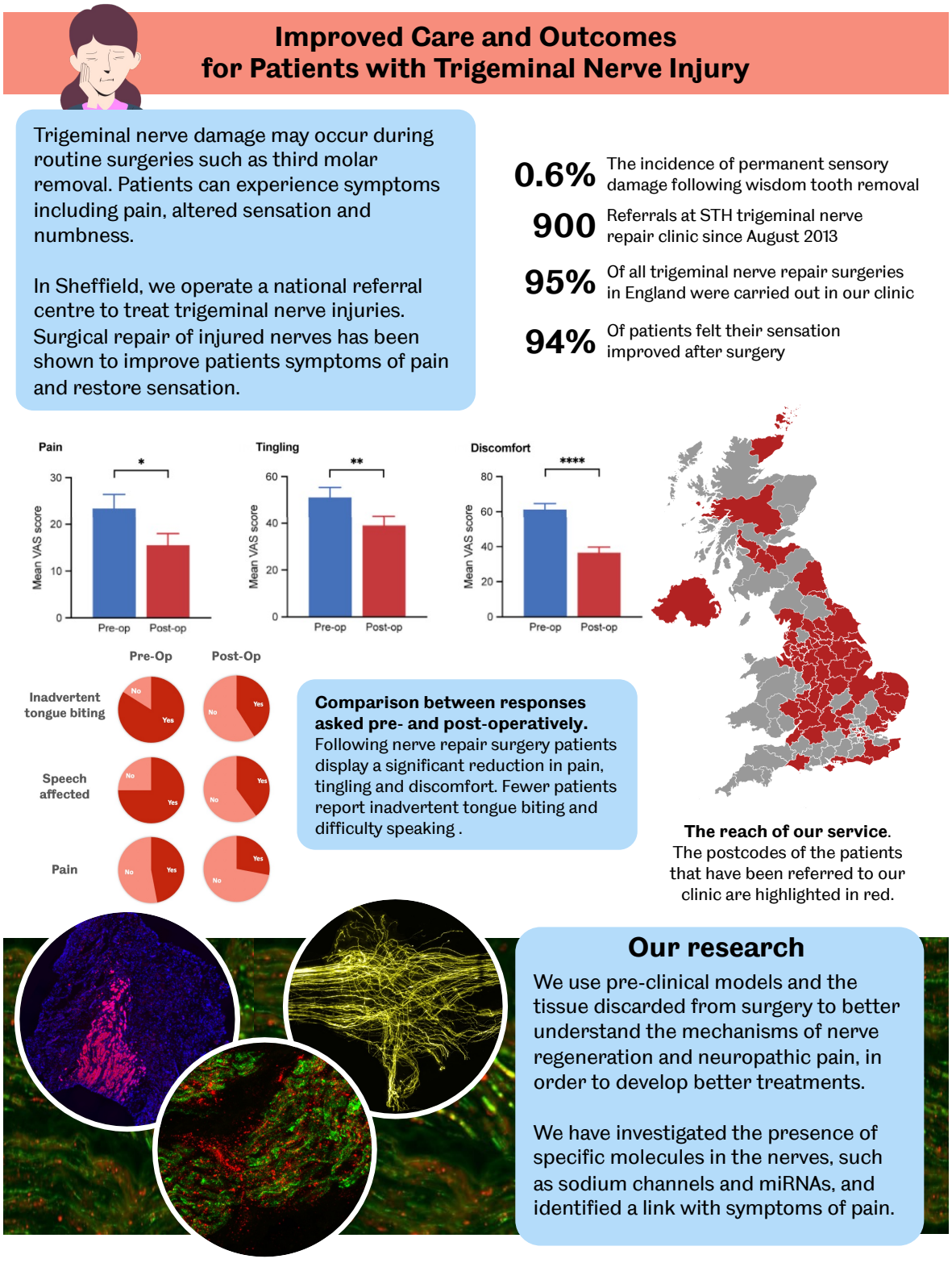

Figure 1.6 Outcomes for patients with trigeminal nerve injuries.
Infographic for the trigeminal nerve repair clinic displaying the clinical outcomes of trigeminal nerve repair surgery. The statistics on the reach of the service and the clinical outcomes of trigeminal nerve repair surgery were obtained from Atkins and Kyriakidou (2021).

1.5.4.1 Anatomy of the lingual nerve

The lingual nerve is a terminal branch of the posterior division of the mandibular nerve, its anatomy is shown in Figure 1.7. It enters the oral cavity between the lateral surface of the medial pterygoid muscle and the medial surface of the ramus of the mandible, and then passes anteriorly adjacent to the mandibular ramus, in close proximity to the third molar (Karakas et al., 2007). It innervates the anterior two thirds of the tongue, the floor of the mouth and lingual gingiva (Rodella et al., 2012).

The lingual nerve also transports special visceral afferent (SVA) and general visceral efferent (GVE) fibers from the chorda tympani, a branch of the facial nerve, which joins the lingual nerve below the skull, near the lower border of the lateral pterygoid muscle, and is responsible for taste perception in the anterior two-thirds of the tongue and for secretory and motor innervation of the sublingual and submandibular glands (Sittitavornwong et al., 2017). The lingual nerve also has anterior, middle, and posterior communicating branches with the hypoglossal nerve (Sittitavornwong et al., 2017).

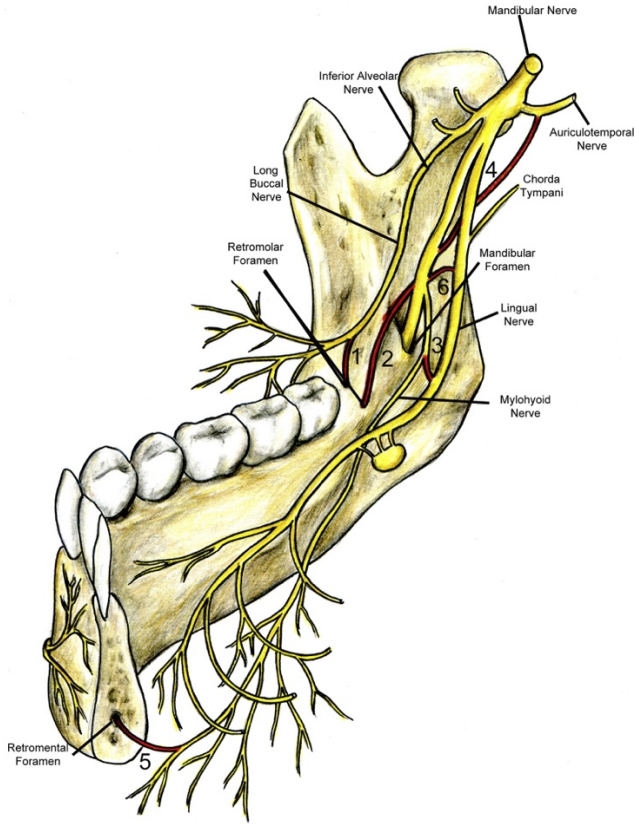

Figure 1.7 The branches of the mandibular nerve
The diagram displays the mandibular nerve and its branches, including the lingual nerve and the inferior alveolar nerve. Obtained with permission from Rodella et al. (2012).

1.5.4.2 Lingual nerve injury and repair

Damage to the lingual nerve may occur during dental procedures such as third molar extraction, mandibular trauma management, periodontal procedures and excision of neoplastic lesions (Rodella et al., 2012). The frequency of lingual nerve injuries during oral and maxillofacial procedures varies between 0.6-2%, resulting in anaesthesia, paraesthesia or hypesthesia of the anterior part of the tongue, potentially affecting taste (Queral-Godoy et al., 2006, Atkins and Kyriakidou, 2021, Robert et al., 2005). The use of lingual flap retractors during third molar removal surgery is associated with an increased risk of lingual nerve injury (Pichler and Beirne, 2001). Other preventative measures to reduce mandibular nerve injury include: pre-operative radiological examination with computed tomography (particularly to prevent IAN injury), the use of local anaesthesia over general anaesthesia, a well-designed mucoperiosteal flap preferably on the buccal side, conservative osteotomy and tooth sectioning (La Monaca et al., 2017).

Nevertheless, the lingual nerve can still be injured resulting in sensory deficits which include lost or altered sensation, reduced or altered taste, impaired speech, inadvertent tongue biting, tingling, discomfort and neuropathic pain, often described as a burning sensation (Atkins and Kyriakidou, 2021). The symptoms may be temporary, but if they don't resolve within three months they are deemed unlikely to resolve spontaneously (Atkins and Kyriakidou, 2021). The diagram in Figure 1.8 displays the suggested clinical management of suspected lingual nerve injury during third molar removal (Atkins and Kyriakidou, 2021).

Lingual nerve repair surgery promotes functional recovery of sensation and reduction of pain, tingling and discomfort VAS scores, as well as a reduction in accidental tongue biting and improvement in taste perception and speech (Atkins and Kyriakidou, 2021, Fujita et al., 2019). Several methods can be used for nerve repair: end-end anastomosis is the most common method, involving microsurgical suturing of the two nerve ends; nerve autograft consists in the insertion of a healthy donor nerve (commonly the sural nerve) to bridge a large injury gap (Poppler et al., 2015, Miloro et al., 2015); and finally, nerve allograft, where the donor nerve is obtained from cadaveric tissue requiring temporary immunosuppression, until the nerve regenerates fully (Myckatyn and Mackinnon, 2004).

Surgical nerve repair involves the resection of the injured part of the nerve, identified as the neuroma, which can present as a swollen neuroma-in-continuity or as a nerve stump completely separated from its distal counterpart (Atkins and Kyriakidou, 2021).

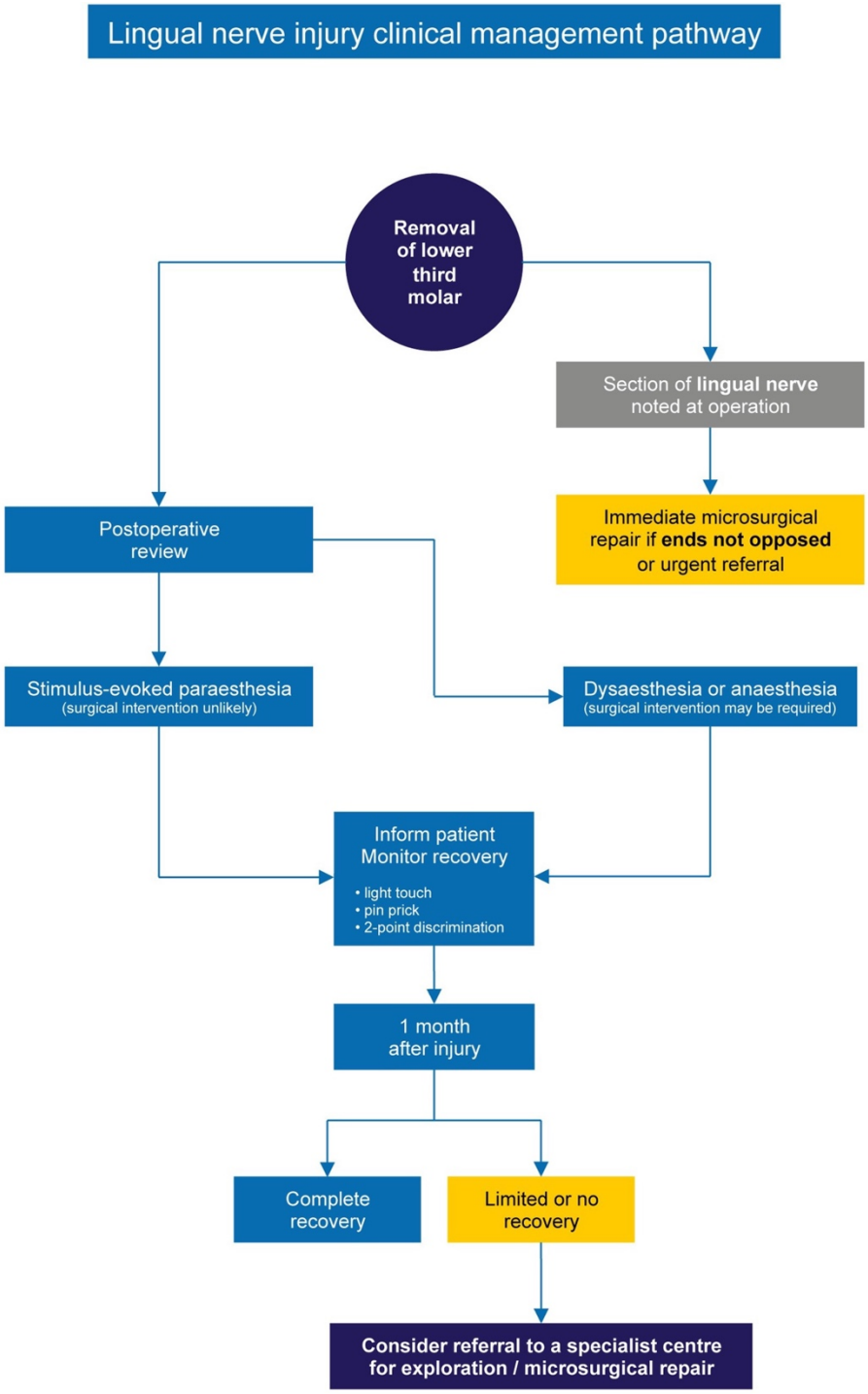

Figure 1.8 Suggested clinical management pathway for lingual nerve injury
The diagram displays the suggested management pathway following third molar extraction to prevent permanent sensory disturbances as a result of lingual nerve injury. Obtained with permission from Atkins and Kyriakidou (2021)

1.6 Overview and aims

As highlighted in the literature review, neuropathic pain is a complex disease involving both peripheral and central mechanisms. Whilst animal models have been used extensively to characterise these mechanisms, validation in humans is difficult due to the lack of accessibility of human clinically relevant samples.

Injuries to branches of the trigeminal nerve, including the lingual nerve, are treated in the trigeminal nerve repair clinic at the Charles Clifford Dental Hospital. Surgical resection of lingual neuromas and nerve repair promote functional recovery of sensation (Atkins and Kyriakidou, 2021). The resected neuromas are collected in the laboratory with linked clinical information, including the patient reported VAS scores on pain, tingling and discomfort, and used for molecular and histological investigation.

The work presented in this thesis aims to characterise the cellular and transcriptional composition of healthy and injured human trigeminal nerves and identify molecular changes in human lingual neuromas linked with the symptoms of pain. Spatial and single nuclei RNA sequencing were used to profile the expression of ~18,000 genes at single cell level within the morphological context. Validation of selected targets was performed with RNAscope and immunohistochemistry. The characterisation of the cellular and molecular landscape of healthy and injured peripheral nerves will contribute to the identification of mechanisms underlying peripheral sensitisation leading to neuropathic pain, as well as provide new targets for novel analgesics development.

The specific aims of this project are described as follows.

Aim 1: Characterise the cellular and transcriptional composition of healthy and injured trigeminal nerves with single-nuclei RNA sequencing (Chapter 2)

In order to characterise the cellular heterogeneity in human lingual neuromas, single nuclei RNA sequencing was performed on human lingual neuromas (n=2) and healthy trigeminal nerve roots (n=2, obtained from organ donors from the Netherland Brain Bank). The cellular composition of peripheral nerves has been investigated in rodents in both healthy and injured states (Yim et al., 2022, Lovatt et al., 2022, Chen et al., 2021) and in human sural nerves using a small number of

nuclei (Chau et al., 2022). Here, we aimed to profile for the first time the transcriptional and cellular composition at single cell level on human trigeminal nerves in healthy and injured samples, linked with clinical information. The dataset generated as part of this aim is of interest to various fields, including nerve regeneration, neuropathic and orofacial pain.

Aim 2: Identify potential cell-cell interactions between cells in the periphery and trigeminal neurons in healthy and injured nerves (Chapter 2)

The communication between axons and cells at the periphery is crucial to their homeostasis and, following nerve damage, it enables the axons to regenerate by activating mechanisms of Wallerian degeneration and repair that underlie successful reinnervation of their end-targets. These interactions, while beneficial to nerve regeneration, may also lead to maladaptive changes leading to hyperexcitability and neuropathic pain generation.

Using the transcriptomic dataset of injured and healthy trigeminal nerves generated in Aim 1 and publicly available data from human trigeminal ganglia (trigeminal ganglia cell atlas, Yang et al., 2022), the potential cell-cell communication taking place between the cells supporting the neurons at the periphery and trigeminal neurons in both healthy and injured conditions was investigated *in silico*, using the publicly available R package CellChat.

Aim 3: Investigate the spatial distribution of the genes expressed in human neuromas with spatial transcriptomics (Chapter 3)

Human lingual neuromas are characterised by a heterogenous cellular composition due to the presence of several tissue types, mainly scar tissue and nerve fascicles, but also muscle tissue due to the anatomical proximity of the lingual nerve to several muscle groups. In order to identify the spatial organisation of the transcripts and cell-types detected, spatial transcriptomics was used, in combination with the snRNA-seq dataset generated in Aim 1, in samples of human neuromas with and without pain. The aim of this work was to characterise the transcriptional landscape within the morphological context of human lingual neuromas.

Aim 4: Identify differentially expressed genes in the nerve fascicles of painful and non-painful neuromas (Chapter 3)

Differential gene expression analysis in painful and non-painful neuromas was performed in order to identify novel genes linked with the presence of neuropathic pain. The heterogeneous cellular architecture of the neuromas, which includes scar tissue, muscle tissue and nerve fascicles, makes the use of bulk RNA sequencing challenging for this aim. The cells and genes in close proximity to the nerve fibres are more likely to sensitise the axons producing a state of hyperexcitability, leading to neuropathic pain, while adjacent tissues such as scar and muscle tissue are less likely to interact with the axons to produce sensitisation.

In order to identify changes in gene expression from the cells within the nerve fascicles, including Schwann cells, endothelial cells, immune cells, endoneurial and perineurial fibroblasts; the spatial transcriptomics dataset was subset to include only the areas overlying nerve fascicles, manually selected based on haematoxylin & eosin staining. Pseudo-bulk differential expression analysis was performed to identify changes in gene expression between painful and non-painful samples only in areas containing nerve fascicles.

Aim 5: Validate the single cell and spatial transcriptomics data with RNAscope and immunohistochemistry (Chapter 4)

Several targets relevant to neuropathic pain generation and maintenance, involved in signal transduction and conduction (SCN9A, SCN10A, TRPV1), Schwann cell differentiation (SOX10), prostaglandin signalling (PTGDS) and inflammation (OSM, CD68), were investigated using RNAscope to validate the spatial and snRNA sequencing data and further identify with higher spatial resolution their patterns of expression. Additionally, perineurial cell markers (GLUT-1, NGFR) were investigated with immunohistochemistry to validate their co-expression at the protein level.

Aim 6: Investigate the potential correlation between PI16 protein expression and symptoms of pain in human neuromas (Chapter 4)

PI16 was recently identified to be secreted by perineurial fibroblasts in rats and contribute to neuropathic pain development (Singhmar et al., 2020, Garrity et al.,

2023). The data generated from Aim 1 and Aim 3 highlighted PI16 expression in the human neuromas, particularly in cells classified as endoneurial fibroblasts. This part of the project aimed to validate PI16 expression at the protein level in the human neuromas and investigate a potential correlation with symptoms of pain.

Chapter 2. Characterising the cellular landscape of uninjured trigeminal nerves and human lingual nerve neuromas

2.1 Introduction

In this chapter, the cellular and transcriptional composition of trigeminal nerve roots and human lingual neuromas will be characterised using single nuclei RNA sequencing. Furtherly, the potential communication between the cell types at the periphery and trigeminal neurons will be computationally inferred using CellChat, using the dataset generated by Yang et al. (2022) from human trigeminal ganglia.

The analysis of single nuclei RNA sequencing data generated from trigeminal nerves presented the challenge of identifying suitable markers for cell-type annotation. In this introduction, a summary of the body of literature on peripheral nerves' cellular composition will be described, including recent studies attempting to perform an unbiased characterisation of cellular composition and markers using single cell/nuclei RNA sequencing in both rodents and human.

2.1.1 Structure of peripheral nerves

Peripheral nerves contain the axons of sensory, motor and autonomic neurons, providing a nourishing environment, where axons are protected from injury and regeneration is supported in the event of damage. Peripheral nerves are characterised by a fascicular organization with different protecting layers (Figure 2.1). The axons, which can be myelinated by Schwann cells or sheathed by non-myelinating Schwann cells (also called Remak cells), are grouped within the endoneurium, where they are physically supported by endoneurial fibroblasts-derived collagen fibres and nourished by endoneurial blood vessels (Sunderland, 1990). The endoneurium is surrounded by the perineurium, a protective layer made up of specialised fibroblasts sealed by tight junctions, which absorbs external stretching and compressing forces and acts as a diffusion barrier to prevent the exposure of the endoneurial environment to pathogens, toxins and changes in ionic or pH composition (Iwanaga et al., 2022). The perineurium together with endoneurial blood vessels forms the blood-nerve barrier, a continuation in peripheral nerves of

the blood-brain barrier (Iwanaga et al., 2022). Finally, multiple fascicles are grouped and cushioned by the epineurium, composed of fibroblasts, blood vessels and occasional clusters of adipocytes (Weerasuriya and Mizisin, 2011).

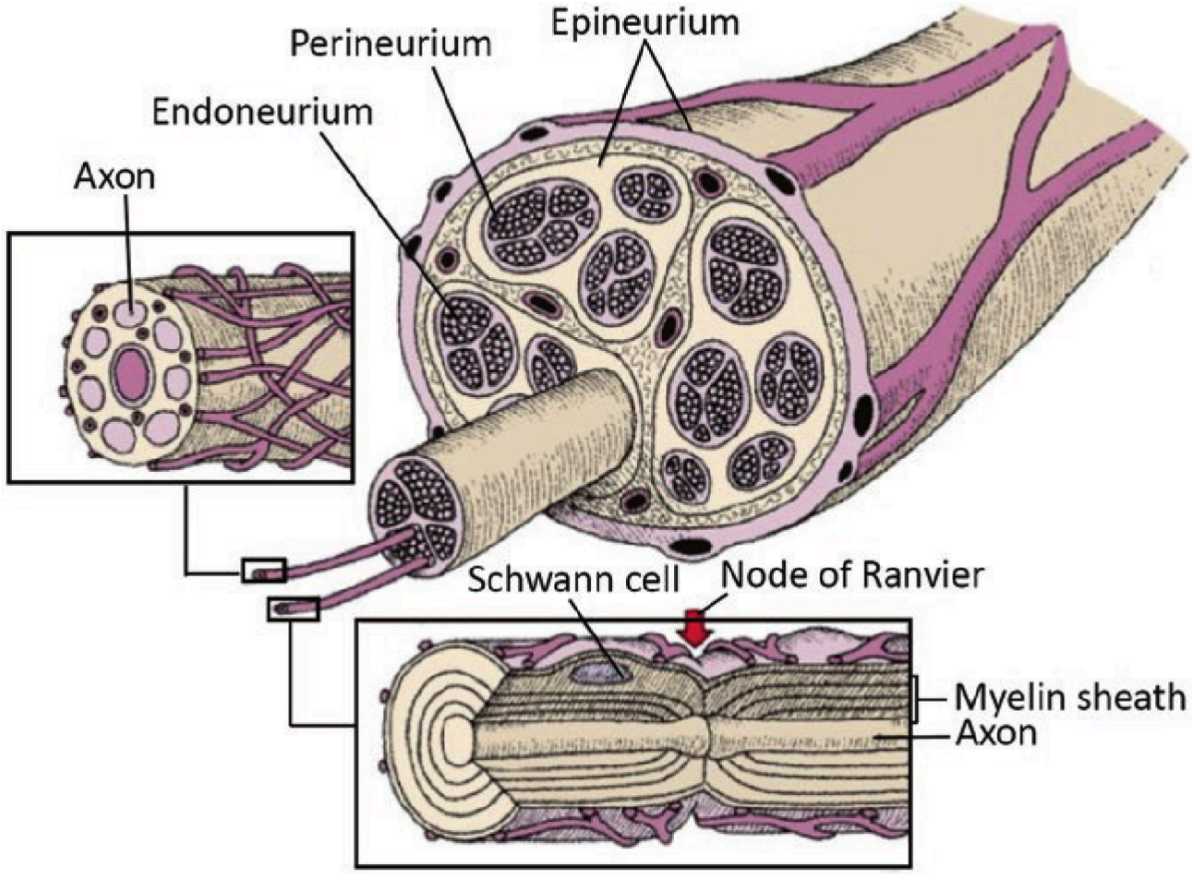

Figure 2.1 Structure of a peripheral nerve.
The diagram displays the cross section of a peripheral nerve, highlighting its anatomical structure. Axons are enwrapped by myelin sheaths or Remak cells, and grouped in the endoneurium, which is surrounded by a perineurial sheath, forming the perineurium. Multiple nerve fascicles are grouped in the endoneurium. Image obtained with permission from Pope and Deer (2017).

2.1.2 The cell types that populate peripheral nerves

Historically, much of the structural and cellular characterization of peripheral nerves has been performed using electron microscopy and immunohistochemistry; more recently, advances in single cell transcriptomics have led to the unbiased characterization of the cellular populations found in nerves (Zhao et al., 2023). A handful of single cell studies have been performed in murine nerves, including in naïve, developing and injured states (Chen et al., 2021, Carr et al., 2019, Toma et al., 2020, Yim et al., 2022, Wolbert et al., 2020, Gerber et al., 2021), one study on rat

naïve and injured sciatic nerves (Lovatt et al., 2022) and one on injured human sural nerves (Chau et al., 2022).

Carr et al. (2019), Wolbert et al. (2020) and Toma et al. (2020) paved the way in the identification of the cellular composition of murine sciatic nerves in health and injury. Some inaccuracies in the annotation of cell types prompted Chen et al. (2021) to combine and reanalyse their datasets, establishing markers for various peripheral cell types and identifying changes in the sciatic nerve at 3 and 9 days following sciatic nerve resection. Gerber et al. (2021) focused on Schwann cells phenotypes in development and created a single-cell atlas of murine sciatic nerve at early and mature developmental stages. A challenge encountered in the aforementioned studies is the underrepresentation of myelinating Schwann cells (mSCs) compared to what is reported in the literature from histological studies, caused by the difficulty in the isolation of mSCs due to their large shape and long processes (Yim et al., 2022, Chen et al., 2021). Yim et al. (2022) performed an elegant study to circumvent this issue: by using ActB-Sun1 and Mpz-Sun1 mice, which display GFP expression in cells where the ubiquitously expressed gene ActB or myelination-specific gene Mpz was active at any point of development, they could purify nuclei from all the cells in the nerve or exclusively from cells that expressed Mpz. This resulted in the precise characterization of the sciatic nerve cellular composition, which was then compared to that of the peroneal, sural and vagus nerve, along a detailed Schwann cell atlas to identify several previously uncharacterised subtypes of mSCs and nmSCs (Yim et al., 2022). For example, a Schwann cell subtype marked by Pmp2 was shown to preferentially myelinate motor neurons, whilst Pmp2 expression was shown to be reduced in ALS mouse models and patient samples (Yim et al., 2022).

While previous studies had been performed in mice, Lovatt et al. (2022) performed single nuclei RNA sequencing of the peripheral sciatic nerves of rat in the naïve state and at 3, 12 and 60 days following nerve constriction. Finally, Chau et al. (2022) performed single nuclei RNA sequencing on human sural nerves two weeks following nerve transection, obtained as part of a clinical trial for a new treatment for Parkinson’s disease.

These datasets provide a great wealth of information on the cellular composition and potential cell-cell interactions within peripheral nerves, and how these are altered during development and injury. A major challenge when analysing this type of data lies in the correct annotation of cell types, where markers might not be reliable across all conditions or species. An example is Ngfr, commonly used as a repair Schwann cell marker, which led Wolbert et al. (2020) to incorrectly annotate an endoneurial fibroblast cluster as nmSCs, suggesting that other SCs markers could be Smoc2 and Apod, while in fact, Ngfr is also expressed in NG2+ cells in mice that can be classified as endoneurial fibroblasts (Chen et al., 2021, Stierli et al., 2018). In Chau et al. (2022), NGFR and SLC2A1, a marker for perineurial cells (Piña et al., 2015), were co-expressed in a cluster which was classified as heterogeneous, containing both perineurial and repair Schwann cells. However, evidence of NGFR expression in the perineurium of rats and human nerves has been reported (Wyatt et al., 1990, Yamamoto et al., 1992), hinting to the possibility that the $NGFR^{+}$ $SLC2A1^{+}$ cluster should be identified as purely perineurial.

In the following paragraphs, the cell types that make up peripheral nerves and their markers will be described to set the scene for the cellular populations expected to be identified in the trigeminal injured and healthy nerve samples sequenced and analysed in this thesis.

2.1.2.1 The endoneurial environment

Early investigations of the contents of the endoneurium were performed by Causey and Barton (1959), identifying the high prevalence of Schwann cells, as well as the presence of endothelial cells and other uncharacterised cell types, which were later identified as endoneurial fibroblasts and macrophages (Arvidson, 1977, Gamble and Eames, 1964).

Schwann cells are highly plastic cells able to transition across various phenotypes during development or following injury. Schwann cell subtypes in adult mice have been characterised in depth by Yim et al. (2022), who showed that SCs in the sciatic nerve make up 45% of the cells. Of these, 26% were identified as non-myelinating (marked by Ncam1, Slc35f, Scn7a and Csmd1 expression) and 73% were annotated as myelinating (Prx, Qk and Mbp expression). Gerber et al. (2021) provides further in-depth characterization of Schwann cells across development,

identifying an immature phenotype found between E13.5 and P14 ($Ngfr^+$/$Ncam1^+$/$L1cam^+$) and a pro-myelinating subtype ($Pou3f1^+$/$Cdkn1c^+$) found at P1 to P5.

Schwann cells' response to injury has been characterised by Lovatt et al. (2022) in rat sciatic nerves at various timepoints following CCI, reporting an increase in Sox10+ nuclei, peaking at day 12 with a reduction to baseline by day 60. In human nerves the sox10+ nuclei expansion occurs at a different timescale, with a peak at 90-100 days following injury returning to baseline after 200 days (Wilcox et al., 2020). Sox10 is involved in SCs specification from neural crest progenitors, its expression is sustained in the adult nerve and is suitable as a pan-SC marker (Liu et al., 2015). Following injury there is a change in the proportion of SCs subtypes: in the naïve state, myelinating and non-myelinating SCs make up 94% of Schwann cells, while less than 1% are marked as dividing ($Top2a^+$/$Cdk1^+$/$Mki67^+$); then, at day 3 post-CCI, the dividing SC cluster increases to 20%, and the repair phenotype ($Ngfr^+$/$Erbb3^+$/$Sox2^+$) emerges, making up 18% of the SCs, which is then reduced to 3% 60 days following injury (Lovatt et al., 2022).

Another cell type sparsely found in the endoneurium consists in endoneurial fibroblasts (EFs), who share a common developmental lineage with Schwann cells, as both are derived from neural crest stem cells (Joseph et al., 2004), although a small amount of bone marrow-derived EFs has been identified in pathogenic conditions (Mäurer et al., 2003). In rat and human nerves they can be identified by the expression of P4HB, important in collagen deposition, as well as NG2 and CD34 (Richard et al., 2014). EFs' function involves collagen synthesis, phagocytosis, immune surveillance and cytokine production, and, although their role following nerve injury hasn't been extensively characterised, they are thought to contribute to axon guidance for target reinnervation (Richard et al., 2012).

Finally, endoneurial macrophages make up 2-9% of the healthy sciatic nerve population (Griffin et al., 1993). The distinction between nerve resident macrophages and monocyte-derived macrophages has been a challenge due to the lack of specific markers (Mueller et al., 2001). Advances in genetic manipulations allowed the identification of endoneurial macrophages markers in mice including Cx3cr1, Csf1r and Trem2 (Wang et al., 2020). Ydens et al. (2020) identified

Relmα^{+}/Mg11^{+} and Relmα^{-}/Mg11^{-} macrophages as resident epineurial and endoneurial macrophages, respectively, and identified their distinct response to nerve injury: endoneurial macrophages activate the transcription of early response genes such as Atf3, Fos, Jun or Ler2 and produce monocyte chemoattractants, while epineurial macrophages do not significantly respond to nerve injury (Ydens et al., 2020). Resident macrophages can have both pro-nociceptive and anti-nociceptive roles in the endoneurial environment (Domoto et al., 2021).

2.1.2.2 The blood-nerve barrier

The blood-nerve barrier (BNB), also known as the blood-nerve interface (BNI), is composed of the endoneurial microvessels and the perineurium (Weerasuriya and Mizisin, 2011).

Endoneurial microvessels are made up by pericytes and endothelial cells, which are joined by tight junctions without fenestrations and in direct contact with circulating blood. Endoneurial endothelial cells can be identified with common endothelial markers (Egfl7, Pecam1, Tie1) in addition to the expression of Lrg1 and Icam1 to distinguish them from lymphatic and epineurial endothelial cells, while pericytes can be identified by the expression of Acta2 and Pdgfrb (Chen et al., 2021).

The perineurium surrounds each endoneurial compartment and is composed of concentric layers (up to 15 in large fascicles) of perineurial cells, which are flattened cells with fibroblast origin (Weerasuriya and Mizisin, 2011). GLUT-1, encoded by SLC2A1, has been suggested as the best marker for perineurial cells (Piña et al., 2015).

The increased permeability of the BNB, also termed as BNB breakdown, plays a role in several neuropathies such as Guillen-Barré Syndrome and diabetic peripheral neuropathy (Weerasuriya and Mizisin, 2011). Changes in endoneurial blood vessels have been reported in the sural nerves of patients with diabetes mellitus, including reduplication of the basement membrane and pericyte degeneration (Giannini and Dyck, 1994). Endoneurial hypoxia was observed in nerve injury-induced painful neuropathy and might be caused by structural changes, including endothelial cells hypertrophy and enlargement of the basement membrane, as well as perineurial

fibrosis, which might restrict oxygen access to the highly metabolically demanding regenerating neurons (Lim et al., 2015).

2.1.2.3 The epineurium

The epineurium consists of collagenous ECM which also contains arteries, arterioles, venules and veins that are collectively named epineurial macrovessels, as well as lymphatic vessels and occasional adipocyte clusters (Sunderland, 1990). The cell types identified in this anatomical structure from single cell studies include epineurial fibroblasts (Sfrp2^{+} and Pcolce2^{+}), epineurial macrophages (Retnla^{+} and Clec10a^{+}), lymphatic endothelial cells (Lyve1^{+} and Prox1^{+}), adipocytes and cells involved in vasculature: vascular smooth muscle cells (Des^{+}, Tpm2^{+}, Myh11^{+}, Acta2^{+}) and pericytes (Rgs5^{+}, Kcnj8^{+}, and Pdgfrb^{+}), which are collectively known as mural cells, and epineurial endothelial cells (Sox17^{+}, Spock2^{+}, and Rgcc^{+}) (Chen et al., 2021, Lovatt et al., 2022).

2.1.2.4 Immune cells

Non-resident immune cells infiltrate the nerve following insult or injury, facilitated by the breakdown of the BNB (Weerasuriya and Mizisin, 2011). Firstly, the innate immune system, involving neutrophils, macrophages, mast cells and dendritic cells, comes into action (Totsch and Sorge, 2017). Neutrophils (Csf3r^{+}) transiently infiltrate the damaged nerves following injury and contribute to myelin removal during Wallerian degeneration (Lindborg et al., 2017). Chemoattractants released by Schwann cells, neutrophils and resident macrophages recruit monocyte-derived macrophages at the site of injury (Metzemaekers et al., 2020). Dendritic cells are detected in human sural nerve biopsies in the perineurial and epineurial space of both control and chronic inflammatory demyelinating polyradiculoneuropathy (CIPD) patients (Press et al., 2005). Mast cells are found in proximity to peripheral sensory nerve endings and have a role in pruritus and inflammation through the secretion of histamine and substance P (Nakashima et al., 2019).

Following the induction of the innate immune system, the adaptive immune system is activated, involving T and B lymphocytes (Totsch and Sorge, 2017). T-cells infiltrate both the epineurium and endoneurium of injured nerves and have been detected starting from 3 days following injury in rodents, while natural killer

(NK) cells have been shown to infiltrate to a larger degree in the epineurium (Lovatt et al., 2022, Tang et al., 2022).

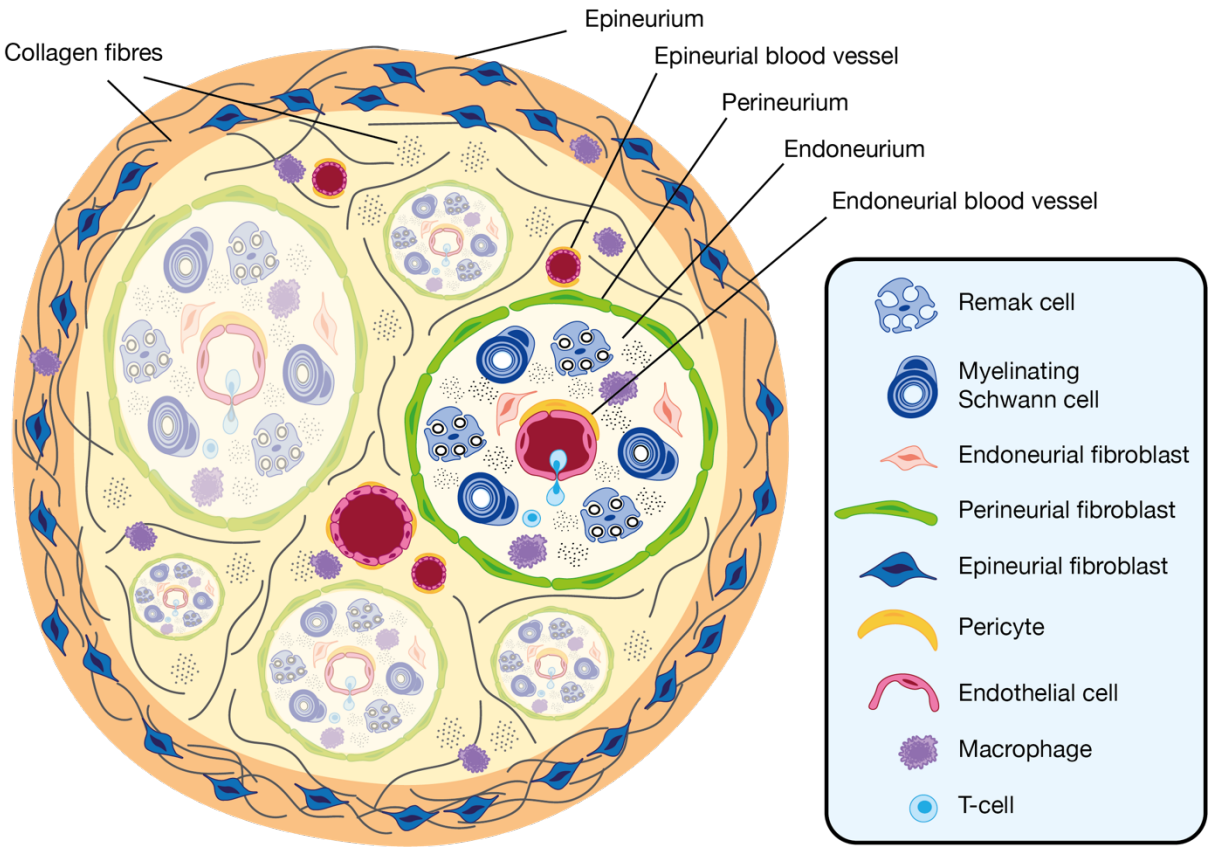

Figure 2.2 Cell types found in peripheral nerves.
Diagram showing the cell types found in the structural components of peripheral nerves. The epineurium is made up of epineurial fibroblasts and an extensive network of collagen fibres, as well as epineurial blood vessels which contains both vascular smooth muscle cells, epithelial cells and pericytes, and epineurial resident macrophages. The perineurium is mainly composed of perineurial fibroblasts. The endoneurium contains axons associated with both myelinating and non-myelinating (Remak) Schwann cells, as well as endoneurial blood vessels, macrophages and fibroblasts. T-cells and other immune cells can infiltrate in the endoneurial and epineurial space due to the breakdown of the BNB following injury and inflammation.

2.1.3 Summary and Experimental Design

Peripheral nerves display extensive cellular heterogeneity that varies according to the state (naïve, developing or injured), anatomical location and neuronal composition (sensory, motor or autonomic). The interactions between peripheral cell types and the axons play a role in nerve injury, repair and neuropathic pain development.

As part of this project, which aimed to characterise the transcriptional changes in human lingual neuromas linked with neuropathic pain, single nuclei RNA sequencing was performed in two samples of human lingual neuromas, in order to characterise the cell-types present at the site of injury. Two samples of trigeminal nerve roots from the Netherland Brain Bank were obtained from healthy organ donors in order to compare the cellular composition of the nerve injury-induced lingual neuromas to healthy trigeminal nerves. The anatomical origin of the samples are displayed in Figure 2.3.

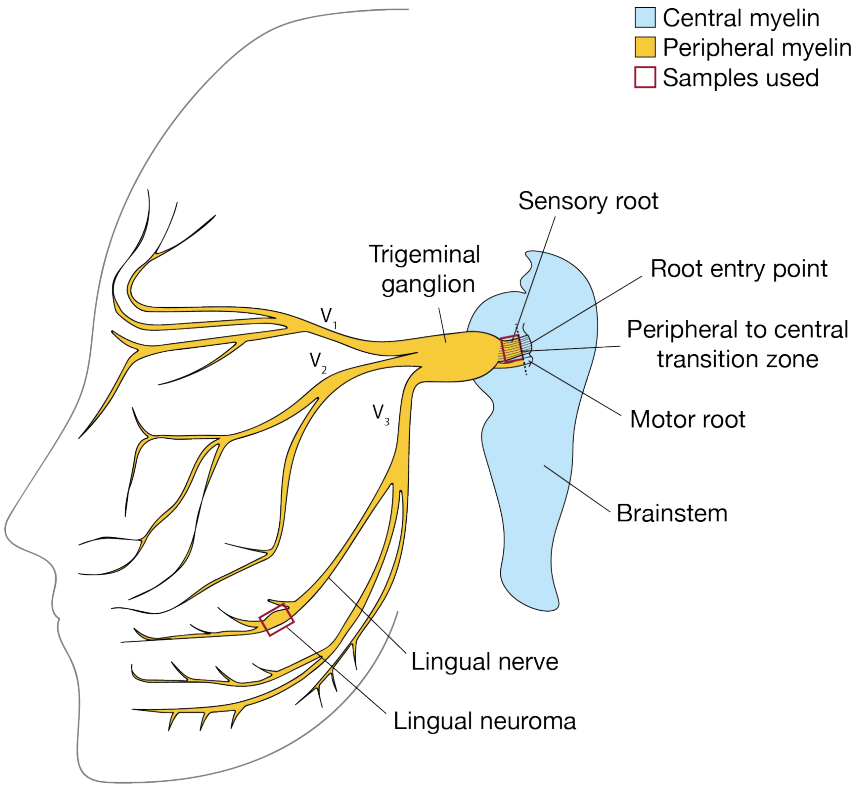

Figure 2.3 The anatomical origin of the samples used for single nuclei RNA sequencing. The diagram illustrates the trigeminal nerve as well as its sensory and motor root, and its entry point in the pons. In yellow, areas where myelin is peripheral in nature, i.e. deposited by Schwann cells, is shown; while in blue, areas where myelin is deposited by central glial cells (oligodendrocytes) is marked. The transition zone is indicated by a dashed line. The samples used for snRNAseq are outlined by red squares and identify a lingual neuroma from the lingual nerve and the distal portion of the sensory root.

The trigeminal nerve root is located between the trigeminal ganglia and the root entry point of the nerve in the pons (Peker et al., 2006). It was deemed as a suitable healthy control since both nerve segments are innervated by neurons whose soma resides in the trigeminal ganglia. It must be noted however, that the different

anatomical origin of these samples can result in differences in the cellular composition. The trigeminal nerve root is located proximally to the trigeminal ganglia and contains the peripheral to central transition zone where peripheral myelin is replaced by central myelin, deposited by oligodendrocytes (Peker et al., 2006). In the samples used, there was minimal detection of central glial cells (astrocytes and oligodendrocytes), indicating that the major part of the nerve roots used were from the most distal portion of the root and were peripheral in nature, enabling the comparison with the lingual neuromas.

The cell types present in the lingual neuromas and trigeminal nerve roots were characterised, and their transcriptional profile across conditions was compared. Finally, the potential cell-cell interaction between the cell types identified at the periphery and human trigeminal neurons, whose transcriptomic signature was obtained from Yang et al. (2022), was inferred using the publicly available R package CellChat.

2.2 Methods

2.2.1 Human Lingual Neuromas

Lingual neuromas were obtained from patients attending the trigeminal nerve injury clinic at the Charles Clifford Dental Hospital, Sheffield, UK. Neuromas were collected during nerve repair surgery, carried out by Dr. Simon Atkins. All neuromas were collected with the informed consent from the patients, in accordance with ethical approvals received by the NHS Health Research Authority (HRA) and Sheffield Teaching Hospitals (STH) (19/SC/0308 STH20664). Clinical information including patients' age, sex and pain history was recorded preoperatively and anonymised.

The samples intended for single nuclei RNA sequencing were immediately placed in cryovials following surgical removal, flash frozen in liquid nitrogen and stored at -80°C for shipment on dry ice to the University of Texas at Dallas (Richardson, TX), where they were further processed.

2.2.2 Human Trigeminal Nerve Samples

Trigeminal nerve samples were obtained from The Netherlands Brain Bank, Netherlands Institute for Neuroscience, Amsterdam (NBB). All material has been collected from donors for or from whom a written informed consent for a brain autopsy and the use of the material and clinical information for research purposes had been obtained by the NBB.

2.2.3 Nuclei isolation

Nuclei isolation was kindly performed by Dr Ishwarya Sankaranarayanan and Dr Diana Tavares Ferreira. On the day of isolation, utensils including forceps, scissors and Dounce homogenizers were sterilised and pre-chilled. Surfaces were cleaned with 70% ethanol followed by RNase Zap. Nuclei isolation media (0.25 M sucrose, 150 mM KCl, 5 mM MgCl2, 1 M Tris Buffer pH 8.0) was prepared in advance. Homogenization buffer was made freshly on the day by supplementing the nuclei isolation media with 0.1 mM DTT, cOmplete protease inhibitor, 0.1% Triton-X and 0.2 U/µL RNA inhibitor. Wash buffer was made freshly on the day by supplementing the nuclei isolation media with 1% BSA and 0.2 U/µL RNA inhibitor. The procedure was performed on ice, using low retention pipette tips and soft touch pipettes to prevent nuclei disruption and maximise recovery.

Briefly, the tissue was chopped up into smaller pieces (<1 mm) using sterile scissors in 2 mL of homogenization buffer on ice. Up to four samples were processed in parallel. The homogenate was transferred using a wide bore pipette tip to a glass Dounce homogenizer, further homogenized with a pestle for 15 strokes and left to incubate for up to 2 minutes on ice. The homogenate was filtered through a 70 µm strainer and centrifuged at 800 x g for 7 minutes. The supernatant was discarded, the nuclei were resuspended in wash buffer, centrifuged again, and resuspended in 1 mL 4% formaldehyde fixative solution and fixation buffer (10X Genomics, PN 2000517). A small aliquot of the sample was used to count the nuclei using trypan blue staining and assess their integrity and the presence of debris and clumping.

2.2.4 Single nuclei RNA sequencing

The samples were prepared for single nuclei RNA-sequencing with the Chromium Single Cell Fixed RNA Profiling for Multiplexed Samples kit (10X Genomics, PN-1000456) by Dr Diana Tavares Ferreira and Dr Ishwarya Sankaranarayanan according to the manufacturer's instructions. The protocol is summarised in Figure 2.1. Following overnight fixation (16-17 h), the nuclei from each sample were hybridized with barcoded probes targeting the whole human transcriptome. Two barcodes were used for each sample to recover a higher number of nuclei. The samples were then combined and loaded in the microfluidic chip. In the chip, the nuclei are partitioned into droplets containing gel beads. By loading the optimal dilution of nuclei suspension, a total of 8,000 nuclei per barcode were targeted, aiming to recover 16,000 nuclei per sample. Following the Gel Beads-in Emulsion (GEM) generation, the left-hand and right-hand probes were ligated and the barcoded primers on the gel bead were hybridized to the probes. The probes were extended to include the unique molecular identifier (UMI), the 10x GEM barcode and a partial TruSeq 1 sequence for Illumina sequencing. Library preparation and sequencing was performed by the Genome Center at the University of Texas at Dallas. Libraries were quality controlled by verifying optimal size using the High Sensitivity DNA Agilent Bioanalyzer kit and sequenced on an Illumina Nextseq 2000.

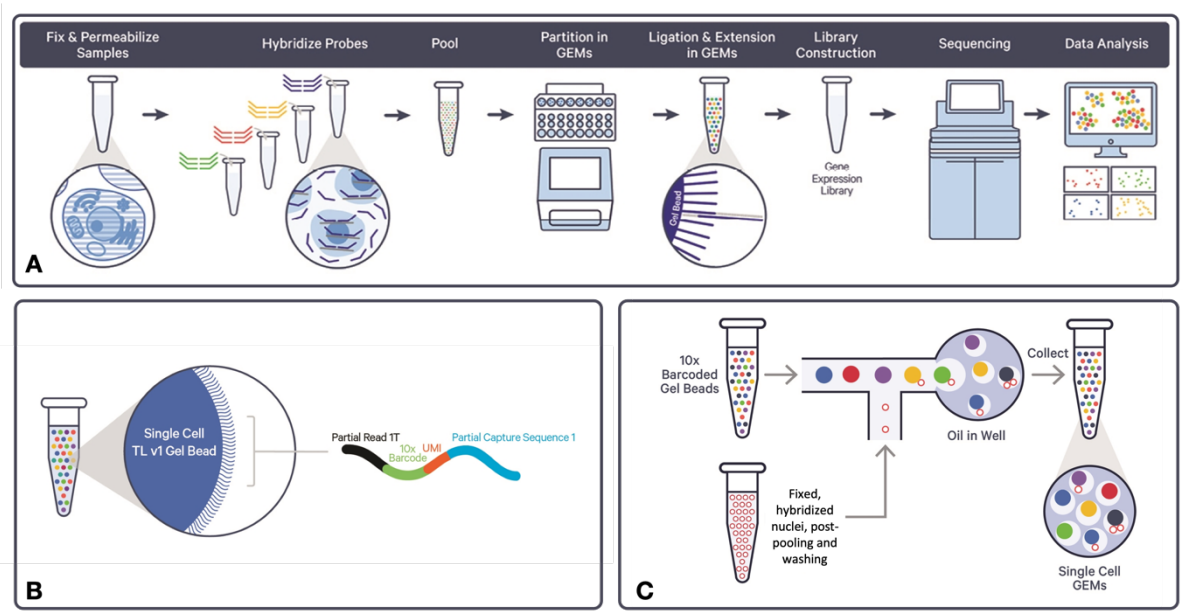

Figure 2.4. Experimental overview of single cell/nuclei RNA sequencing experiments.
The diagram illustrates the protocol for single nuclei RNA sequencing (A), the composition of the Gel Beads-in-emulsion (GEMs) (B) and how the nuclei are incorporated in oil droplets containing GEMs

in the microfluidic wells of the Chromium X controller, allowing the capture and barcoding of the probes hybridised to the transcripts expressed in individual nuclei within the partitioned cells. Image provided by 10X Genomics.

2.2.5 Data analysis

The reads were demultiplexed, converted to fastq files, aligned to the human genome reference GRCh38 and counted using the Cellranger software provided by 10X Genomics. The workflow used to analyse the data is illustrated in Figure 2.5. Analysing single nuclei RNA sequencing datasets presents a variety of challenges resulting from the experimental protocol, including the presence of ambient RNA and doublets, which can have a significant impact on the quality of the data and the ability to annotate cell types (Figure 2.6).

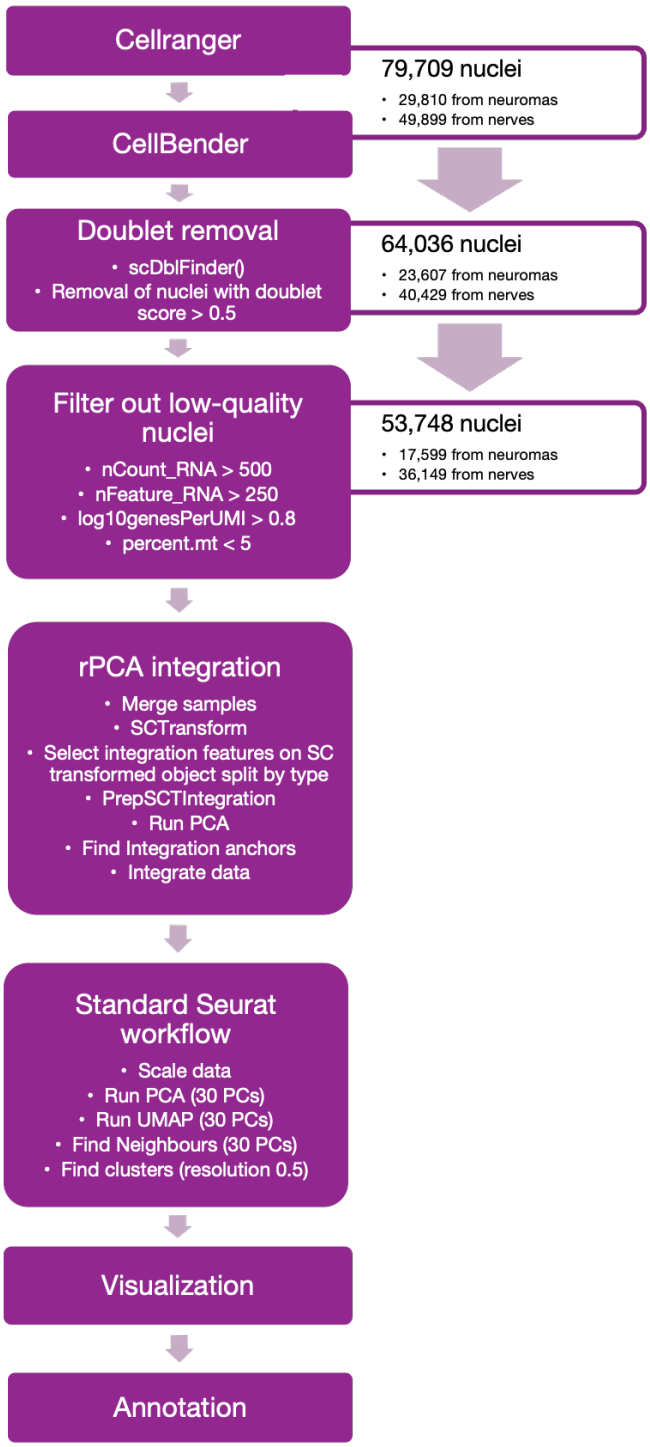

Figure 2.5. Diagram illustrating the workflow for single nuclei RNA sequencing analysis. The diagram illustrates the steps involved in single nuclei RNA sequencing analysis in the purple boxes with information on the parameters used in each step. In the white boxes, the number of nuclei retained are shown.

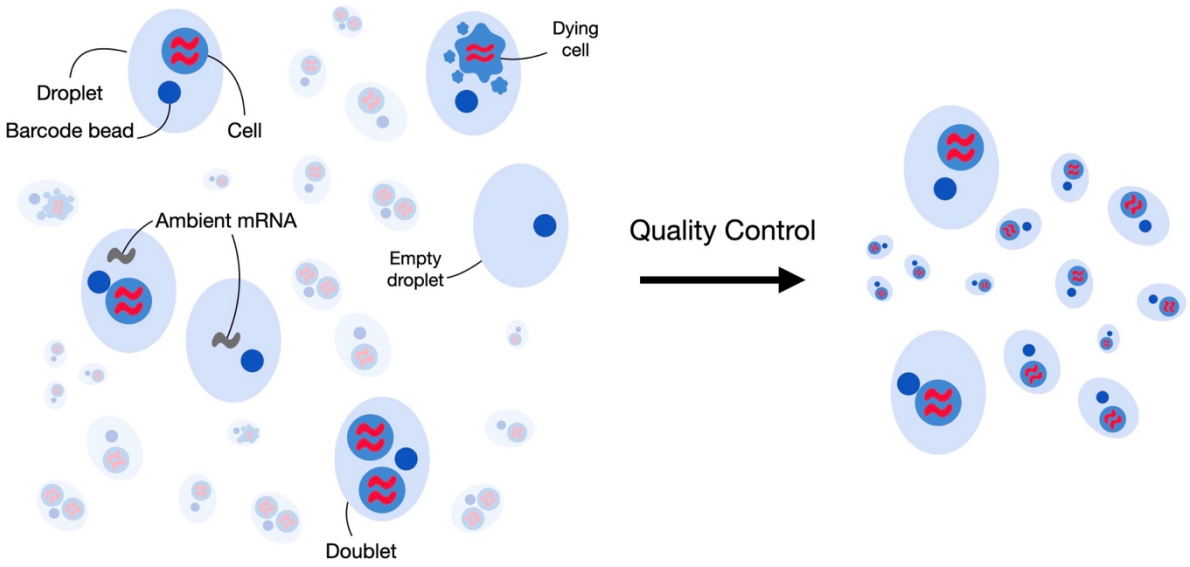

Figure 2.6. Common issues affecting single cell/nuclei RNA sequencing datasets. Diagram displaying some of the common issues that affect single cell/nuclei datasets, including ambient RNA contamination and the presence of doublets. Image obtained with permission from (Heumos et al., 2023)

2.2.5.1 Ambient RNA removal

Ambient RNA arises from the harsh dissociation protocol required to isolate the nuclei, which involves cell lysis and the release of cytoplasmic RNA. The mixture of RNAs released following cell lysis is incorporated in the partitioned beads and creates background noise in the gene expression counts that can mask the variability across nuclei, preventing the correct identification of cell types. In order to remove ambient RNA, the h5 files containing the feature barcode matrices were processed with Cellbender, a fully unsupervised deep generative model for inferring cell-free and cell-containing droplets that enables the identification and removal of background noise (Fleming et al., 2023). The number expected cells in each and the number of total droplets to include was estimated from the GEX barcode rank plot generated from the Cellranger pipeline (example shown in Figure 2.7). The number of epochs to train and the fpr (target 'delta' false positive rate) parameters were kept as default. The pipeline was run on a GPU hosted by the Stanage high performance computing clusters of the University of Sheffield.

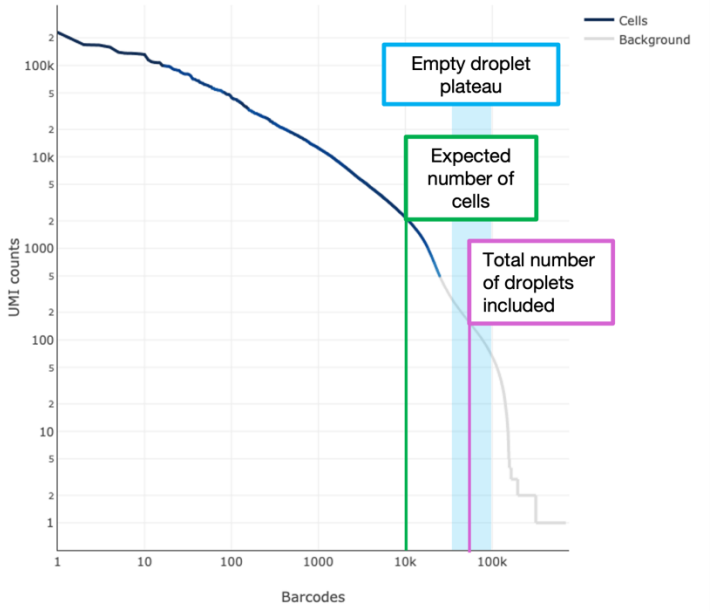

Figure 2.7 Example of a GEX Barcode Rank Plot generated by Cellranger.
The graph displays the counts of filtered UMIs mapped to each barcode, used to identify the parameters to run the function remove-background from CellBender. UMI counts might be detected in barcodes associated with empty droplets due to the presence of background RNA: this creates an "empty droplet plateau" in the Barcode Rank plot (identified in the light blue rectangle in the graph), a plateau consisting of low UMI counts associated with a few barcodes which are deemed empty droplets. To remove background RNA, CellBender requires the user to set the expected number of cells and the total number of droplets to be included in the analysis. The expected number of cells is set by identifying the lowest number of barcodes deemed to contain a nucleus, identified by the green line in the graph. The total droplets included in the analysis are identified by selecting a number a few thousand of barcodes into the empty droplet plateau, identified by the pink line. In this example, the expected cells were set at 10,000 and the total included cells were set at 60,000.

2.2.5.2 Doublets' removal

Following ambient RNA removal, the presence of potential doublets was assessed. Doublets arise as a consequence of the stochastic incorporation of nuclei into partitioned beads: depending on the concentration of the nuclei suspension, a proportion of the beads will be partitioned with two or more nuclei and, if originating from the same sample, the transcriptome of the nuclei in the same droplet can't be differentiated. In this instance, the presence of multiple nuclei in one droplet will confound the expression data, which will resemble that of a cell type in-between the real cell types incorporated in the droplet. Several methods have been published to remove doublets from single-cell experiments: scDblFinder (v1.12), a publicly available R package that combines multiple approaches to identify doublets (Germain et al., 2021), was used to remove doublets from this dataset. The function scDblFinder() was used with default parameters to calculate a doublet score

associated with each barcode. Barcodes with a doublet score higher than 0.5 were removed from the dataset.

2.2.5.3 Quality control, integration and annotation

Downstream analysis was performed on R (v4.2.3) and Seurat (v4.9.9). The following filters were used to retain high quality nuclei:

- At least 500 UMIs per barcode
- At least 250 genes per barcode
- A novelty score higher than 0.8
- A mitochondrial ratio lower than 5%

The novelty score is the logarithmic ratio of the number of genes and the number of UMIs detected in each barcode and represents the complexity of the RNA species.

$$Novelty\ score = \frac{log_{10}nFeature\_RNA}{log_{10}nCount\_RNA}$$

The data was then normalized with SCtransform, with the method “glmGamPoi” to improve the speed. Integration was performed using Seurat v5. After an initial exploratory analysis of the data, a subset of cell types was identified to be specific to the trigeminal nerve samples, such as a small number of astrocytes, oligodendrocytes and meningeal fibroblasts, or to the neuromas, such as salivary gland cells or myocytes. To retain the cellular heterogeneity of the different sample types, integration with reciprocal PCA (rPCA) was chosen over canonical correlation analysis (CCA), where by determining the anchors between two datasets (nerves and neuromas), each dataset is projected into the others’ PCA space and the anchors are constrained by the same mutual neighbourhood requirement. This results in fewer overlaps between two datasets following integration, enabling the identification of cell types that are unique to each sample type (Luecken et al., 2022). The rPCA workflow involved selecting 3000 integration features on the SCT transformed objects, which are used as anchors to prepare the SCT integration. PCA analysis is performed on the object split by the sample type, and the integration anchors are identified with the reduction “rpca” using 30 dimensions.

Finally, the data is integrated using the previously identified anchors with 30 dimensions, with the normalization method “SCT”.

The standard Seurat workflow was performed for downstream analysis, involving scaling the data, running the UMAP dimensional reduction technique (30 PCs), finding nearest neighbours (30 PCs) and clusters at resolution 0.5. The clusters were annotated using marker genes obtained from the literature, summarised in Table 2.1. Markers for each cluster were calculated with the function FindAllMarkers() from Seurat, genes with p-value < 0.05 and log2 Fold Change > 0.5 were used for further enrichment analysis.

2.2.5.4 Differential expression analysis between trigeminal nerve root and neuroma samples

Differential expression (DE) analysis was performed comparing subsets of specific cell-types belonging to “nerve” or “neuroma” identity using the Seurat function FindMarkers() using the MAST (Model-based Analysis of Single-cell Transcriptomics) test, which is tailored for sc datasets which contain many zero counts, treating the overall expression level in each barcode as a covariate (Finak et al., 2015). Genes with an average log2FC > 0.5 and a p-value < 0.05 were deemed differentially expressed. The plots in Figure 2.11.A and Figure 2.13.E-F were generated by plotting the logarithmic average expression of gene in the neuroma and nerve samples, whilst DE genes were colour-coded in purple and the top 20 DE genes were labelled on the graphs.

2.2.5.5 Inference of cell-cell communication

CellChat (v1.6.1) was used to identify potential cell-cell interactions. CellChat is based on a manually curated database, CellChatDB, which takes into account ligand-receptor (L-R) interactions as well as the presence of co-factors and multimeric complexes. Intercellular communication is calculated based on a mass action model, along with differential expression analysis and statistical tests on cell groups (Jin et al., 2021). The interactions can then be visualized with a variety of plots, focusing on the communication patterns between cell types or on specific L-R interactions.

To perform the analysis, the Seurat object was split by the sample type (nerve and neuroma), each of these were then merged with the neuronal barcodes from

Yang et al. (2022) and normalised with Seurat. Variable features were identified and the data was scaled following standard Seurat workflow. The cellchat objects for nerves and neuromas were created separately following the CellChat manual with the createCellChat() function, adding the normalized RNA scaled data assay and the annotation labels from each Seurat object.

The CellChat protocol was followed: briefly the over-expressed genes in each cell group and the over-expressed interactions were identified with identifyOverExpressedGenes() and identifyOverExpressedInteractions(). The communication probability was computed with computeCommunProb() with the default parameters. This function uses the trimean statistical method, assuming that the average expression of a certain gene is 0 if it's expressed in less than 25% of cells, which produces fewer interactions but is statistically more robust. The communication network was filtered with filterCommunication(), which removes cell groups with fewer than 10 cells by default. The communication at the level of individual pathways was estimated with computeCommunProbPathway(). The interactions were visualised with the plotting functions provided by CellChat, including chord plots, circos plots and heatmaps.

Table 2.1. Summary of the marker genes used for cell type annotation.

Cell Type	Abbreviation	Marker Genes	References
General Fibroblasts	Fibro	DCN, GSN, VIM, COL1A1, FN1	
Endoneurial Fibroblasts	EndoF	OSR2, ABCA8, ABCA9, ABCA10, PLXDC1, COL15A1	
Perineurial Fibroblasts	PeriF_1-4	CLDN1, SLC2A1, PTCH1, LMO7, ITGB4, KLF5, NGFR	
Meningeal Fibroblasts	MenF_1-2	OGN, PTGDS, FXYD5, ALPL, CRABP2	
Endothelial cells	Endo_1-3	EGFL7, PECAM1, TIE1, EMCN, CDH5, VWF, CLDN5, ECSCR	
Vascular Smooth Muscle Cells / Pericytes	Mural	TPM2, MYH11, ACTA2, MYLK, PDGFRB	Chen et al. (2021), Lovatt et al. (2022) DeSisto et al. (2020), Chau et al. (2022), Gong et al. (2022)
Schwann cells	SC	SOX10, PLP1, ERBB3, NCAM1, S100B	
Non-Myelinating Schwann Cells	NMSC	L1CAM, NRXN1, NCAM1	
Myelinating Schwann Cells	MSC_1-3	MBP, MPZ, EGR2, NCMAP	
Repair Schwann Cells	N/A	NGFR, BDNF, GDNF, ERBB3, SOX2, CADM1, ATF3, RUNX2	
Lymphocytes	Lymphocytes	PTPRC, CD3G, CXCR6, TRAC, CD3E, SKAP1, THEMIS, IL7R	
Myeloid	Myeloid	AIF1, CD68, MRC1, SIGLEC1, ITGAM, CSF1R	
Myocytes	Myo	MYL1, TNNT1, TNNT3, TNNI1	
Oligodendrocytes		OLIG2, OLIG1, MOG, CNP, PLP1	
Astrocytes	Astro	GFAP	
Salivary Gland Cells	SGC_1-3	MUC5B, AQP5, KRT19, KRT7, KRT14	

2.3 Results

2.3.1 Overview of samples and quality control

To investigate the cellular composition of the trigeminal nerves with and without injury in humans, single nuclei RNA sequencing was used on mechanically dissociated samples of human lingual nerve neuromas and trigeminal nerves. The trigeminal nerves were obtained from the Netherland Brain Bank, from two donors who died of non-neurological causes and without a diagnosis of dementia (Table 2.2). The samples were obtained by the University of Texas at Dallas for trigeminal ganglia investigation; however, due to the absence of neuronal cell bodies and the morphology typical of peripheral nerves, evidenced by H&E staining (shown in Figure 2.8.A,B) the specimens were classified as trigeminal root nerves. Therefore,

they were included in the study as a healthy control of uninjured trigeminal nerve for comparison with the injured lingual neuromas. The lingual nerve neuromas were obtained from lingual nerve repair surgeries carried out at the Royal Hallamshire Hospital in Sheffield, UK. The clinical information linked to each sample is shown in Table 2.3.

Table 2.2 Human trigeminal nerves information.
Donor information is shown for trigeminal nerve samples used for single nuclei RNA sequencing.

Sample ID	Donor #	Tissue	Sex	Age	Collection Site
TG1	2013-022	Trigeminal Nerve	F	92	Netherlands Brain Bank
TG2	2012-104	Trigeminal Nerve	M	79	Netherlands Brain Bank

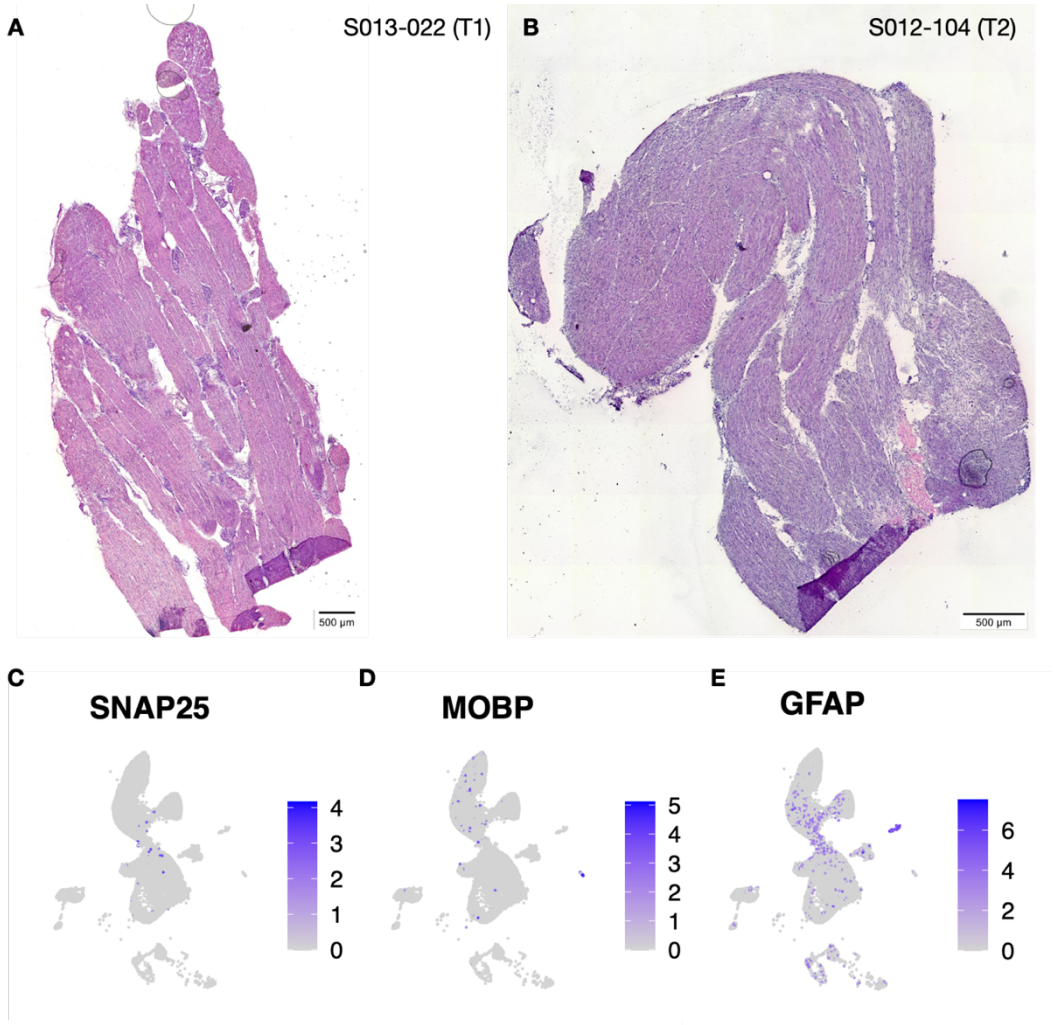

Figure 2.8. Quality control evidencing that the nerve samples from the NBB are trigeminal nerve roots rather than trigeminal ganglia.

A,B: H&E images of the samples used are shown, where the morphology typical of nerve fascicles and the lack of neuronal cell bodies can be observed. Courtesy of Dr Stephanie Shiers.
C, D, E: Feature plots of SNAP25 (C), a neuronal marker which encodes for a SNARE protein, showing the absence of a neuronal cluster in the trigeminal nerve roots, MOBP (D), a marker for oligodendrocytes, and GFAP (E), a marker for astrocytes.

Table 2.3 Human lingual nerve neuromas information.
Clinical information is given for human lingual nerve neuroma samples used for single nuclei RNA sequencing.

Sample ID	Clinical Code	Tissue	Sex	Age	Time since Injury (months)	Subjective sensation	Pain VAS	Tingling VAS	Discomfort VAS	Collection Site
N2	LN13	Lingual Nerve Neuroma	F	28	4	20%	65	100	87	Sheffield, UK
N1	LN14	Lingual Nerve Neuroma	F	31	13	0%	0	0	0	Sheffield, UK

A total of 79,709 nuclei were sequenced, 49,899 from two trigeminal nerve samples and 29,810 from two neuroma samples, with an average of 1,214 genes detected per nuclei. Ambient RNA was removed with CellBender and doublets were removed using scDblFinder, removing nuclei with a doublet score higher than 0.5. Nuclei with fewer than 500 reads and 250 genes detected, a novelty score lower than 0.8 and the presence of mitochondrial genes higher than 5% were removed. Finally, after cell-type annotation, a small number of nuclei belonging to sample type-specific clusters were incorrectly detected in the wrong sample type, i.e. some nuclei classified as meningeal fibroblasts were found in the neuromas and some salivary gland cells were found in the trigeminal nerve samples, which might have been an effect of Seurat's integration process. Since only 19 nuclei were identified as incorrectly labelled, they were removed from downstream analysis. After quality control and clean-up of the data, 53,729 nuclei were kept, 17,591 from lingual neuromas and 36,137 from the trigeminal root nerves.

Low expression of the Synaptosome Associated Protein 25 (SNAP25), commonly used as a neuronal marker (Tavares-Ferreira et al., 2022b, Tafoya et al., 2008), in the nerve root samples (Figure 2.8.C) confirms the absence of neuronal cell bodies, while the presence of a small cluster positive for the astrocyte marker GFAP (Figure

2.8.D) and one positive for the oligodendrocyte marker MOBP (Figure 2.8.E), indicates that a small number of cells sequenced from the trigeminal root nerves samples are glial cells from the peripheral – central myelin transition zone (Peker et al., 2006).

2.3.2 The cellular landscape of peripheral trigeminal nerves

The nuclei from lingual neuromas and healthy trigeminal nerves were integrated using rPCA integration with SCT normalization, analysed following standard Seurat workflow and clustered at resolution 0.5. A total of 24 clusters were identified in the integrated dataset, shown in Figure 2.9. Three types of myelinating Schwann cells were identified: MSC_1 and MSC_2 were found in both sample types, MSC_3 in the neuromas only, while one non-myelinating Schwann cell (NMSC) cluster was identified in both sample types. In the healthy nerve samples, one cluster was annotated as astrocytes (Astro) and one as oligodendrocytes (Oligo), which were absent in the neuromas. A total of 8 fibroblasts clusters were identified, including one cluster of endoneurial fibroblasts (EndoF), 4 clusters of perineurial fibroblasts (PeriF_1-4), which were found in all samples; one type of general fibroblast enriched in PRRX1 expression (Fibro_PRRX1+) and particularly abundant in the neuroma samples; and finally, 2 types of meningeal fibroblasts, only found in the trigeminal root nerve samples. Three subtypes of endothelial cells were identified in all samples (Endo_1, Endo_2, Endo_3). One cluster was identified as containing mural cells (Mural), i.e. the cells that make up the vascular barrier: vascular smooth muscle cells and pericytes. Myeloid cells and lymphocytes were identified in both sample types. Finally, three subtypes of salivary gland cells (SGC_1, SGC_2, SGC_3) and one cluster of myocytes (Myo) were identified in the neuroma samples. The distribution of the clusters between sample types is shown in Figure 2.9.D. A few of the marker genes used to annotate the clusters are shown in the dotplot in Figure 2.9.E.

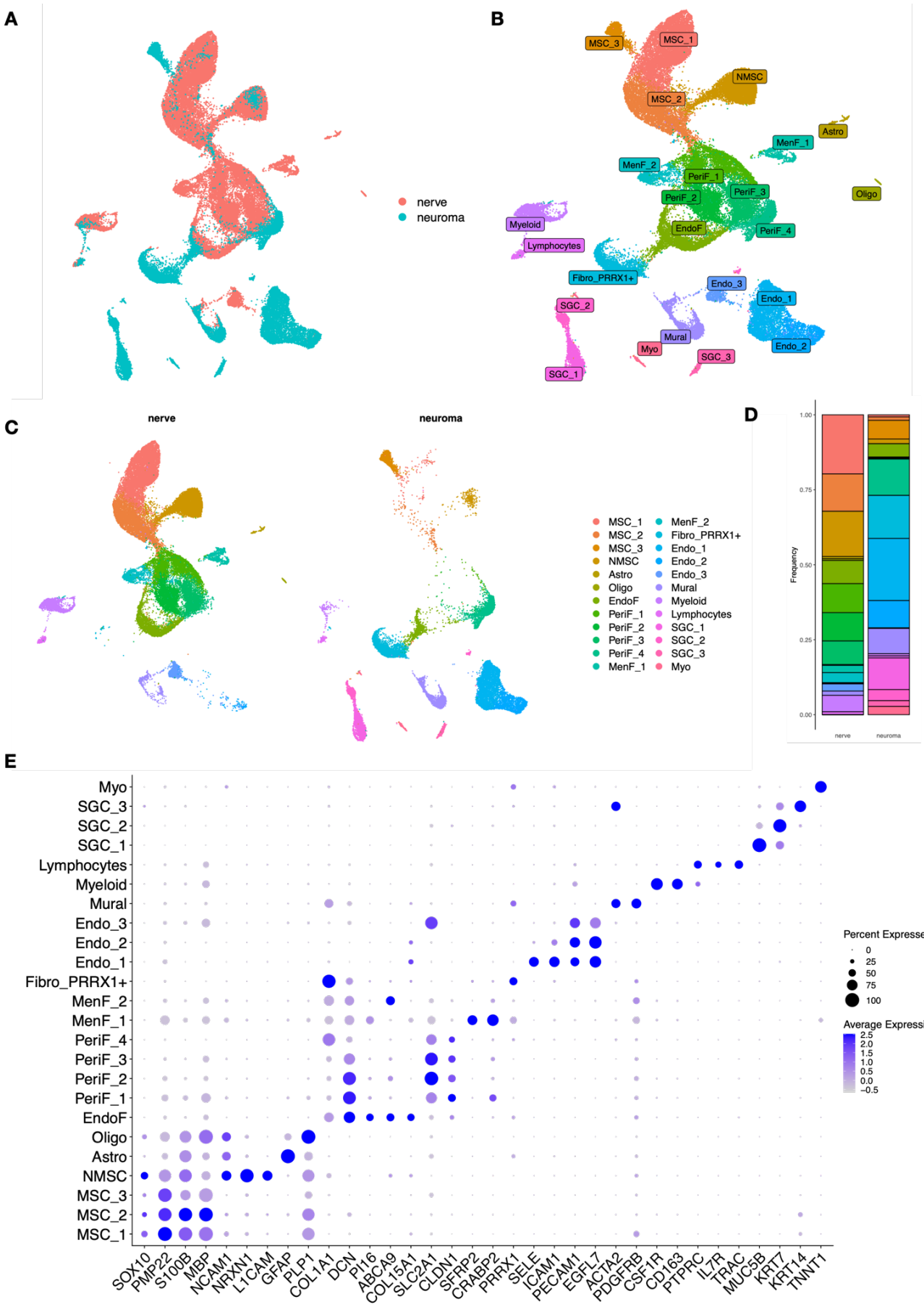
A
nerve
neuroma
B
MSC_3
MSC_1
NMSC
MSC_2
Astro
MenF_1
MenF_2
PeriF_1
PeriF_3
PeriF_2
Oligo
Myeloid
EndoF
PeriF_4
Lymphocytes
Fibro_PRRX1+
Endo_3
Endo_1
SGC_2
Mural
Myo
Endo_2
SGC_3
SGC_1
C
nerve
neuroma
MSC_1
MSC_2
MSC_3
NMSC
Astro
Oligo
EndoF
PeriF_1
PeriF_2
PeriF_3
PeriF_4
MenF_1
MenF_2
Fibro_PRRX1+
Endo_1
Endo_2
Endo_3
Mural
Myeloid
Lymphocytes
SGC_1
SGC_2
SGC_3
Myo
D
Frequency
1.00
0.75
0.50
0.25
0.00
nerve
neuroma
E
Myo
SGC_3
SGC_2
SGC_1
Lymphocytes
Myeloid
Mural
Endo_3
Endo_2
Endo_1
Fibro_PRRX1+
MenF_2
MenF_1
PeriF_4
PeriF_3
PeriF_2
PeriF_1
EndoF
Oligo
Astro
NMSC
MSC_3
MSC_2
MSC_1
SOX10
PMP22
S100B
MBP
NCAM1
NRXN1
L1CAM
GFAP
PLP1
COL1A1
DCN
PI16
ABCA9
COL15A1
SLC2A1
CLDN1
SFRP2
CRABP2
PRRX1
SELE
ICAM1
PECAM1
EGFL7
ACTA2
PDGFRB
CSF1R
CD163
PTPRC
IL7R
TRAC
MUC5B
KRT7
KRT14
TNNT1
Percent Expressed
0
25
50
75
100
Average Expression
2.5
2.0
1.5
1.0
0.5
0.0
−0.5

Figure 2.9. snRNA-seq of human healthy and injured trigeminal nerves.
A: UMAP plot where 53,729 nuclei from injured and healthy trigeminal nerves are grouped by sample type and overlapped.
B: UMAP plot of the nuclei showing the cell type annotation.
C: UMAP plot of the nuclei split by sample type.
D: Bar plot displaying the distribution of cell types across the healthy and injured nerve samples, expressed as a percentage of the total nuclei in each sample type.
E: Dot plot showing a few marker genes used to annotate the dataset, where the diameter of each dot represents the percentage of cells in each cluster that expresses the gene, and the shade of purple represents the average expression in the scaled RNA assay.

2.3.2.1 Schwann Cells

Three clusters were annotated as myelinating Schwann cells: MSC_1, MSC_2 and MSC_3. MSC_1 and MSC_2 were found in both neuromas and trigeminal nerve root samples and are enriched in markers for myelination such as PRX, a gene encoding for periaxin, required for maintenance of myelination in peripheral nerves, PMP22, encoding for peripheral myelin 22, and MBP, encoding for myelin basic protein (Figure 2.10). The top marker genes identified in MSC_1 are SLC25A48, a gene encoding for a solute carrier transporter, MLIP, a gene encoding for the muscular LMNA interacting protein, previously identified to be expressed in Schwann cells (Bargagna-Mohan et al., 2021), PRX, PMP22 and SLC36A2, a member of a family of amino acid transporters identified as a biomarker for vestibular Schwannoma (Shi et al., 2022). Marker genes for MSC_2 were PMP2, encoding for peripheral myelin protein 2, MBP, S100B and CRYAB, encoding for a small heat shock protein involved in myelination (Lim et al., 2021). A third myelinating Schwann cell cluster, MSC_3, was found only in the neuroma samples. MSC_3 expresses markers for myelinating SCs such as PRX but is enriched in genes including AATK, an apoptosis induced gene, PLEKHG5, involved in autophagy of vesicles, TNFRSF25, member of the TNF receptor family and COL18A1, encoding for the alpha chain of type 18 collagen.

One cluster was annotated as non-myelinating Schwann cells (NMSC), found in both neuromas and trigeminal nerve roots, and expresses markers such as L1CAM, ERBB3, and SOX10. This cluster is enriched in genes common in non-myelinating SCs including NRXN1, which encodes for a cell surface protein involved in forming intracellular junctions, SCN7A, a voltage gated sodium channel, also identified as a NMSC marker in mice by Yim et al. (2022), PRIMA1, encoding for an

acetylcholinesterase membrane anchor precursor protein and CHL1, member of the L1 gene family of neural cell adhesion molecules.

Interestingly, Yim et al. (2022) identified a myelinating Schwann cell subpopulation in mouse and human nerves that expresses high levels of PMP2 and preferentially myelinates large diameter axons, in particular motor axons, which might correspond to the MSC_2 cluster, where PMP2 expression is significantly upregulated. While motor axons would be found in the motor root of the trigeminal nerve, other large-diameter axons such as Aβ low threshold mechanoreceptors present in the sensory root of the trigeminal nerve might be preferentially myelinated by the MSC_2 cluster. However, ADAMTSL1 and CLDN14, also identified as markers of the PMP2+ subpopulation in mice in Yim et al. (2022), aren't found in the present dataset, which could represent a species or anatomical difference.

Classic markers of repair Schwann phenotype displayed a very low level of expression, such as NGFR (shown in Figure 2.10), NGF, BDNF and GDNF (not shown). The absence of the repair Schwann cell phenotype in the injured neuromas can be explained by the interval between nerve injury and surgery, which is greater than 3 months in both samples, while the repair Schwann cell phenotype is known to deteriorate within 2-3 months following injury (Jessen and Mirsky, 2019).

ERBB3 and SOX10 are markers for immature Schwann cells (Jessen et al., 2015) and are expressed to a higher degree in the NMSC cluster, but there isn't a specific cluster that can be identified as the immature Schwann cell phenotype. In Lovatt et al. (2022) all cells were classified as myelinating or non-myelinating SCs in the naïve sciatic nerve of rats, while less than 1% were classified as dividing Schwann cells. The authors also found no Sox10 ISH signal in naïve nerves, whilst this increased after injury. However, Bremer et al. (2011) has shown that SOX10 is required in adult naïve peripheral nerves to maintain structural and functional integrity of the nerve, and the lack of Sox10+ nuclei in Lovatt et al. (2022) could be caused by the investigation of a restricted area of tissue. In the present dataset, SOX10 is expressed in all Schwann cells subtypes of the healthy trigeminal nerve root, while it's only expressed in the MSC_1 cluster in neuromas. The presence of SOX10 mRNA in the neuromas is confirmed by RNAscope (Section 4.3.1.4). Overall, an immature Schwann cell cluster couldn't be identified. Again, this is in line with the

timeframe following nerve injury, where immature Schwann cells develop from dedifferentiated Schwann cells and then differentiate into repair Schwann cells, within the first 3 months following injury (Jessen and Mirsky, 2019).

DHH is a gene encoding for desert hedgehog, a gene important for peripheral nerve development expressed in precursor Schwann cells (Parmantier et al., 1999) and important for peripheral nerve sheath development (Sharghi-Namini et al., 2006). Interestingly, in the present dataset, DHH expression is prominent in the MSC_3 cluster only found in the lingual neuromas; while only present to a smaller degree in the trigeminal root MSC_1 cluster, indicating the potential upregulation of DHH following nerve injury for the establishment of the peripheral nerve sheath architecture.

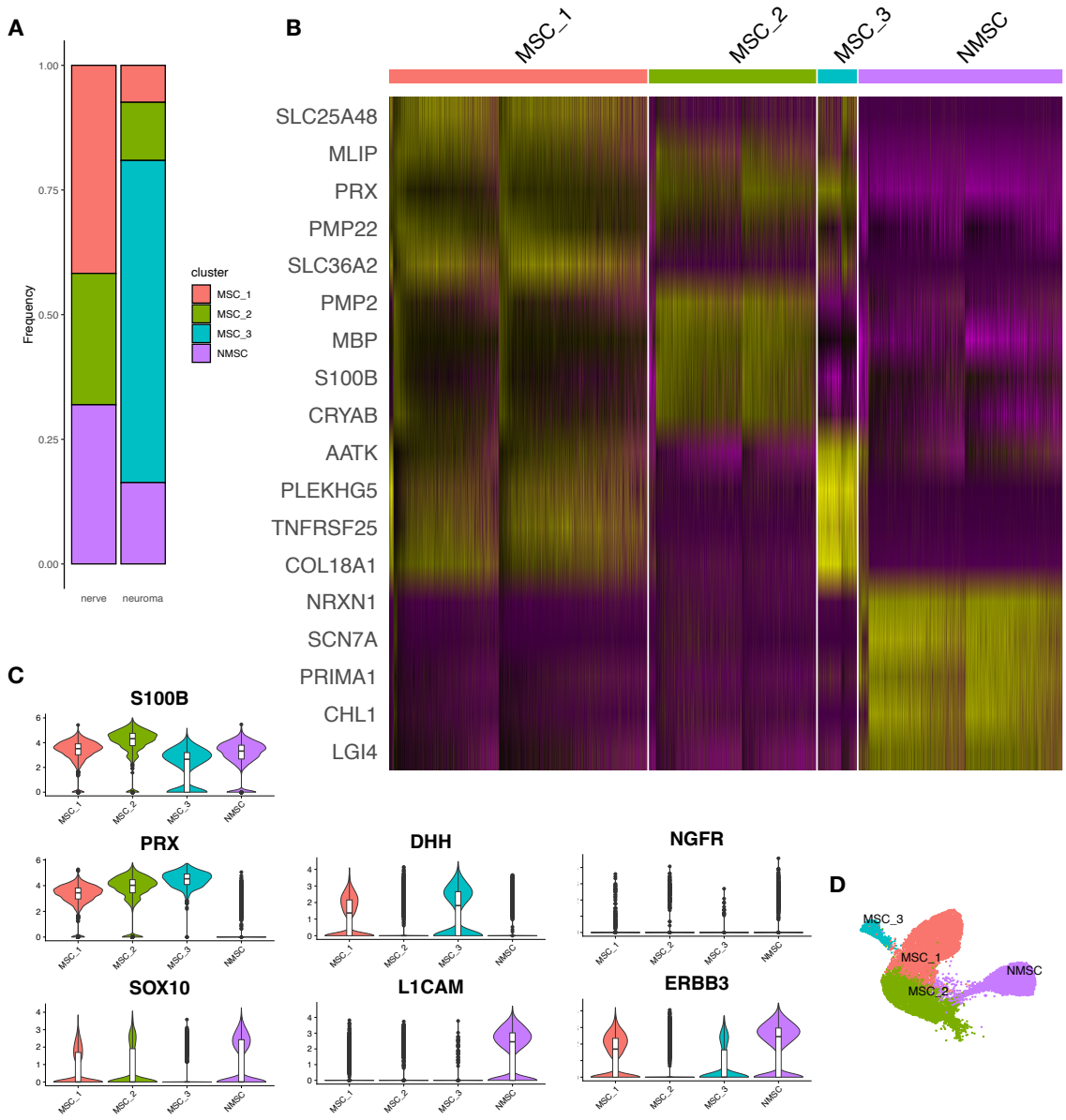

Figure 2.10. Identification of molecular subtypes of Schwann cells in lingual neuromas and trigeminal root healthy nerves.
A: Distribution of Schwann cell subtypes between the trigeminal root and neuroma samples.
B: Heatmap highlighting the top 5 marker genes in each cluster, where the expression from low to high is colour coded on a scale from purple to yellow.
C: Violin plots showing the expression levels of S100B, PRX, SOX10, DHH, L1CAM, NGFR and ERBB3 across each Schwann cluster.
D: UMAP plot of the Schwann cell clusters.
MSC: myelinating Schwann cells; NMSC: non-myelinating Schwann cell

Differences in gene expression between Schwann cell subtypes in the neuromas and the healthy trigeminal nerve roots were investigated by separating the myelinating and non-myelinating clusters and performing the MAST test with the FindMarker() function in Seurat. The average expression of all genes in the nerve and neuroma samples is plotted in Figure 2.11, where purple dots indicate that the gene is differentially expressed with an average p-value < 0.05 and a log2FC > 0.5, and the labelled dots are the top 20 DE genes.

In both myelinating and non-myelinating Schwann cells, genes associated with nerve repair are upregulated in the Schwann cells from the neuromas compared to the ones from the nerve roots, including the AP-1 transcription factor subunits JUN, JUNB, JUND, FOS and FOSB, known to direct the transcriptional switch following peripheral nerve injury (Jessen and Mirsky, 2019), and EGR1 which is upregulated following PNI (Balakrishnan et al., 2021). NR4A1 is an orphan nuclear receptor which has been linked with Schwann cell differentiation following nerve injury (Zhang et al., 2015a) and is upregulated in the neuroma samples. Mutations in the LMNA gene have been shown to cause peripheral neuropathies (Benedetti et al., 2005) and are linked with morphological abnormalities in Schwann cells (Vital et al., 2005). Clusterin (CLU) has also been linked with the nerve injury response: Wright et al. (2014) found that CLU is required for neurite outgrowth and peripheral nerve regeneration, with its transcriptional levels increasing in the DRG 7 days following denervation and returning to baseline a month following denervation. Interestingly, in this dataset, CLU expression levels are downregulated in the neuromas, but its role in late-stage peripheral nerve injuries hasn’t been investigated yet.

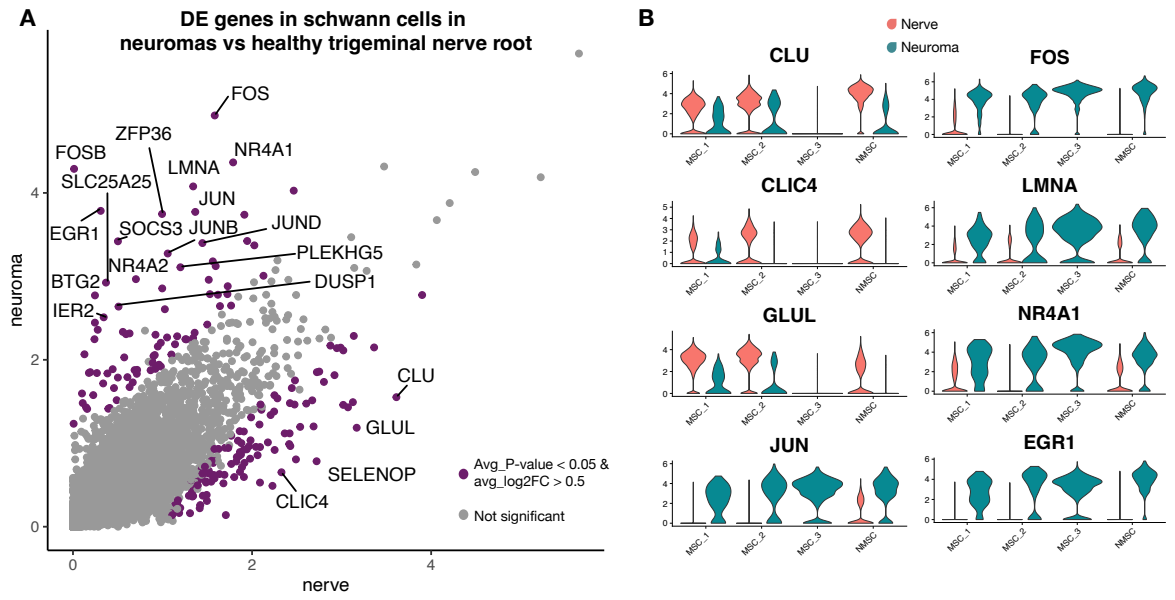

Figure 2.11 Differentially expressed genes in Schwann cells of healthy trigeminal nerve roots and lingual neuromas.
A: the logarithmic average gene expression level of nuclei classified as Schwann cells from healthy trigeminal root nuclei (nerve) and lingual neuromas (neuroma) plotted against each other. The significantly differentially expressed (DE) genes (avg_log2FC > 0.5, p-value < 0.05) are colour coded in purple, and the top 20 DE genes are labelled.
B: CLU, CLIC4, GLUL, JUN, FOS, LMNA, NR4A1 and EGR1 expression levels are shown across in violin plots across SC clusters, separated by sample type, where pink represents nuclei belonging to nerve samples, while teal represents nuclei from neuroma samples.

2.3.2.2 Fibroblasts

Six fibroblast clusters were identified across all samples (EndoF, PeriF_1-4 and Fibro_PRRX1+), whilst two clusters identified as meningeal fibroblasts were found in the nerve samples and aren't included in this section. All clusters express a high level of general fibroblast marker genes such as VIM and DCN (Figure 2.12). The endoneurial cluster, found in both neuroma and healthy nerve samples, is enriched in ABCA10 and ABCA5, members of the ATP-binding cassette (ABC) superfamily, APOD, a gene encoding for the apolipoprotein D, and PI16, encoding for peptidase inhibitor 16. PI16 has been described as an epineurial fibroblast marker in rodents (Singhmar et al., 2020, Yim et al., 2022). However, in the present dataset it was found to be co-expressed with CSPG4, also known as NG2, identified as a marker for endoneurial fibroblasts by Richard et al. (2014), indicating a potential species difference. Its localization in the endoneurium was validated with immunohistochemistry in the human neuromas as described in section 4.3.3 PI16

was identified by Singhmar et al. (2020) to promote neuropathic pain by inducing permeability of the blood-nerve barrier and increasing immune cell infiltration.

The four perineurial fibroblast clusters are found in varying proportions across sample types: PeriF_1,2,3 are largely found in the trigeminal root samples, while PeriF_4 is found primarily in the neuroma samples. PeriF_1,2,3 are enriched in genes such as IGFBP6, encoding for the insulin growth factor binding protein 6 and SLC2A1, a gene encoding for a glucose transporter, also known as Glut-1, and widely used as a perineurial marker gene (Piña et al., 2015). PeriF_4 has increased expression of THBS1, encoding for thrombospondin 1, CCN1, encoding for Cellular Communication Network Factor 1, a protein found to promote SCs proliferation and upregulation of c-Jun (Cheng et al., 2021), and ADAMTS14, encoding for a metalloprotease with a thrombospondin 1 motif, among others. THBS1 was shown to be secreted by fibroblasts in peripheral nerves following transection injury and to promote neurite outgrowth (Hara et al., 2023). NGFR is also found in the perineurial clusters to a higher expression level compared to Schwann cells, which was validated with immunohistochemistry, as discussed in chapter 4. NGFR expression in perineurial cells was also previously identified in human peripheral nerves by Yamamoto et al. (1992) and Chau et al. (2022).

Finally, one fibroblast cluster particularly abundant in the neuromas was classified as Fibro_PRRX1+ and displays a pro-fibrotic phenotype similar to the fibroblast lineage described in Leavitt et al. (2020). This cluster is enriched in ECM-related genes including COL1A1, FBLN1 and COL5A3, as well as inflammation-related genes such as FOSB, involved in promoting a profibrotic programme in pulmonary fibrosis (Cui et al., 2020) and LSP1, which mediates neutrophil activation (Le et al., 2015).

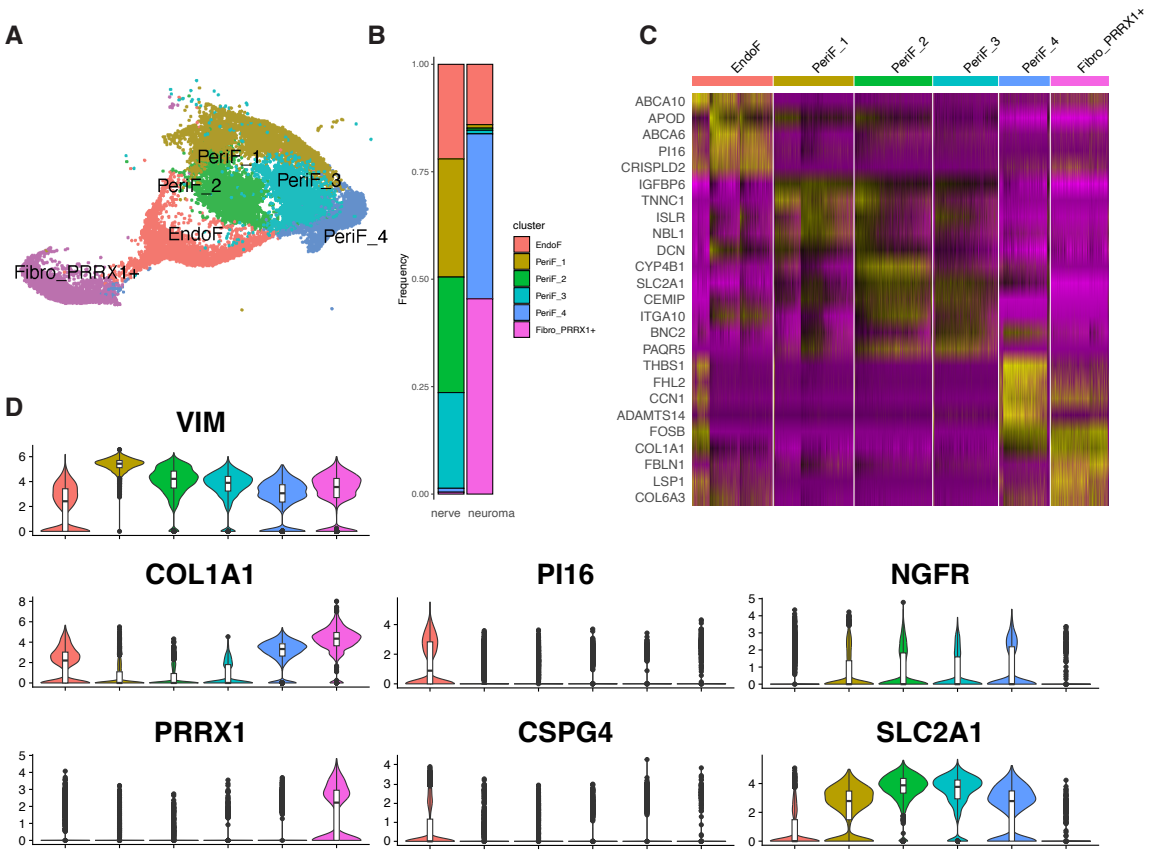

Figure 2.12. Identification of fibroblasts subtypes in lingual neuromas and trigeminal root nerves.
A: UMAP plot showing the different fibroblasts clusters in the nerve and neuromas.
B: Distribution of fibroblasts subtypes between the trigeminal root and neuroma samples.
C: Heatmap highlighting the top 5 marker genes in each fibroblast cluster.
D: Violin plots showing the expression levels of VIM, COL1A1, PI16, NGFR, PRRX1, CSPG4 and SLC2A1 across each fibroblast subtype.
EndoF: endoneurial fibroblasts; PeriF: perineurial fibroblasts; Fibro_PRRX1+: PRRX1+ fibroblasts

2.3.2.3 Immune Cells

A total of 2,578 nuclei were classified as immune cells, making up 6.5% of the nuclei sequenced in the trigeminal nerve root and 1.4% of the nuclei sequenced in the neuromas. Two immune cell subpopulations were identified: lymphocytes and macrophages, shown in Figure 2.13. The macrophage cluster expressed high levels of RGS1, encoding for regulator of G protein signalling 1 found in macrophages as well as T-cells (Feng et al., 2022, Bai et al., 2021), CSF1R and CLEC7A commonly used as a macrophage markers (Lovatt et al., 2022, Wang et al., 2022b), CD163, a marker for M2 macrophages (Hu et al., 2017) and MS4A5A, another potential M2 macrophage marker (Zhang et al., 2022a).

The lymphocyte cluster displayed high levels of CXCR4 and CD69, T-cell markers (Mousset et al., 2019), CYTIP, also found to be expressed in T cells (Queiroz et al., 2022), IKZF1, a regulator of lymphocyte differentiation (Ronni et al., 2007) and TRBC2, also known as T-cell Receptor Beta Constant 2, involved in antigen binding activity (Maciocia et al., 2017).

In the neuroma samples a higher proportion of lymphocytes are detected compared to the macrophages. T-cells have been identified to have an important role in nerve repair, modulating remyelination and inflammation (Tang et al., 2022).

DE analysis was performed comparing macrophages and lymphocytes from the trigeminal nerve root and the lingual neuroma samples. Members of the AP-1 family of transcription factors, such as FOS, FOSB, JUN and JUND, were upregulated in the neuromas in both macrophages and lymphocytes. This is in accordance with Li et al. (2021), where the AP-1 TF family was found to be upregulated following nerve injury by both Schwann cells and immune cells of the mouse sciatic nerve and high JUN and JUNB immunoreactivity was observed in immune cells 9 days after nerve injury.

KLF4, encoding for Kruppel Like Factor 4, is a transcription factors involved in axonal regeneration (Qin et al., 2013, Xu et al., 2021). In the current dataset, its expression, as well as KLF6 expression, another member of the same TF family, are increased in the neuroma samples specifically in macrophages. Interestingly, KLF6 was reported to promote M2 macrophage polarization (Kim et al., 2016). NLRP3

inflammasome was also upregulated in the macrophages found in the neuromas, in concordance with the literature which identified a role for NLRP3 in nerve damage (Li et al., 2022b)

The lymphocytes from the neuromas displayed a downregulation of genes that have been linked with the interplay between immune cells and axonal regeneration such as CXCR4, found to cause nerve entrapment following axotomy of the optic nerve (Hilla et al., 2021), and CCL5, which was found to promote robust optic nerve regeneration (Xie et al., 2021).

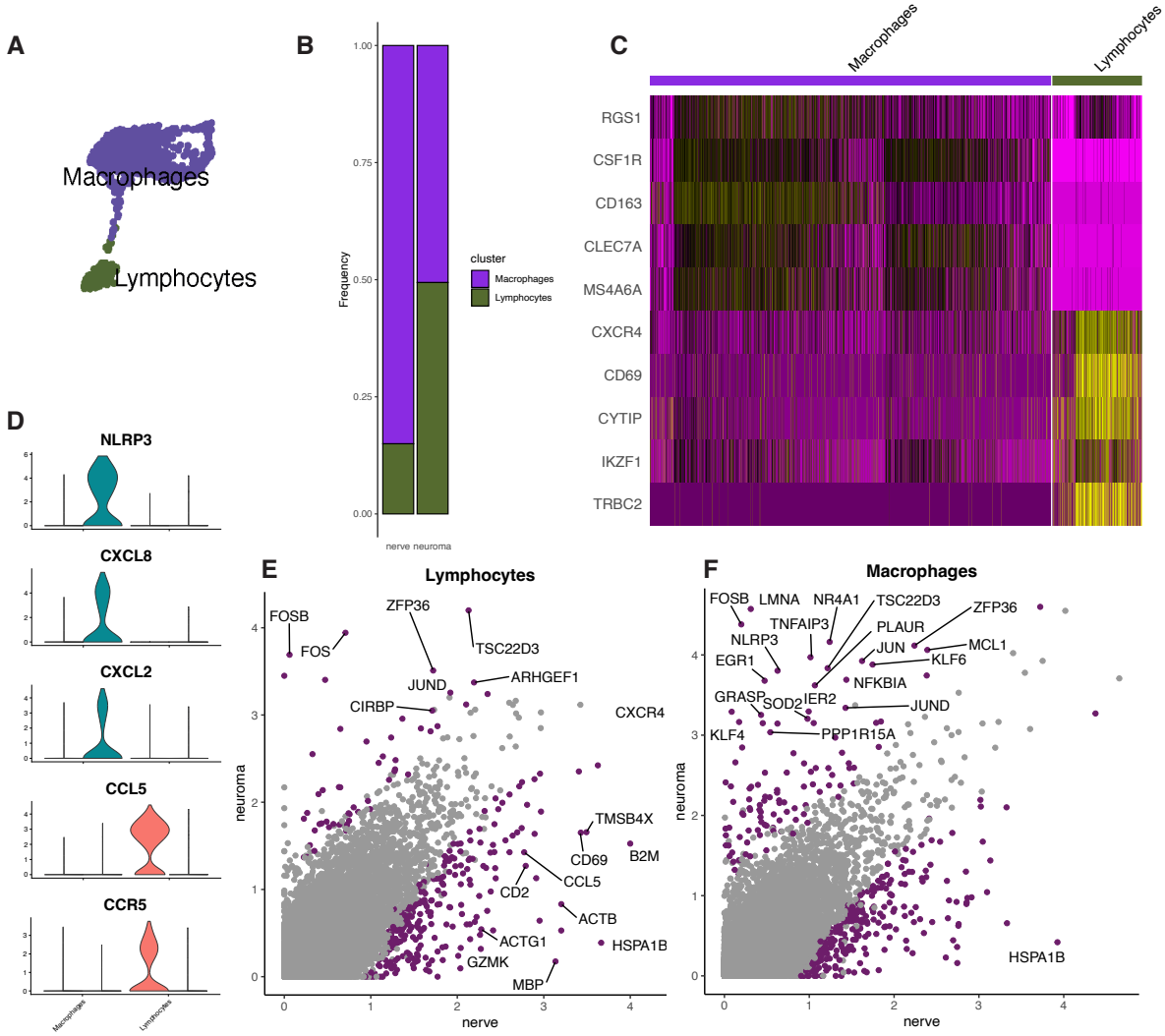

Figure 2.13. Identification of molecular subtypes of immune cells in lingual neuromas and trigeminal root nerves.
A: UMAP plot displaying the macrophages and lymphocytes clusters represented in a 2-dimensional plane in the nerve and neuromas.
B: Distribution of immune cell subtypes between the trigeminal root and neuroma samples.
C: Heatmap highlighting the top 5 marker genes in each immune cell cluster.
D: Violin plots showing the expression levels split by sample type of NLRP3, CXCL8, CXCL2, CCL2, CCR5; which were identified as differentially expressed between the nerve and the neuromas in the

immune subclusters. The red filled violin plots represent the expression level in the trigeminal nerve root, while the teal filled violin plots represent the expression levels in the neuroma samples. E, F: Differentially expressed genes in the lymphocytes (E) and in the macrophages (F) between the nerve and neuromas. The x-y coordinate of each dot in the graph represents the average gene expression of a gene in the nerve (x-axis) and in the neuroma (y-axis). The dots that were identified as differentially expressed (p-value<0.05, avg_log2FC > 0.5) are colour-coded in purple. The top 20 DE genes are labelled.

2.3.2.4 Vasculature

Endothelial cells, vascular smooth muscle cells and pericytes make up the vasculature that supplies peripheral nerves. A total of 8,242 nuclei were annotated as vascular, where three clusters of endothelial cells (Endo_1, Endo_2, Endo_3) and one cluster of mural cells, containing vascular smooth muscle cells and pericytes, were identified, shown in Figure 2.14. In the neuromas, a higher proportion of endothelial cells were identified, making up 30% of the nuclei in those samples, while only 3% of the nuclei in the nerves were annotated as endothelial, the majority of which belong to the Endo_3 cluster.

All the endothelial cell clusters expressed high levels of canonical endothelial cell markers such as EGFL7 and CLDN5 (Chen et al., 2021). Additionally, the Endo_1 cluster is enriched with genes usually found in cytokine activated endothelial cells and involved in leukocyte recruitment at the site of injury, such as SELE (Wu et al., 2017), ICAM-1, considered a master regulator of inflammation and injury resolution (Bui et al., 2020) and interleukin-6 (IL6), a hallmark of inflammation arising following nerve injury (Sandy-Hindmarch et al., 2022).

Although several papers performing snRNA-seq on peripheral nerves have identified lymphatic endothelial cells, characterised by LYVE1 and CCL21 expression (Lovatt et al., 2022, Chen et al., 2021, Gong et al., 2022), we were unable to identify this cluster in this dataset.

The mural cells cluster was characterized by high ACTA2, MYH11 and PDGFRA expression which are markers for both vascular smooth muscle cells and pericytes (Muhl et al., 2020). As noted by Muhl et al. (2020), mural cells displayed less heterogeneity than fibroblasts, displaying a more continuous phenotype despite including two cell types with a marked morphological difference.

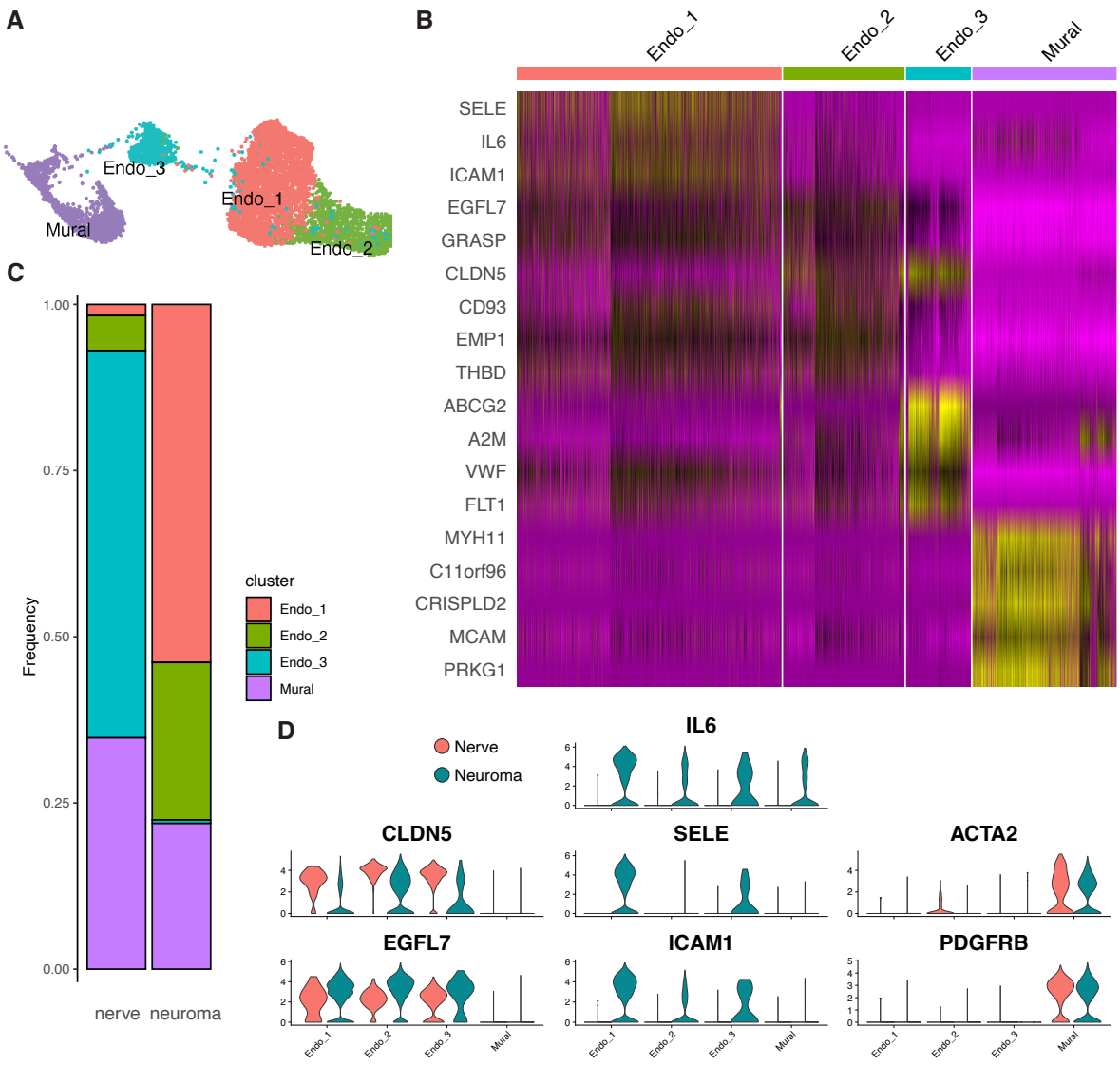

Figure 2.14. Identification of molecular subtypes of vascular cells in lingual neuromas and trigeminal root nerves.
A: UMAP plot displaying the vascular cell clusters represented in a 2-dimensional plane in the nerve and neuromas.
B: Heatmap highlighting the top 5 marker genes in each vascular cell cluster.
C: Distribution of vascular cell subtypes between the trigeminal root (nerve) and neuroma samples.
D: Violin plots showing the expression levels split by sample type of IL6, CLDN5, SELE, ACTA2, EGFL7, ICAM1, PDGFRB. The red filled violin plots represent the expression level in the trigeminal nerve root, while the teal filled violin plots represent the expression levels in the neuroma samples.

2.3.3 Inferring neuronal communication in the trigeminal nerve roots and lingual neuromas using CellChat

The cell types discussed in the previous paragraphs make up the microenvironment which supports the axons with cell bodies situated in the trigeminal ganglia. The interaction between the trigeminal axons and the various cell

types that make up the trigeminal nerve is important for neuronal homeostasis, providing support, activating a pro-regenerative program after nerve injury but also contributing to neuronal sensitization and neuropathic pain following injury. In order to disentangle the complex communication network taking place between trigeminal axons and peripheral cell types, CellChat, an open-source R package, was adopted to computationally infer cell-cell communication in the trigeminal nerve roots and the lingual neuromas.

In order to estimate the communication with trigeminal neurons, the dataset generated by Yang et al. (2022) with the trigeminal ganglia from three human donors (1 male, 2 female) was combined with the present dataset. The trigeminal ganglia cell atlas was generated with single nuclei RNA sequencing using the 10X Genomics Chromium platform. A total of 3,873 nuclei annotated by the authors as “neuronal” were used in this analysis. The neurons were furtherly classified by the authors according to the expression of marker genes in the following subtypes: peptidergic nociceptors (PEP, TAC1+), non-peptidergic nociceptors (NP, CD55+), pruriceptors (SST, SST+), C-fibre low threshold mechanoreceptors (cLTMR, FAM19A4), A-fibre low threshold mechanoreceptors (NF, NEFH+). The trigeminal neurons were merged, normalised and scaled with the trigeminal root nerves and the lingual neuromas. The communication in each sample type was analysed independently in order to preserve the different pathways that might be overexpressed in each sample type, characterised by different injury status and anatomical location. The CellChat database contains a total of 2,201 manually curated ligand-receptor (L-R) pairs, including information from the KEGG pathway database, across 229 signalling pathways, overviewed in Figure 2.15.E. A total of 11,737 interactions were identified in the neuromas, including 10,569 involving at least a neuronal subtype, while 18,335 were identified in the trigeminal nerve root, including 12,908 involving a neuronal subtype.

A total of 96 and 77 signalling pathways within the CellChat database displayed significant interactions with the nerves and the neuromas respectively, including laminin, collagen, thrombospondin, selectin, claudin, WNT, semaphorin 3, 5 and 6, neuregulin, NGF, FGF, VEGF, PARs and ephrins. The interactions inferred in the CXCL and CCL pathways are discussed in more depth in the following paragraph.

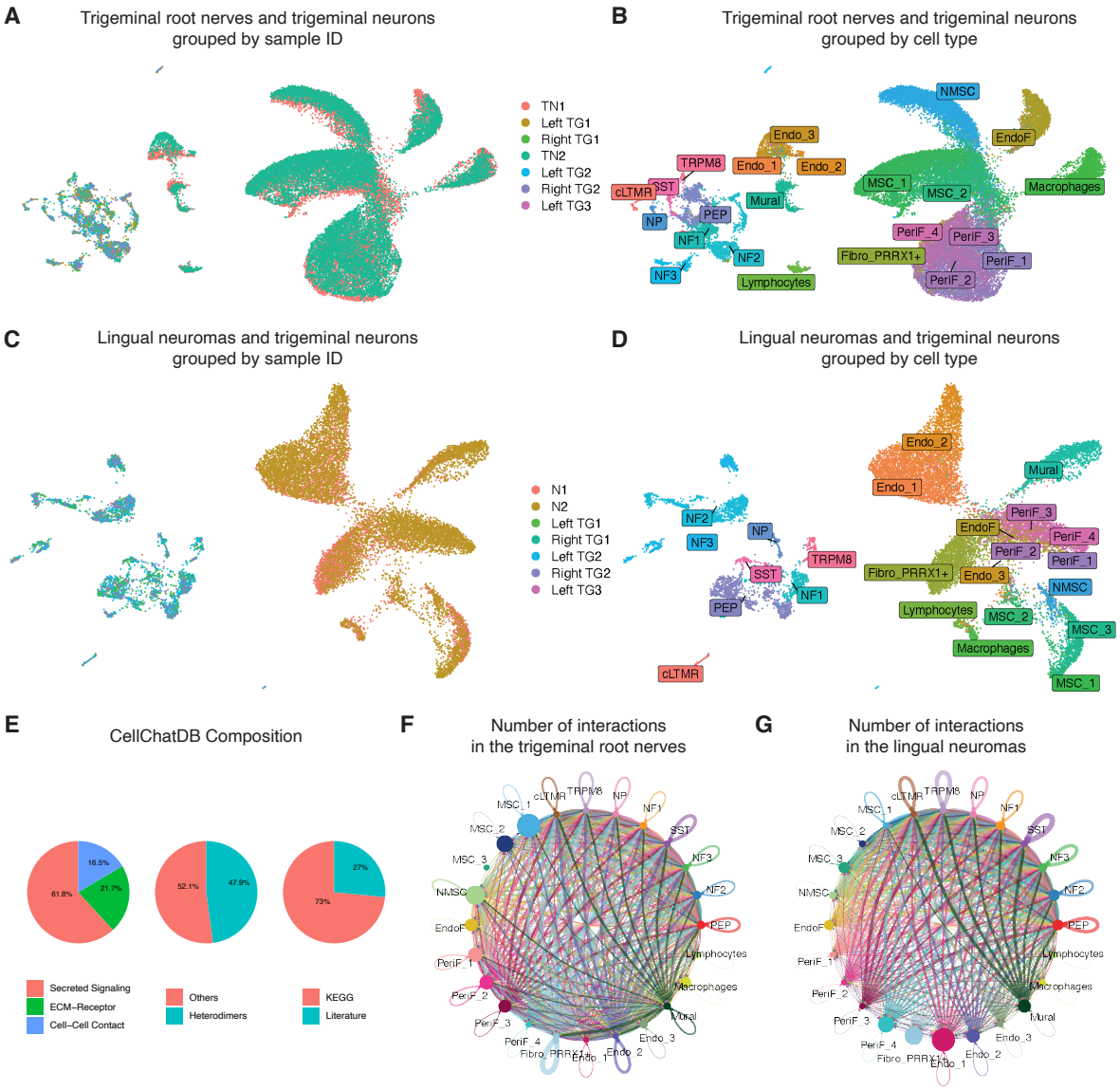

Figure 2.15. Overview of the Cell-cell interaction analysis performed with CellChat.
A, B: UMAP plot displaying the 2D representation of the nuclei from trigeminal root nerves and the trigeminal neurons used for CellChat analysis. In A they are colour-coded based on the sample ID: the trigeminal neurons were sequenced from three human donors (left and right from TG1, left and right from TG2 and left from TG3) and the trigeminal nerve root from two organ donors (TN1, TN2). In B the nuclei are colour coded by cell-type annotation.
C, D: UMAP plot displaying the 2D representation of the nuclei from lingual neuromas and the trigeminal neurons used for CellChat annotation, grouped by sample ID (A) and by annotation (B).
E: Pie charts displaying the CellChat database categories, showing the proportion of interactions classified as secreted signalling, ECM-Receptor or Cell-Cell contact (left); as heterodimers or others (middle); and as interactions identified from the KEGG database or from experiments published in the literature (right).
F, G: Circle plot generated with the CellChat package displaying all the interactions in each group, in the trigeminal nerve root (F) and in the neuromas (G). The thickness of each line represents the number of interactions between two specific cell-types, while the size of each dot represents the total number of interactions involving that cell type.

2.3.3.1 Chemokines signalling pathways in the trigeminal nerve root and the human neuromas

Among the interactions inferred by CellChat, several belonging to the chemokine signalling pathways CCL and CXCL reached statistical significance. Chemokines are inflammatory mediators released following nerve injury, which are primarily involved in chemotaxis but can also activate and sensitize nociceptors, leading to persistent pain (Solis-Castro et al., 2021, Cambier et al., 2023, Abbadie, 2005). The classification of chemokines is based on the arrangement of two cysteine residues: the CC group has two adjacent cysteine residues, while the CXC group has one amino acid separating the two cysteine residues (Abbadie, 2005). Significant interactions between the trigeminal nerve roots and the neuromas with the trigeminal axons were identified in the CXCL (Figure 2.16) and CCL (Figure 2.17) pathways.

In the CXCL signalling pathway, the interactions CXCL12 - CXCR4 and CXCL2 – ACKR1 reached statistical significance in both the trigeminal root nerves and the neuromas, accounting for most of the communication in this category in both sample types. The CXCL12/CXCR4 axis has been reported to contribute to neuropathic pain generation in rodents (Yu et al., 2017). In the present dataset, CXCL12 is expressed by a variety of cell types, including endoneurial fibroblasts, injury responsive fibroblasts (Fibro_PRRX1+), endothelial cells (Endo_2, Endo_3) and in the trigeminal root nerves, in mural cells and macrophages, as well. CXCR4 is found in macrophages and lymphocytes in both sample types. In Yu et al. (2017), the proteins encoded by CXCL12 and CXCR4 were detected in murine DRG neurons; however, in the human trigeminal neurons sequenced by Yang et al. (2022), the expression of these two genes was low. Nevertheless, components of the CXCL12-CXCR4 signalling axis are expressed in both naïve and injured human trigeminal nerves in a variety of cell types that make up the nerve.

The second ligand-receptor (L-R) pair with the highest contribution is CXCL2-ACKR1. CXCL2 is expressed by endothelial cells (Endo_1, Endo_2) in both sample types and in macrophages in the lingual neuromas. ACKR1, also known as Duffy antigen, a highly promiscuous receptor for several chemokines, is expressed in the trigeminal neurons. The CXCL2-ACKR1 axis is involved in neutrophil homeostasis

(Metzemaekers et al., 2020) but the role of ACKR1 activation in sensory neurons hasn't been investigated yet.

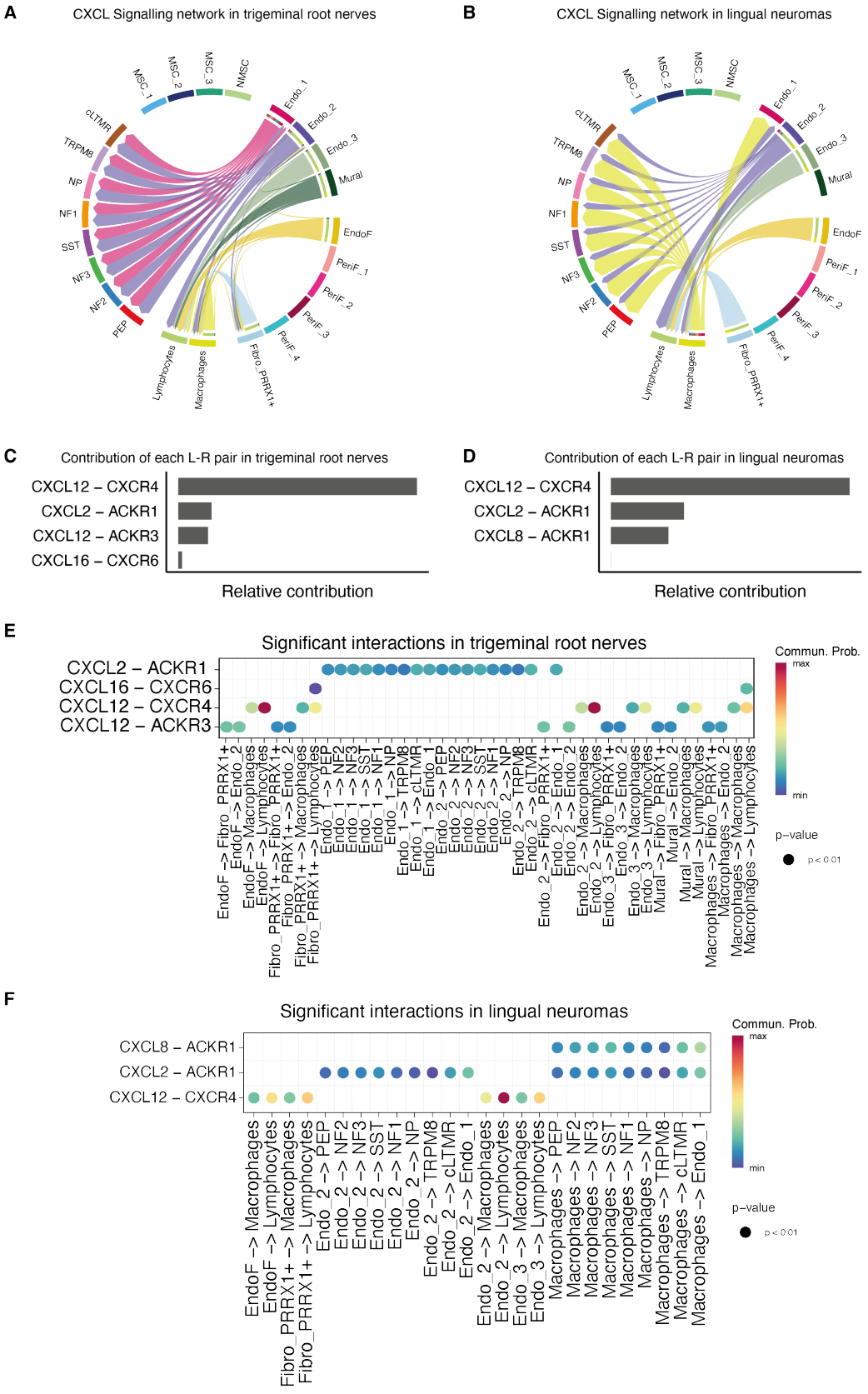

Figure 2.16. CXCL signalling network in the trigeminal root nerves and the lingual neuromas.

A: Chord diagram displaying the interaction network in the CXCL category in the trigeminal root nerves (A) and in the neuromas (B).
C, D: Bar plot displaying the relative contribution of each L-R pair in the trigeminal nerve roots (C) and in the neuromas (D).
E, F: Bubble plots displaying the inferred significant L-R interactions between cell types in the trigeminal root nerves (E) and in the lingual neuromas (F).

Several interactions annotated as part of the CCL signalling pathways in CellChatDB resulted as significant in the trigeminal root nerves and the neuromas. In the trigeminal root nerves, interactions involving CCL4 and CCL5, both expressed in lymphocytes, and the atypical chemokine receptor. ACKR1, expressed in neurons, and CCR5, expressed in lymphocytes, were identified. On the other hand, in the neuromas, interactions between the ligands CCL2 and CCL14 and the receptor encoded by ACKR1 were statistically significant. In the neuromas, CCL2 is expressed on perineurial fibroblasts (PeriF_1, PeriF_2) and CCL14 is expressed in endothelial cells (Endo_1), which might interact with ACKR1, expressed in trigeminal neurons. CCL2, also known as monocyte chemoattractant protein-1 (MCP-1) is a chemokine involved in macrophage chemotaxis which has been linked to neuropathic pain (Van Steenwinckel et al., 2011), while the role of CCL14 in chronic pain hasn’t been investigated.

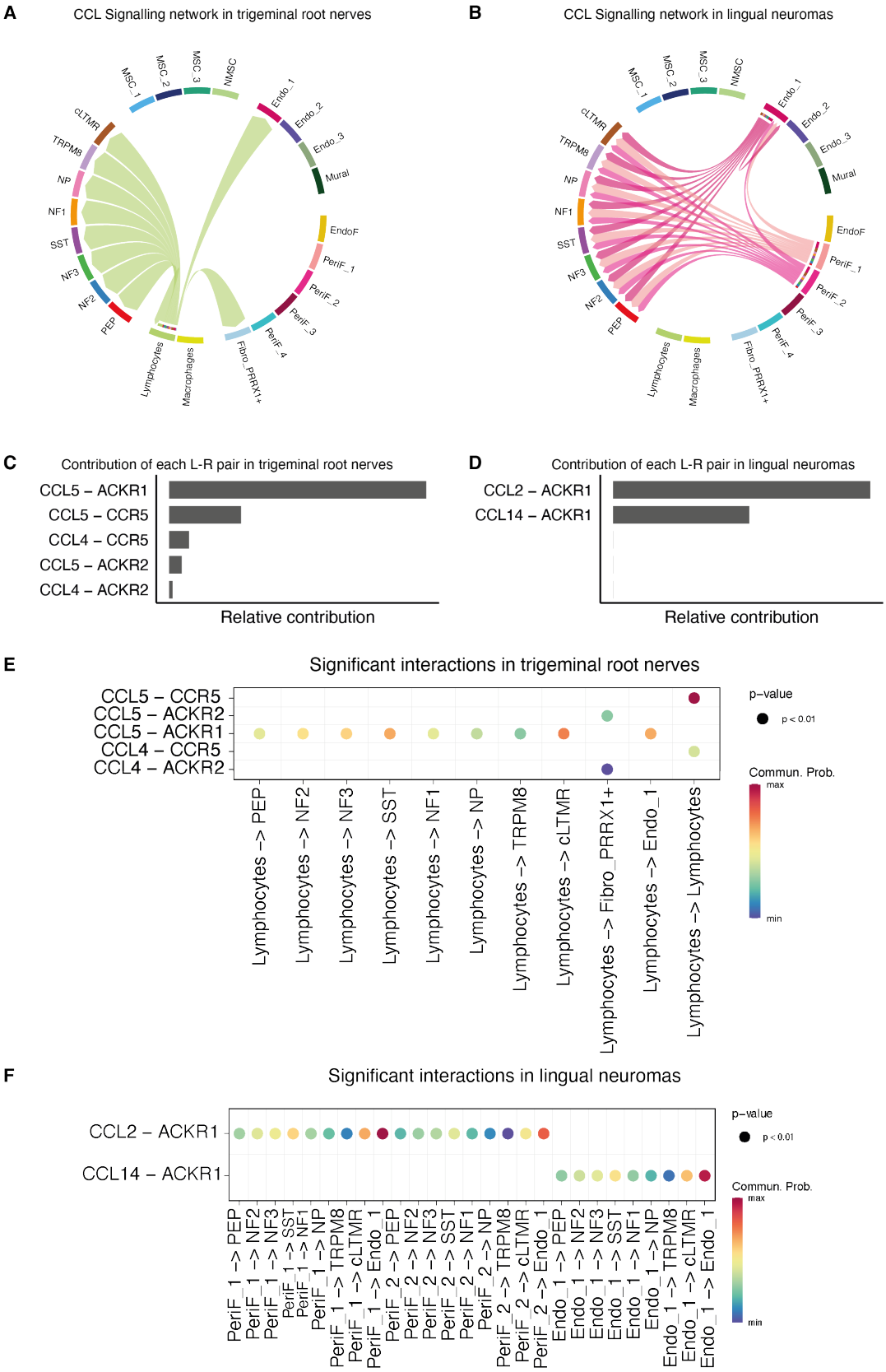

Figure 2.17. CCL signalling network in the trigeminal root nerves and the lingual neuromas.
A: Chord diagram displaying the interaction network in the CCL category in the trigeminal root nerves (A) and in the neuromas (B).
C, D: Bar plot displaying the relative contribution of each ligand-receptor (L-R) pair in the trigeminal nerve roots (C) and in the neuromas (D).

E, F: Bubble plots displaying the inferred significant L-R interactions between cell types in the trigeminal root nerves (E) and in the lingual neuromas (F).

2.4 Discussion

Single nuclei RNA sequencing highlighted the heterogeneity of cell types within the lingual neuromas and trigeminal nerve root samples which were annotated using markers from the literature. In Schwann cells and immune cells, the differentially expressed genes in naïve and injured nerves were investigated, due to the importance of these cell-types in nerve repair and peripheral sensitisation, respectively. Finally, the communication between cells in the periphery and trigeminal neurons was inferred with CellChat using the dataset of human trigeminal ganglia generated by Yang et al. (2022), focusing on the CCL and CXCL chemokine signalling due to their role in chronic pain (Jiang et al., 2020, Solis-Castro et al., 2021).

2.4.1 AP-1 transcription factor complex is upregulated in Schwann cells several months following injury

Myelinating and non-myelinating Schwann cells were identified in both sample types. Myelinating Schwann cells were further subdivided in three clusters (MSC_1, 2 and 3). Interestingly, MSC_2, which displays increased Pmp2 expression, might correspond to a myelinating SC subtype identified by Yim et al. (2022) in murine peripheral nerves which preferentially myelinates large diameter axons. In particular, Yim et al. (2022) found that $Pmp2^{+}$ Schwann cells were more likely to be associated with motor neurons, as well as $Chat^{-}$ large diameter sensory neurons in sural nerves. Further immunohistochemical validation is required to confirm this finding.

MSC_3 was found exclusively in the human neuromas and due to its expression of AATK, an apoptosis induced gene, might represent degenerating or dying Schwann cells (Gordon et al., 2019). Another highly expressed gene in this cluster, PLEKHG5, has also been linked with apoptosis through the activation of the NF-kB pathway (Witte et al., 2020).

The gene expression across Schwann cells in neuromas and trigeminal nerve roots was compared and several differentially expressed genes were identified, including FOS, FOSB, JUN, JUND and EGR1, part of the AP-1 transcription factor

family that regulates Wallerian degeneration. Additionally, inflammation-related genes were also dysregulated, including SOCS3 and EGR1 (Balakrishnan et al., 2021, Duclot and Kabbaj, 2017, Sobah et al., 2021). These findings underline the long-lasting changes in gene expression following nerve injury in Schwann cells, which can be observed even in neuromas collected 4 to 13 months following nerve injury.

Interestingly, repair Schwann cells, typically marked by NGFR and the upregulation of neurotrophic factors (Jessen and Mirsky, 2019, Lovatt et al., 2022), couldn't be identified. It has been proposed that the fading of repair Schwann cells is dependent on the downregulation of c-Jun and STAT3 (Jessen and Mirsky, 2019, Wagstaff et al., 2021). However, in this dataset, despite the increased c-Jun expression in the injured neuromas compared to the uninjured nerve roots, the repair phenotype couldn't be detected. This might be due to a bias in the dissociation method in the neuromas, where fibrotic tissue might prevent the successful dissociation of particular Schwann cell subtypes. However, it could also indicate that other mechanisms besides c-Jun downregulation are at play in the loss of the repair phenotype after long intervals following injury.

2.4.2 Fibroblasts in peripheral nerves are highly heterogeneous.

The data highlights the variety and complexity of the fibroblast subtypes present in peripheral nerves. Endoneurial, perineurial, pro-fibrotic and meningeal fibroblasts were identified based on markers from the literature. Interestingly, epineurial fibroblasts weren't detected. In the neuromas, this might be explained by the degree of nerve injury, where transection during dental surgery might have severed the epineurial sheath which never regenerated. On the other hand, in the trigeminal nerve root samples, epineurial fibroblasts are replaced by meningeal fibroblasts, as spinal and trigeminal ganglia and their roots are enclosed by the spinal and cranial meninges, respectively (Sakka et al., 2016).

Four different subtypes of perineurial fibroblasts were identified by their high level of SLC2A1 expression. In the neuromas, most of the perineurial fibroblasts belonged to the PeriF_4 cluster, which displayed a high level of expression of matricellular genes with pro-inflammatory effects such as THBS1, CCN1 and

ADAMTS14 (Emre and Imhof, 2014, Bornstein, 2009, Mead and Apte, 2018). Thrombospondin-1 (THSB-1) has been shown to promote neurite outgrowth (Hara et al., 2023, O'Shea et al., 1991), however, it has a clear role in inflammation through the interaction with CD63 and the activation of the NF-kB pathway leading to cytokine secretion (Lopez-Dee et al., 2011, Xing et al., 2017). On the other hand, in the trigeminal nerve roots, perineurial fibroblasts were equally distributed among clusters PeriF_1, 2 and 3. Further characterisation of these subtypes would be required to identify differences in their function or anatomical distribution.

Interestingly, in this dataset, NGFR is found primarily in perineurial, rather than endoneurial, fibroblasts, as observed in mice peripheral nerves (Chen et al., 2021, Yim et al., 2022). There is evidence in the literature of NGFR expression in perineurial cells of human and rat nerves; in particular, increased NGFR immunoreactivity was observed in injured nerves distal to the site of injury (Yamamoto et al., 1992). Chau et al. (2022) also noted NGFR expression in a cluster which contained perineurial cells, but annotated it as a heterogeneous cell cluster; however, considering that the samples in Chau et al. (2022) are derived from injured sural nerves, it is likely that the perineurial cells in that dataset would express high levels of NGFR and therefore this cluster should be annotated as perineurial. The expression of NGFR at the protein level in GLUT-1^{+} cells will be validated in Chapter 4.

Another interesting finding is that PI16 is enriched in endoneurial fibroblasts cluster, marked by CSPG4 expression (Richard et al., 2014). PI16 has been proposed as a regulator of neuropathic pain and its expression was observed in perineurial fibroblasts in murine sciatic nerves (Singhmar et al., 2020). However, in the present dataset, PI16 is markedly expressed in endoneurial fibroblasts, which represents a potential species difference. This observation will be further investigated in Chapter 4.

Finally, a fibroblast cluster particularly abundant in the neuromas was characterised by high PRRX1 expression, as well as high expression of ECM-related genes such as COL1A1, FBLN1, COL5A3 and FOSB, involved in fibrosis (Cui et al., 2020). Prrx1+ fibroblasts were recently defined as a profibrotic lineage in the mouse ventral dermis (Leavitt et al., 2020). Targeting this fibroblast population when nerve

injury is suspected during surgical procedures or at the time of nerve repair might be a promising route for the prevention of neuroma formation.

2.4.3 The expression of AP-1 TF family members in immune cells from lingual neuromas

Amongst the immune cells, two main clusters were identified: one comprising myeloid cells, which broadly include resident and monocyte-derived macrophages, as well as dendritic cells and mast cells, and another including T and B lymphocytes. There was a higher proportion of lymphocytes in the trigeminal nerve roots than in the neuromas (0.97% and 0.69%, respectively). It would be expected to detect a higher proportion of T cells in injured nerves, as T cells are known to be present to a very low number in naïve nervous tissue, while injury triggers their infiltration which is thought to contribute to neuropathic pain (Galvin and C, 2021). Similarly, myeloid cells make up 5% of the trigeminal nerve roots but only 1% of the neuromas. Due to the small number of immune cells isolated, a more detailed characterization of further subtypes, such as endoneurial and epineurial macrophages, neutrophils, dendritic cells, mast cells and T or B lymphocytes was impossible.

Myeloid cells and lymphocytes from neuromas and trigeminal nerve roots display several differentially expressed genes. Members of the AP-1 complex FOS, FOSB, JUN, JUND are upregulated in the neuromas, in agreement with Li et al. (2021), who have shown that the AP-1 TF family is upregulated in immune cells following nerve injury. Additionally, several inflammation related genes are upregulated in the neuromas, including NLRP3, EGR-1 and KLF4 and 6. The leukocytes in the trigeminal nerve display an upregulation of cytokines such as CCL5 and chemokine receptors such as CXCR4, previously identified in the literature to affect nerve regeneration (Hilla et al., 2021, Xie et al., 2021).

2.4.4 Expansion of vascular cell types in the neuromas

There is a marked difference in the proportion of endothelial and mural cells detected in the two sample types: 30% of nuclei are annotated as endothelial and 8% as mural in the neuromas, whereas in the trigeminal nerve roots 3% and 1% were annotated as endothelial and mural cells, respectively. This might be due to

several factors, both biological and technical. A biological explanation might be that neuroma formation might be accompanied by increased vascularization, as tissue injury, repair and inflammation are linked with angiogenesis (DiPietro, 2016). Technical factors include the inclusion of neighbouring tissue types in the neuromas with a high vascular content, such as muscle tissue, and the dissociation method that might be biased against Schwann cell isolation in highly fibrotic tissues such as the neuromas, potentially leading to a higher proportion of cells being vascular in nature.

Half of the vascular cells annotated in the neuromas belong to Endo_1 (20% of total nuclei), while in the trigeminal nerve roots only 0.7% of total nuclei are classified in this cluster. Endo_1 is characterised by the expression of cytokine-activated genes such as ICAM-1, SELE and IL-6, which play a role in inflammation and leukocyte infiltration (Bui et al., 2020, Wu et al., 2017). On the other hand, in trigeminal nerve root samples, the majority of endothelial cells are clustered in Endo_3, which express typical endothelial cell markers such as FLT-1, VWF and A2M (Lovatt et al., 2022).

2.4.5 Chemokine signalling and the atypical chemokine receptor 1

Investigating the potential cell-cell communication taking place between neurons and cells at the periphery represents an interesting route to generate new hypothesis on how the cellular microenvironment might contribute to peripheral sensitisation. Nerve injury leads to the secretion of pro-inflammatory mediators from axons, Schwann cells and immune cells that promote debris clearance and regeneration, but may also lead to inflammation and peripheral sensitisation, resulting in changes in gene expression and neuronal hyperexcitability (Chapter 1). It was decided to focus on the CCL and CXCL chemokine signalling, due to its relevance in peripheral sensitization and chronic pain development (Jiang et al., 2020, Solis-Castro et al., 2021).

To infer cell-cell communication with sensory neurons, the dataset generated by Yang et al. (2022), which includes trigeminal neurons from healthy donors, was used. The neurons from this dataset haven't been exposed to the sensitizing pro-inflammatory milieu that results from peripheral nerve injury, therefore they are in a

naive state and lack the expression of several chemokine and cytokine receptors, which might be, on the other hand, upregulated following injury (Miller et al., 2009).

Nevertheless, the trigeminal neurons from Yang et al. (2022) did express a variety of chemokine receptors, including CCR5, ACKR1, ACKR3, CXCR4 and CXCR6, which might potentially interact with chemokines secreted by cell types in the periphery. Of interest, in the neuromas, CXCL8 is expressed in macrophages and might interact with ACKR1 in the trigeminal neurons. Interestingly, the main CXCL8 receptor, CXCR2, was shown to be upregulated in trigeminal sensory neurons following itch induction producing sensitization (Li et al., 2023a).

While few chemokine receptors are expressed in the unsensitised naïve trigeminal neurons, the atypical chemokine receptor ACKR1, which can bind to several chemokines (CCL2, 5, 7, 11, 13, 14, 17; CXCL5, 6, 8, 11) (Bonecchi and Graham, 2016), is expressed on both naïve trigeminal and dorsal root ganglia sensory neurons, and particularly enriched in putative silent nociceptors (Tavares-Ferreira et al., 2022b). ACKR1 has been studied in the context of erythrocytes and malaria infection (Horuk, 2015), while a global knockout highlighted its effect on motor coordination and anxiety, through negative regulation of Purkinje cells in the cerebellum (Schneider et al., 2014). The receptor is termed atypical since it doesn't elicit GPCR-mediated intracellular signalling cascades; instead, it acts by scavenging chemokines, thereby reducing local inflammation and preventing leukocytes extravasation (Horuk, 2015). However, one might wonder what would happen in the context of peripheral nerve injury, where ACKR1 on sensory neurons might potentially scavenge an increasing number and variety of chemokines. Would ACKR1-mediated chemokine scavenging by sensory neurons reduce peripheral inflammation? Are the internalised chemokines inert or could they activate internal signalling pathways leading to peripheral sensitization in the sensory neurons? These questions warrant further investigation; but first, validation of ACKR1 expression in peripheral axons is required.

2.4.6 Limitations of the study

This study generated a large amount of data from rare human samples of naïve and injured trigeminal nerves, that could be of use to several researches in the field

of pain and nerve regeneration. However, some limitations should be recognised. Only two neuromas and two trigeminal nerve roots were used, while usually, a minimum of three biological replicates are required to make comparisons across different conditions. Due to the rarity of peripheral nerve samples, it is still useful to observe changes in gene expression in injured and naïve samples; however, in the future, a larger pool of samples should be included. Nevertheless, single cell atlases even in a small number of samples are still beneficial, as they can be integrated with spatial and bulk RNA sequencing data generated on a larger pool of samples to deconvolute cell type composition (Avila Cobos et al., 2020), as will be performed in the next chapter.

In this study, trigeminal nerve roots were used as an uninjured control to be compared to injured lingual neuromas. Ideally, healthy lingual nerves from age and sex-matched individuals would have been used as a healthy control, allowing the clear identification of differences linked with injury status. The comparison with trigeminal nerve roots prevents the clear attribution of the differences found with the neuromas to the injury state, as they could also be associated with the different anatomical location of the samples, as well as the differences in ages and sex of the donors. Other control tissues were considered for the study, such as sural nerves from organ donors, but they were deemed unsuitable due to their spinal origin and the extensive length of their axons, which would also underpin differences in gene expression and cell-type composition. Ultimately, due to the scarcity of the relevant control tissue types, the comparison with trigeminal nerve roots was deemed as the best option available, and yielded fruitful comparisons and several avenues that warrant further investigation. As relevant datasets are generated and made available in the literature, they can be integrated and compared with the one presented here.

2.4.7 Conclusion

The RNA expression at single cell level in human trigeminal nerve roots and injured lingual neuromas was investigated with single nuclei RNA sequencing, in order to characterise the cellular composition of trigeminal nerves in healthy and injured conditions and identify changes in gene expression. The data highlights the sustained expression of genes part of the AP-1 transcription factor family in both

Schwann cells and immune cells following injury, as well as the heterogeneity of fibroblast subtypes that support peripheral nerves. This dataset represents a useful resource for researchers in the field of orofacial pain and nerve regeneration, as well as to the pharmaceutical industry, enabling the expression of drug targets identified in animal models or in genomic studies to be verified in human tissue.

Chapter 3. Identifying novel targets for the treatment of neuropathic pain using spatial transcriptomics

3.1 Introduction

In this chapter, the transcriptome of human lingual neuromas from patients with and without symptoms of neuropathic pain will be analysed within the context of the tissue morphology using spatial transcriptomics.

A fundamental question in the field of pain is why in certain individuals the acute pain caused by tissue injury or disease transitions to chronic pain, while in others, affected by the same injury or disease, this transition doesn't occur (Costigan et al., 2009). Human lingual nerve neuromas obtained from nerve repair surgeries provide a valuable opportunity to answer this question, as patients are affected by the same type of nerve injury, but only a minority develops neuropathic pain (Atkins and Kyriakidou, 2021). This enables the identification of changes at the molecular and cellular level that correlate with the presence of pain and are unrelated to the pathophysiological mechanisms underlying nerve regeneration. The correlation between symptoms of pain and the expression of specific proteins, such as $Na_v1.7$, $Na_v1.8$, $Na_v1.9$, P2XR, TRPV1 and TRPA1, as well as miRNAs, has been previously investigated in our laboratory (Bird et al., 2007, Morgan et al., 2009b, Morgan et al., 2009a, Bird et al., 2013, Biggs et al., 2007, Tavares-Ferreira et al., 2019). However, the unbiased analysis of whole transcriptome in human neuromas hasn't been performed yet and will be the focus of this chapter.

3.1.1 Methodological considerations

A commonly used and cost-effective method to analyse whole transcriptome is by bulk RNA sequencing, where the RNA content of the homogenised tissue is isolated, reverse transcribed and sequenced, obtaining an averaged count of each RNA species in the whole tissue (Stark et al., 2019). A pilot study using bulk RNA sequencing was performed on the neuromas (not discussed in this thesis) but yielded disappointing results stemming from the difficulty of isolating RNA from such highly fibrotic tissue. The resulting RNA was highly degraded and of low

abundance, as a result of the harsh mechanical and chemical dissociation required to extract the RNA. While the protocol could have been further optimised to improve the quality of RNA, spatial transcriptomics methodologies that enabled the analysis of RNA content in the spatial context were advancing. Visium spatial transcriptomics provided a highly validated method with demonstrated efficacy in fixed clinical samples to measure gene expression within the spatial context of the tissue (Gracia Villacampa et al., 2021). Importantly, this method, unlike bulk RNA sequencing, enabled the analysis of pathologically relevant areas such as the nerve fascicles, excluding other tissue types present in the neuromas such as muscle and fibrotic tissue.

3.1.2 Spatial transcriptomics to identify the transcriptional profile within the morphological context of human neuromas.

Spatial transcriptomics refers to the measurement of RNA transcripts of several genes within the spatial context of the tissue or cells. In recent years, technical advances have evolved rapidly and several commercially available methods can be used to detect hundreds or thousands of transcripts at variable resolution (Moses and Pachter, 2022). Currently, several options for spatial transcriptomics are available with variable resolution, number of transcripts that can be detected, cost-effectiveness and extent of optimization required. *In situ* hybridisation-based technologies such as MERFISH (Chen et al., 2015) or seqFISH+ (Eng et al., 2019) enable the subcellular visualization of individual transcripts based on their detection with probes, where probe panels are limited to a restricted number of targets (up to 10,000 targets in MERFISH) (Yue et al., 2023). In situ sequencing based technologies rely on the reverse transcription of RNA within the tissue, for example through the use of padlock probes and rolling circle amplification (Ke et al., 2013), commercialised by 10X Genomics with the Xenium platform. Next Generation Sequencing (NGS)-based technologies include 10X Genomics Visium (Ståhl et al., 2016), Slide-seq and Slide-seqV2 (Stickels et al., 2021) and stereo-seq (Chen et al., 2022), which are based on the capture of RNA molecules in a barcoded area, reverse transcribed and sequenced by NGS. The spatial location is inferred based on the barcode attached to each transcript with computational analysis. These technologies enable the high-throughput untargeted analysis of the whole

transcriptome but are limited by the resolution of each barcoded area, which started off as 100 μm in Ståhl et al. (2016) and has now reached 500 nm with Stereo-seq (Chen et al., 2022), with the drawback that more sequencing is required, increasing costs. Finally, other methods to obtain transcriptomic information within a spatially-defined area involve the selection of areas of interest, for example with laser dissection microscopy (Brown et al., 2002) or with the GeoMX Digital Spatial Profiling (Merritt et al., 2020).

For this project, the unbiased profiling of the whole transcriptome was a priority, rather than the use of selected probes, therefore an NGS-based method was chosen over targeted methods. Pilot in situ hybridization experiments at the start of the project highlighted tissue autofluorescence as a significant issue for image-based techniques, such as MERFISH (Xia et al., 2019). Therefore, an NGS method targeting the whole transcriptome was deemed the most suitable. After considerations of cost-effectiveness, Visium spatial transcriptomics was chosen above other technologies commercially available at the time, such as the GeoMX DSP, due to the increased cost-effectiveness for the analysis of large areas of tissue. Additionally, Visium had been validated in FFPE clinical samples, characterised by lower RNA quality compared to fresh-frozen samples, taking advantage of probes targeting the whole transcriptome that would enable the detection of RNA in fixed and slightly degraded samples (Gracia Villacampa et al., 2021).

The main limitation of Visium is the size of the barcoded spots, which limits its resolution at 55 μm. However, by integrating single nuclei RNA sequencing data discussed in Chapter 2, information at single cell resolution can be inferred in a process known as cell-type deconvolution (Li et al., 2023b). This approach has its drawbacks and limitations since the cellular composition is virtually inferred from a similar but separate tissue. Nevertheless, the combination of these techniques enables the detection of the cellular populations within a sample in the spatial context, providing valuable insight in the cellular and transcriptional composition of human neuromas.

3.1.3 Aims and objectives

The overall aim of this chapter is to characterise the cellular and transcriptional composition of human neuromas within the spatial context and identify genes differentially expressed in human neuromas from patients with and without pain. The specific objectives were:

1. Perform clustering analysis to identify patterns in the spatial distribution of gene expression across samples.
2. Integrate the single nuclei RNA sequencing data to perform cell-type deconvolution in the spatial transcriptomics dataset.
3. Perform pseudo-bulk differential expression analysis of pathologically relevant areas between painful and non-painful samples.
4. Validate the trends displayed by the top differentially expressed genes in the single nuclei RNA sequencing data.

3.2 Methods

3.2.1 Human Lingual Neuroma Processing

Lingual neuromas were obtained from patients attending the trigeminal nerve injury clinic at the Clifford Dental Hospital in Sheffield, UK. Neuromas were collected during nerve repair surgery, carried out by Dr. Simon Atkins. All neuromas were collected with the informed consent from the patients, in accordance with ethical approvals received by the NHS Health Research Authority (HRA) and Sheffield Teaching Hospitals (STH) (19/SC/0308 STH20664). Clinical information including patients' age, sex and pain history was recorded preoperatively and anonymised. Patients reported the symptoms of pain, tingling and discomfort on the day of surgery on a visual analog scale (VAS) ranging from 1 to 100. Based on the pain VAS scores, the neuromas chosen for this study were divided in two groups: 'painful' (pain VAS score higher than 40) and 'non-painful' (pain VAS score lower than 15). Differences in VAS scores between painful and non-painful groups were evaluated using an unpaired t-test assuming equal variance.

After surgical removal, the samples were placed in Zamboni's fixative (0.1 mol/L phosphate buffer, pH 7.4, containing 4% paraformaldehyde and 0.2% picric acid)

and fixed overnight at 4°C, then transferred to 30% sucrose overnight at 4°C and finally cryoprotected in OCT and stored at -80°C.

3.2.2 Assessment of RNA quality in samples for Visium

To assess the suitability of the samples for spatial transcriptomics, total RNA was extracted from a few sections of each sample with the RNeasy FFPE kit (Qiagen, 73504), according to the manufacturer instructions. The incubation with the deparaffinization solution was omitted since the samples weren't embedded in paraffin. Briefly, 6-10 sections were cut using a cryostat and placed in a pre-chilled Eppendorf tube. Buffer PKD was added to the sections and vortexed to lyse the sample. Formaldehyde bonds were decrosslinked by incubating the lysate with proteinase K at 56°C and at 80°C for 15 minutes respectively. The mixture was incubated on ice for 3 minutes, then centrifuged for 7.5 minutes at 20,000 x g. DNase Booster buffer and DNase I were added to the sample, mixed and incubated for 15 minutes to ensure DNA degradation. Buffer RBC was added to the sample to adjust binding conditions, then 100% ethanol was added and transferred to the RNeasy MinElute spin column. The RNA was captured on the column, washed twice with buffer RPE and eluted in 14 µl of RNase-free water.

The quality of the RNA was assessed using the Bioanalyzer RNA 6000 Pico chip (Agilent, 5067-1513). Samples with a DV200 higher than 50, indicating that more than 50% of the ribonucleic acids are 200 nucleotides or longer, were deemed to be of satisfactory quality to proceed with the Visium protocol. Some examples of the Bioanalyzer traces are shown in Figure 3.1. The adherence of the tissue sections from a few samples was tested using the tissue adherence test slides (10X

Genomics, 1000347).

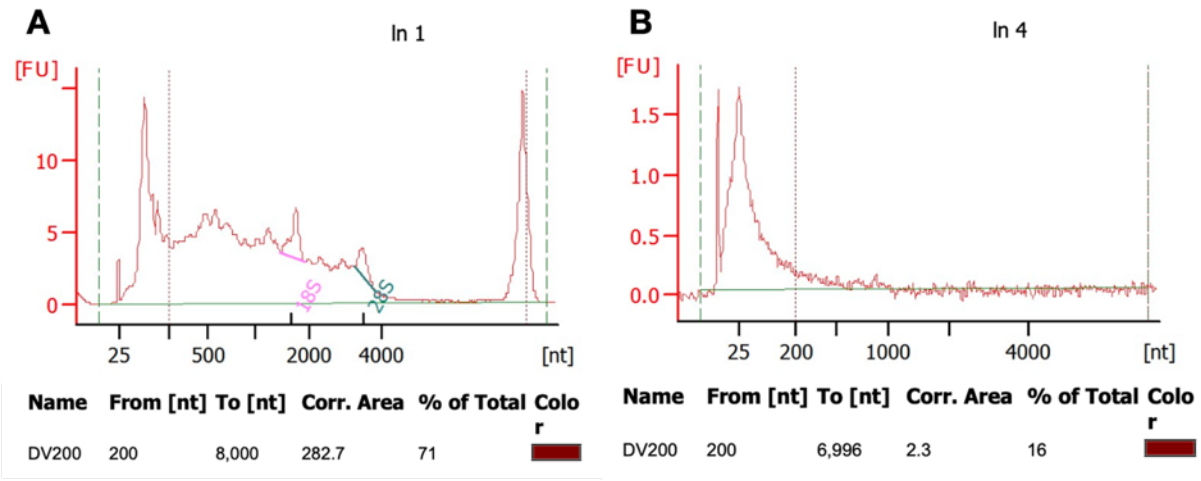

Figure 3.1. Example Bioanalyzer traces of RNA extracted from fixed-frozen human neuromas to assess the samples' suitability for Visium spatial transcriptomics.
A, B: The image summarises the result of the RNA quality assessment with the Bioanalyzer of two samples of human neuromas. In the graphs, the fluorescence units (FU) are plotted against the size distribution of the RNA molecules in nucleotides (nt). The DV200 calculated by the Bioanalyzer estimates the proportion of RNA molecules longer than 200 nt, marked by the dotted brown line. The presence of peaks for ribosomial RNA (18S and 28S in A) is another positive indicator of RNA quality. The sample in A has a DV200 of 71, therefore 71% of RNAs are longer than 200 nt and is suitable for Visium. On the other hand, in the sample shown in B, only 16% of the RNA molecules are longer than 200, making the sample unsuitable for Visium due to the poor RNA quality.

3.2.3 Spatial Transcriptomics

Spatial transcriptomics was performed with the Visium Spatial Gene Expression for FFPE kit for the Human Transcriptome (10X Genomics, 1000338). An overview of the protocol is shown in Figure 3.2, all reagents used are listed in Table 3.1. Briefly, fixed-frozen sections of human neuromas embedded in OCT were sectioned at a thickness of 7 µm, placed on the capture areas of Visium slides and dried for 45 minutes. Deparaffinization was omitted and the sections were stained with haematoxylin and eosin (H&E) following manufacturer's instructions. The slides were mounted with 100% glycerol and cover-slipped without sealing. The tissue sections were imaged through the glass slide with a Leica Thunder DMi8 inverted microscope equipped with a FlexaCam C1 Camera system at 10X magnification. Tile-scans were merged using the Leica Application Suite X (LAS X) software. The coverslip was removed and the slide was placed in the Visium cassette (shown in

Figure 3.3), sealing each capture area and enabling the localized administration of liquid solutions over each section. Decrosslinking for 1 hour at 70°C with TE

buffer was performed to reverse the formaldehyde bonds and expose the nucleic acids. The sections were hybridised overnight with probes targeting the whole human transcriptome: 19,144 genes are targeted by the probe set, 17,943 genes without off-target activity are filtered and present in the final output. After probe hybridization, stringent washes with 2X SSC were performed to remove non-specifically bound probes. Then, the left-handed and right-handed probes were ligated with a ligase enzyme and the RNA was digested to allow the release of the probes, which were captured by the oligos present on the surface of the Visium slide. The probes were extended to incorporate the unique molecular identifier, the spatial barcode information and the TruSeq Read 1 index. The extended probes were eluted in 0.8M KOH and transferred to PCR tubes. Quantitative PCR was performed on 1 µl of each library with the KAPA SYBR FAST qPCR Master Mix (Merck, KK4600) to estimate the number of PCR cycles required to amplify each library. Library amplification was performed with a unique 10X Sample Index from the Plate TS Set A (10X Genomics, PN-1000251) for each sample. The library was then cleaned using SPRIselect magnetic beads, removing short fragments, consisting in primer dimers or singlet probes, that would take up sequencing reads (Beckman Coulter, B23317). Quality control was performed with the High Sensitivity DNA kit (Agilent, 5067-4626) on a Bioanalyzer. The libraries were sequenced on a NovaSeq 6000 S4 platform with 2x150 cycles (PE150) by Novogene Co., Ltd. The minimum sequencing depth required was 25,000 reads per spot covered by tissue, which was estimated by uploading the H&E images in Loupe browser (10X Genomics), manually selecting the area covered by tissue and multiplying the number of spots counted by the software by 25,000, as recommended by the manufacturer.

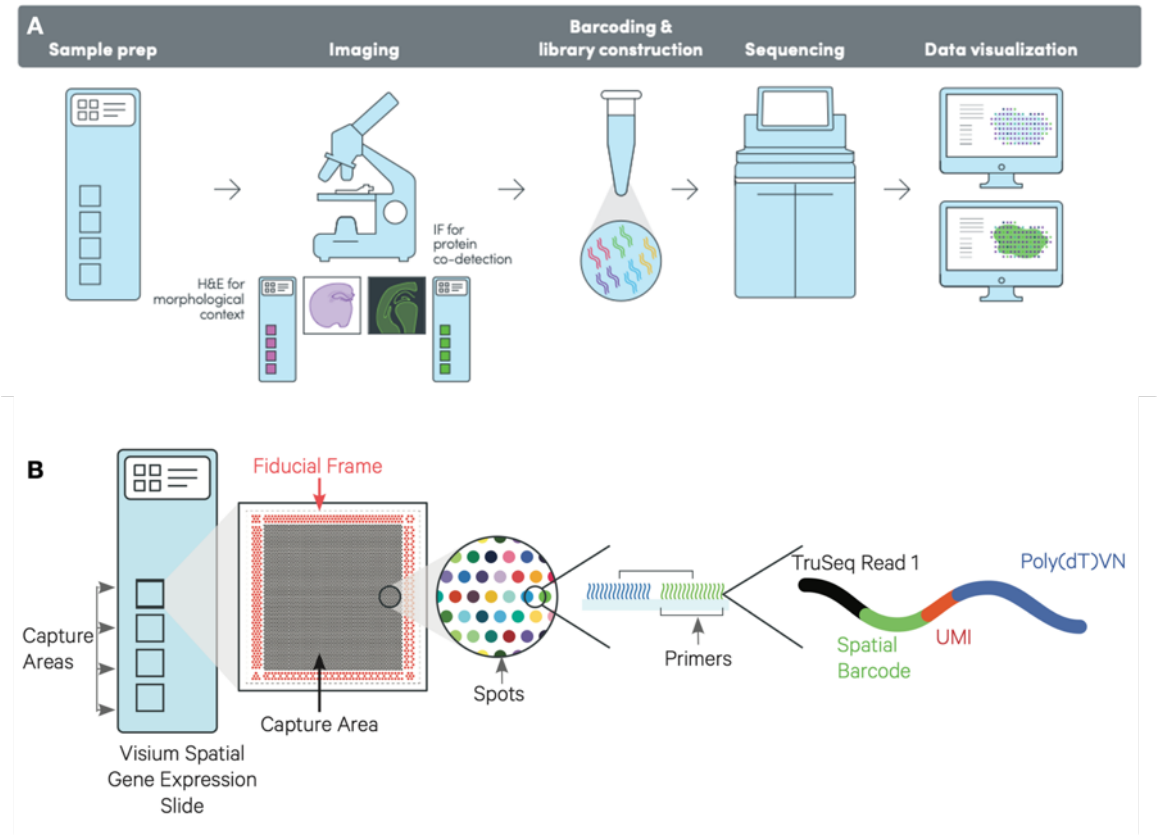

Figure 3.2. Overview of the spatial transcriptomics protocol.
The diagrams summarise the spatial transcriptomics protocol by 10x Genomics. The sections are placed on the capture areas and stained with H&E, imaged and hybridised to probes targeting the whole transcriptome. The hybridised probes are captured by the barcoded oligos shown in panel B, which tag them with a spatial barcode that enables the localization of each transcript on the tissue section following sequencing and data processing. Diagrams are obtained with permission from 10X Genomics' user manual.

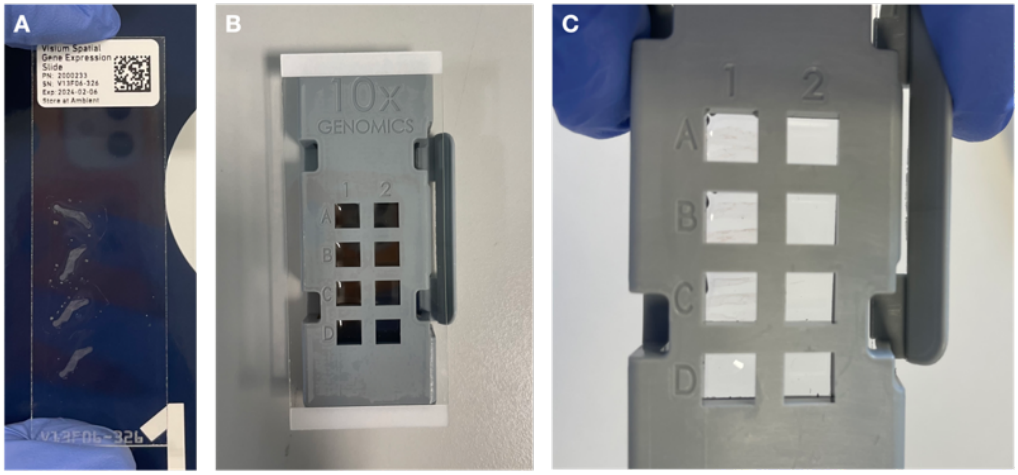

Figure 3.3. Placement of the tissue on the Visium gene expression slide.
Images showing the placement of tissue sections on the capture areas of the slide (A), the slide placed in the sealed cassette (B) and the sections in the capture areas incubating in the cassette (C).

Table 3.1. List of reagents used in the spatial transcriptomics experiments.

Item	Vendor	Product code
Visium Spatial for FFPE Gene Expression Kit, Human Transcriptome, 4 rxns	10x Genomics	1000338
Invitrogen Utrapure RNase/DNase free water	Fisher Scientific	10977035
DNA LoBind Tubes	SLS	EP0030108051-250EA
RNeasy FFPE kit	Qiagen	73504
Visium Accessory kit	10 X Genomics	1000194
Visium Tissue Section test Slides, 4 Slide Pack	10 X Genomics	1000347
Dual Index Plate TS Set A, 96 rxns	10 X Genomics	1000251
Eosin Y-solution, Alcoholic	SLS	HT110116
Haematoxylin Solution According to Mayer	Merck	51275
TE Buffer	Fisher	12090015
Tris 1 M	Fisher	AM9850G
10x PBS	Fisher	AM9624
KAPA SYBR FAST qPCR master mix 2x	Merck	KK4600
SPRIselect Reagent kit	Beckman Coulter	B23317
8 M KOH	SLS	P4494-50ML
20x SSC	SLS	S6639-1L

3.2.4 Data Analysis

Sequencing files in fastq format were processed with Spaceranger (10X Genomics) to align the reads to the human reference assembly GRCh38 and process H&E images to align the fiducial frame and detect the tissue. Downstream processing was performed with the R packages Giotto, Seurat, PCAtools and DEseq2. The analysis consisted in three main workflows, summarised in Figure 3.4.

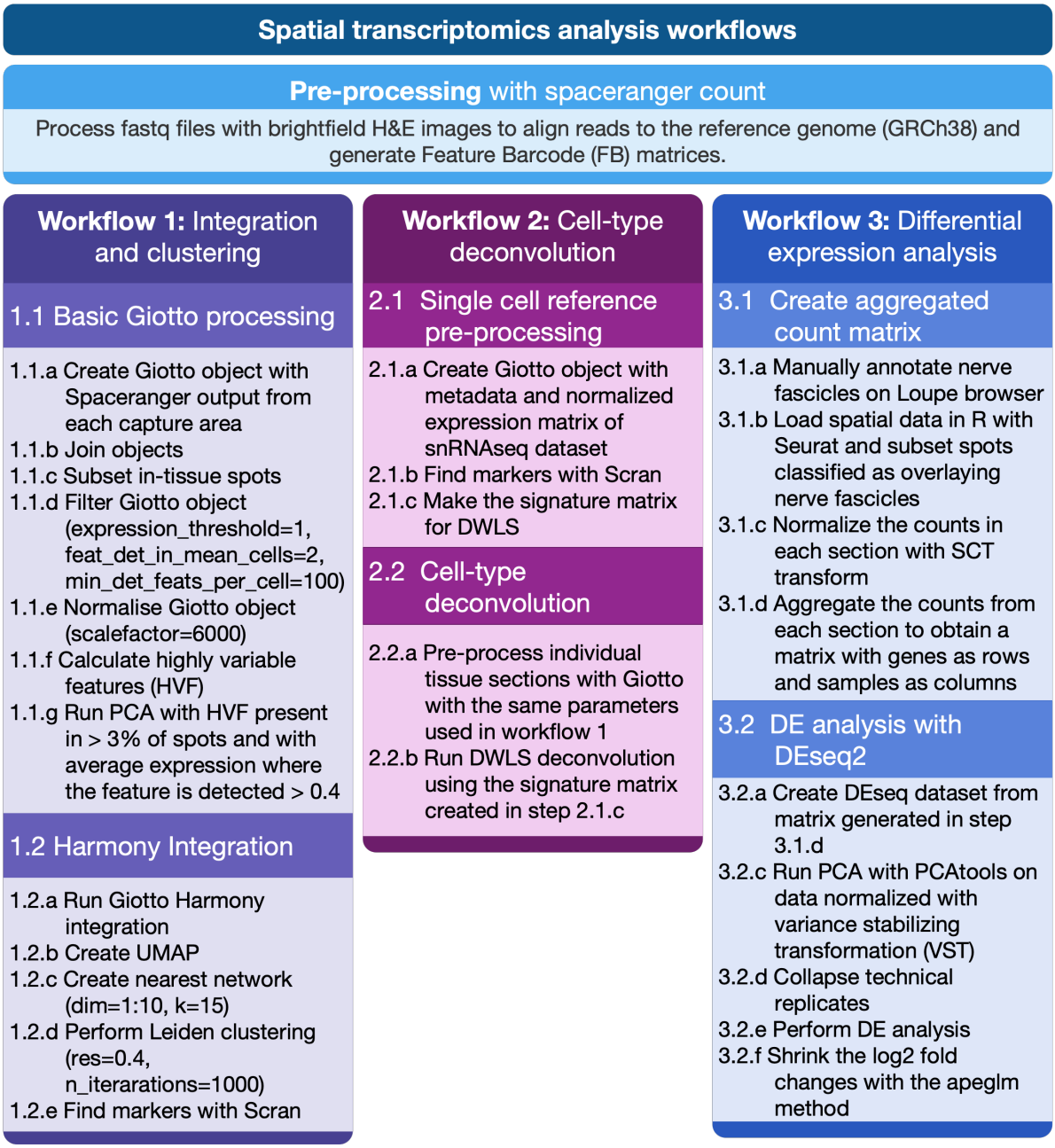

Figure 3.4 Workflows for the analysis of the Visium experiments on the human lingual nerve neuromas.
The diagram summarises the workflows used for the analysis of Visium spatial gene expression data on the human neuromas. The aim of Workflow 1 was to perform an integrated clustering analysis across all samples, in order to identify cell type enrichment signatures. The aim of Workflow 2 was to integrate the single nuclei RNA sequencing data discussed in Chapter 2 with the spatial transcriptomics data and perform cell-type deconvolution. The aim of Workflow 3 was to perform differential expression analysis between painful and non-painful samples.

3.2.4.1 Integration and clustering with Giotto

All sections were processed with the R package Giotto (Dries et al., 2021). The Giotto objects for each section were merged, genes were filtered so that the expression threshold would be 1 and they were detected in a minimum of two

spots, while spots with less than 100 genes were excluded. The sections were normalised with a scale factor of 6000. Highly variable features were calculated with the calculateHVF() function. PCA was performed with the runPCA() function using the highly variable features expressed in more than 3% of spots with a mininum average detection threshold of 0.4. The sections were integrated using the Harmony package with the runGiottoHarmony() function. The UMAP representation was calculated with the runUMAP() function, the nearest neighbour graph was mapped with createNearestNetwork() with the first 10 harmony dimensions and clustering was performed with doLeidenCluster() at resolution 0.4 with 1000 iterations. Marker genes for each cluster were calculated with find_markers_one_vs_all() using the scran method on the normalized gene expression values.

3.2.4.2 Cell-type deconvolution with SpatialDWLS

Several methods have been developed to perform cell-type deconvolution on spatial transcriptomics datasets using single cell datasets generated on the same or similar type of tissue as a reference, as reviewed and benchmarked in Li et al. (2022a) and Li et al. (2023b). SpatialDWLS (dampened weighted least squares) was chosen as it consistently performed well across simulated and real-world datasets without requiring large computing resources (Dong and Yuan, 2021). Spatial DWLS is implemented in the Giotto package and was adapted from a method developed to estimate cell-type composition from bulk RNA sequencing experiments (Tsoucas et al., 2019), whereby each spot is treated as a bulk RNA sequencing experiment, with extra steps to adjust for the fewer cells that can be present within a spot of a Visium slide (5-10 cells). SpatialDWLS involves a first round of deconvolution using enrichment analysis with the Parametric Analysis of Gene Set Enrichment (PAGE) method to identify the cell types that are likely to be present in each spot, followed by a second round of deconvolution using the DWLS method to infer the composition of the cell-types using a weighted least square to minimise the overall relative rate (Dong and Yuan, 2021).

To achieve this, a reference single cell dataset on the same or similar type of tissue is required: in this case the snRNAseq dataset generated in chapter 2 was used for this purpose. To create the reference dataset, the expression matrix normalized with Seurat as described in section 2.2.5 and the associated metadata

containing cell-type annotation was loaded in Giotto and DE genes were calculated with findMarkers_one_vs_all() using the Scran method. The top 10 markers of each cluster were used as the signature gene list to create the reference matrix for DWLS. Cell-type deconvolution was performed with runDWLSDeconv() on each individual tissue section processed with Giotto using the parameters described in the previous section. In 18% of the samples (3 technical replicates of LN1, one replicate of LN7 and one replicate of LN13), the function wasn't able to run, outputting the error message 'matrix D in quadratic function is not positive definite!'. The root cause of this error couldn't be identified.

3.2.4.3 Differential expression analysis with DEseq2

The feature count matrices in h5 format were loaded in R with the package Seurat (Hao et al., 2022). In order to subset the barcodes associated with nerve fascicles, the data was accessed on Loupe browser (10X Genomics). The spots overlapping nerve fascicles were manually selected and exported as a comma-separated file format. Barcodes classified as containing nerve fascicles were selected as shown in Figure 3.5. When multiple sections were placed on the same capture area, the nerve fascicles from each section were classified as separate technical replicates. The counts from each section were aggregated for pseudo-bulk differential expression analysis, performed with DEseq2 (Love et al., 2014).

The DEseq dataset was created with the function DESeqDataSetFromMatrix(), including pain status (P if pain VAS>30, NP if pain VAS <30) in the design formula and sex as a covariate, using the unnormalized counts from the Seurat object. The replicates from each sample were collapsed using the DEseq2 function collapseReplicates(). After performing variance-stabilizing transformation with the vst() function from DEseq2, principal component analysis (PCA) analysis was conducted with the package PCAtools to summarize the data and investigate correlations of the principal components with clinical information (Blighe, 2019). The correlation of the PCs with clinical information was performed with the function eigencorplot(), using the Pearson correlation method with multiple hypothesis testing correction with the FDR method.

DE analysis was performed with the DESeq() function from DEseq2 as described by Love et al. (2014). The logarithmic fold changes (LFC) were shrunk with the

approximate posterior estimation for generalized linear model (apeglm) method to reduce the variance of LFCs caused by low or variable gene counts (Zhu et al., 2019). Genes with an adjusted p-value lower than 0.05 were deemed to be differentially expressed. The volcano plot and graphs of normalized counts were generated with the R package ggplot, while the heatmap was generated with the R package pheatmap and the visualization of single nuclei and spatial data was generated with Seurat.

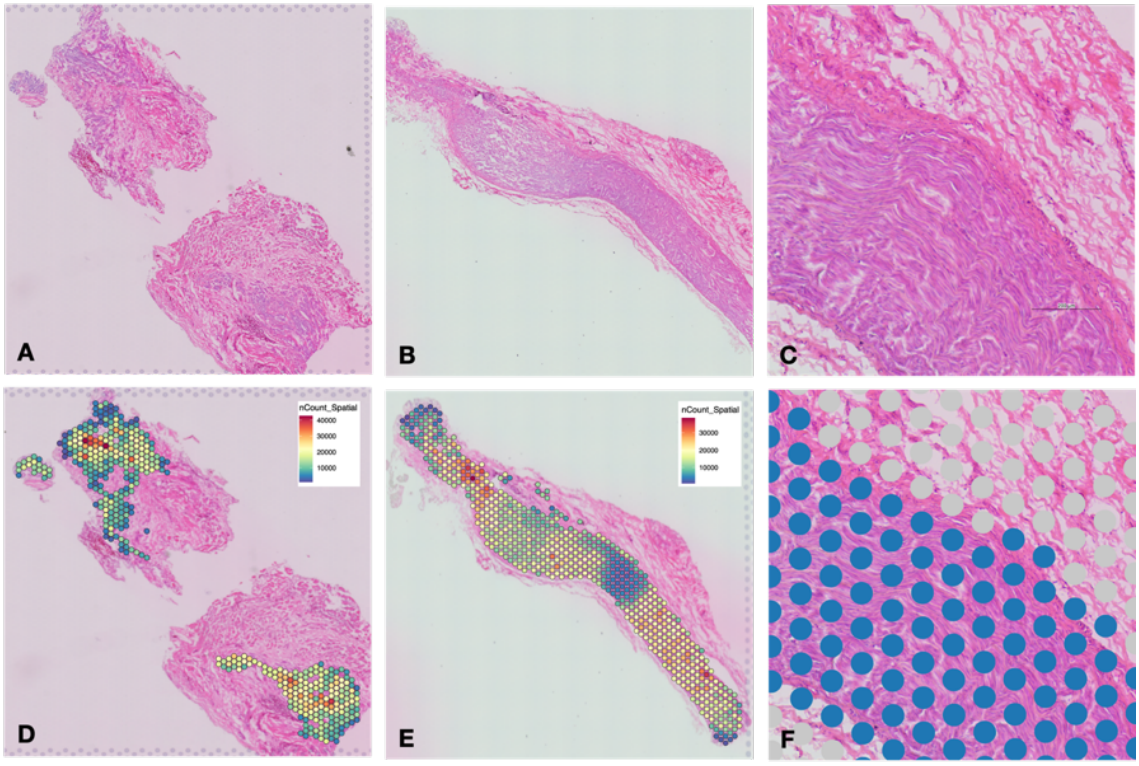

Figure 3.5. Annotation of the nerve fascicles using H&E images on Loupe browser. Nerve fascicles identified with the H&E staining were manually selected on Loupe browser and exported on Seurat to perform pseudo-bulk differential expression analysis. H&E images of two samples are shown in A and B. The spots overlapping the nerve fascicles are shown in D and E, colour-coded by the number of UMIs detected. One sample is magnified in C and F, where the spots overlapping nerve fascicles are displayed in blue.

3.2.4.4 Validation of DE genes with the single nuclei RNA sequencing data

In Chapter 2, single nuclei RNA sequencing (snRNAseq) data of human lingual neuromas and trigeminal nerve roots was presented. The human neuromas were obtained from a patient reporting pain (N2, VAS=65) and one reporting no pain (N1, VAS=0). For more clinical information, the reader can refer to Table 2.3 in Chapter 2. In order to assess whether the genes that were identified as differentially expressed in the spatial dataset display a similar trend of expression in the painful and non-

painful samples analysed with snRNAseq, their fold change was compared. The most highly DE genes identified with DEseq2 ($p<0.01$, $LFC>1.33$) were selected, the expression of these genes in the samples used for snRNAseq was summed across all nuclei and normalised with Seurat's function AggregateExpression(), using the normalization method "LogNormalize". The log fold change (LFC) of expression of each DE gene between the two samples analysed with snRNAseq was calculated as:

$$LFC_{gene\ A} = log_2 \frac{aggregated\ expression\ of\ gene\ A\ in\ N2}{aggregated\ expression\ of\ gene\ A\ in\ N1}$$

3.3 Results

3.3.1 Overview of the data

In order to characterise the transcriptome of human lingual nerve neuromas, sections from a total of 7 samples were processed with Visium spatial transcriptomics. Spatial transcriptomics enables sequencing of the RNA content in a tissue section retaining information on the location of each transcript within the tissue, paired with information on the morphological context provided by an H&E image of the section. A total of 4 to 5 consecutive tissue sections from the same sample were processed as technical replicates. The clinical information linked to each sample used for Visium is reported in Table 3.2.

Table 3.2 Clinical information linked to samples used for spatial transcriptomics

Clinical Code	Sex	Age	Time since Injury (months)	Subjective sensation (%)	Pain status	Pain VAS	Tingling VAS	Discomfort VAS
LN1	F	27	12	0	P	55	100	80
LN2	M	41	7	50	NP	2	85	85
LN7	F	30	17	20	NP	4	100	84
LN8	M	36	4	0	NP	14	77	66
LN12	F	34	16	0	P	43	10	88
LN13	F	28	4	20	P	65	100	87
LN15	F	34	12	20	P	61	10	77

Patients in the non-painful group reported an average pain VAS score of 6.7, while patients in the painful group had VAS scores ranging between 43 and 65, with an average of 56. Overall, there was a significant difference in the pain VAS score between the high and low pain groups ($p<0.001$).

A total of 1-3 sections were placed in each capture area: due to the smaller size of LN12 and LN13, multiple sections (2-3) were placed within the same capture area, while one section per capture area was used for all the other samples. One section of LN13 lifted off during the protocol, while other sections from this sample generally experienced a higher degree of tissue detachment, indicating a potential issue with the sample's adhesion to the Visium slide or the placement of multiple sections in the same capture area.

Sequencing metrics are reported in Table 3.3. On average, the median unique molecular identifiers (UMIs) detected per spot in each sample was 7,285, with a total of 16,079 genes detected in each sample out of a panel of 17,943 genes.

Table 3.3 Sequencing results of spatial transcriptomics
The spaceranger output for each capture area, summarised in the table, was used to create an object with the R package Giotto. All sections were then normalised, integrated and further analysed together.

Sample ID	Number of Spots Under Tissue	Mean Reads Under Tissue per Spot	Median Genes per Spot	Median UMI Counts per Spot
LN1_0	1,477.00	20,646.79	3,043	5,790.00
LN1_A1	1,345.00	20,522.41	3,168	6,509.00
LN1_B1	1,347.00	24,288.17	2,882	5,543.00
LN1_C1	1,374.00	20,038.56	529	749.50
LN1_D1	1,350.00	19,204.66	2,987	5,901.50
LN12_A1	2,849.00	27,745.64	4,362	10,647.00
LN12_B1	2,804.00	26,309.51	3,915	9,093.50
LN13_C1	2,031.00	19,525.61	2,828	5,463.00
LN13_D1	827.00	25,173.44	4,887	12,349.00
LN15_A1	960.00	7,809.64	938	1,305.50
LN15_B1	1,165.00	24,411.25	3,909	8,472.00
LN15_C1	1,075.00	23,084.38	4,185	9,396.00
LN15_D1	1,159.00	23,340.80	3,978	8,480.00
LN2_0	1,648.00	29,393.81	3,754	8,862.00
LN2_A1	1,906.00	17,447.52	2,799	5,684.50
LN2_B1	1,867.00	20,335.68	2,998	6,329.00
LN2_C1	1,719.00	26,430.18	3,342	7,283.00
LN2_D1	1,710.00	23,645.65	3,268	7,175.50
LN7_0	746.00	16,364.15	1,757	3,067.50
LN7_A1	834.00	18,835.28	1,395	2,354.50
LN7_B1	866.00	21,709.14	1,516	2,610.00
LN7_C1	815.00	21,798.02	2,573	5,100.00
LN7_D1	845.00	21,131.52	2,580	5,306.00
LN8_0	1,802.00	26,547.31	4,365	12,570.50
LN8_A1	1,674.00	24,163.83	4,250	11,704.00
LN8_B1	1,950.00	20,207.69	4,021	10,921.00
LN8_C1	2,049.00	21,215.12	4,384	12,485.00
LN8_D1	2,073.00	20,795.47	4,433	12,822.00
Average	**1,509.54**	**21,861.47**	**3,180**	**7,284.77**

3.3.2 Cluster analysis identifies spatial compartments with specific cell-type enrichment.

The R package Giotto was used to merge all sections and perform an integrated clustering analysis (Dries et al., 2021). The spaceranger output from each capture area, corresponding to one or more sections from the same sample, was used as the input to create each Giotto object. The Giotto objects were joined, filtered, integrated and clustered as described in the methods in workflow 1 (Figure 3.4). A total of 17 clusters were identified with the Leiden clustering method (Traag et al., 2019), shown in a UMAP plot in Figure 3.6.A. The clusters were annotated based on the expression of cell-type specific markers, representing the enrichment of a certain cell-type in the spots belonging to each cluster. The differentially expressed genes in each cluster are displayed in a heatmap in Figure 3.6.B and in Table 3.4. Representative images of the H&E staining and the cluster distribution on sections from the samples classified as non-painful and painful are shown in Figure 3.7 and Figure 3.8, respectively.

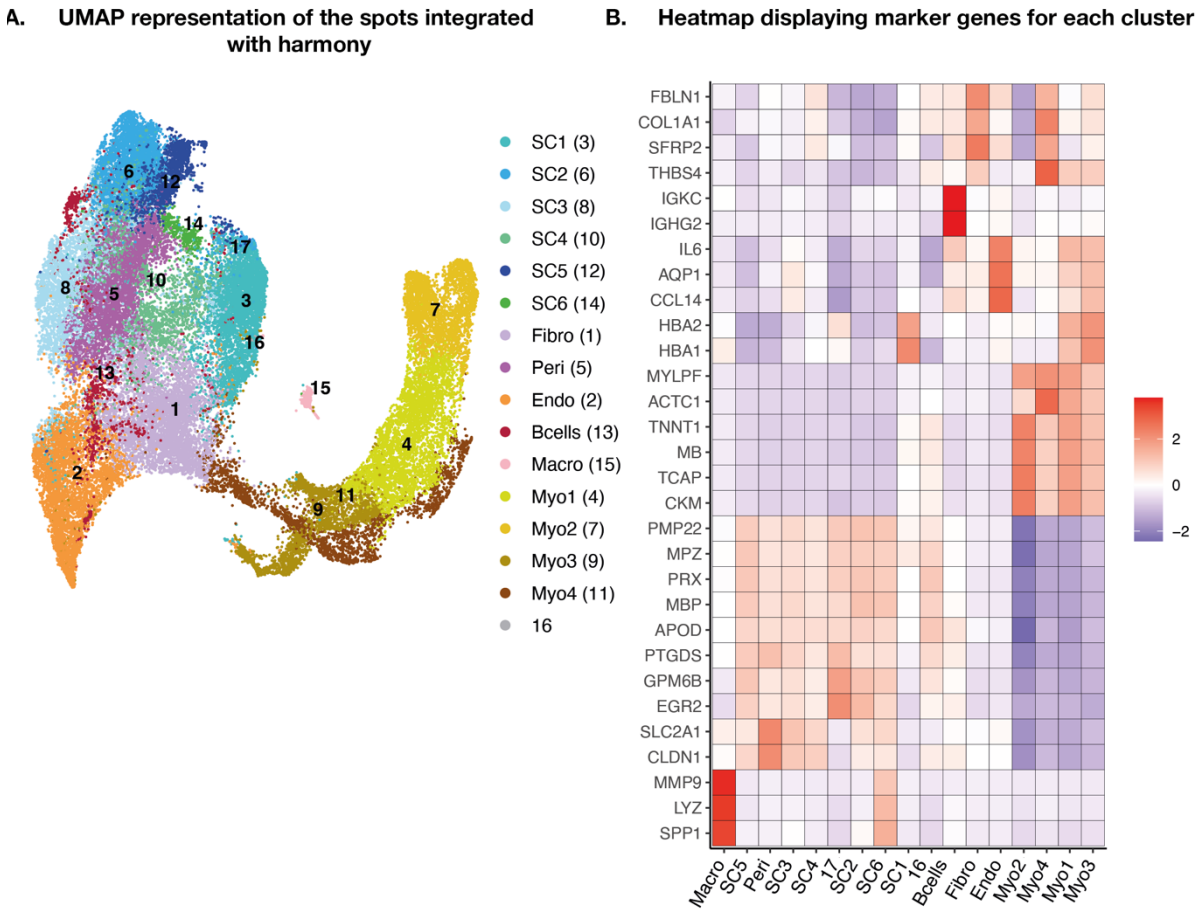

Figure 3.6 Overview of the clusters identified in the integrated human neuromas and their marker genes.
A: UMAP of all the spots colour-coded by their cluster classification, each cluster was assigned a number and then annotated based on the gene expression.
B: Heatmap of the most differentially expressed genes in each cluster colour-coded by the average normalized expression level in each cluster, where purple indicates below average expression, while red indicates above average expression.

Six clusters displayed an enrichment in Schwann cell marker genes such as MPZ, PMP22, MBP, PRX and S100B and therefore were classified as SC1-6. SC1 is enriched with HBA1 and HBA2, markers for erythrocytes, and is localised to the outer edge of the tissue sections, potentially indicating the presence of residual red blood cells as a result of the surgical removal of the sample. The other five clusters were found across all samples mostly overlaying areas containing nerve fascicles.

The most ubiquitous cluster expressed genes enriched in fibroblasts including COL1A1, FBLN1 and COL1A2 (Muhl et al., 2020) and was therefore classed as Fibro. The cluster is localised in areas surrounding the nerve fascicles but not directly overlaid on them, which might indicate the presence of fibrotic tissue. This

cluster displayed over-expression of SFRP2 and 4, secreted frizzled-related proteins that act as extracellular regulators of the Wnt signalling pathway by competing for Wnt ligand binding (Wawrzak et al., 2007). The Wnt pathway has been identified as a critical mediator of fibrosis, contributing to fibroblast activation and differentiation into myofibroblasts (Burgy and Königshoff, 2018). Changes in Wnt gene expression have been reported in both human and animal models of peripheral nerve injury, including SFRP4 over-expression (van Vliet et al., 2021).

The second most ubiquitous cluster (Endo) expressed AQP1, TM4SF1 and SELE, indicating the presence of endothelial cells (Hong et al., 2023, Verkman, 2002, Chen et al., 2021). IL6 and CCL14 were also enriched in this cluster suggesting a pro-inflammatory phenotype of the endothelial cells present in these samples: the role of IL-6 as a pro-inflammatory molecule is well-known (Tanaka et al., 2014), while CCL14 has been shown to bind to CCR1, 3 and 5, potentially inducing leukocyte infiltration (Gu et al., 2020).

Cluster 5 (Peri) is enriched in PTGDS, CLDN1 and SLC2A1, which are marker genes of perineurial cells (Piña et al., 2015, Chen et al., 2021), and is found across all samples in areas associated with nerve fascicles. In samples LN15 and LN12, which display a more ordered fascicular organization compared to the other samples, evidenced by the H&E staining (Figure 3.8C,E), this cluster is distributed along the edges of the nerve fascicles, in line with the expected morphology of the perineurial barrier.

Four clusters enriched in myocyte markers, such as MB, TNNT1, CKM and ACTC1, were identified, but their distribution varies across the samples. No myocyte clusters are identified in LN12, while only two clusters are identified in a small number of spots in LN15. These clusters overlay areas with a morphology typical of skeletal muscles, characterized by the presence of multinucleated myocytes, and are not directly associated with nerve fascicles.

Finally, two clusters were enriched with immune cell markers: cluster 13 and cluster 15. Cluster 13 was enriched in IGKC, encoding the Immunoglobulin Kappa Constant and IGHG1-2, encoding the immunoglobulin heavy constant gamma 1 and 2, respectively. This suggests the presence of immunoglobulin-producing B

cells (Hoffman et al., 2016) and was therefore classified as B cells. This cluster was found across all samples but is particularly abundant in LN12, LN8 and LN15.

Cluster 15, classified as Macro, was enriched in genes such as LYZ, encoding for lysozyme, a marker for macrophage activation (Keshav et al., 1991), SPP1, encoding for Secreted Phosphoprotein 1 and secreted by activated macrophages (Dong et al., 2021), LAPTM5, encoding for a transmembrane receptor associated with lysosomes and associated with pro-inflammatory activation of macrophages (Glowacka et al., 2012) and CHIT1, encoding for chitotriosidase, an enzyme involved in macrophage polarization and activation (Sklepkiewicz et al., 2023). This cluster also expresses high levels of MMP9, encoding for metalloprotease 9, which is known to be secreted by Schwann cells in the early stages following nerve injury, promoting blood-nerve barrier breakdown and leukocyte influx at the site of injury (Ji et al., 2009). This cluster was particularly abundant in LN15 (Figure 3.8.F), one of the samples classified as painful based on the patient's reported VAS score.

Table 3.4 Top 5 marker genes for each cluster and the putative enriched cell-type.

Cluster number	Cluster name	Top 5 DE genes					N of spots	Putative enriched cell type
1	Fibro	COL1A1	SFRP2	FBLN1	COL1A2	SFRP4	4607	Fibroblast
2	Endo	AQP1	CCL14	IL6	TM4SF1	SELE	4422	Endothelial cells
3	SC1	HBA2	MPZ	HBA1	PMP22	MBP	4327	Schwann cells
4	Myo1	MB	TNNT1	TCAP	CKM	TTN	4214	Myocytes
5	Peri	PTGDS	CLDN1	SLC2A1	IGFBP6	MPZ	3873	Perineurial cells
6	SC2	MBP	PMP22	MPZ	PRX	S100B	3571	Schwann cells
7	Myo2	MB	TNNT1	TCAP	CKM	TNNI1	2936	Myocytes
8	SC3	PMP22	MBP	MPZ	PRX	APOD	2882	Schwann cells
9	Myo3	MB	TNNT1	CKM	TCAP	TTN	2458	Myocytes
10	SC4	APOD	MPZ	PMP22	MBP	PRX	2162	Schwann cells
11	Myo4	ACTC1	THBS4	MYLPF	CA3	COL1A1	1937	Myocytes
12	SC5	MPZ	PRX	MBP	PMP22	S100B	1549	Schwann cells
13	Bcells	IGKC	IGHG2	APOD	IGHG1	S100B	1083	B cells
14	SC6	PMP22	MBP	MPZ	PRX	S100B	449	Schwann cells
15	Macro	LYZ	MMP9	SPP1	LAPTM5	CHIT1	353	Macrophages
16	NA	PRX	APOD	MPZ	CNP	MBP	8	NA
17	NA	GPM6B	EGR2	MPZ	CARD8	FGFBP2	5	NA

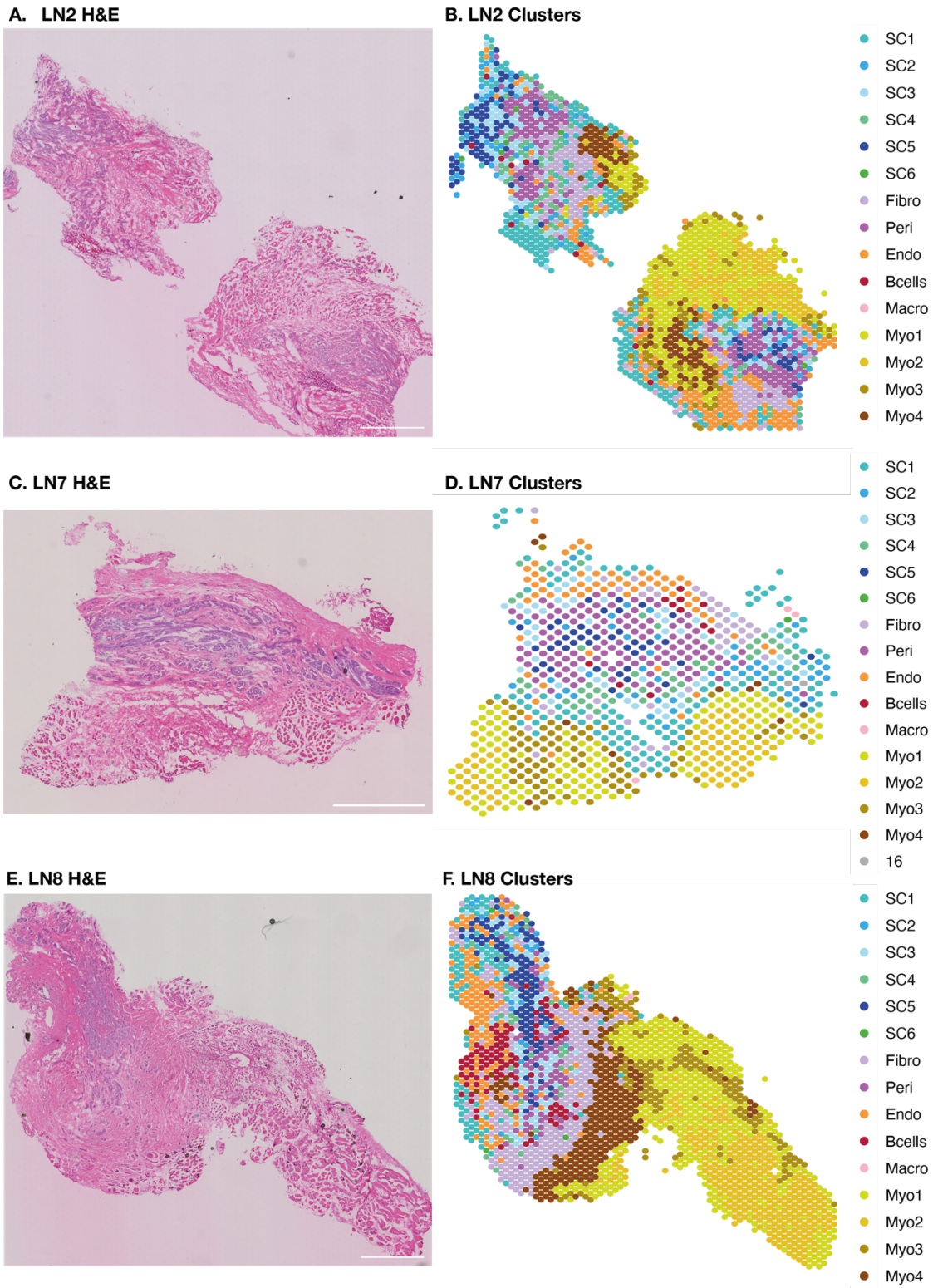

Figure 3.7 Representative H&E staining and clusters overlay of lingual neuromas classified as non-painful.
A, C, E: H&E tiled image of a representative replicate of LN2, LN7 and LN8; the samples classified as non-painful used in the Visium experiments. Scale bar: 1 mm.
B, D, F: Spatial plot displaying the spots from each adjacent tissue section colour-coded by the cluster classification.

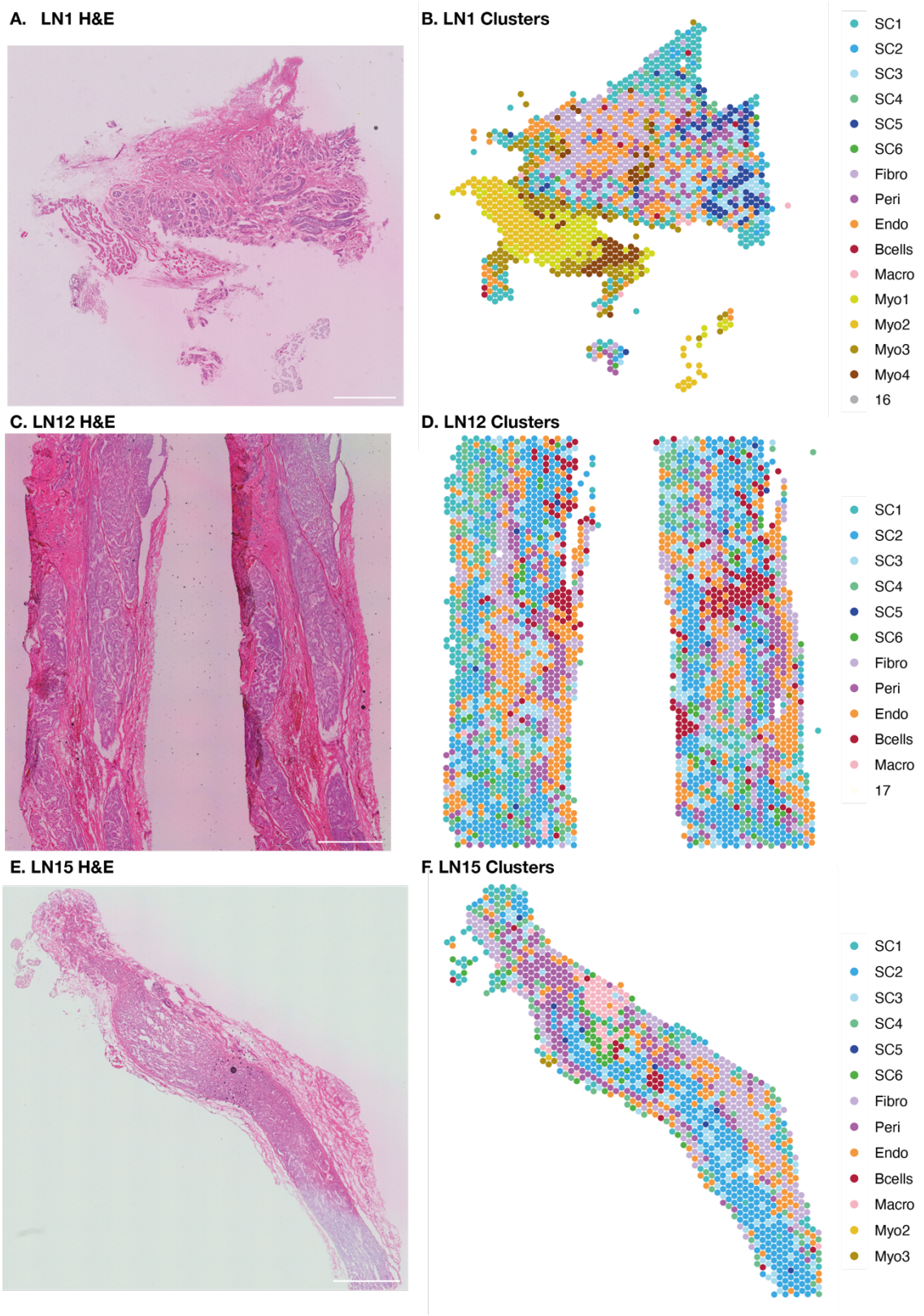

Figure 3.8 Representative H&E staining and cluster overlay of lingual neuromas classified as painful.
A, C, E: H&E tiled image of a representative replicate of LN1, LN12 and LN15; three of the samples classified as painful used in the Visium experiments. Scale bar: 1 mm.
B, D, F: Spatial plots displaying the spots from each adjacent tissue section colour-coded by the cluster classification.

3.3.3 Deconvolution of cell-types using single nuclei RNA sequencing labels

Since each barcoded spot has a diameter of 55 μm which is larger than the average size of most cells, the Visium technology is unable to capture the transcriptome at single cell resolution. Clustering and differential expression analysis enables the inference of cell-type enrichment in each spot based on markers from the literature but is unable to accurately identify all the cell types present at each location and quantify their proportion. Several computational methods have been developed to overcome this limitation and identify the cell-type identities and distribution in the Visium barcodes with the use of a single cell reference dataset from the same or similar type of tissue (Li et al., 2022a, Li et al., 2023b). Here, cell-type deconvolution was performed using the spatial DWLS algorithm developed by Dong and Yuan (2021) with the snRNAseq dataset generated in Chapter 2 as reference, using the neuroma samples only. This algorithm is based on DWLS, a previously developed cell-type deconvolution method for bulk RNA sequencing, which was adapted to spatial datasets (Dong and Yuan, 2021). Spatial DWLS was run on each section individually. The results of cell-type deconvolution are shown in Figure 3.9. In a few technical replicates (LN1_C1, D1, 0; LN7_C1 and LN13_D1), the algorithm couldn't run to completion and the reason couldn't be identified.

The cell types identified are consistent across samples. Out of the Schwann cell clusters, MSC_2 and MSC_3 are the most abundant, accounting for 27.0% and 14.6% of all samples on average, while MSC_1 and NMSC are identified in fewer spots, but are still present across all samples, accounting for 2.3% and 0.8% of cell types across all samples on average. Among the fibroblast subtypes, PeriF_1 is most common subtype of perineurial fibroblasts identified, accounting for 12.0% of cellular composition. Endoneurial fibroblasts and PRRX1+ fibroblasts are identified across all samples, on average making up 4.4% and 9.7% of cellular composition. Among the endothelial cell subtypes, Endo_3 is the most abundant (13.6%). Macrophages and lymphocytes make up 0.5% and 0.1% of cellular composition, respectively. Myocytes are present only in LN1, LN2, LN7 and LN8, where they make up around 18% of each tissue section, but they are absent from LN12, LN13

and LN15. None of the salivary gland cells are detected to a significant degree in any of the samples.

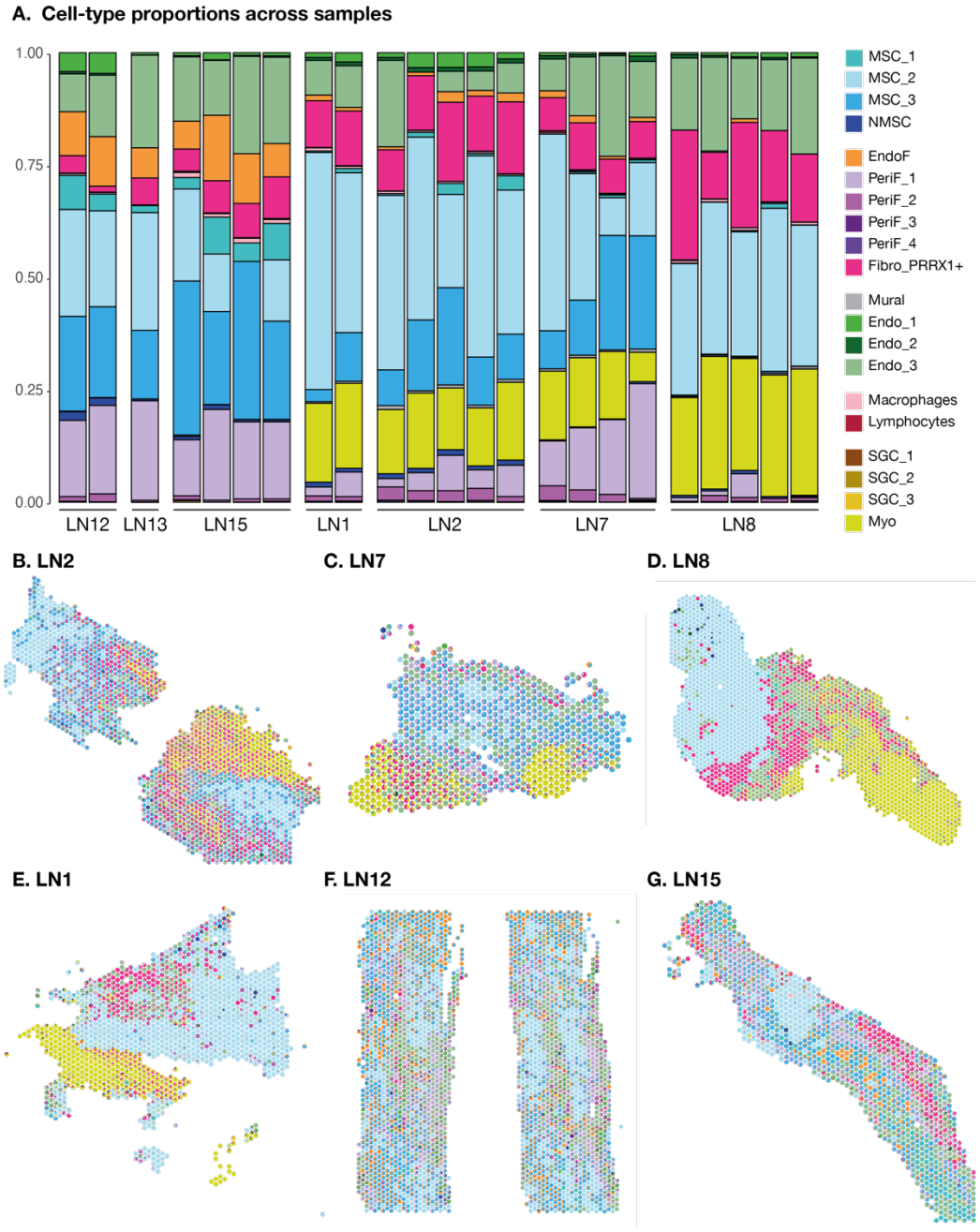

Figure 3.9 Cell-type composition of the Visium dataset across the samples.
A: Barplot displaying the proportion of the cell-types annotated in the snRNAseq dataset identified in each Visium sample with spatial DWLS deconvolution. Technical replicates from each sample are grouped together, each bar represents a capture area. Some replicates are missing as the deconvolution algorithm was unable to run on specific Giotto objects.
B-G: Cell-type deconvolution shown on representative sections of LN2 (B), LN7 (C), LN8 (D), LN1 (E), LN12 (F) and LN15 (G). Each spot is represented by a pie-chart displaying the cell-types predicted to be present in each location and their proportion.

Table 3.5. Distribution of cell-types in the human neuromas calculated with spatial DWLS. The proportion of each cell type was averaged across technical replicates of each sample and expressed as a percentage.

	LN1	LN2	LN7	LN8	LN12	LN13	LN15	Average
MSC_1	0.60%	1.51%	0.39%	0.29%	5.65%	1.55%	5.73%	2.25%
MSC_2	44.16%	35.42%	24.16%	31.48%	22.57%	26.20%	11.72%	27.96%
MSC_3	6.80%	13.23%	17.86%	0.26%	20.64%	15.25%	28.01%	14.58%
NMSC	0.95%	1.05%	0.27%	0.46%	1.78%	0.39%	0.67%	0.80%
EndoF	1.03%	1.41%	1.17%	0.23%	10.40%	6.73%	9.81%	4.40%
PeriF_1	3.70%	4.95%	16.47%	1.46%	18.31%	22.12%	16.72%	11.96%
PeriF_2	1.11%	2.31%	1.98%	0.81%	1.42%	0.36%	0.65%	1.23%
PeriF_3	0.07%	0.07%	0.07%	0.06%	0.04%	0.07%	0.07%	0.07%
PeriF_4	0.13%	0.22%	0.05%	0.11%	0.06%	0.07%	0.03%	0.09%
Fibro_PRRX1+	11.28%	13.42%	8.38%	18.63%	2.61%	5.99%	7.24%	9.65%
Mural	0.38%	0.65%	0.51%	0.34%	0.11%	0.01%	0.09%	0.30%
Endo_1	1.54%	2.43%	0.53%	0.77%	4.39%	0.52%	0.89%	1.58%
Endo_2	0.76%	0.87%	0.71%	0.46%	0.46%	0.03%	0.23%	0.50%
Endo_3	8.49%	6.94%	13.73%	17.33%	11.03%	20.58%	16.83%	13.56%
Macrophages	0.63%	0.43%	0.29%	0.54%	0.39%	0.14%	0.97%	0.49%
Lymphocytes	0.11%	0.07%	0.21%	0.07%	0.09%	0.02%	0.20%	0.11%
SGC_1	0.08%	0.01%	0.01%	0.01%	0.00%	0.00%	0.00%	0.02%
SGC_2	0.00%	0.00%	0.02%	0.00%	0.00%	0.00%	0.00%	0.00%
SGC_3	0.02%	0.03%	0.13%	0.00%	0.05%	0.00%	0.16%	0.05%
Myo	18.23%	15.02%	13.08%	26.09%	0.00%	0.00%	0.03%	10.35%

3.3.4 Pseudo-bulk differential expression analysis comparing painful and non-painful neuromas.

The human neuromas collected as part of this study are linked with clinical information including the patients' self-reported score of pain. The patients they are derived from are affected by the same type of injury to the lingual nerve, but only a portion of them report symptoms of pain. Are there any differences in gene expression among painful and non-painful samples that might be contributing to neuropathic pain development and maintenance?

Characterization of the cellular composition of the neuromas with single nuclei RNA sequencing highlighted the heterogeneity within these samples, which contain several subtypes of Schwann cells, fibroblasts, endothelial cells, myocytes, immune cells and salivary gland cells. Spatial transcriptomics uncovered the spatial distribution of these cell types within the morphological context, highlighting the

presence of nerve fascicles containing Schwann cells, endoneurial and perineurial fibroblasts and endothelial cells, and areas containing scar tissue and myocytes not directly associated with the nerve fascicles.

Bulk RNA sequencing is widely used as a technique to compare gene expression among different samples in an unbiased fashion, which often involves the lysis of the whole sample. Therefore, the transcriptional profile of specific morphological structures is lost. Nociception is a process driven by the nervous system, however these samples also contain muscle tissue incidentally resected during surgery and scar tissue developed as a result of tissue injury. In order to identify changes in gene expression that might be driving neuropathic pain generation and maintenance, differential gene expression analysis was focused on the areas involved with nociception, i.e. the nerve fascicles.

H&E sections were manually annotated to identify the barcodes that contain nerve fascicles, which can be identified by the presence of densely packed nuclei characterised by an elongated shape, typical of Schwann cells. The gene expression of all the nerve fascicles from each section was aggregated and analysed with pseudo-bulk differential expression analysis. The technical replicates were collapsed and exploratory PCA analysis was performed with PCAtools.

3.3.4.1 Principal Component Analysis

Principal component analysis is a widely used technique for data exploration that enables the summary of multivariate data to identify its fundamental structure (Blighe, 2019). RNA sequencing data consists in the measurement of several thousands of genes (in this case ~18,000) for each sample. PCA is performed to identify the trends and patterns that can most accurately explain the variation of the data (Blighe, 2019). This involves the reduction of the dimensionality of the data, where each variable is geometrically projected onto lower dimensions called the principal components (PCs) and the goal is to identify the best summary of the data using the lowest number of PCs (Lever et al., 2017). The first component (PC1) is obtained by minimizing the distance between the data and its projection, the following PCs are chosen similarly, but in addition they need to be uncorrelated with previous PCs (Lever et al., 2017). The resulting PCs are always smaller or equal to the number of samples or variables (whichever is smallest). In other words, the PCs

are linear combinations of the data's original variables, where the coefficients, stored in the loadings matrix, can be interpreted as a rotation matrix such that the rotated values with the greatest variance go along the first principal component (Lever et al., 2017). The first few PCs capture the greatest variance and are the most useful to explain the data variability, while the latter PCs capture noisy fluctuations and explain only a small percentage of the variance (Lever et al., 2017).

PCA analysis was performed on the pseudo-bulk RNA sequencing dataset in order to explore the source of the variability of the dataset. The biplot shown in Figure 3.10.A shows the samples' distribution in the PCA space according to the first two principal components, which account for 31% and 21% of the variability, respectively, overlaid with a loadings plot, which highlights the variables (genes) that have the highest effect on each component. LN12, LN13 and LN15 (painful samples) cluster closely together, whilst LN1 (painful sample) clusters more closely to the other non-painful samples. The genes driving most of the variation are shown in the plots in Figure 3.10.A and B. Variation is driven by the expression of muscle marker genes (MB, CKM, MYH7, CA3) and genes associated with the immune response (HLA-A, CHIT1, MMP9, IGKC). The expression of muscle marker genes is highest in the samples LN8, LN7, LN2 and LN1, which as highlighted in the previous paragraphs, contain a large proportion of myocytes – despite this analysis including only spots that overlay morphologically resembling nerve fascicles.

Since there are several sample-specific variables in the dataset, including age, sex, interval between injury and neuroma resection, patient-reported subjective sensation and discomfort, pain, discomfort and tingling VAS (reported in Table 3.2); the correlation of each of these variables with the principal components that summarise the variation in the data was investigated. The Eigencor plot (Figure 3.10.C) displays the r^2 coefficient of determination for the correlations between each principal component and clinical variable. Following multiple test correction with the false discovery rate, none of the correlations were statistically significant ($p<0.05$). However, PC1 displays a stronger relationship with pain status and tingling, while PC3 with sex, age and time since injury.

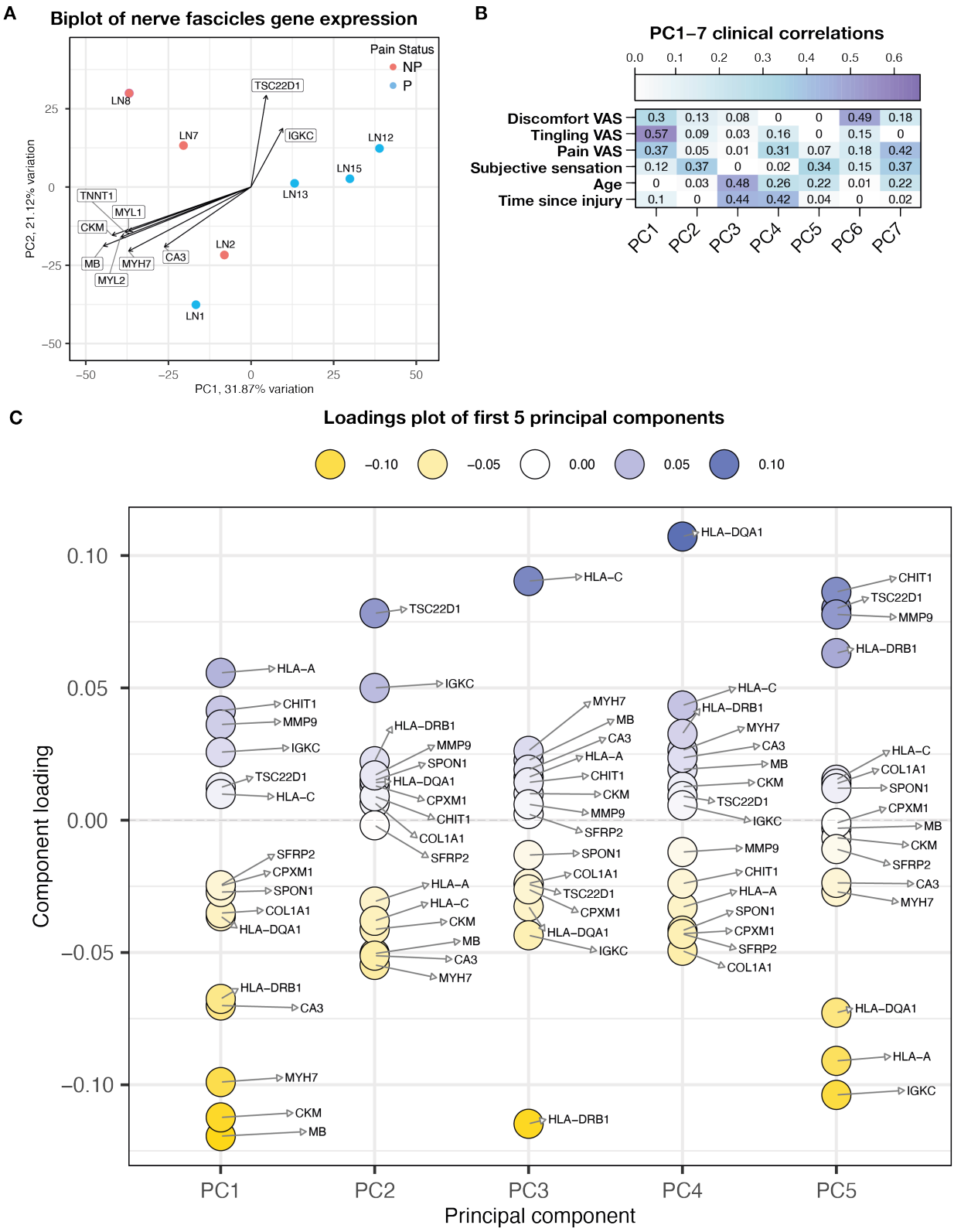

Figure 3.10 Principal component analysis of gene expression in nerve fascicles from human lingual neuromas

A: Biplot showing the samples' first two principal components and the genes explaining most of the variance in the dataset.

B: Coefficient of determination r^2 between the first 7 principal components and clinical metadata. The correlation coefficients are calculated with the Pearson correlation test and corrected for multiple testing with the false discovery rate. None of the correlations are statistically significant.

C: Loading plot showing the correlation coefficient of variables (i.e. gene) driving the variation in the first 5 PCs.

Overall, the principal component analysis was useful to explain the source of the variability in the data in an unsupervised manner. A large part of the variability between samples can be traced back to the presence of muscle, where genes related to muscles might diffuse in areas that were selected as morphologically resembling nerve fascicles. Nevertheless, there are trends of correlations (although not significant) with pain and tingling in PC1 and with sex in PC3, indicating that these clinical features might also influence the variability in the data.

3.3.4.2 Differential Expression analysis

Differential expression analysis was performed with DEseq2. 59 genes were significantly dysregulated (adjusted p-value < 0.05). The DE genes are displayed in Figure 3.11. Among the most highly upregulated genes in the painful group compared to the non-painful are HLA-A, belonging to the antigen-presenting Major Histocompatibility Complex (MHC) Class I family, NID2, a gene encoding for a basement protein, the chemokines CXCL2 and CXCL8, JMJ1DC, encoding for a protein interacting with the thyroid hormone receptor, and SLC52A3, encoding for a riboflavin transporter protein. All the DE genes are displayed in a heatmap in Figure 3.11.B, while the normalized counts of the top 20 DE genes are shown in Figure 3.11.C.

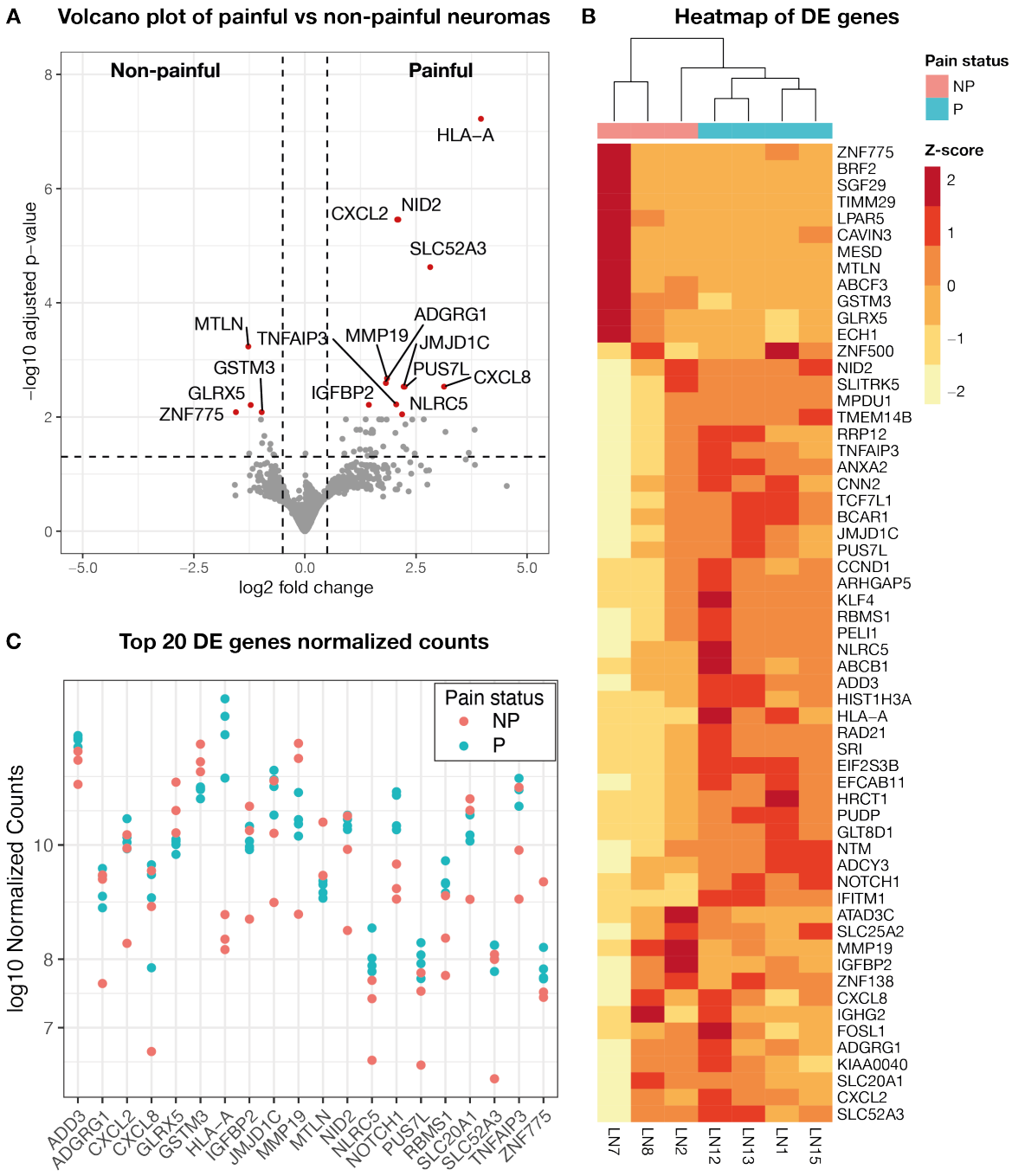

Figure 3.11 Differentially expressed genes between nerve fascicles of painful and non-painful neuromas.
A: Volcano plot displaying the fold change (x-axis) and adjusted p-value (y-axis) of genes after differential expression analysis with DEseq2. DE genes with adjusted p-value of less than 0.01 are colour coded in red and labelled. The vertical dotted lines represent a logarithmic fold change of 0.5, and the horizontal line represent a p-value of 0.05.
B: Heatmap displaying the z-scores, representing the centred and scaled normalized expression, of all significant DE genes (adjusted p-value < 0.05), colour coded on a scale from yellow (under-expression) to red (over-expression).
C: Graph displaying the normalised counts of the top 20 DE genes colour-coded by pain status. The counts are normalized with variance-stabilizing transformation.

3.3.4.3 Validation of the DE genes in the snRNA-seq dataset

The expression of the top DE genes (adjusted p-value < 0.01, LFC>1.33) was investigated in the single nuclei RNA sequencing dataset discussed in chapter 2, where nuclei from one painful and one non-painful neuroma sample were sequenced and annotated by their cell-type. The counts across the nuclei in each neuroma sample were aggregated and log2-normalized. The change in expression in the snRNAseq data is compared to the fold change of the top DE genes in the spatial data (Figure 3.12.A). The aggregated expression of each DE gene in the neuromas' single nuclei dataset is shown in Figure 3.12.B. The expression of 10 out of 12 genes found as most highly DE in the spatial dataset is in concordance with the single nuclei dataset. The expression of HLA-A couldn't be compared, as probes for HLA genes are excluded from the probe set used for single nuclei RNA sequencing. CXCL8, SLC52A3, JMJD1C, NLRC5, NID2, CXCL2, TNFAIP3, MMP19, ADGRG1 and IGFBP2 were found to be upregulated in the spatial dataset in painful samples, and their aggregated expression is higher in the painful sample in the single nuclei dataset. However, two genes display an opposite trend in expression in the snRNA-seq dataset: PUS7L, which is upregulated in the spatial dataset, displays a lower level of expression in the snRNA-seq dataset, and ZNF77, which is downregulated in painful samples in the spatial dataset, displays a higher level of expression in the painful neuroma used for snRNA-seq. Of note, these genes display low counts in the single nuclei dataset, detecting less than 350 log-transformed counts across all sequenced nuclei in each sample.

In Figure 3.12.C, the cell-type distribution of the top DE genes in the single nuclei dataset is shown. CXCL8 and CXCL2 are found in macrophages. Endothelial cells also express CXCL2, JMJD1C, ADGRG1, encoding for Adhesion G Protein-Coupled Receptor G1, and NLRC5, member of the NLR family that regulates the expression of MHC class I genes (Meissner et al., 2010) - which is also expressed in lymphocytes. NID2 is found in non-myelinating SCs. TNFAIP3, encoding for TNF Alpha induced protein 13, is found in lymphocytes and macrophages.

A Comparison of top DE genes LFC in spatial dataset with single nuclei

Gene	snRNAseq LFC	Spatial LFC
NID2	1.88	2.10
CXCL2	0.89	2.08
SLC52A3	1.47	2.82
MMP19	0.36	1.85
ADGRG1	0.14	1.82
CXCL8	0.23	3.13
JMJD1C	1.32	2.22
PUS7L	-0.43	2.24
TNFAIP3	0.31	2.06
IGFBP2	0.38	1.44
ZNF775	0.67	-1.55
NLRC5	1.75	2.19

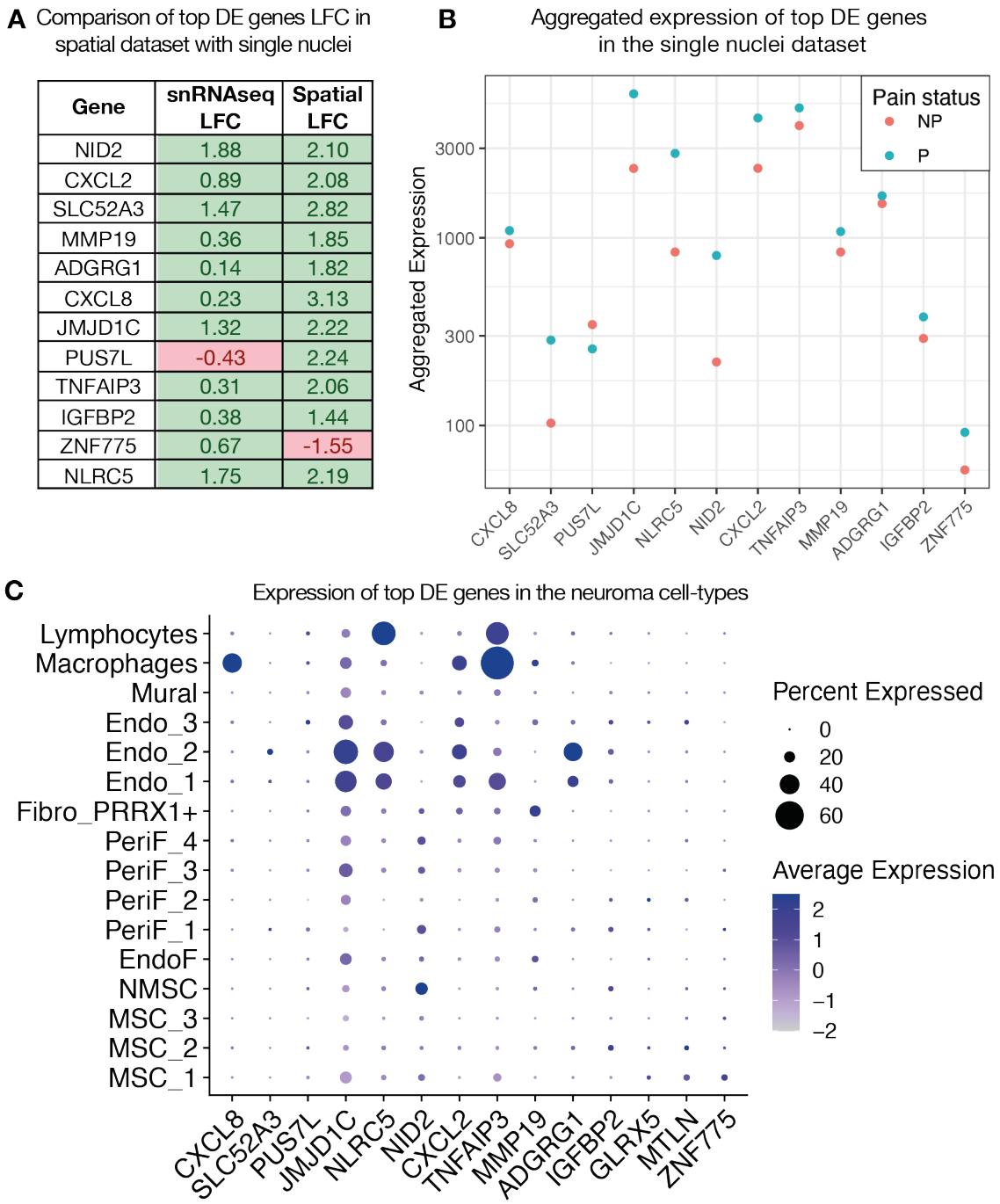

Figure 3.12 Validation of DE genes in the single nuclei dataset.
A: Comparison of the non-painful versus painful gene expression change in the snRNAseq data (calculated as log2(n2/n1)) and the fold change expression from DEseq2 analysis of the spatial dataset. A green cell indicates a gene that has increased expression in the painful sample(s), a red cell indicates a gene that has decreased expression in the painful sample(s). The genes displayed are the top DE genes in the spatial dataset ($p<0.01$, LFC>1.3). LFC= log fold change.
B: Aggregated expression (y-axis) of the top DE genes in the spatial dataset (x-axis) in the snRNA-seq data of the neuromas are shown, colour-coded by the pain status of the neuromas used for snRNA-seq.
C: Dotplot displaying the average expression of the top DE genes (x-axis) across the cell types in the snRNA-seq dataset (y-axis), where the size of each dot represents the percentage of cells that express each gene, and the colour of the dots represents the scaled average expression in each cell-type.

3.3.4.4 Spatial expression of selected DE genes

DE analysis was performed by aggregating the counts detected in the barcodes classified as nerve fascicles. Figure 3.13 displays the distribution of normalized counts in representative sections of the samples used for DE analysis. HLA-A displays a stark difference in expression in painful and non-painful samples (Figure 3.13.A), while the level of expression of the other DE genes isn't as obvious (Figure 3.13.B-D).

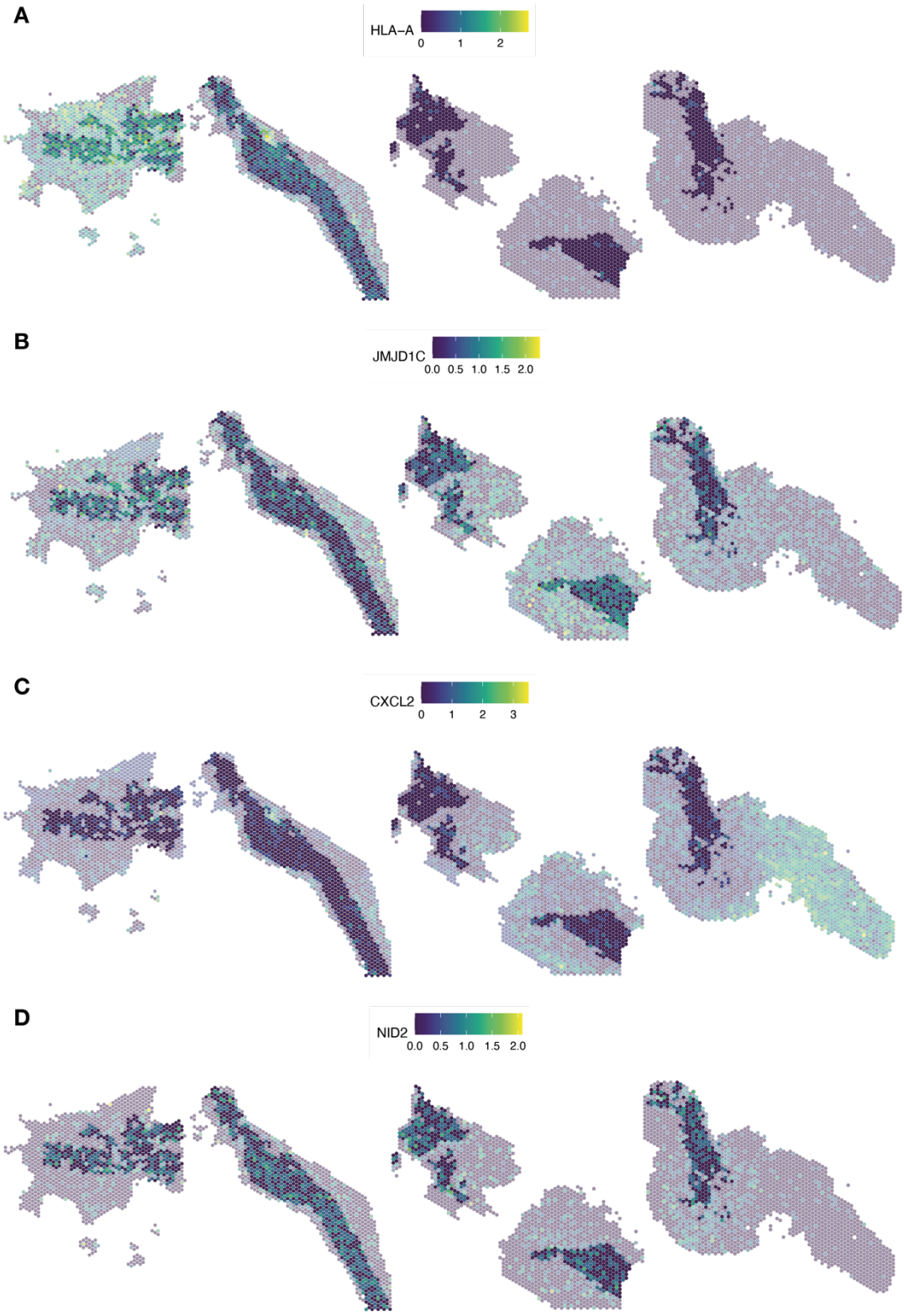

Figure 3.13 Spatial expression of HLA-A, JMJD1C, CXCL2 and NID2 in the lingual neuromas. A-D: Spatial plots displaying 4 of the top DE genes in representative sections (from left to right: LN1 and LN15, painful; LN2 and LN8, non-painful). SCT normalized counts across the sections are displayed for HLA-A (A), JMJD1C (B), CXCL2 (C) and NID2 (D). Spots classified as nerve fascicles are displayed at full saturation, while other spots are semi-transparent.

3.4 Discussion

In this chapter, the analysis of the gene expression in human lingual neuromas within their morphological context was presented. Spatial transcriptomics was chosen to measure the unbiased expression of 17,943 genes within tissue sections from 7 samples of human neuromas linked with clinical information including self-reported symptoms of pain. The use of spatial transcriptomics on human neuromas enabled a large amount of information to be obtained from a small portion of tissue and allowed the selection of pathologically relevant areas during post-processing by the examination of the H&E associated image. In this way, several differentially expressed genes were identified in painful and non-painful neuromas.

3.4.1 Cell-type characterization with spatial transcriptomics combined with single nuclei RNA sequencing.

Despite the lack of single cell resolution, clustering analysis revealed areas enriched in cell-type specific genes, in agreement with the histology of the tissue. For example, Schwann cell markers were enriched in areas overlaying nerve fascicles, perineurial cell markers were enriched in areas directly surrounding nerve fascicles and myocyte-associated genes were primarily located in areas containing muscle tissue.

Additionally, clustering analysis enabled the identification of cell types which sparsely populate the samples, such as immune cells. One cluster displayed the expression of lysosome specific genes (LYZ, MMP9, SPP1, LAPTM5, CHIT1*)*, typical of degranulating cells such as macrophages and dendritic cells. Lyzozyme (LYZ) is a bacteriolytic enzyme found in phagocytes such as macrophages, neutrophils and dendritic cells. It was shown to contribute to neuropathic pain via TLR4-mediated neuronal sensitization (Yadav and Surolia, 2019, Yadav et al., 2023b). MMP9 is also present in the late phase of peripheral nerve injury regeneration in rat nerves (Remacle et al., 2018) and promotes mechanical nociception (Kobayashi et al., 2008). Although there wasn't any difference in the frequency of the distribution of this cluster between painful and non-painful samples, this cluster is highly abundant in one specific sample, LN15. Further characterization of the microenvironment within this sample would be of interest, as

it emerges from spatial transcriptomics analysis that an area adjacent to the nerve fascicle at the site of injury is enriched with genes linked to the immune response, which might result in neuronal sensitization through the activation of specific receptors, such as TLR4 (Yadav and Surolia, 2019, Yadav et al., 2023b).

On the other hand, another cluster displayed an enrichment of genes encoding for immunoglobulins (IGKC, IGHG2, IGHG1), indicating the potential presence of B cells. In the single nuclei RNA sequencing data, a B cell cluster couldn't be identified, perhaps due to the absence of B lymphocytes in the samples used, by the lack of probes targeting IG variable regions in the probe set or due to the use of nuclei which excludes cytoplasmic transcripts. Nevertheless, the transcripts enriched in this cluster could be detected using spatial transcriptomics and were particularly enriched in LN12, where spots classed as "Bcells" are found overlapping nerve fascicles, indicating the infiltration of B lymphocytes in the nerve. Immunoglobulins have been linked to autoimmune pain disorders, where they can attack components of the somatosensory pathway (Xu et al., 2018), in this case however, it's impossible to establish the relevance of the presence of immunoglobulin genes in the sample and what their targets are. Further validation of the presence of immunoglobulins and antibody-secreting plasma cells derived from B cells is required.

3.4.1.1 Cell-type deconvolution to increase the resolution of spatial transcriptomics data.

Cell-type deconvolution provides another way to identify cell-specific signatures in a spatial dataset, benefitting from the integration of a single cell or single nuclei reference dataset, where the cell types likely to be present in the spatial dataset are previously identified and transcriptionally characterised. With this method, the presence of endoneurial fibroblasts located within the nerve fascicles could be identified, which was otherwise missed due to the overwhelming expression of Schwann cell-specific genes in these areas. The annotation of Fibro_PRRX1 as a profibrotic fibroblast cluster, is also confirmed in the spatial dataset, where this cluster is highly abundant and overlays areas where H&E staining indicates the presence of fibrosis.

The cell-type assignment among replicates, which were run independently, is consistent, providing reassurance in the cell-type deconvolution method to predict the cell-types present within each spot. The predictions are dependent on the quality of the single cell reference data, where it's possible that some cell-types were missed due to technical factors, such as the use of a limited number of samples, the use of nuclei rather than whole cells, and the different genes included in the probe set. However, the combination of these two types of data presents the advantage of overcoming each technique's limitation, inferring single cell information within the spatial context of the tissue.

The use of more samples would enable the identification of trends and correlations linked with clinical information, including longitudinal changes linked with time since injury, sex differences and correlations with other clinical measures such as levels of pain, tingling and discomfort. In this work, the samples were divided into a painful and non-painful group and differentially expressed genes within nerve fascicles were identified.

3.4.2 Pseudo-bulk analysis identified several differentially expressed genes

Spatial transcriptomics was adopted to perform pseudo-bulk RNA sequencing due to the ability to select pathologically relevant areas of the tissue, in this case the nerve fascicles. Human lingual neuromas display a high degree of heterogeneity within the histological composition, including muscle and scar tissue, which might not be directly relevant to neuropathic pain generation. Among the differentially expressed genes, several were previously identified to be linked with chronic pain.

3.4.2.1 HLA-A and its transactivator NLRC5 are upregulated in painful neuromas.

HLA-A is a group of the Human Leukocyte Antigens, part of the major histocompatibility complex (MHC) class I antigens. Variation in this region is associated with a large number of human diseases, primarily with an immunological component (Dendrou et al., 2018). Genetic variants in the HLA-A gene have previously been shown to correlate with the risk of developing neuropathic pain following traumatic nerve injury (Miclescu et al., 2023) and postherpetic neuralgia following Herpes Zooster infection (Sato-Takeda et al., 2004, Sato et al., 2002). Other HLA loci have also been associated with increased risk of developing

neuropathic pain following inguinal hernia surgery and lumbar disc herniation (Dominguez et al., 2013) and complex regional pain syndrome type I with dystonia (de Rooij et al., 2009). Additionally, variants in the HLA class II region were shown to bear a protective role against the development of peripheral neuropathy in patients with type 2 diabetes (Marzban et al., 2016). Finally, rat strains with different susceptibility to autoimmune neuroinflammation, characterised by allelic variants in the MHC regions, displayed increased susceptibility to the development of mechanical allodynia following nerve injury (Dominguez et al., 2008). These findings highlight the role of genes in the HLA region in neuropathic pain development in conditions where tissue injury, whether caused by viral infection, trauma or diabetes, leads to neuropathic pain in some, but not all, patients.

The functional effects of the variants identified in the aforementioned studies haven't been investigated, however one might hypothesise that variation in the HLA region might be indicative of a hyperactive immune system where tissue injury triggers exaggerated immune responses that lead to maladaptive changes in the nervous system. This might occur with increased antigen presentation by the MHC molecules, caused by increased expression of the HLA genes, triggering immune activation.

HLA-A significant upregulation is observed in lingual neuromas from patients that report neuropathic pain, compared to those who do not report pain. Additionally, its transactivator NLRC5 (Carey et al., 2019, Meissner et al., 2012, Kobayashi and van den Elsen, 2012) is also upregulated in the painful samples. NLRC5 is activated by IFNγ and is involved in the inflammatory response by regulating the NF-kB, inflammasome and IFN1 signalling pathways, and is associated with several nervous system disorders (Zhang et al., 2021).

Accumulating evidence points to the importance of MHC molecules in the development of neuropathic pain (Dominguez et al., 2008, Hartlehnert et al., 2017), but it's unknown whether their effect might occur due to immune activation alone or via neuronal-specific pathways as well. Nevertheless, identifying biomarkers of immune activation from patients with neuropathic pain might help to stratify patients and identify potential subgroups that could benefit from therapies targeting the immune response. Additionally, genotyping for variants in the HLA region might help

to identify patients more susceptible to the development of neuropathic pain following surgery or infection and take preventative measures.

3.4.2.2 Chemokines and trigeminal neuropathic pain

While HLA class I antigens are critical for the lymphocytes-mediated acquired immune response, on the other hand, chemokines are mediators of the innate immune response and accumulating evidence attributes them a role in the pathogenesis of neuropathic pain (White et al., 2007, Abbadie, 2005, Solis-Castro et al., 2021).

In human lingual neuromas, CXCL2 and CXCL8 are upregulated in patients with neuropathic pain. These chemokines and their receptor, CXCR2, have previously been associated with pain conditions affecting the trigeminal system (Solis-Castro et al., 2021). Infraorbital nerve constriction leads to the increase of CXCL2 in the trigeminal ganglia, while anti-CXCL2 injection resulted in the reduction of nerve injury induced-mechanical hypersensitivity (Iwasa et al., 2019). CXCL8 was shown to be increased in the serum of patients with migraines (Duarte et al., 2015) and trigeminal neuralgia (Liu et al., 2019), and its receptor, CXCR2, was upregulated in trigeminal neurons following sensitization by pruritogens (Li et al., 2023a). CXCR2 contributes to peripheral and central sensitization both through intracellular Calcium release and by increasing TRPV1 function (Silva et al., 2017, Dong et al., 2012). CXCR2 is upregulated in DRG neurons following nerve injury and its inhibition reduces symptoms of nerve injury induced neuropathic pain (Piotrowska et al., 2019) as well as chemotherapy-induced neuropathic pain, specifically through the suppression of CXCL8 signalling in the DRG (Brandolini et al., 2019).

Overall, there is plenty of evidence for CXCL2 and CXCL8 involvement in pain generation, particularly in the trigeminal system, through the expression of their receptor CXCR2 on primary afferents following sensitization. The effect of their interaction with the atypical chemokine receptor ACKR1, expressed in trigeminal neurons in naïve states as discussed in Chapter 2, hasn't been explored yet. Several mechanisms might drive the effect of chemokines on neuropathic pain, including both leukocyte recruitment and secretion of pro-nociceptive molecules, as well as in the direct neuronal stimulation and sensitization.

3.4.2.3 Other genes identified as differentially expressed.

A total of 59 genes displayed a statistically significant change in expression between painful and non-painful samples. Among the top dysregulated genes besides HLA-A, CXCL2 and CXCL8, there were several genes with a previous link with neuropathic pain or peripheral nerve biology.

A member of the solute carrier family 5, SLC52A3, was upregulated in samples linked with neuropathic pain. This gene encodes for a plasma membrane transporter which mediates the uptake by cells of vitamin B2/riboflavin. Congenital mutations in SLC52A3 are associated with Brown-Vialetto-Van Laere syndrome, where patients present neuropathies and other neurological symptoms (Thulasi et al., 2017, Manole et al., 2017). The supplementation of B12 partially ameliorates the progression of the condition (Foley et al., 2014), and, while evidence for benefits of B12 to neuropathic pain is scarce, it might be effective in some subgroups (Buesing et al., 2019).

Another gene upregulated in the painful samples and expressed in profibrotic fibroblasts is matrix metalloprotease 19 (MMP19), involved in the breakdown of the extracellular matrix. Some members of the metalloprotease family have been linked to neuropathic pain development (Ji et al., 2009, Marcianò et al., 2023, Lakhan and Avramut, 2012).

The Adhesion G-protein-Coupled Receptor G1 (ADGRG1, also known as GPR56), upregulated in the painful samples and expressed in endothelial cells, is involved in cell matrix adhesion and regulates the development and maintenance of peripheral myelin (Ackerman et al., 2018).

The Jumonji Domain Containing 1C (JMJD1C) interacts with thyroid hormone receptors and is thought to be a histone demethylase and a coactivator for key transcription factors (Viscarra et al., 2020). It’s upregulated in the neuromas and expressed in endothelial cells. Other members of the JMJD family were found to be involved in neuropathic pain development in animal models (Wen et al., 2018, Li et al., 2023c).

GSTM3 is a glutathione S-transferase downregulated in the painful samples. Its protein and transcriptomic expression was associated with stomach or abdominal pain in a study investigating pain in individuals with depression (Zhang et al., 2022b). It was also reported to synthetise the prostaglandin PGE_2 in the brain, known for its pro-inflammatory effects (Beuckmann et al., 2000).

NID2 encodes a member of the nidogen family which makes up basement membrane proteins which plays a role in Schwann cell migration following nerve transection (Lee et al., 2007), and was found to be expressed in non-myelinating Schwann cells in the human neuromas by single nuclei RNA sequencing.

Insulin-like growth factor binding protein 2 (IGFBP2) binds to insulin-like growth factors I and II (IGF-I and IGF-II) and is upregulated in the painful samples. IGF-I was shown to be upregulated in the TG and infraorbital nerve following injury, contributing to sensitization (Miura et al., 2011, Sugawara et al., 2019).

Notch signalling was shown to be activated and required for neuropathic pain development (Xie et al., 2015). NOTCH-1, encoding one of the four receptors involved in Notch signalling, is upregulated in the painful samples.

Validation in a larger pool of samples is required to draw any definite conclusions, however, the results show promise as several of the genes identified are already linked specifically with neuropathic pain, and this list might include novel potential biomarkers or candidates involved in neuropathic pain development or maintenance in humans.

3.4.3 Limitations of this study

Analysis of human neuromas by spatial transcriptomics is a valuable method to obtain a high amount of information from a single tissue section from these rare samples. The use of Visium provided a relatively cost-effective approach to profile RNA expression within the spatial context. However, it prevented single cell resolution, allowing only the identification of enriched cell types in each barcoded spot. With cell-type deconvolution, the resolution was improved, but this approach is based on computational inference and requires validation with cell-type specific markers. In Chapter 4, a few cell types will be further characterised using immunohistochemistry and RNAscope, including macrophages, perineurial cells

and endoneurial fibroblasts. However, more extensive work to confirm the cell-types present, the best markers to identify them and whether there are any correlations linked with sex, age, time since injury, tingling, discomfort and pain scores is required.

Another drawback of spatial transcriptomics is the potential of transcript diffusion, where the RNA molecules in the tissue diffuse horizontally and are captured by adjacent barcodes, affecting the accurate representation of the spatial distribution of gene expression. While transcript diffusion is observed to a minimal degree with the Visium technology, there is variation between samples due to tissue detachment and other technical factors (Ståhl et al., 2016). Potential RNA diffusion was observed in the present dataset when selecting areas containing nerve fascicles for pseudo-bulk analysis, where myocyte-specific genes were still detected in the samples that contained muscle tissue in other areas of the section. Nevertheless, several differentially expressed genes with a previous link to neuropathic pain were detected, despite the small sample size, and warrant further investigation in the future. Future studies are required to confirm the differential expression of these genes at the protein level in a larger pool of samples. Additionally, analysis of the biofluids collected from the patients, including saliva, whole blood and serum, would be of interest to identify whether any biomarkers that correlate with the gene expression at the site of injury can be detected.

3.4.4 Conclusion

Spatial transcriptomics provided a complementary tool to analyse the transcriptome of human neuromas that, when integrated with single nuclei RNA sequencing, generates a vast amount of information on the microenvironment within these samples. In this chapter, the spatial distribution of gene expression was discussed, highlighting immune-specific signatures, including antibody-secreting B cells and degranulating macrophages, enriched in a subset of samples. Spatial transcriptomics was integrated with snRNAseq to infer the cellular composition at higher resolution. Pseudo-bulk analysis on the pathologically-relevant areas of the tissue identified several dysregulated genes between painful and non-painful samples. Some of the dysregulated genes were previously identified to be linked

with neuropathic pain, including HLA-A, CXCL2 and CXCL8, highlighting the role of neuroimmune interactions in neuropathic pain generation. This approach has paved the way for future studies, which should aim to identify the role of chemokine signalling and HLA genes in chronic neuropathic pain, in order to further elucidate the pathophysiological mechanisms, identify potential therapeutic targets, and identify biomarkers that might recapitulate the gene expression at the site of injury and inform the clinician on the best courses of treatment.

Chapter 4. Immunohistochemistry and in situ hybridisation investigation of human lingual nerve neuromas

4.1 Introduction

In this chapter the protein and RNA expression of several genes will be investigated to validate single nuclei RNA sequencing and spatial transcriptomics experiments, attempt to quantify their expression in a broader pool of samples and investigate potential correlations with patients' reported pain scores.

The molecules chosen for investigation were selected based on their relevance to neuropathic pain generation and maintenance as evidenced in the literature. RNAscope was employed to investigate the expression of ion channels, including SCN9A, SCN10A and TRPV1, the Schwann cell marker SOX10, the macrophage marker CD68, the macrophage-secreted cytokine Oncostatin M and the prostaglandin synthase encoded by PTGDS, involved in the inflammatory response. Immunohistochemistry was employed to validate the expression of NGFR in GLUT-1-labelled perineurial fibroblasts and to investigate PI16 expression in human injured nerves and its correlation with symptoms of pain.

4.1.1 The expression of ion channels in the neuromas.

The protein expression of several ion channels, including $Na_v1.7$, $Na_v1.8$, $Na_v1.9$ and TRPV1 in human neuromas was investigated in previous work (Bird et al., 2007, Bird et al., 2013, Biggs et al., 2007). These studies demonstrate that the above ion channels are expressed in human lingual nerve neuromas and that expression of $Na_v1.8$ correlates with the presence of neuropathic pain. In the spatial transcriptomics dataset presented in Chapter 3, the expression of $Na_v1.7$ and TRPV1 was detected at the mRNA level, while $Na_v1.8$ and $Na_v1.9$ transcripts weren't detected.

In this chapter, the expression of these genes will be investigated with RNAscope to verify that the lack of signal for specific ion channels' mRNAs was not caused by the probes used in the spatial transcriptomics protocol, and whether it might reflect

biological differences in how ion channels are trafficked and inserted in the plasma membrane.

SCN9A ($Na_v1.7$), SCN10A ($Na_v1.8$) and TRPV1 were selected for validation using RNAscope to investigate whether their pattern of expression reflects that detected with spatial transcriptomics.

4.1.2 The role of macrophages and Oncostatin M in neuropathic pain.

Previous work from our laboratory identified the infiltration of CD68+ macrophages within nerve fascicles in human lingual nerve neuromas (Vora et al., 2007). In Chapter 2, macrophages were found to potentially interact with trigeminal neurons in the neuromas through CXCL8/ACKR1 interaction, and CXCL8 was identified as differentially expressed in painful neuromas compared to non-painful ones in chapter 3.

In this chapter, the presence of CD68+ macrophages within nerve fascicles will be validated with RNAscope, along with the expression of Oncostatin M (OSM). OSM is a pro-inflammatory cytokine secreted by macrophages (Repovic and Benveniste, 2002) and highly expressed in human DRGs from male donors associated with a history of neuropathic pain (Ray et al., 2023).

4.1.3 Perineurial cells and prostaglandin signalling in neuropathic pain.

Perineurial cells surround nerve fascicles and make up the blood-nerve barrier, protecting axons from pathogens, toxins and external fluctuations in ionic composition and pH. In Chapter 2, perineurial cells were identified by the expression of GLUT-1, encoded by SLC2A1 (Piña et al., 2015). Additionally, this cluster expressed NGFR, which encodes for the neurotrophin p75 NGF receptor, involved in nerve regeneration following injury (Cosgaya et al., 2002), as well as PTGDS, which encodes Prostaglandin D2 synthase - an enzyme that catalyses the conversion of prostaglandin H2 to prostaglandin D2, involved in inflammation and pain (Tavares-Ferreira et al., 2022a).

This cell type will be further investigated in this chapter: PTGDS expression in the neuromas will be validated with RNAscope, while co-localisation of GLUT-1 and NGFR receptor will be investigated with immunohistochemistry.

4.1.4 PI16 as a regulator of neuropathic pain.

Peptidase Inhibitor 16 (PI16) is a fibroblast-derived protein recently proposed as a regulator of neuropathic and inflammatory pain (Singhmar et al., 2020, Garrity et al., 2023). In these studies, PI16 was shown to be expressed in perineurial and epineurial fibroblasts in injured mouse sciatic nerves; however, in Chapter 2 single nuclei RNA sequencing highlighted its expression in endoneurial fibroblasts in human trigeminal nerves.

In this chapter, the expression of PI16 in human neuromas will be further investigated with immunohistochemistry, with the aim to identify a potential correlation between PI16 expression and pain in human neuromas.

4.1.5 Aims and objectives.

The overall aim of this chapter is to provide a broad overview of the genes and proteins expressed in human lingual neuromas and whether Visium and single nuclei RNA sequencing data can be qualitatively confirmed with different methodologies.

The specific objectives are as follows:

1. Optimise combined RNA detection and immunohistochemistry in fixed human neuromas.
2. Validate the RNA expression of SCN9A, SCN10A, TRPV1, CD68, OSM and PTGDS in TUJ1+ areas in human neuromas with RNAscope.
3. Validate PI16 expression associated with TUJ1-labelled axons in human neuromas with immunohistochemistry.
4. Identify the correlation between PI16 expression in human neuromas and symptoms of pain.
5. Validate NGFR expression in GLUT-1-labelled perineurial cells in human neuromas with immunohistochemistry.

Due to the small number of samples where RNAscope could be successfully performed, quantification and comparison across painful and non-painful samples wasn't possible. Nevertheless, the findings described here provide evidence of the

expression of selected pain-relevant targets in human injured nerves, stimulating questions for future studies.

4.2 Methods

4.2.1 Human Lingual Neuromas

As indicated in Table 4.1, a portion of the samples used in this chapter were also used in previous chapters for spatial and single nuclei RNA sequencing. Lingual neuromas were obtained from patients attending the trigeminal nerve injury clinic at the Clifford Dental Hospital in Sheffield, UK. Neuromas were collected during nerve repair surgery, carried out by Dr Simon Atkins. All neuromas were collected with the informed consent from the patients, in accordance with the South Sheffield Research Ethics Committee (06/Q2305/151) STH13926 and East of England - Cambridge Central Research Ethics Committee (17/EE/0238) STH 19847. Clinical information including patients' age, sex and pain history was recorded preoperatively and anonymised. Patients reported symptoms of pain, tingling and discomfort on the day of surgery on a visual analogue scale (VAS) ranging from 0 to 100.

After the surgical removal, the neuromas were placed in Zamboni's fixative (0.1 mol/L phosphate buffer, pH 7.4, containing 4% paraformaldehyde and 0.2% picric acid) for immunohistochemistry and in situ hybridization. Each sample was fixed overnight at 4°C, then transferred to 30% sucrose for 12 h at 4°C and finally cryoprotected in OCT and stored at -80°C. The tissue was sectioned in a cryostat at a thickness of 10 µm and placed on Superfrost Plus slides (Epredia, 10149870). Sections were dried for 45 minutes and stored at -80°C.

Table 4.1 Summary of samples used for RNAscope and immunohistochemistry
For each sample clinical information including age, sex and pain VAS are reported, as well as the assays they have been used for. The table includes information on whether they have been tested for RNAscope, immunohistochemistry and which antibodies combinations have been used, spatial transcriptomics (ST) and single nuclei RNA sequencing (snRNA-seq).

Sample	Age	Sex	Pain VAS	RNAscope	IHC Experiments			Other uses	
					PI16 + TUJ1	PI16 + CD45	NGFR + GLUT-1	ST	SnRNA-seq
LN7	30	F	4		+			+	
LN6	25	F	0		+	+	+		
LN17	41	M	0		+	+	+		
LN10	39	F	0	+	+				
LN11	33	F	3	+	+	+	+		
LN1	27	F	55	+	+			+	
LN4	65	F	100	+	+	+	+		
LN15	34	F	61		+			+	
LN12	34	F	43	+	+			+	
LN13	28	F	65	+	+			+	+

4.2.2 Immunohistochemistry

Indirect immunofluorescence assays were used to determine the expression of several cell-type specific markers including NGFR, GLUT-1, CD45, TUJ1 and PI16. Several of the immunohistochemistry experiments were performed by Evgeniya Anisimova as part of a Wellcome Trust Biomedical Vacation Scholarship. Based on recommendations on the data sheets provided by the manufacturers, different dilutions of antibodies were first evaluated to determine the optimal dilution for each antibody, detailed in Table 4.2.

Sections were thawed and dried for 45 minutes at room temperature prior to the start of the protocol. Slides were washed in phosphate buffered saline (PBS) for 5 minutes with agitation, then washed with PBS-T (0.2% Triton-X in PBS) twice for 7 minutes. A hydrophobic barrier was drawn surrounding each section with ImmEdge

Hydrophobic Barrier PAP Pen (Vector Laboratories, H-4000). The sections were incubated with 20% Normal Donkey Serum (NDS, Jackson Laboratories, 017-000-121) in PBS-T for 1 hour at room temperature. Primary antibodies were diluted in 5% NDS in PBS-T and incubated overnight at 4°C. The following day, the slides were washed twice with PBS-T for 7 minutes and a secondary antibody was diluted in 1.5% NDS in PBS-T and incubated for 90 minutes in the dark. In dual-labelling experiments, the incubation steps were repeated with markers of specific cell types and a secondary antibody (Table 4.2). Finally, they were mounted in Vectashield Antifade Mounting Medium with DAPI (Vector Laboratories, H-1200-10), cover-slipped and sealed.

Table 4.2. Details of the antibodies used for fluorescent immunohistochemistry

Antibody	Source	Cat number	Lot number	Antibody type	Optimal dilution
Rabbit anti-PI16	Cambridge Bioscience	HPA043763	000038964	Polyclonal	1/200
Mouse anti-NGFR	abcam	ab3125	1016053-5	Monoclonal	1/200
Mouse anti-CD45	Abcam	ab8216	1037004-6	Monoclonal MEM-28	1/400
Rabbit anti-S100B	Proteintech	15146-1-AP	103243	Polyclonal	1/100
Rabbit anti-GLUT1	Abcam	ab115730	1030236-10	Monoclonal EPR3915	1/400
Mouse anti-TUJ1	BioLegend	801202	B354042	Monoclonal	1/200
Donkey anti-mouse Cy3	Jackson ImmunoResearch	715-165-150	163873	Polyclonal (H&L)	1/500
Donkey anti-rabbit Cy3	Jackson ImmunoResearch	711-165-152	165051	Polyclonal (H&L)	1/500
Donkey anti-mouse FITC	Jackson ImmunoResearch	715-095-150	146034	Polyclonal (H&L)	1/500
Donkey anti-rabbit FITC	Jackson ImmunoResearch	711-095-152	122195	Polyclonal (H&L)	1/500

4.2.2.1 Specificity control

A pre-absorption control was used to confirm the specificity of the antibody against PI16. The antibody was diluted at the optimal dilution (Table 4.2) in 5% NDS in PBS-T and then mixed with its blocking peptide (Cat# APrEST84407, SLS), 5 µg peptide per 1 µg antibody. The solution was then left at 4°C for approximately 18 hours prior to performing the immunofluorescence staining assay. For the remaining

antibodies a blocking peptide wasn't available, therefore a negative control was performed where the protocol was conducted as described above but the primary antibody was omitted.

4.2.3 Simultaneous detection of mRNAs and proteins using RNAscope.

RNAscope enables the detection of up to four RNA molecules by *in situ* hybridization within one tissue section. Immunohistochemistry can be incorporated in the RNAscope protocol to enable simultaneous detection of proteins and mRNAs. RNAscope Multiplex Fluorescent v2 Assay (ACD, 323100) was used to visualise several RNA targets (listed in Table 4.3) in TUJ1 labelled human neuromas. Tissue sections were dried at room temperature for 30 minutes, washed in PBS and post-fixed by immersing in 10% Normal Buffered Formalin (NBF) for 15 minutes at 4°C. The sections were dehydrated by immersion in increasing ethanol concentrations (50%, 70%, 100% and 100%) for 5 minutes each, dried, then treated with 0.3% hydrogen peroxide for 10 minutes at room temperature and washed in fresh distilled water. Antigen retrieval was performed in a steamer at 95°C with ACD 1X Antigen Retrieval reagent. Incubation times of 5 and 15 minutes were tested. A hydrophobic barrier was drawn around the tissue sections with ImmEdge Hydrophobic Barrier PAP Pen (Vector Laboratories, H-4000). Protease treatment was performed with Protease III at room temperature. Incubation times of 1, 3 and 5 minutes were tested. The probes were mixed at the dilution suggested by the manufacturer, with the proportion between the probe in channel 1 (C1), channel 2 (C2) and channel 3 (C3) as C1:C2:C3=50:1:1,and were hybridised in the hybridization oven for 2 hours at 40°C. In order to detect the probes, a series of channel-specific signal amplifications were performed, as illustrated in Figure 4.1. All incubations were performed in the hybridization oven at 40°C and slides were washed twice with 1X RNAscope wash buffer in a Coplin jar between all incubations. The sections were incubated with the amplification reagents for each channel, AMP1, AMP2 and AMP3 for 30, 30 and 15 minutes respectively. The signal from each channel was amplified by incubating the slides with a channel-specific horseradish peroxidase (HRP) enzyme (HRP-C1, HRP-C2 or HRP-C3) for 15 minutes, then with a TSA vivid fluorophore 520, 570 or 650 diluted 1:1,500 in RNAscope TSA Buffer (ACD, 322809) for 30 minutes, and finally with HRP blocker

for 15 minutes to stop the reaction. This process was repeated for each probe channel for labelling with the desired fluorophore.

When all channels were amplified, immunolabelling of TUJ1 was performed. The slides were washed in PBS-T, blocked with 20% normal goat serum (NGS, Abcam, ab7481) for 1 hour at room temperature and incubated with mouse anti-TUJ1 (BioLegend, 801202) in 10% NGS in PBS-T (1:100) overnight at 4°C. The slides were washed with PBS-T and incubated with goat anti-mouse secondary antibody (H+L) conjugated with AlexaFluor 488 (Invitrogen, A28175) in 10% NGS in PBS-T (1:500) for 90 minutes at room temperature. The slides were washed in PBS-T and incubated with DAPI in PBS (1:3,000) for 1 minute. The slides were washed in PBS, mounted with ProLong Gold, coverslipped and stored in the darkness until imaging.

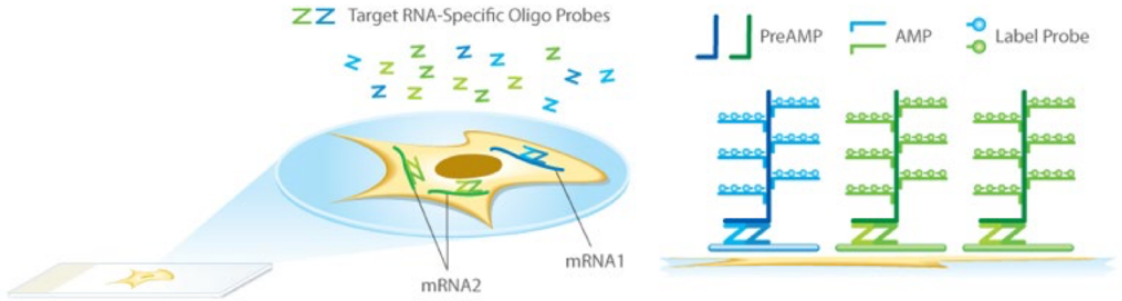

Figure 4.1. Overview of RNAscope-based detection of RNA molecules.
The diagram illustrates how RNA molecules are detected with RNAscope. The probes are designed to detect the target mRNA through the binding of multiple short oligos: only when all oligos are hybridised to the target sequence the signal can be detected, which reduces background staining due to unspecific binding of the probes. The signal is detected through a series of amplification rounds specific for each mRNA targeted by the probes. Image obtained with permission from Advanced Cell Diagnostics (ACD), USA.

Table 4.3. Details of the probes used for the RNAscope experiments.

Item	Probe target	Channel	Fluorophore
RNAscope™ 3-plex Positive Control Probe- Hs	POL2RA	C1	Cy5
	PPIB	C2	Cy3
RNAscope™ 3-plex Hs-CD68-C1	CD68	C1	Cy3
RNAscope™ 3-plex Hs-TRPV1-C2	TRPV1	C2	Cy3
RNAscope™ 3-plex Hs-SCN9A-C1	SCN9A	C1	Cy5
RNAscope™ 3-plex Hs-SCN10A-C2	SCN10A	C2	Cy3
RNAscope™ 3-plex Hs-OSM-C1	OSM	C1	Cy5
RNAscope™ 3-plex Hs-SOX10-C1	SOX10	C1	Cy5
RNAscope™ 3-plex Hs-PTGDS-C2	PTGDS	C2	Cy3

4.2.4 Imaging

4.2.4.1 Widefield Fluorescence Microscopy

Images for the immunohistochemistry experiments were acquired using a Leica DMi8 inverted microscope fitted with a Leica K5 sCMOS microscope camera system. The microscope was equipped with a LED 3 fluorescent light source in the 390-680 range, and 4 filter cubes for epifluorescence excitation: DAPI, FITC, Cy3 and Cy5. Tile scans and z-stacks were acquired at 20X and 40X magnification and processed on the Leica Application Suite X (LAS X) software and on Fiji (v2.14).

4.2.4.2 Confocal Microscopy

Confocal microscopy of the RNAscope experiments was performed on an Olympus FV3000RS Confocal Laser Scanning inverted microscope at the University of Texas at Dallas. The samples were imaged with 405 nm, 488 nm, 561 nm and 640 nm diode laser lines at 20x, 40x and 100x magnification. Images were acquired on the Fluoview acquisition software and processed on Fiji.

Confocal microscopy of immunohistochemistry experiments was performed on a Zeiss LSM980 Airyscan 2 system at the University of Sheffield, using a blue diode 405 nm laser, an argon 488 nm laser and a HeNe 543 nm laser. The images were acquired using Airyscan with the ZEN software and processed on Fiji (2.14).

4.2.5 Image Analysis and Quantification

Based on the pain VAS scores, the neuromas chosen for the PI16 immunohistochemical analysis were divided in two groups: ‘painful’ (pain VAS score higher than 40) and ‘non-painful’ (pain VAS score lower than 15). Differences in VAS scores between painful and non-painful groups were evaluated using an unpaired t-test assuming equal variance.

Images labelled with PI16 and TUJ1 were analysed in Fiji (2.14) by Evgeniya Anisimova as part of a Wellcome Trust Biomedical Vacation Scholarship. She was blinded to the clinical information linked to each sample. Maximal intensity projections were generated from z-stacks of tile-scans of the tissue sections imaged at 20X magnification. The areas of the tissue positive for TUJ1 were selected and PI16 average signal intensity in the TUJ1 positive areas was recorded. Statistical analysis of PI16 signal intensity between the samples classified as painful

and non-painful were performed using GraphPad Prism (10.0.2, GraphPad software, San Diego, CA, USA). Unpaired Student's t-test was used to test the statistical difference between PI16 signal intensity in painful and non-painful neuromas, and Pearson correlation test was used to test the correlation of PI16 signal intensity with the patient's self-reported pain VAS scores.

4.3 Results

4.3.1 Validation of spatial transcriptomics and single cell RNA sequencing with RNAscope.

4.3.1.1 Rationale of target selection for RNAscope validation.

RNAscope was employed in order to validate the expression of selected targets from spatial transcriptomics and single nuclei RNA sequencing in human neuromas. The choice of the targets to validate was based on their relevance to neuropathic pain development and peripheral nerve homeostasis.

Firstly, the RNAscope protocol was optimised to enable combined detection of RNA molecules in TUJ1+ putative axons labelled by immunohistochemistry. The RNA expression of genes important for nociceptive transduction (SCN9A, SCN10A, TRPV1) was investigated in TUJ1-labelled axons. The protein expression of these genes in axons is well-established in the literature and has been previously investigated in lingual nerve neuromas (Biggs et al., 2007, Bird et al., 2007, Bird et al., 2013). However, the presence of axonal mRNAs, which would suggests local translation, is a topic that has more recently come into focus (Holt et al., 2019). Visium data indicated that SCN9A and TRPV1 transcripts are expressed in the neuromas, while SCN10A mRNA is absent. We aimed to confirm these findings with RNAscope-based mRNA detection.

SOX10 expression was also validated with RNAscope, to confirm whether Schwann cells in the neuromas still express the transcript several months after nerve injury, as suggested from the single nuclei data.

Another target that was chosen to validate with RNAscope is PTGDS, encoding for an enzyme involved in prostaglandin synthesis, due to its relevance in inflammation and sex-specific pain perception (Shen et al., 2023). PTGDS was found to be expressed in perineurial fibroblasts and to a lower degree in

endoneurial fibroblasts and Schwann cells in single nuclei RNA sequencing data (Chapter 2).

Finally, CD68 and OSM expression was validated with RNAscope. CD68 was investigated to confirm the presence of macrophages in the nerve fascicles and identify co-expression of OSM, a cytokine with an emerging role in neuropathic pain development (Ray et al., 2023).

In the following sections, the RNA expression of these molecules detected with RNAscope will be compared to the signal detected with Visium spatial transcriptomics. Due to the high variability of RNAscope signal across samples, the investigation was focused on one sample, LN8, which displayed a strong signal for the positive control probes, as will be explained in more detail in the following section.

4.3.1.2 Optimization of combined RNAscope and immunofluorescence detection

RNAscope enables the detection of up to four RNA molecules within a tissue section. The protocol includes a protease treatment to expose RNAs in the tissue, enabling the probes to hybridise to their complementary sequences. The protease treatment causes digestion of protein antigens, which results in decreased immunoreactivity affecting the detection of protein targets with immunohistochemistry (Ball et al., 2023). Human lingual neuromas contain a variety of tissue types, including scar tissue, muscle tissue and nerve fascicles. In order to detect RNAs associated with nerve fascicles, it was desirable to simultaneously detect axons. TUJ1 was chosen as a marker for neuronal axons (Geisert and Frankfurter, 1989). This required optimisation to identify the optimal protease and antigen retrieval (AR) treatment to enable combined RNA and protein detection.

Sections were incubated with different durations of protease treatment and AR and labelled with the positive control RNAscope probes, targeting house-keeping genes PPIB and POL2RA (Highet et al., 2021). Following the RNAscope protocol, the sections were immunolabelled with an antibody targeted against TUJ1 and detected by a secondary antibody conjugated to FITC. The negative control consisted in the use of RNAscope negative control probes, targeting bacterial

genes, and the omission of the primary antibody targeted against TUJ1 (Figure 4.2.E).

Different incubations of protease treatment and AR were tested to identify which combination would yield positive RNA and protein signals. Protease treatment was tested for 1 and 5 minutes and AR was tested for 5 and 15 minutes: representative images of the fluorescence from the tissue with a combination of these treatments is shown in Figure 4.2.A-D. With 5 minutes of protease incubation, TUJ1 immunofluorescence was severely reduced compared to 1 minute incubation. The sections treated with 15 minutes AR displayed a stronger signal for both TUJ1 immunoreactivity and RNA hybridisation, while the sections treated with 5 minutes AR exhibited high autofluorescence (Figure 4.2.A). Therefore, subsequent experiments were performed with 1 minute protease treatment and 15 minutes AR.

This optimization experiment was performed on one sample assuming that these parameters would be suitable for all samples. However, when multiple samples were tested using the optimised protocol, the signal detected for the positive control probes varied considerably, as summarised in Table 4.4 and shown in Figure 4.3. This may be caused by variable RNA quality across samples and differences in fixation length, which can vary from 16 to 24 hours and may affect the accessibility of RNAs due to varying degrees of cross-linkage (Mostegl et al., 2011). Due to the high variability in RNAscope signal across samples, direct comparison between samples and pain levels couldn't be performed. Localised expression of the RNAs of interest in selected targets could still be assessed qualitatively in the samples that displayed a positive signal of the house-keeping genes. LN8 was used for the majority of the RNAscope experiments showed in the following sections due to the strong signal detected with the positive control probes (Figure 4.3.B).

Table 4.4 Summary of clinical information across samples of human neuromas tested in the RNAscope experiments.

ID	Time since injury (months)	Age	Sex	Subjective Sensation	Pain	Pain VAS	RNAscope positive control signal
LN4	19	65	F	0	Yes	100	Low
LN8	4	36	M	0	No	14	High
LN10	69	39	F	0	No	0	Low

LN11	18	33	F	0	No	3	Medium
LN12	16	34	F	0	Yes	43	Medium
LN13	4	28	F	20	Yes	65	Low

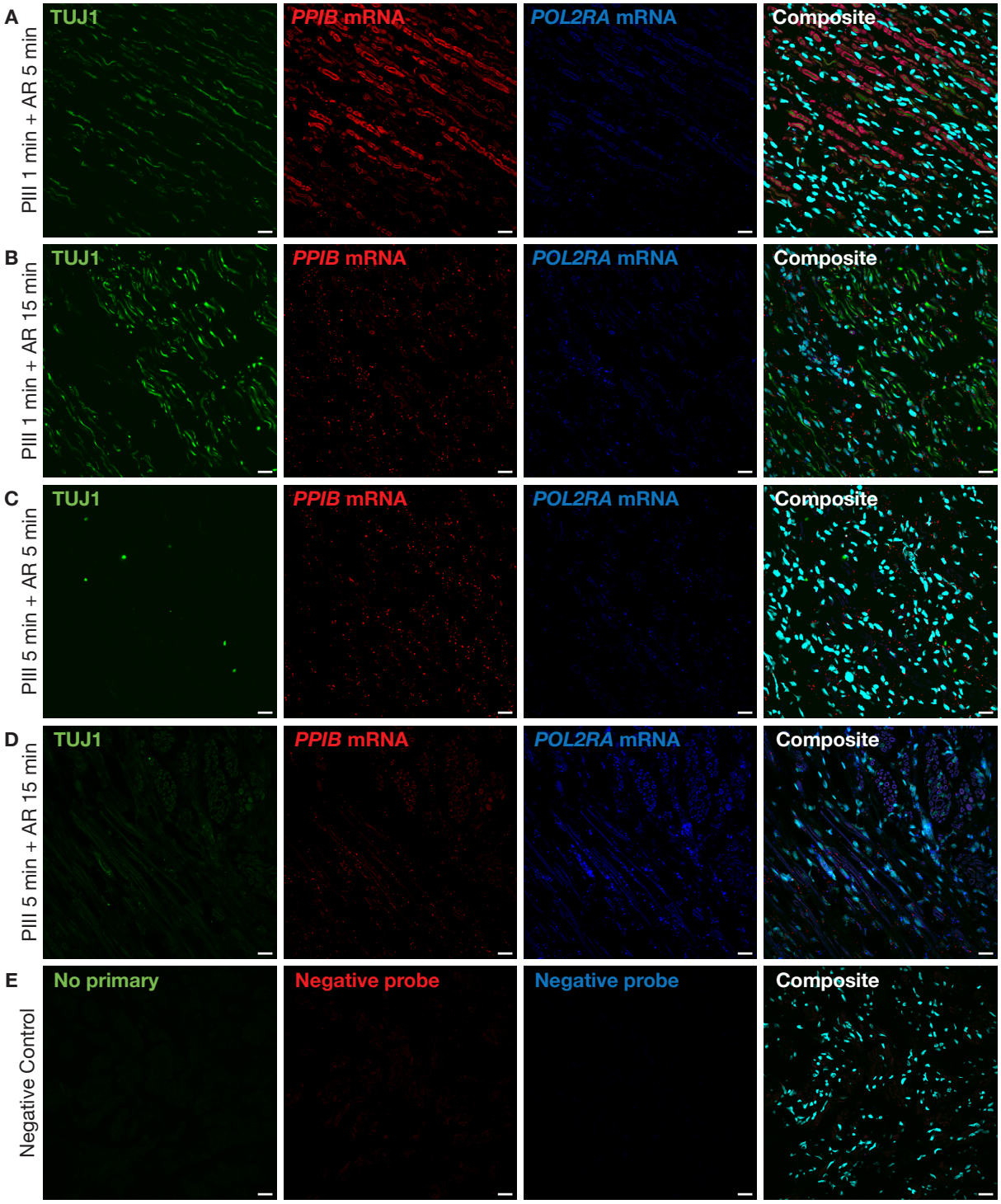

Figure 4.2 Optimization of combined immunofluorescence and RNAscope on human lingual neuromas.
Confocal images displaying TUJ1 (FITC) immunofluorescence combined with PPIB (Cy3) and POL2RA (Cy5) RNAscope in samples of human neuromas. Each row of images displays a different treatment: treatment with protease III was tested for 1 min (A, B) and 5 min (C, D), while antigen

retrieval was tested for 5 min (A, C) and 15 min (B, D). The negative control (E) was treated with PIII of 1 min and AR of 15 min, no primary antibody and negative control probes. Scale bar: 20 µm, 40x magnification.

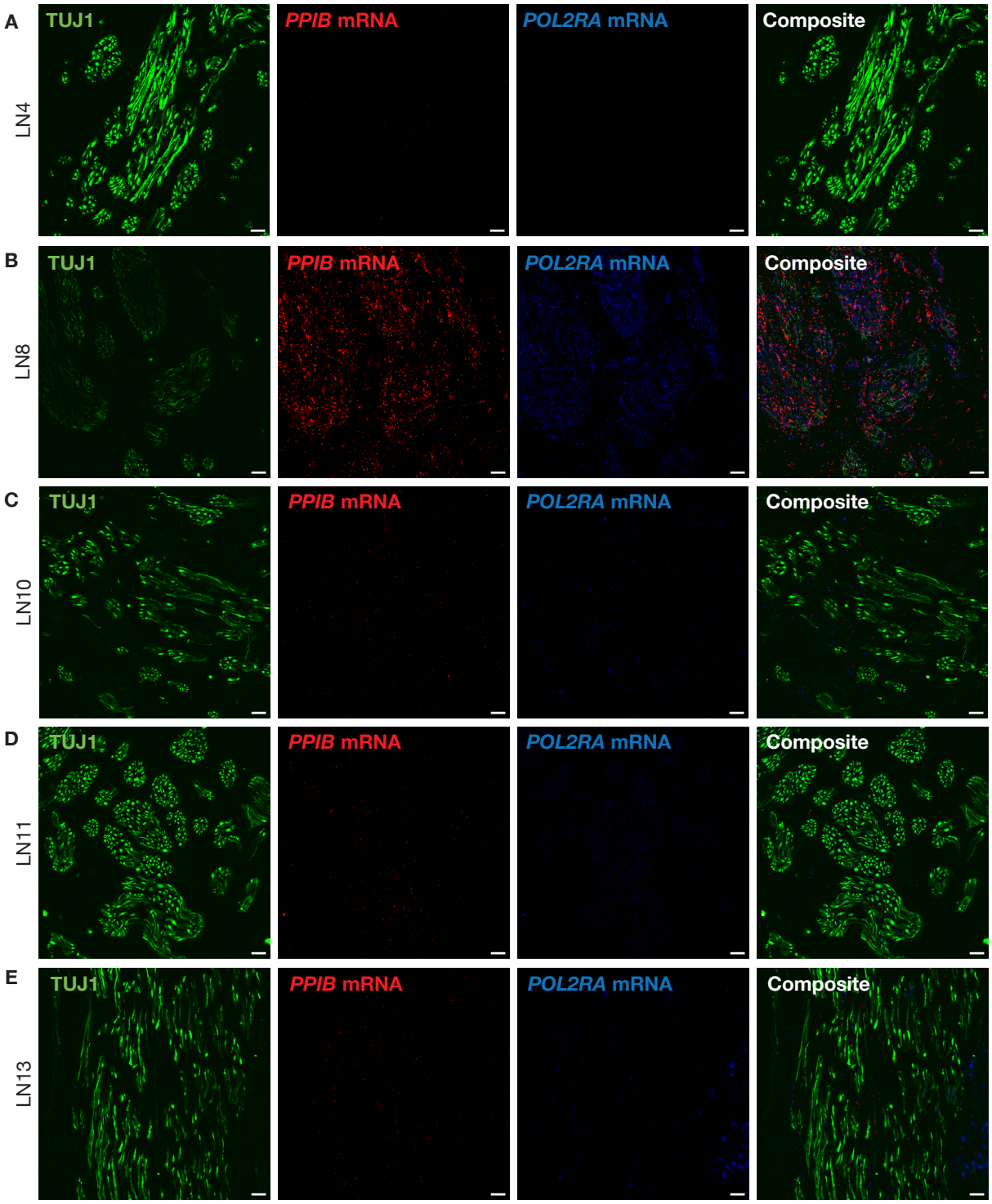

Figure 4.3 Variability in the positive control RNAscope probes' signal among different samples of human neuromas.
Confocal images displaying TUJ1 (FITC) immunofluorescence combined with PPIB (Cy3) and POL2RA (Cy5) RNAscope in samples of human neuromas. Each row displays a different sample. Scale bar: 20 µm, 40x magnification.

4.3.1.3 SCN9A and SCN10A

SCN9A and SCN10A encode for $Na_v1.7$ and $Na_v1.8$ respectively, two voltage gated sodium channels specifically expressed in the peripheral nervous system. The protein expression of these channels in human lingual neuromas was confirmed in earlier studies from our group (Bird et al., 2013, Bird et al., 2007). Using Visium spatial transcriptomics, SCN9A mRNA was detected across all tissue sections while SCN10A mRNA was detected at a very low level in a small number of spots across sections. A representative Visium section from LN8 showing the spatial distribution of SCN9A and SCN10A mRNA is shown in Figure 4.4.C-D. For reference, a section from the same sample labelled with anti-TUJ1 and an H&E image of the section used for Visium are shown in Figure 4.5.A-B, to highlight the location of nerve fascicles.

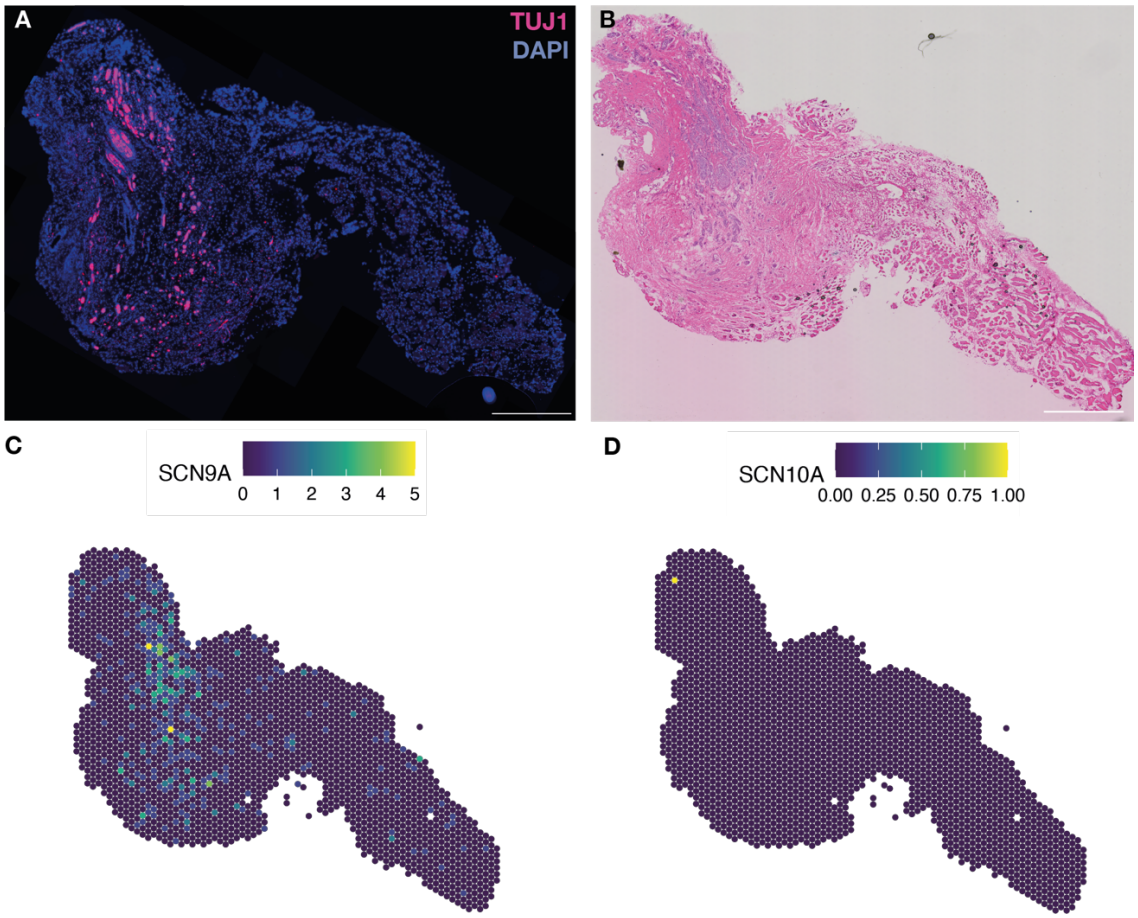

Figure 4.4 Spatially resolved expression of SCN10A and SCN9A detected with Visium in a human neuroma.
Section of LN8 immunolabelled with TUJ1 (Cy3) (A) and stained with H&E for Visium spatial transcriptomics (B). The sections displayed are 100 µm apart within the same sample. The transcript counts detected with Visium of SCN9A (C) and SCN10A (D) from one representative section of LN8 are displayed. The spots are colour-coded from blue to yellow by the number of transcripts

detected, where yellow spots contain a higher number of transcripts. The diameter of each spot is 55 µm.

We investigated the mRNA expression of SCN9A and SCN10A using RNAscope *in situ* hybridisation in order to validate the Visium data and, by simultaneous TUJ1 immunolabelling, observe whether any putative axonal transcripts could be detected.

RNAscope for SCN9A identifies several puncta (Figure 4.5.A) co-localised with cell nuclei, indicating the expression of SCN9A mRNA in cell-types associated with axons. Puncta that are closely associated to TUJ1+ labelling were also observed, indicating potential axonal SCN9A transcript expression.

On the other hand, only a few puncta could be detected for SCN10A RNAscope (Figure 4.5.A). The signal for the SCN10A probe is slightly more abundant than in the negative control and a few puncta are associated with TUJ1+ labelling, indicating potential axonal SCN10A transcript expression. However, the few transcripts that were detected with RNAscope cannot confidently be differentiated from background signal observed with the negative control probes.

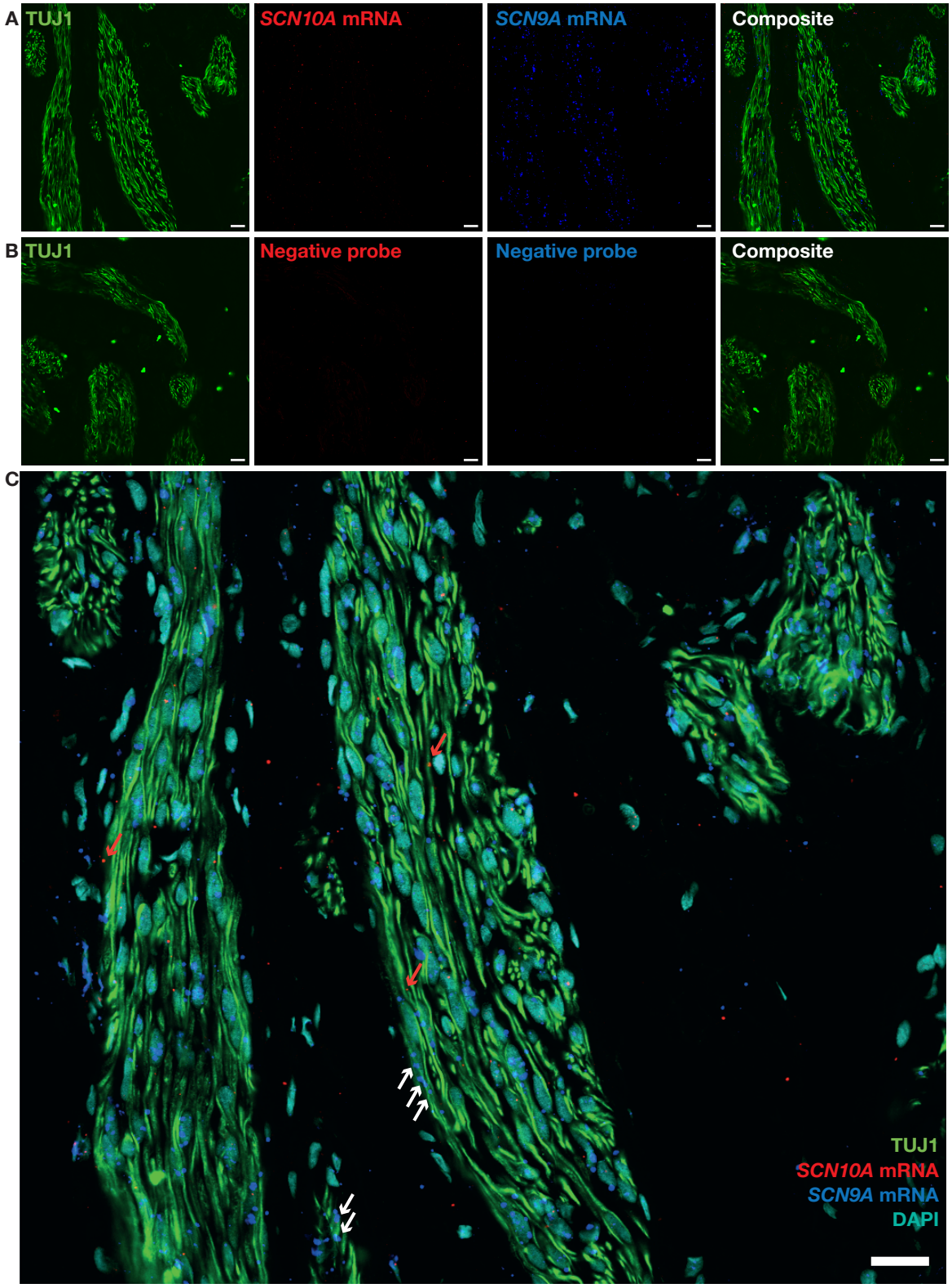

Figure 4.5 Combined SCN9A and SCN10 RNAscope and TUJ1 immunofluorescence in human lingual neuromas.
Confocal images displaying TUJ1 immunofluorescence (FITC), SCN10A mRNA (Cy3) and SCN9A mRNA (Cy5) in LN8 (A) and negative control for the same sample (B). A few puncta can be identified for SCN10A, while SCN9A expression is clearly visible. In C, white and red arrowheads point to SCN9A and SCN10A puncta, respectively, closely associated to TUJ1+ labelling. Scale bar: 20 μm, all images were taken at 40x magnification.

4.3.1.4 TRPV1 and SOX10

TRPV1, transient receptor potential vanilloid 1, is an ion channel expressed in most human nociceptors (Shiers et al., 2020). TRPV1 protein was previously detected in human neuromas in our group (Biggs et al., 2007). Using Visium spatial transcriptomics, TRPV1 mRNA was detected across all tissue sections. Representative Visium sections from LN8 showing the spatial distribution of TRPV1 mRNA is shown in Figure 4.7.A.

The SRY-box transcription factor 10 (SOX10) plays a key role in glial differentiation during development. In peripheral nerves, SOX10 is key to establish Schwann cells' cellular identity and its knockout leads to loss of structural integrity of peripheral nerves (Finzsch et al., 2010, Bremer et al., 2011). In injured human nerves, SOX10+ cells' density was found to peak at 90-100 days following injury and to severely decrease following this time point (Wilcox et al., 2020).

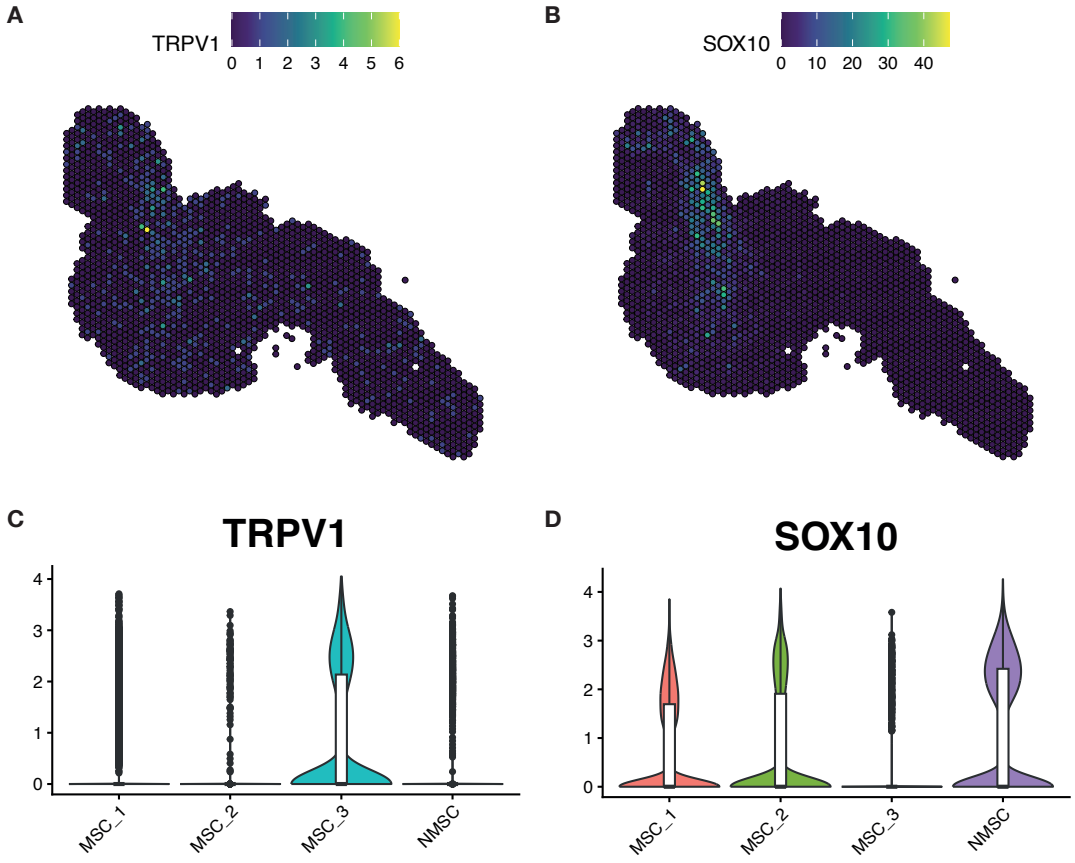

Figure 4.6 Spatially resolved expression of TRPV1 and SOX10 detected with Visium in a human neuroma.
Transcript counts of TRPV1 (A) and SOX10 (B) in Visium barcodes of one representative section of LN8. The spots are colour-coded from blue to yellow by the number of transcripts detected, where yellow spots contain a higher number of transcripts. Each spot's diameter is 55 µm.

C-D: TRPV1 (C) and SOX10 (D) mRNA expression in single nuclei annotated as Schwann cells in human trigeminal nerves and neuromas. The x-axis represents the number of transcripts detected in each nuclei.

The expression of TRPV1 and SOX10 mRNA was investigated using RNAscope *in situ* hybridisation in order to validate the Visium data. SOX10 is detected in several nuclei associated with TUJ1+ labelling (Figure 4.7.A), indicating the presence of SOX10+ cells in LN8, which was removed 120 days following nerve injury.

RNAscope *in situ* hybridization for TRPV1 identifies a small number of puncta (Figure 4.7.A) associated with TUJ1+ labelling, which can be differentiated from the negative control probe, indicating potential TRPV1 transcript expression in the axons. At the same time, several TRPV1+ puncta are found in association with SOX10+ puncta, which hints to the potential expression of TRPV1 mRNA in a subset of Schwann cells. The expression of TRPV1 in Schwann cells was also observed in the snRNAseq data (Figure 4.6.C), particularly abundant in MSC_3, a cluster of myelinating Schwann cells only found in the neuromas and absent in the healthy trigeminal nerve roots. TRPV1 protein expression in Schwann cells cultured from rat sciatic nerve has been previously reported (Grüter et al., 2020). Whether the transcript is translated into a functional protein in Schwann cells in human neuromas should be further investigated.

Overall, in the sample analysed with RNAscope, it's impossible to conclude whether TRPV1 mRNA detected is axonal in origin. However, the RNAscope signal taken together with evidence from single nuclei RNA sequencing hints to the expression of TRPV1 mRNA in Schwann cells.

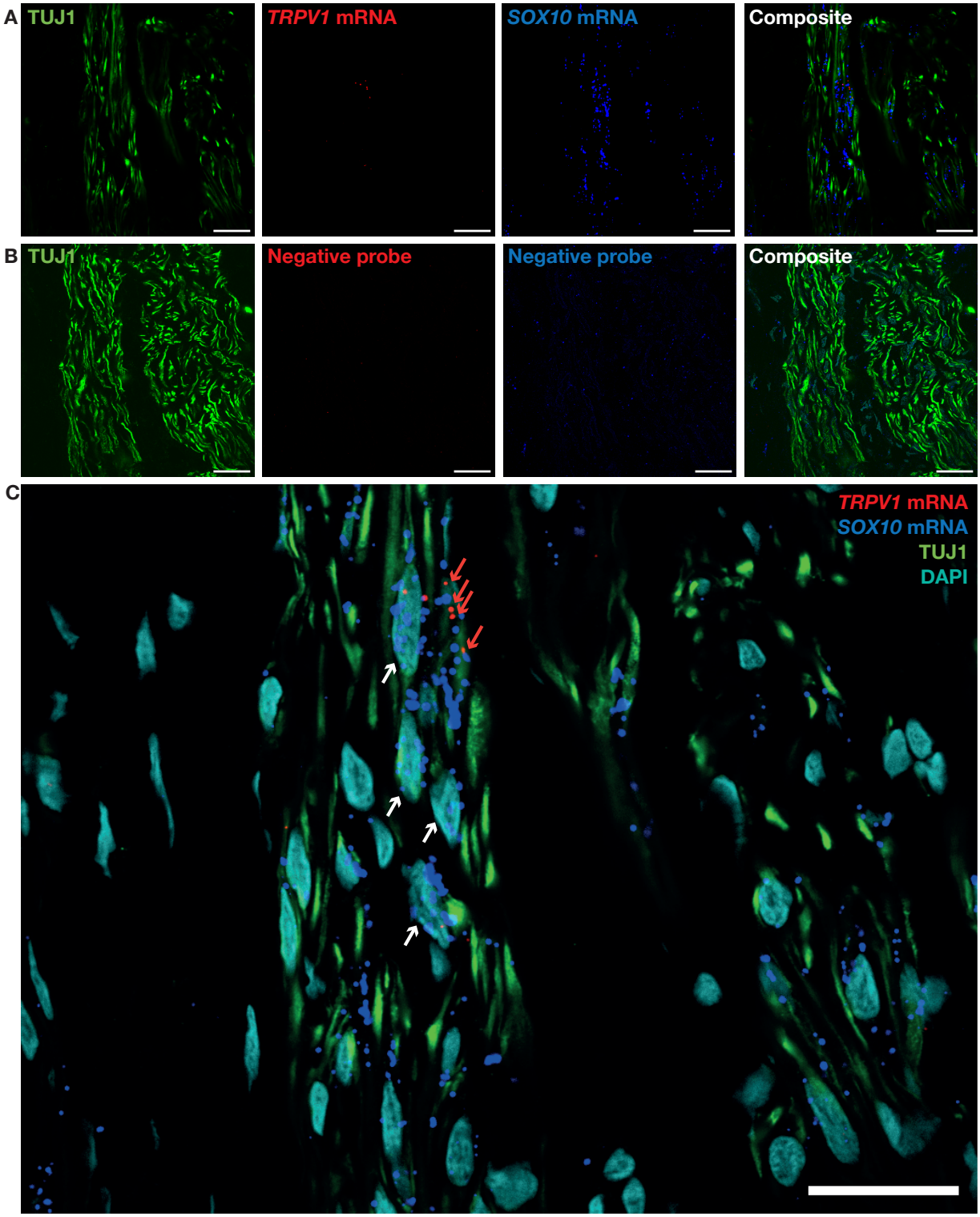

Figure 4.7 Combined TRPV1 and SOX10 RNAscope and TUJ1 immunofluorescence in samples of human neuromas.
Confocal images displaying TUJ1 immunofluorescence (FITC), TRPV1 mRNA (Cy3) and SOX10 mRNA (Cy5) in one sample of human neuroma (A) and negative control for the same sample (B). A few puncta can be identified for TRPV1 (red arrows), while SOX10 expression is clearly visible in cell nuclei associated with TUJ1+ labelling (white arrows). Scale bar: 20 µm, all images were taken at 100x magnification.

4.3.1.5 CD68 and OSM

CD68 encodes for a glycoprotein expressed in macrophages (Chistiakov et al., 2017). Nerve resident macrophages are activated following nerve injury to clear tissue debris and attract circulating macrophages to the site of injury through the release of cytokines and other pro-inflammatory mediators, which can sensitize sensory neurons resulting in neuropathic pain (Silva et al., 2021). One of the cytokines released by macrophages during the inflammatory response is Oncostatin M (OSM) (Repovic and Benveniste, 2002), which is required for noxious behavioural responses to nociceptive stimuli (Morikawa et al., 2004). OSM mRNA expression is increased in human DRG from male patients with neuropathic pain undergoing thoracic vertebrectomy in a sex-specific manner (Ray et al., 2023). The presence of CD68+ cells in human lingual neuromas was identified with immunohistochemistry but no correlation with the symptoms of pain were identified (Vora et al., 2007).

Data from Visium spatial transcriptomics confirms CD68 mRNA expression in human lingual neuromas (a representative section from LN8 is shown in Figure 4.8.A). OSM mRNA was detected at a low level in all samples analysed with Visium (LN8 is shown in Figure 4.8.B). Single nuclei RNA sequencing evidenced the expression of OSM mRNA in a small subset of CD68+ macrophages (Figure 4.8.D).

We aimed to investigate whether any CD68+ OSM+ cells could be identified in the neuromas with RNAscope *in situ* hybridization (Figure 4.9). Several CD68+ cells were identified with RNAscope in association with nerve fibres labelled by TUJ1. A few OSM mRNA puncta could be observed, in agreement with the Visium data. A few cells displayed positive signal for both CD68 and OSM mRNA (Figure 4.9.C-D). Due to the high variability of RNA quality between samples, sex and pain-related differences in OSM expression couldn't be quantified. Positive RNAscope signal for OSM could only be identified in the male sample LN8 out of the samples examined (Table 4.4).

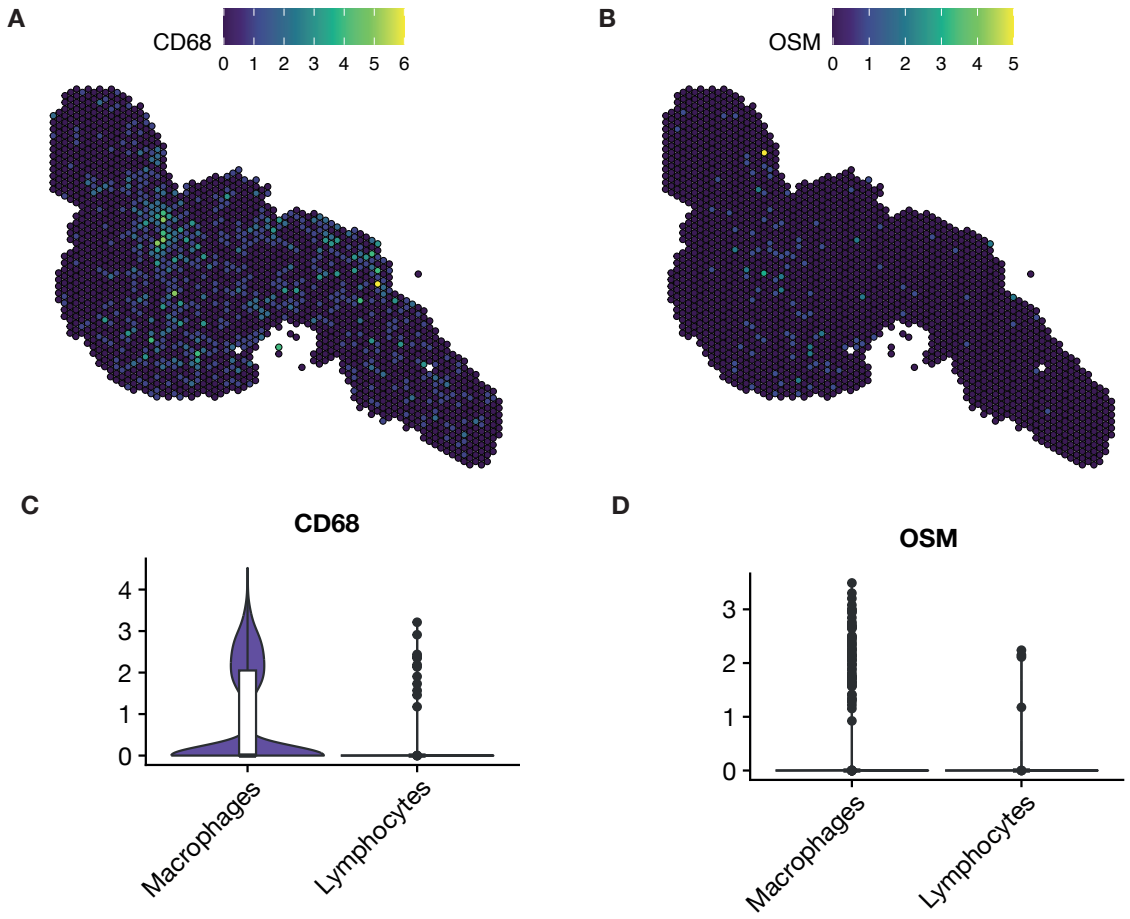

Figure 4.8 Spatially resolved and single cell expression of CD68 and OSM mRNA in human neuromas and trigeminal nerves.
A-B: Transcript counts of CD68 (A) and OSM (B) mRNA in Visium barcodes of one representative section of LN8. The spots are colour-coded from blue to yellow by the number of transcripts detected, where yellow spots contain a higher number of transcripts. Each spot's diameter is 55 µm. C-D: CD68 (C) and OSM (D) mRNA expression in single nuclei annotated as immune cells in human trigeminal nerves and neuromas. The x-axis represents the number of transcripts detected in each nuclei.

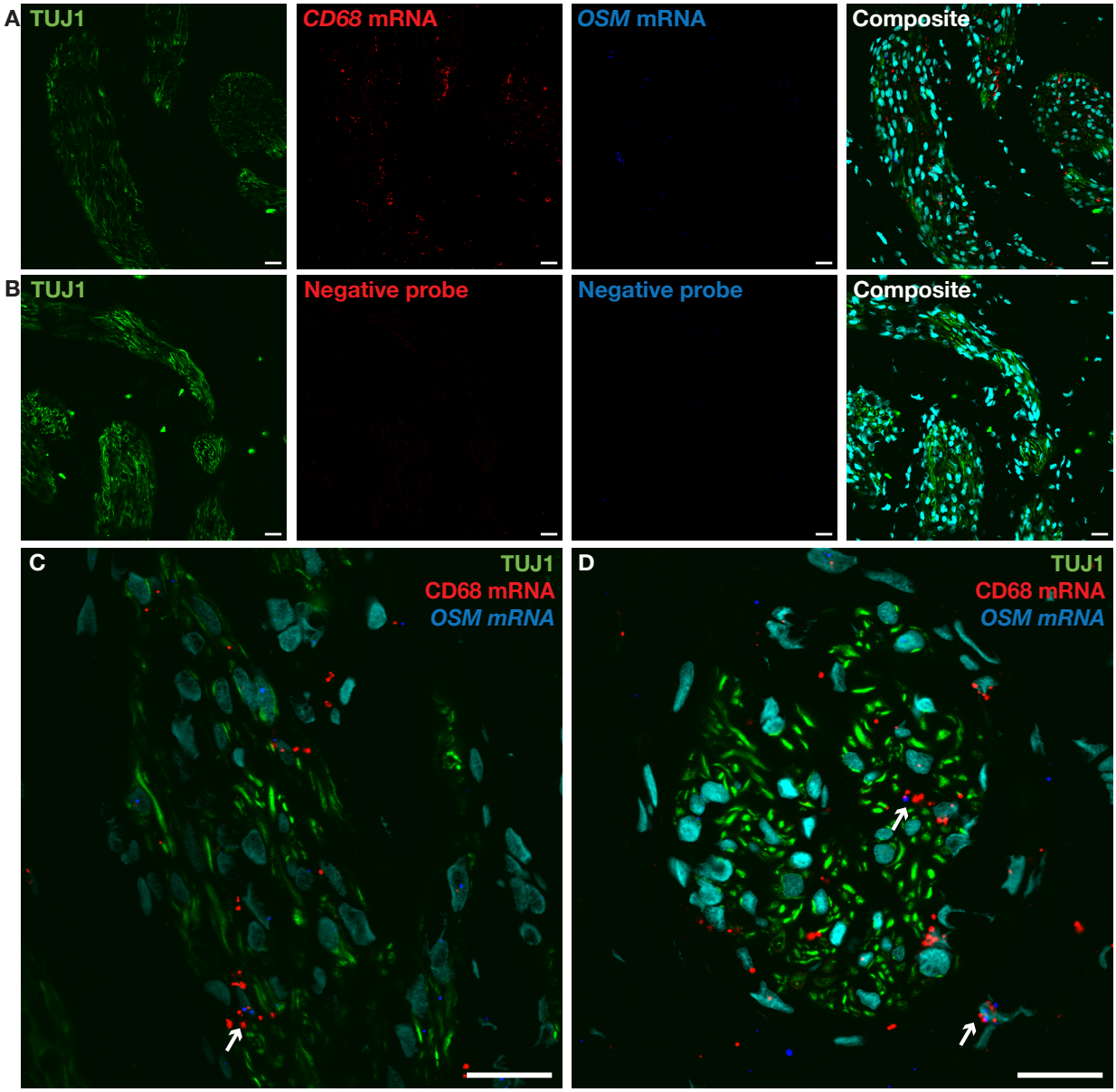

Figure 4.9 Combined CD68 and OSM RNAscope and TUJ1 immunofluorescence in samples of human neuromas.
TUJ1 immunofluorescence (FITC), CD68 mRNA (Cy3) and OSM mRNA (Cy5) in LN8 (A) and negative control for the same sample (B). The signal is displayed at higher magnification in C and D. The white arrows point to cells that display puncta for both CD68 and OSM mRNA. Scale bar: 20 µm, 40x and 100x magnification.

4.3.1.6 PTGDS

PTGDS encodes for prostaglandin D2 synthase, an enzyme involved in the conversion of PGH_2 to PGD_2 (Shen et al., 2023). PGD_2 is one of several prostaglandins (PGs): bioactive lipids converted from arachidonic acid through the action of COX1-2 enzymes. PGs can bind to several receptors coupled to GPCRs, leading to intracellular signalling cascades mediated by cAMP or Ca^{2+} that lead to neuronal sensitization and pro-nociceptive effects (Jang et al., 2020). PTGDS mRNA

in murine neurons is differentially expressed in a sex-specific manner, potentially driving the sex-specific behavioural response to PGE_2 induced algesia (Tavares-Ferreira et al., 2022a). Increased expression of PTGDS in female neurons was also identified in human DRGs (Shen et al., 2023).

In human lingual neuromas, PTGDS mRNA was detected across all samples with Visium (representative section shown in Figure 4.10.A) in areas associated with nerve fascicles. However, due to the low resolution of Visium it was impossible to infer the cellular origin of PTGDS mRNA. Single nuclei RNA sequencing evidenced a high level of expression of PTGDS in perineurial fibroblasts, followed by endoneurial fibroblasts and to a lower degree by Schwann cells (Figure 4.10.B).

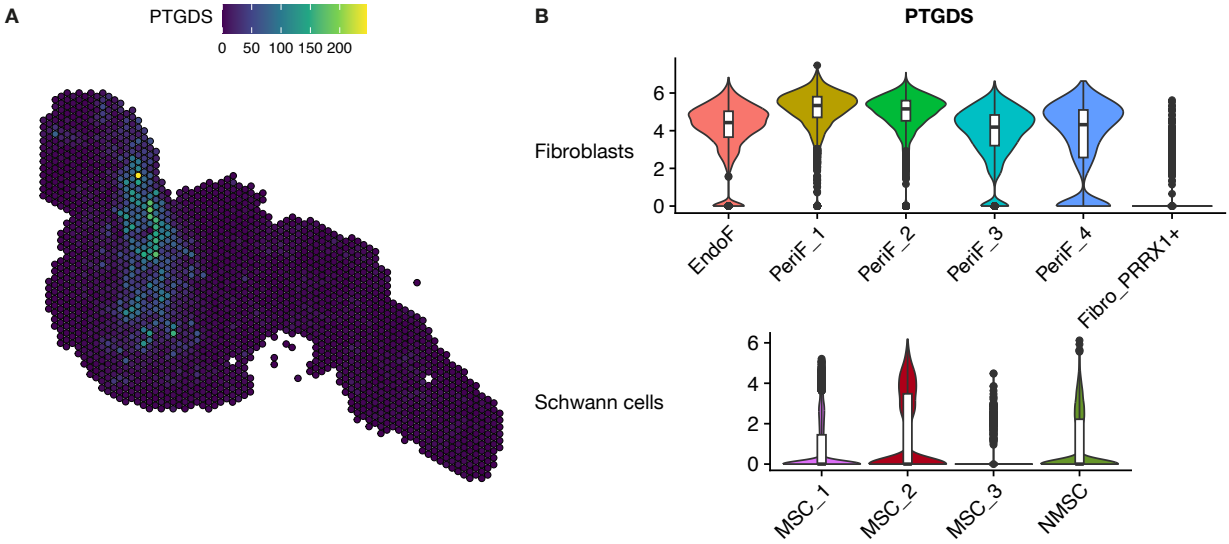

Figure 4.10 Spatially resolved and single cell expression of PTGDS mRNA in human neuromas and trigeminal nerves.
A: Transcript counts of PTGDS in Visium barcodes of one representative section of LN8. The spots are colour-coded from blue to yellow by the number of transcripts detected, where yellow spots contain a higher number of transcripts. Each spot's diameter is 55 µm. B: PTGDS mRNA expression in single nuclei annotated by cell-type in human trigeminal nerves and neuromas. The x-axis represents the transcripts detected in each nuclei. The expression is highest in perineurial fibroblasts followed by endoneurial fibroblast and Schwann cells. EndoF: endoneurial fibroblasts, PeriF: perineurial fibroblasts, Fibro_PRRX1+: PRRX1+ fibroblasts, MSC: myelinating Schwann cells, NMSC: non-myelinating Schwann cells.

RNAscope *in situ* hybridization confirms PTGDS expression in perineurial-like structures surrounding TUJ1+ labelling of putative axons (Figure 4.11). Co-labelling with SOX10 RNAscope indicates the presence of a few putative Schwann cells that express PTGDS mRNA in the neuromas (Figure 4.11.C-D).

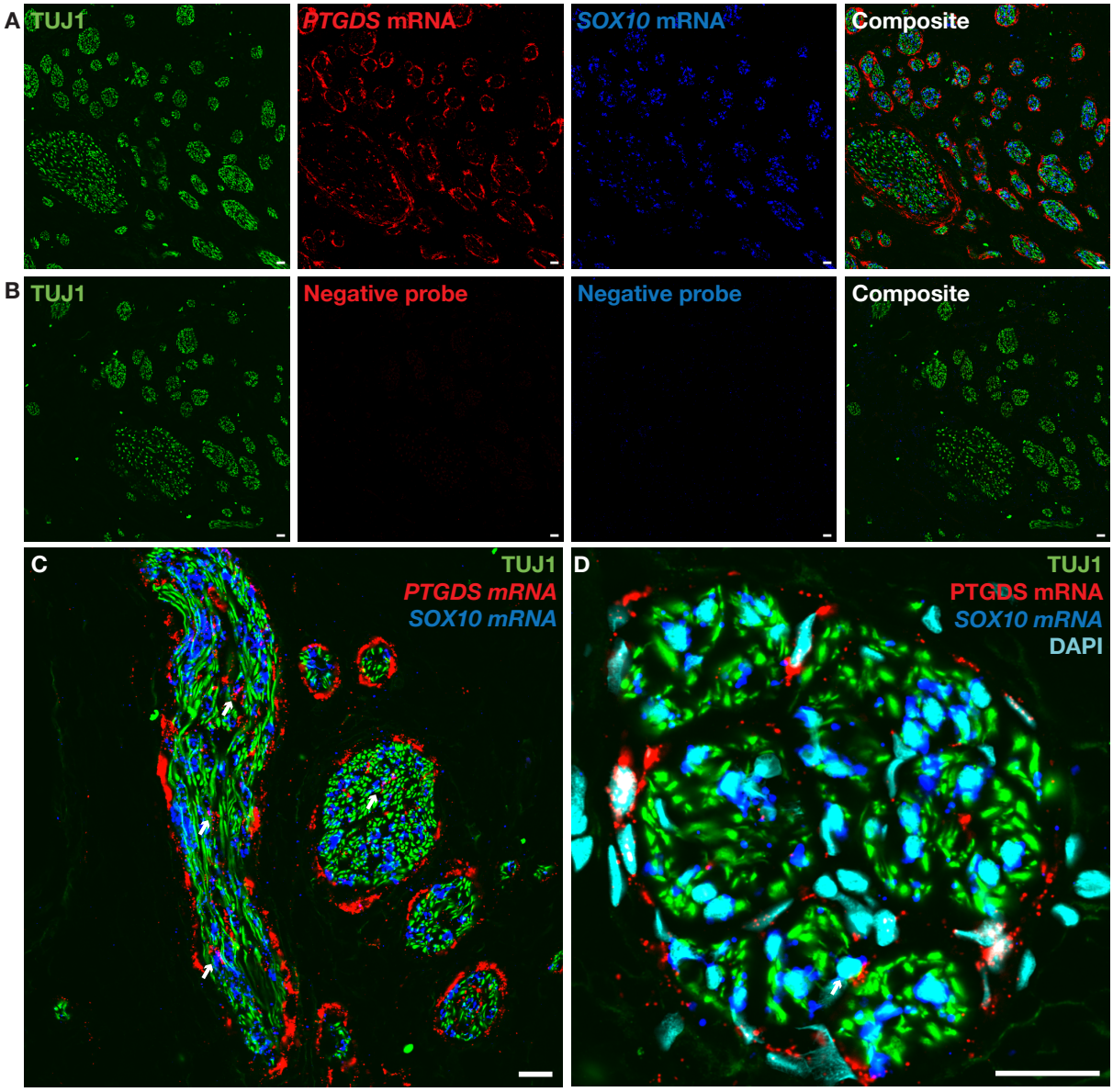

Figure 4.11 Combined PTGDS and SOX10 RNAscope and TUJ1 immunofluorescence in samples of human neuromas.
Confocal images displaying TUJ1 immunofluorescence (FITC), PTGDS mRNA (Cy3) and SOX10 mRNA (Cy5) in one sample of human neuroma (A) and negative control for the same sample (B). The signal is displayed at higher magnification in C and D. PTDGS mRNA is localised to perineurial-like structures surrounding TUJ1+ labelling. Small white arrows indicate SOX10 and PTGDS co-expression in putative Schwann cells (C). Scale bar: 20 µm, 20x and 40x magnification.

Overall, RNAscope validation of selected targets was in accordance with Visium spatial transcriptomics, providing information at a higher resolution in the sample analysed. This should be confirmed in a larger pool of samples, where potential differences in mRNA expression could be quantified and correlated with pain intensity, sex, time since injury and other clinical information. Unfortunately, this was impossible in the samples analysed due to the high variability of the signal

generated by hybridization with the positive control probe. In future, protease and antigen retrieval optimization of samples should be performed on an individual basis, since different treatment durations might be optimal in different samples due to the slight differences in fixation times, which might affect RNA accessibility.

4.3.2 Characterization of perineural cells with immunohistochemistry in human neuromas

Perineurial cells are specialised fibroblasts that form the blood-nerve barrier, protecting axons from antigens, invading pathogens, toxins and changes in extracellular ionic composition (Bunge et al., 1989, Iwanaga et al., 2022). They make up a continuous barrier separated by tight junctions surrounding the axon-schwann cell complexes and express GLUT-1, encoded by SLC2A1, a glucose transporter that enables the transport of nutrients into the endoneurial space to sustain the high energetic demand of axons (Piña et al., 2015, Rawat and Morrison, 2021). NGFR protein expression in perineurial cells was first reported in rat peripheral nerves (Yamamoto et al., 1992, Byers, 1990). Its presence in perineurial-like cells was observed by Chau et al. (2022) in human sural nerves analysed with single nuclei RNA-seq. NGFR, also known as p75 neurotrophin receptor and member of the tumour necrosis factor receptor superfamily, is a receptor for neurotrophins that mediates their neurotrophic actions but also regulates apoptosis (Roux and Barker, 2002, Dechant and Barde, 2002). The function of NGFR in perineurial cells has not been characterised yet.

NGFR and SLC2A1 mRNA is detected across all samples in the Visium data (Figure 4.12). In samples which exhibit an ordered fascicular organization such as LN15, their expression is localised at the boundary of the nerve fascicles where the perineurial barrier would be expected (Figure 4.12.B,F). Single nuclei RNA sequencing confirms NGFR and SLC2A1 mRNA expression in the clusters annotated as perineurial fibroblast in the neuromas and trigeminal nerve roots (Figure 4.12.I-J).

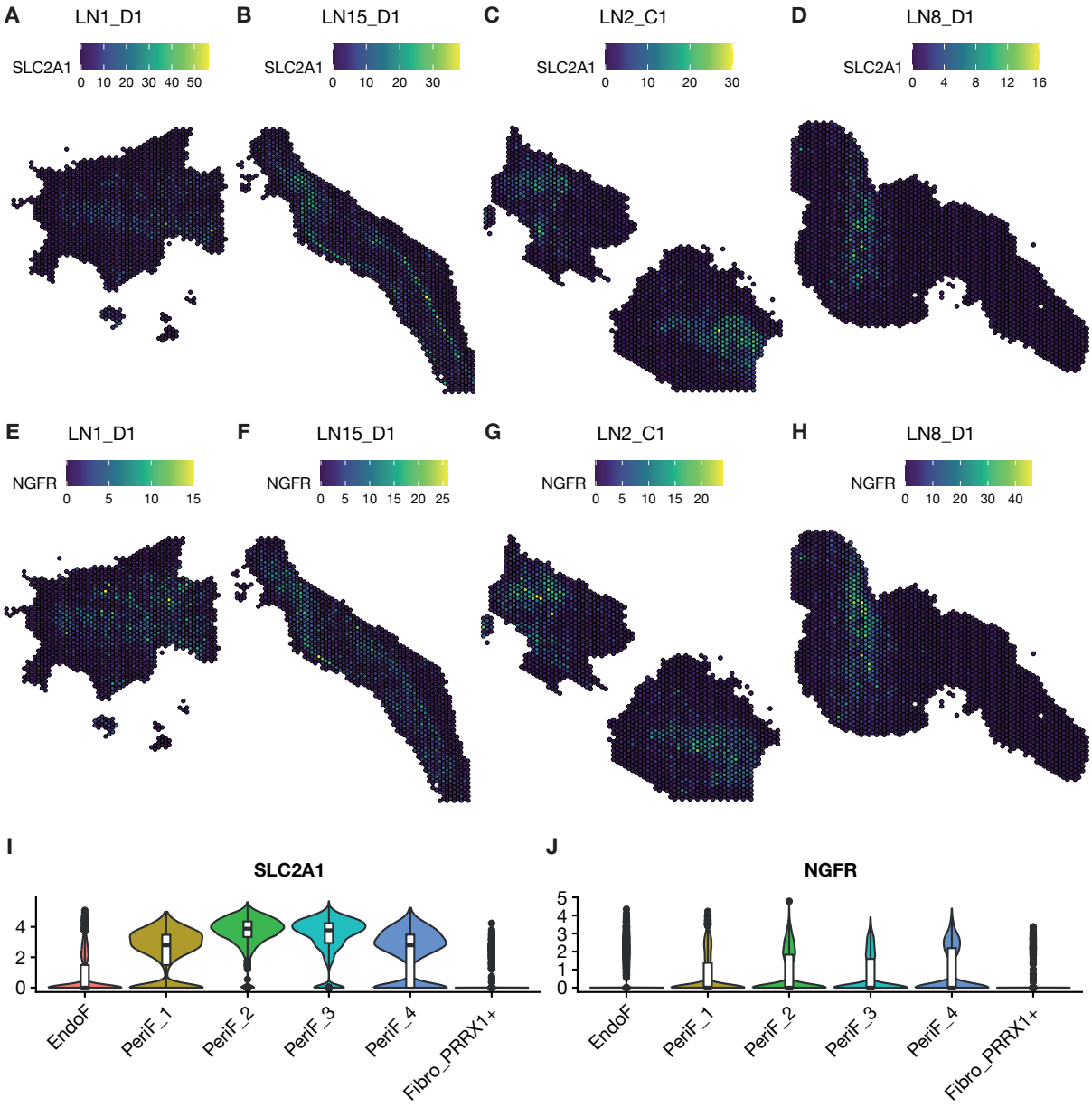

Figure 4.12 Spatially resolved and single cell expression of SLC2A1 and NGFR mRNA in human neuromas and trigeminal nerves.
A-H: Transcript counts of SLC2A1 (A-D) and NGFR (E-H) mRNA in Visium barcodes of representative sections from painful human neuromas, LN1 (A) and LN15 (B) and non-painful human neuromas, LN2 (C) and LN8 (D). The spots are colour-coded from blue to yellow by the number of transcripts detected, where yellow spots contain a higher number of transcripts. Each spot's diameter is 55 µm. I-J: SLC2A1 (I) and NGFR (J) mRNA expression in single nuclei annotated as fibroblasts in human trigeminal nerves and neuromas. Both transcripts are expressed in perineurial fibroblasts. EndoF: endoneurial fibroblasts, PeriF: perineurial fibroblasts, Fibro_PRRX1+: PRRX1+ fibroblasts.

NGFR and GLUT-1 (encoded by SLC2A1) protein expression was investigated with immunohistochemistry in human lingual neuromas (Figure 4.13), which confirmed the observations from Visium and single nuclei RNA sequencing data. GLUT-1 strongly localises to perineurial-like structures (Figure 4.13.B). NGFR co-

localizes with GLUT-1 (Figure 4.13.C and H). NGFR immunoreactivity is also observed in structures resembling axons, which is expected (Wyatt et al., 1990).

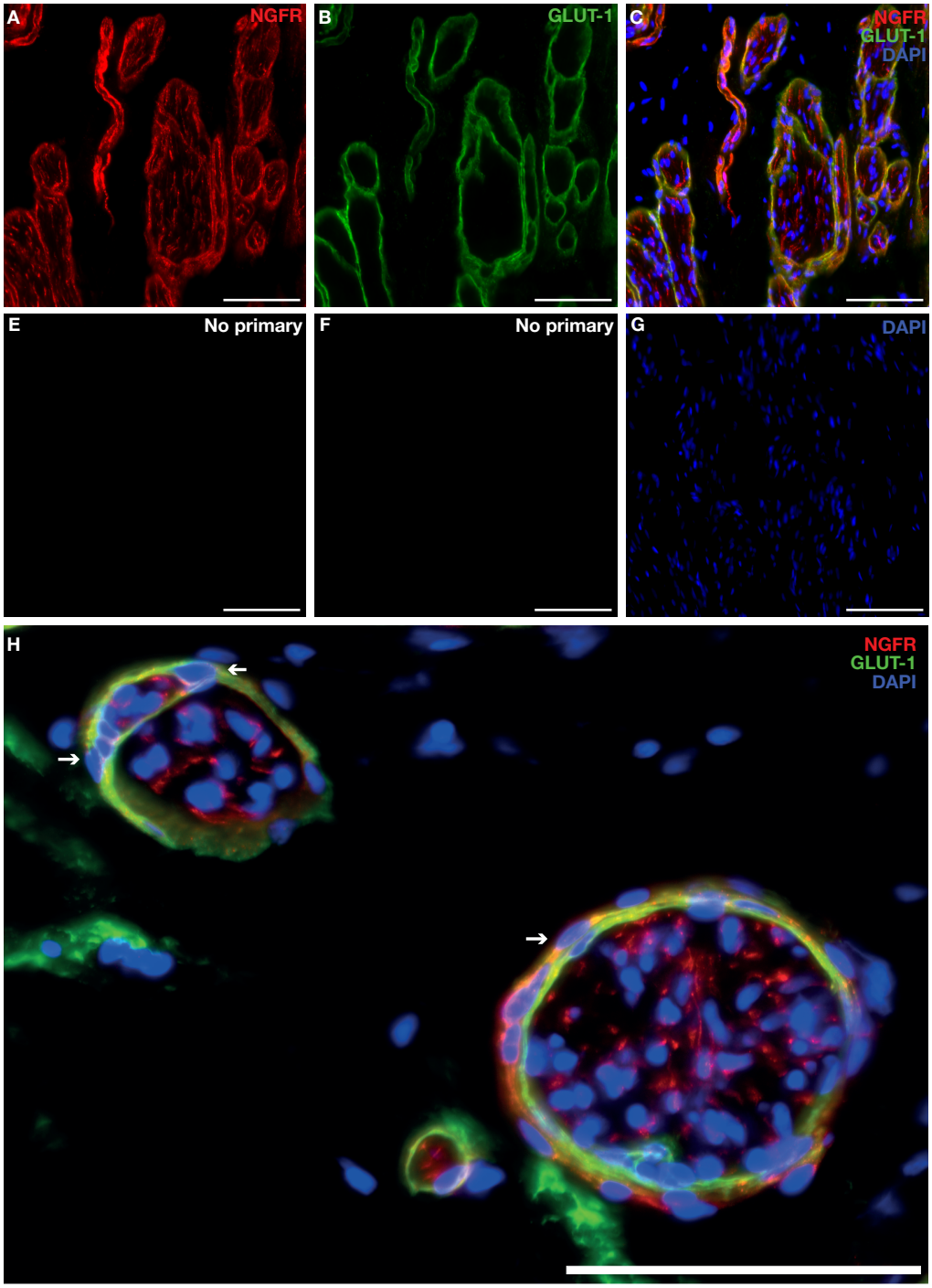

Figure 4.13 Protein expression of GLUT-1 and NGFR in human neuromas.
A-C: Representative section of NGFR (Cy3) and GLUT-1 (FITC) immunofluorescence showing co-localization in one sample of human neuroma. E-F: Negative control where both primary antibodies were omitted. H: Detailed view of two small nerve fascicles (LN6) displaying co-localization of NGFR and GLUT-1 in perineurial cells, pointed out by the white arrows. NGFR+ putative axons are also visible within the nerve fascicle. Scale bar: 100 µm, magnification 40x.

4.3.3 Immunohistochemical investigation of PI16 and potential correlation with symptoms of pain in human neuromas

Using single nuclei RNA sequencing, PI16 was identified as a marker for endoneurial cells, as shown in section 2.3.2.2 PI16, encoding for peptidase inhibitor 16, was recently identified as a regulator of neuropathic pain (Singhmar et al., 2020) and inflammatory pain (Garrity et al., 2023) in animal models, where its deletion reduces behavioural responses indicative of pain following nerve injury and CFA injection, respectively. Its expression was identified in fibroblasts located in the perineurium/epineurium of the murine sciatic nerve and the meninges of the DRG. In human DRG, PI16 mRNA is expressed in fibroblasts surrounding GFRA+ neurons (Garrity et al., 2023). In the SNI-induced neuropathic pain model, PI16 protein expression is associated with an increased epi/perineurial thickness in the murine sciatic nerve (Singhmar et al., 2020). In the absence of PI16 expression, there was a reduction in CD45+ leukocyte influx following SNI, indicating a potential mechanism of neuropathic pain development where PI16 encourages leukocyte infiltration by disrupting the blood-nerve barrier (Singhmar et al., 2020). This mechanism was not confirmed in the CFA-induced model of inflammatory pain, where PI16 expression did not affect leukocyte infiltration or the permeability of the blood-nerve barrier. Instead, its deletion resulted in increased anti-inflammatory macrophages infiltration in the meninges of murine DRG, accelerating the recovery from CFA injections (Garrity et al., 2023).

PI16 mRNA is detected in human neuromas analysed with Visium (representative sections from four samples are shown in Figure 4.14.A-D). Single nuclei RNA sequencing identified PI16 expression to be originating in the cluster annotated as endoneurial fibroblasts (Figure 4.14.E), which is also positive for CSPG4, the gene encoding for NG2, a marker for endoneurial fibroblasts (Richard et al., 2014). This is contraposed to the findings by Singhmar et al. (2020), where PI16 expression was observed in α-SMA and P4HB+ fibroblasts and lacked in NG2+ endoneurial fibroblasts (Singhmar et al., 2020).

Here, validation of PI16 protein expression in human neuromas and the potential correlation between its expression and the symptoms of pain reported by the patients was investigated. A total of 5 painful (pain VAS > 30) and 5 non-painful

(pain VAS < 30) samples were selected for immunohistochemical analysis with TUJ1 dual-labelling to identify PI16 expression associated with TUJ1+ axons. The clinical information of the samples used is reported in Table 4.5.

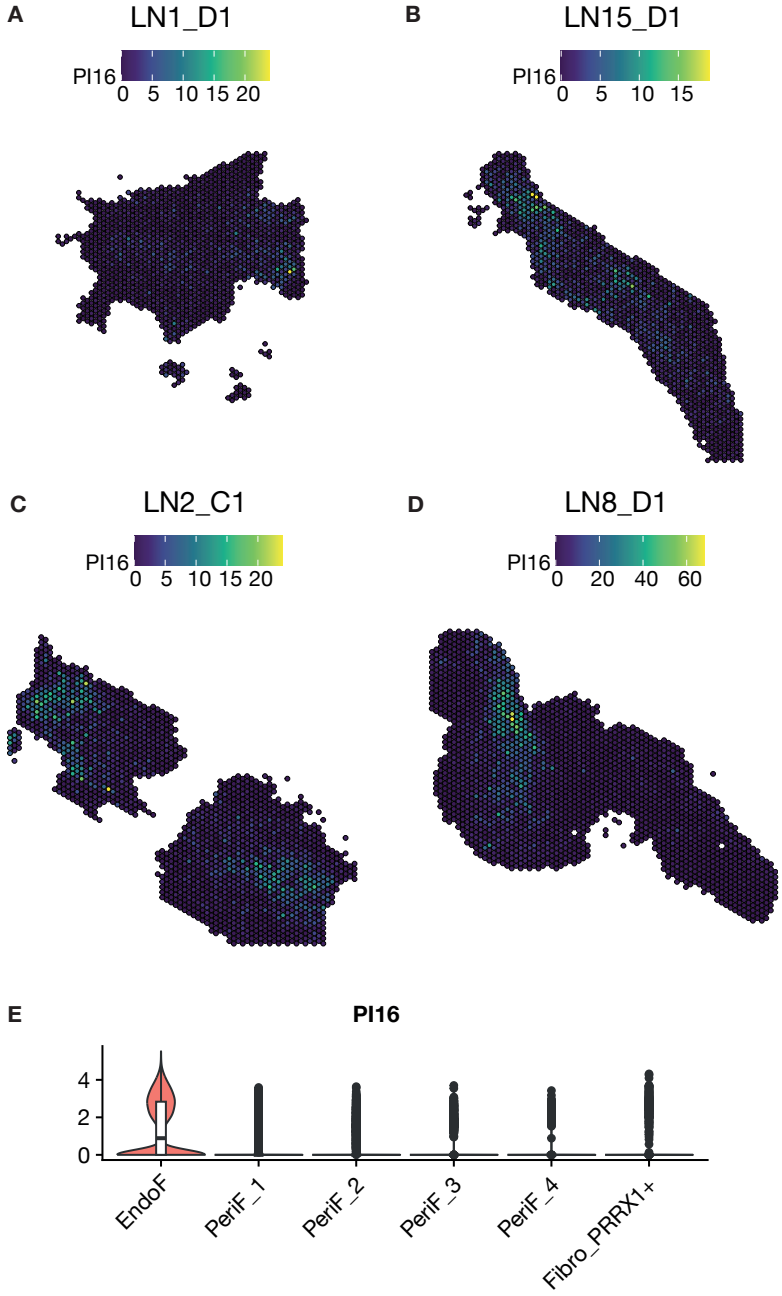

Figure 4.14 Spatially resolved and single cell expression of PI16 mRNA in human neuromas and trigeminal nerves.
A-D: Transcript counts of PI16 mRNA in Visium barcodes of representative sections from painful human neuromas, LN1 (A) and LN15 (B) and non-painful human neuromas, LN2 (C) and LN8 (D). The spots are colour-coded from blue to yellow by the number of transcripts detected, where yellow spots contain a higher number of transcripts. Each spot's diameter is 55 µm. E: PI16 mRNA expression in single nuclei annotated as fibroblasts in human trigeminal nerves and neuromas. PI16 is expressed in endoneurial fibroblasts. EndoF: endoneurial fibroblasts, PeriF: perineurial fibroblasts, Fibro_PRRX1+: PRRX1+ fibroblasts.

Table 4.5 Clinical information of the human neuromas used for the quantification of PI16 protein expression.

Sample	Time since injury (months)	Age	Sex	Pain	Pain VAS	Tingling VAS	Discomfort VAS
LN7	17	30	F	N	4	100	84
LN6	14	25	F	N	0	0	0
LN17	29	41	M	N	0	0	0
LN10	69	39	F	N	0	100	49
LN11	18	33	F	N	3	100	21
LN1	12	27	F	Y	55	100	80
LN4	19	65	F	Y	100	50	100
LN15	12	34	F	Y	61	100	77
LN12	16	34	F	Y	43	10	88
LN13	4	28	F	Y	65	100	87

Patients in the non-painful group reported an average pain VAS score of 1.4, while patients in the painful group had VAS scores ranging between 43 and 100, with an average of 64.8. Overall, there was a significant difference in the pain VAS score between the high and low pain groups ($p < 0.001$).

Immunolabelling and data analysis were performed blinded to the clinical information and the investigator did not know which samples belonged to the painful and non-painful group. All samples analysed were from female patients except of LN17. To assess the antibody's specificity, a pre-absorption control was performed where the antibody was incubated with its blocking peptide prior to the incubation on the tissue (Figure 4.15.B). PI16 immunoreactivity is localised to cells in close proximity to TUJ1-labelled putative axons. Its location within the nerve fascicles suggests the expression of PI16 in endoneurial fibroblasts as suggested by the single nuclei RNA sequencing data, however this needs to be confirmed with endoneurial marker NG2 dual-labelling.

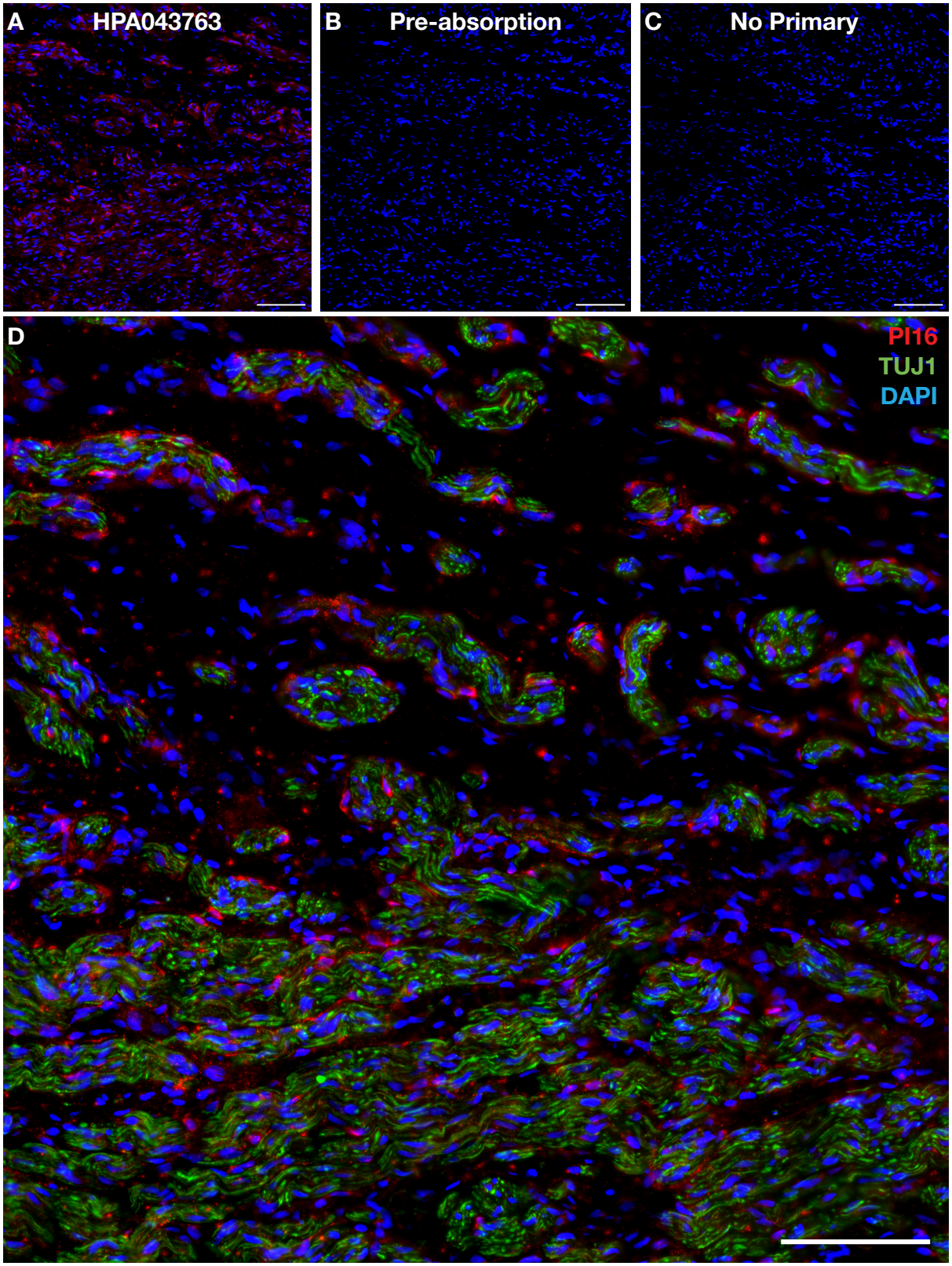

Figure 4.15 Specificity controls of anti-PI16 HPA043763 and expression in TUJ1+ areas.
A: Immunoreactivity of PI16 (Cy3) detected with HPA043763 (Atlas) overlaid with DAPI. B: Pre-absorption control where HPA043763 was incubated with its blocking peptide prior to the incubation with the tissue. C: Negative control where the primary antibody was omitted. D: Dual-labelling of PI16 (Cy3) with TUJ1 (FITC), indicating a close association between PI16-positive cells and putative nerve fibres labelled with TUJ1. Scale bar: 100 um, 40x magnification.

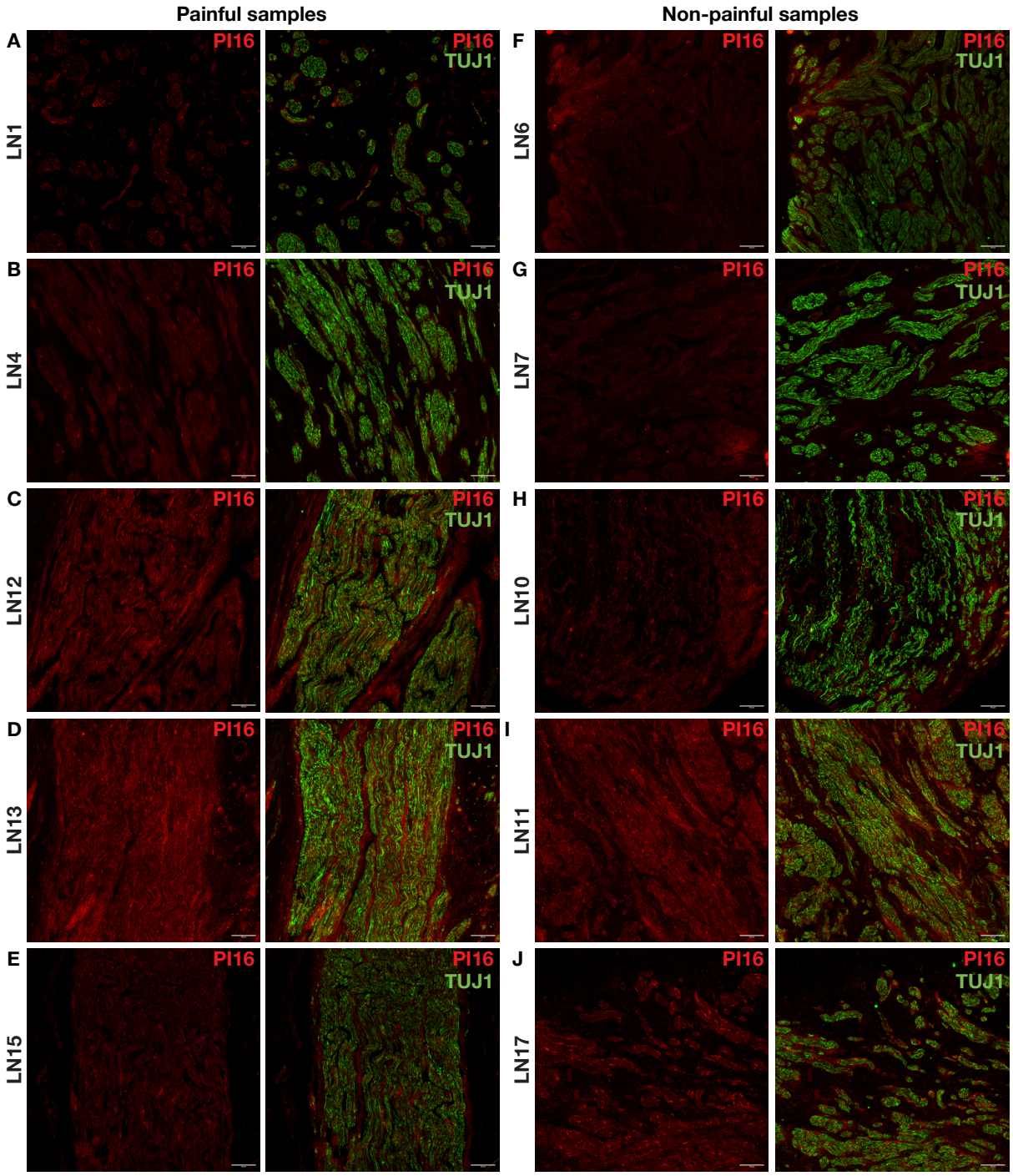

Figure 4.16 PI16 dual labelling with TUJ1 in painful and non-painful neuromas.
Representative images of painful (A-E) and non-painful (F-J) human neuromas dual-labelled with PI16 (Cy3) and TUJ1 (FITC). Each panel includes one representative area from each sample showing Cy3 only (left) and Cy3 overlaid with FITC (right). Scale bar: 100 um, 20x magnification.

Ten samples were dual-labelled with PI16 and TUJ1 antibodies (Figure 4.16) and the entire tissue section was imaged and analysed in at least two technical replicates. PI16 immunoreactivity was variable across samples, with samples displaying localised expression in endoneurial-like cells within the nerve fascicles

(Figure 4.16.A,B,J), while in other samples the signal was more wide-spread and less localised, but still associated with TUJ1+ areas (Figure 4.16.C,D,I).

PI16 fluorescent intensity in areas containing nerve fascicles was analysed by identifying TUJ1+ areas and measuring PI16 mean fluorescent intensity, which was performed in a blinded manner. No significant difference was identified in the mean fluorescent intensity of PI16 immunoreactivity in TUJ1+ areas in painful versus non-painful groups (Figure 4.17.A). No statistically significant correlation between PI16 mean fluorescent intensity and intensity of pain reported by the patient was identified (Figure 4.17.B), and no correlation between discomfort, tingling, time since injury or age was identified.

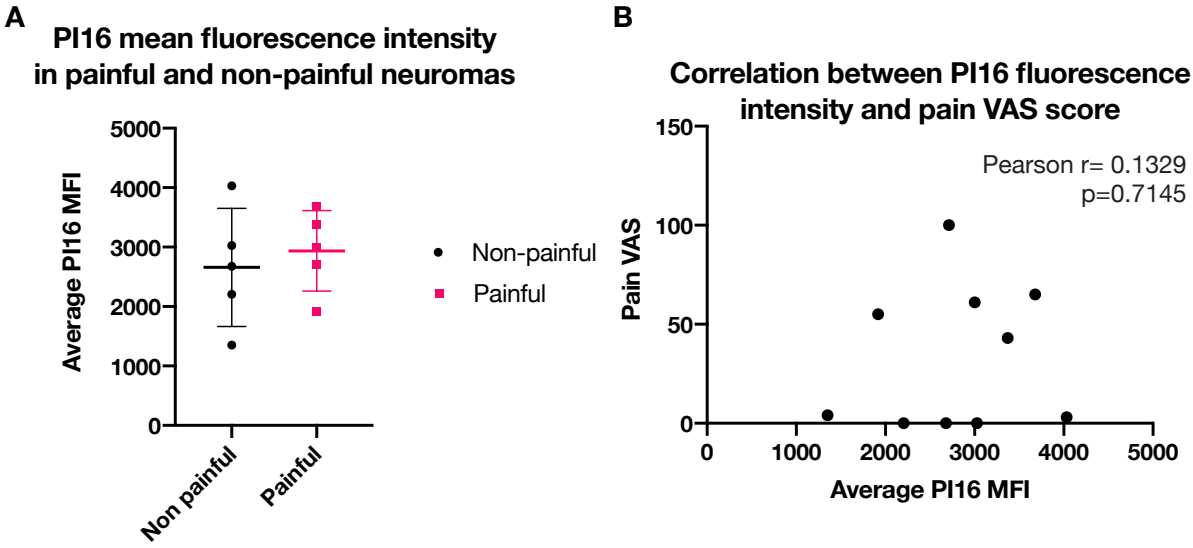

Figure 4.17 Quantification of PI16 fluorescence intensity associated with TUJ1+ areas in human neuromas.
A: Mean fluorescence intensity of PI16 immunoreactivity in areas associated with positive TUJ1+ signal in painful (n=5) and non-painful samples (n=5). No statistical difference was identified between the groups (unpaired t-test). The scatter plot displays each group's mean with standard deviation. B: Correlation between mean fluorescent intensity of PI16 in areas associated with positive TUJ1 signal and the intensity of pain reported by the patient. Pearson r= 0.1329, r^2=0.0165. The correlation wasn't statistically significant.

Singhmar et al. (2020) showed that PI16 expression leads to CD45+ leukocyte infiltration following nerve injury in mice. In the neuromas, it was hypothesised that PI16 immunoreactivity might be correlated with an increase in CD45+ cells. CD45 and PI16 dual labelling was performed on four samples to test this hypothesis (Figure 4.18). From a qualitative observation, the number of CD45+ cells varied

between samples independently from PI16 immunoreactivity: for example LN11, which displays high fluorescent intensity for PI16, has a low number of CD45+ cells (Figure 4.18.B), whilst LN6 shows the opposite trend (Figure 4.18.C).

Overall, PI16 protein expression was demonstrated with immunohistochemistry to be localized to endoneurial-like cells within nerve fascicles of human neuromas. No correlation was identified between PI16 fluorescent intensity and symptoms of pain or leukocyte infiltration in the samples analysed.

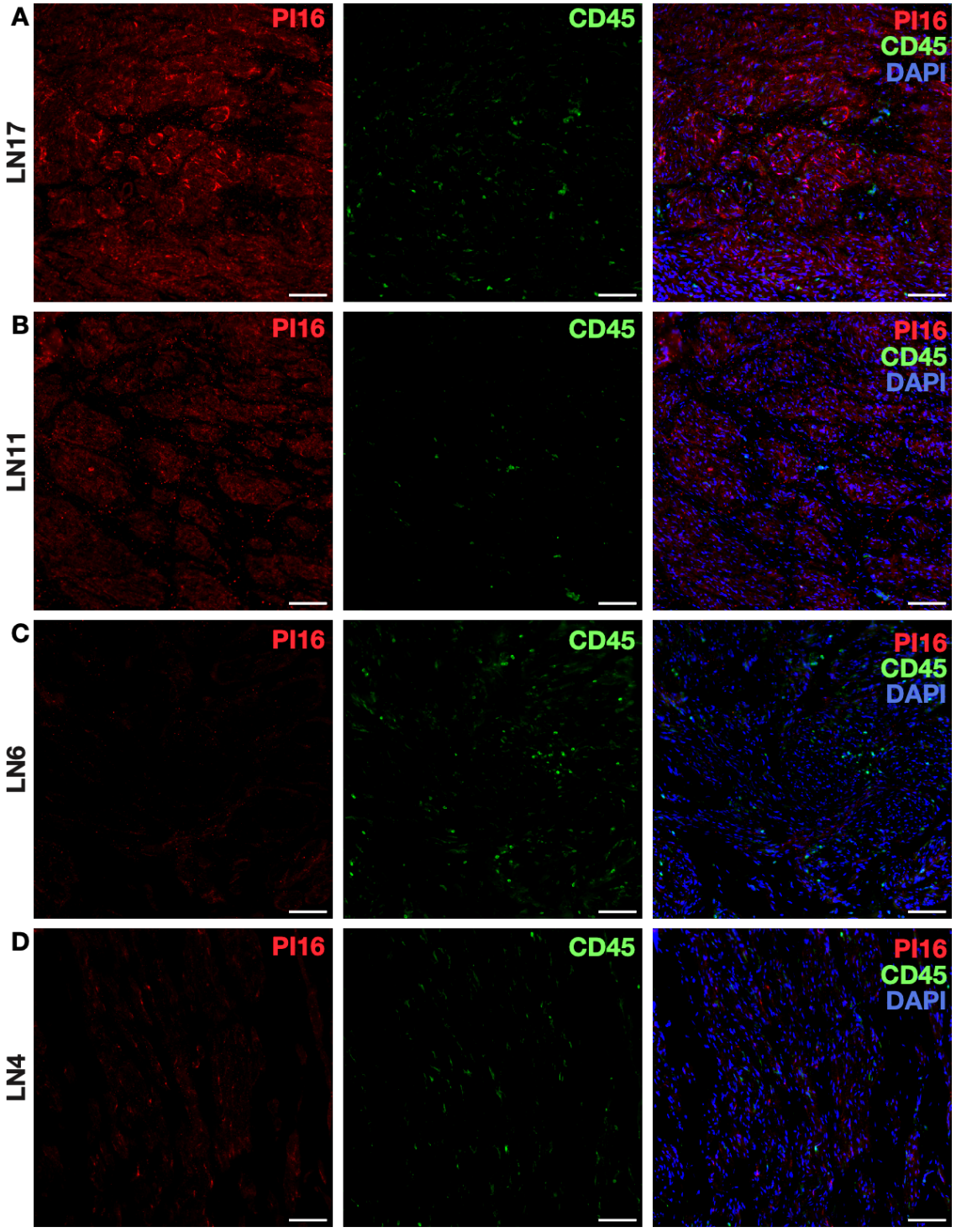

Figure 4.18 Protein expression of PI16 and CD45 in human neuromas.
A-D: PI16 (Cy3) and CD45 (FITC) immunoreactivity is shown in representative areas from different human neuromas. It was hypothesised that PI16 expression might be correlated with leukocyte infiltration, labelled with CD45. No apparent relationship was observed between PI16 and CD45 immunoreactivity. Scale bar: 100 um, 20x magnification.

4.4 Discussion

In this chapter the experiments that aimed to validate the findings from previous chapters were described. Visium and single cell RNA sequencing experiments provide whole-transcriptome information on whole samples or tissue sections, enabling mapping of cell-types in each sample characterised at a molecular level. Selected targets were validated in order to broadly confirm the validity of these techniques. RNAscope and immunohistochemistry were used to validate this data, providing information on selected targets at higher resolution. The cheaper cost per sample of these techniques allowed the analysis of the expression level of specific targets across samples linked with different pain intensities, as performed with PI16, which was investigated to identify potential correlations with the symptoms of pain reported by the patients.

4.4.1 Axonal localization of ion channels transcripts

SCN9A, SCN10A and TRPV1 are well-known genes relevant to pain generation and maintenance (Goodwin and McMahon, 2021, Katz et al., 2023). Whilst their protein expression in the axons of primary sensory afferents is well-characterised (Krishnan et al., 2009), there is also evidence for the presence of mRNA for these channels suggesting local translation, including a few studies observing SCN10A and TRPV1 mRNA in axons of animal models (Ruangsri et al., 2011, Hirai et al., 2017a, Tohda et al., 2001, Thakor et al., 2009). Evidence for mRNA expression of SCN9A in axons of primary afferents is lacking (Akin et al., 2019).

Interestingly, SCN9A and TRPV1 mRNA expression was detected with Visium and RNAscope, while SCN10A was almost undetectable with both techniques. All of the above ion channels were identified to be expressed in human lingual neuromas at the protein level in studies previously performed in our group (Bird et al., 2007, Bird et al., 2013, Biggs et al., 2007).

Ion channels are transported anterogradely in vesicles to the axons, where they are inserted in the membrane (Higerd-Rusli et al., 2023). However, local translation has been identified as another important mechanism of ion channel expression: increased axonal mRNA level of ion channels, including $Na_v1.8$, have been detected at the site of injury in several animal models (Gale et al., 2022, Thakor et al., 2009).

The translocation of mRNAs to the axon might be dependent on the presence of alternative 3'UTR sequences: a novel long 3'UTR sequence in $Na_v1.8$ mRNA was identified exclusively at the site of injury following sciatic nerve entrapment (Hirai et al., 2017b). The probe for SCN10A used in the Visium assay targets the 3' UTR, however the targeted sequence is present in all three transcript variants, including the alternative longer 3'UTR associated with axonal targeting. Whilst it can't be excluded that the presence of a longer 3' UTR in the preferentially axonal $Na_v1.8$ mRNA could affect its conformational structure preventing probe binding, RNAscope confirmed the observations from Visium. The probe used for the RNAscope experiments targets a different region of the SCN10A transcript (nt 2-1090), which is not in the 3'UTR. The low SCN10A mRNA signal detected with both RNAscope and Visium suggests that, at least in human lingual neuromas, local axonal $Na_v1.8$ mRNA expression and translation is rare, unlike what is observed in animal models (Ruangsri et al., 2011, Thakor et al., 2009, Hirai et al., 2017a). Targeting local protein synthesis of ion channels has been suggested as a potential path to pain relief (Obara et al., 2012). The findings discussed above suggest that whilst targeting this mechanism might be promising in animal models (Ruangsri et al., 2011), they might not always translate in humans, as is the case of $Na_v1.8$ mRNA.

$Na_v1.7$, encoded by SCN9A, is another important sodium channel specifically expressed in primary sensory afferents and its trafficking to the membrane has been well characterised (Higerd-Rusli et al., 2023, Akin et al., 2019), whilst evidence of local translation is lacking. SCN9A mRNA expression in the human neuromas was independently detected with both Visium and RNAscope. RNAscope enabled to visualize its expression at a higher resolution, highlighting its localization in axons, but also in association with nuclei within nerve fascicles, hinting to its expression in non-neuronal cell-types. Single nuclei RNA sequencing suggests SCN9A transcript expression in 27% of non-myelinating Schwann cells (Figure 4.19). $Na_v1.7$ expression in non-myelinating Schwann cells has not been previously reported to my knowledge, and its potential function in this cell-type has not been characterised.

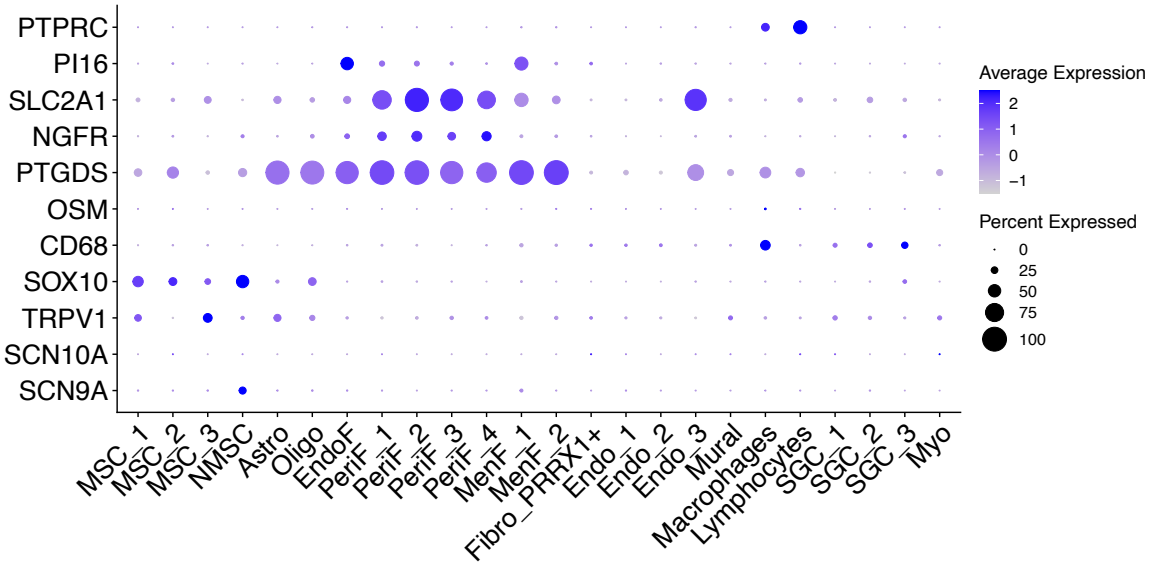

Figure 4.19 Expression of the genes validated by RNAscope or immunohistochemistry in the single nuclei RNA dataset.
Dotplot displaying the cluster-specific expression of the genes validated in this chapter. The size of each dot represents the percentage of cells within one cluster that express the transcript, whilst the colour represents the fold change compared to other clusters, where a darker shade of purple indicates increased expression. MSC: myelinating Schwann cells. NMSC: non-myelinating Schwann cells. Astro: astrocytes. Oligo: oligodendrocytes. EndoF: endoneurial fibroblasts. PeriF: perineurial fibroblasts. MenF: meningeal fibroblasts. Fibro_PRRX1: PRRX1+ fibroblasts. Endo: endothelial cells. SGC: salivary gland cells. Myo: myocytes.

Transient receptor potential vanilloid 1 (TRPV1) is a cation channel activated by capsaicin and heat (Katz et al., 2023). Evidence of increased TRPV1 mRNA axonal transport during inflammation was found in the central and peripheral afferents of primary sensory neurons in mice (Tohda et al., 2001). Whilst TRPV1 mRNA expression in human neuromas was independently detected with both Visium and RNAscope, its location in the axons of human primary afferents couldn't be confirmed. Single nuclei RNA sequencing and RNAscope, however, hint to its expression in myelinating Schwann cells, particularly in the cluster enriched in injured trigeminal nerves (MSC_3). TRPV1 expression in Schwann cells was also reported in rat sciatic nerves by Grüter et al. (2020). Here, the authors show that capsaicin administration on cultured Schwann cells results in the decrease of MHC-II receptor presentation, TLR4 and ICAM1 expression and increased CGRP expression, overall exhibiting an immunomodulatory profile (Grüter et al., 2020). The intracellular mechanisms driving these changes and whether they are specifically driven by TRPV1 activation by capsaicin weren't explored, therefore this requires

further investigation. In the literature, TRPV1 was also reported to be expressed in vascular cells in the rat (Tóth et al., 2014) and in human tooth pulps (Morgan et al., 2005), however this wasn't observed in the neuromas at the transcript level (Figure 4.19). In lingual human neuromas, previous work in our lab identified a negative correlation between TRPV1 protein expression and time since injury (Biggs et al., 2007). TRPV1 was mostly found in PGP9.5-labelled nerve fibres; however, expression of TRPV1 in areas not associated with axons was observed, which might indicate TRPV1 expression in blood vessels (Biggs et al., 2007).

These findings don't exclude the possibility of SCN9A and TRPV1 local translation in human peripheral axons, however, they hint to the expression of these transcripts to a significant degree in non-neuronal cell types, particularly Schwann cells.

4.4.2 SOX10 expression in mature Schwann cells.

SOX10 belongs to the SOX family of transcription factors and is expressed in development in migratory multipotent neural crest cells and the cell-types derived from them, including immature Schwann cells (Pingault et al., 2022). Wilcox et al. (2020) investigated the protein and RNA expression of SOX10 in injured brachial nerves obtained from patients undergoing nerve reconstruction: SOX10 mRNA levels weren't correlated with time since nerve injury, however, the density of cells expressing SOX10 at the protein level peaked at 90-100 days following injury. In animal models, SOX10 is required for Schwann cell specification (Finzsch et al., 2010), whilst the expression of SOX10 mRNA in mature Schwann cells is required to maintain the structural integrity of peripheral nerves in adult mice (Bremer et al., 2011).

In the human neuromas, SOX10 mRNA was detected in a sample obtained 120 days post-injury with RNAscope (Figure 4.7). Immunohistochemical validation is required to establish whether the protein is expressed as well. Since RNAscope resulted in positive signal in only one sample, a correlation between the density of SOX10 positive cells with time since injury in human lingual neuromas couldn't be performed.

4.4.3 OSM expression in CD68+ macrophages in human neuromas.

Nerve resident macrophages are activated following nerve injury to clear tissue debris and attract circulating macrophages to the site of injury through the release of cytokines and other pro-inflammatory mediators, which can sensitize sensory neurons resulting in neuropathic pain (Silva et al., 2021). The presence of CD68+ cells in the neuromas was previously investigated with immunohistochemistry by our group, where CD68+ cells were observed within the nerve fascicles (Vora et al., 2007). This was confirmed at the RNA level with RNAscope.

Additionally, the expression of Oncostatin M (OSM) was investigated. OSM is a cytokine secreted by macrophages during the inflammatory response (Repovic and Benveniste, 2002) and is differentially expressed in human DRGs from male donors associated with a history of neuropathic pain (Ray et al., 2023). OSM mRNA was detected in all samples with Visium, while snRNA sequencing indicates its expression in 3% of macrophages (Figure 4.19). Using RNAscope, a few CD68+ and OSM+ cells could be detected within the nerve fascicles (Figure 4.9). Due to the high variability of RNA quality between samples, sex and pain-related differences in OSM expression couldn't be quantified. However, the role of OSM in human lingual neuromas should be further characterised at the protein level to confirm whether a sex-specific increase of OSM can be detected in the neuromas from patients with neuropathic pain.

4.4.4 Perineurial cells in human neuromas express the p75 neurotrophin receptor.

Perineurial cells surround nerve fascicles and create a protective layer between the endoneurium, containing the axons, and the external environment, protecting it from changes in ionic compositions, toxins, pathogens and other insults (Iwanaga et al., 2022). The role of perineurial cells in peripheral neuropathies and neuropathic pain has not been investigated extensively.

Using single nuclei RNA sequencing and spatial transcriptomics, four clusters of perineurial cells were identified, expressing SLC2A1 (GLUT-1), a widely used marker for this specialised cell-type (Piña et al., 2015). The presence of perineurial

fibroblasts was here validated with immunohistochemistry, showing strong and localised GLUT-1 signal in structures surrounding nerve fascicles.

In the snRNAseq data, perineurial cells were observed to express NGFR to a higher degree compared to Schwann cells (Figure 4.19). NGFR is often used as a marker for repair Schwann cells, however, since the neuroma samples were obtained 4+ months following nerve injury, the lack of NGFR+ Schwann cells can be explained by the decrease of repair Schwann cells several months after injury (Jessen and Mirsky, 2016).

The expression of NGFR in perineurial cells has been previously reported by Yamamoto et al. (1992), who observed increased NGFR immunoreactivity 3 days following nerve transection in rat peripheral nerves. Interestingly, NGFR immunoreactivity was identified in murine endoneurial cells, co-localising with NG2 (Stierli et al., 2018) and was used as an endoneurial fibroblast marker to analyse single cell data from intact murine nerves, where it was also co-expressed with Cspg4 (NG-2) (Chen et al., 2021).

In the human neuromas, co-localization of NGFR with GLUT-1 was validated with immunohistochemistry. NGFR immunoreactivity is strongly co-localized with GLUT-1, whilst also producing a weaker signal in structures resembling axons (Figure 4.13). The immunohistochemical validation confirms the expression of NGFR in human perineurial cells, as observed in rats by Yamamoto et al. (1992). The presence of both mRNA, detected in the snRNA-seq data (Figure 4.19), and protein (Figure 4.13) is observed several months following injury. This highlights species differences where NGFR is expressed in human and rat perineurial cells (GLUT-1+), whilst in mice, NGFR is found in endoneurial cells (NG2+) (Stierli et al., 2018).

Overall, this data suggests sustained production of NGFR in human lingual neuromas, several months following nerve injury. When activated by neurotrophins, NGFR has pro-apoptotic effects (Bruno et al., 2023), but its role in perineurial cells following nerve injury has not been investigated yet. Whilst a global p75-NTR (NGFR) knockout resulted in reduced myelination in murine peripheral nerves, a conditional knockout specific to Schwann cells didn’t produce any major changes in myelination during development or following nerve crush injury (Gonçalves et al.,

2019). Perhaps, NGFR-expressing perineurial cells might have a role in axonal remyelination and regeneration following nerve injury.

4.4.5 Immunohistochemical investigation of PI16 and potential correlation with symptoms of pain in human neuromas.

Fibroblast-derived PI16 is proposed to be a regulator of pain: in its absence, rats were protected from SNI-induced neuropathic pain (Singhmar et al., 2020) and CFA-induced inflammatory pain (Garrity et al., 2023). Its hypothesised mechanism of action in these two injury models differs: whilst in the neuropathic model Pi16 knockout was shown to induce endothelial permeability and CD45+ leukocytes influx in the DRG (Singhmar et al., 2020), in the inflammatory model it promotes a bias towards anti-inflammatory CD206+ macrophages in the DRG and skin (Garrity et al., 2023).

The expression of PI16 was investigated in human neuromas. In the single nuclei data, PI16 is highly expressed in the endoneurial fibroblast cluster (Figure 4.19). Immunohistochemistry confirmed its expression localised to endoneurial-like cells within nerve fascicles (Figure 4.15). This represents a species difference, since Singhmar et al. (2020) identified PI16 expression in rodent perineurial and epineurial cells. Whether this difference has any biological relevance is unknown but should be further investigated: whilst endoneurial cells aren't identified as critical players in the blood-nerve barrier (Weerasuriya and Mizisin, 2011), they are closely associated with axons.

In the neuromas, no correlation was identified with the symptoms of pain and PI16 immunoreactivity (Figure 4.17). No apparent correlation with CD45+ leukocyte infiltration could be identified (Figure 4.18). In the neuropathic pain model, Singhmar et al. (2020) showed that PI16 expression leads to CD45+ leukocyte influx in the DRG. Here, the presence of CD45+ leukocytes was investigated in the neuromas at the site of injury, as the trigeminal ganglion from the patients is inaccessible.

These results don't exclude PI16 involvement in neuropathic pain. Any potential differences at earlier stages of neuropathic pain development might be lost at the time points where the neuromas are usually obtained, ranging from 4 to 69 months post-injury. Nevertheless, PI16 expression in human neuromas supports its role as a

potential novel analgesic target. Its mechanisms of action in human nerves should be further investigated, as it might differ from the rodent models due to the different source of the protein in endoneurial fibroblasts as opposed to perineurial fibroblasts.

4.4.6 Challenges and limitations of the study

RNAscope was used to validate the mRNA expression of selected targets to confirm findings from Visium and snRNAseq in human lingual neuromas. Out of the samples tested, only LN8 displayed strong signal from the positive control probes (Figure 4.3), which was later used to test all the selected combinations of target probes. Visium and snRNAseq data could therefore be validated in this sample. However, due to the reduced signal of the positive control probes in the other samples, the RNA expression of the selected targets couldn't be compared across samples, preventing the assessment of correlations between gene expression and intensity of pain, sex, time since injury or other clinical features.

The RNAscope assays were further complicated by the necessity to visualise TUJ1 immunoreactivity, which required the optimization of the protease treatment to increase protein signal detection (Figure 4.2). A longer protease treatment is beneficial to detect RNA in samples that have been fixed for longer periods of time (Mostegl et al., 2011). Whilst the fixation intervals in the neuroma samples never exceeded 30 hours, they could sometimes be as short as 18 hours. Even small differences in fixation times might affect the degree of cross-linking in the tissue, preventing the accessibility of RNA. Additionally, the variable size of the samples also affects the extent of fixation. Extended protease treatment should reverse the cross-linkage, but can also impact the integrity of protein antigens, reducing immunoreactivity. Individual sample optimization of protease treatment duration might be required to obtain a comparable baseline signal of the positive control probes across samples. Alternative antigen retrieval methods might also be tested in future optimization experiments.

Another reason for the variability of the RNAscope signal across samples might be caused by RNA degradation of the samples during surgical removal. The RNA quality of a subset of samples was tested with a fragment analyzer following RNA

isolation to test the samples' suitability for Visium spatial gene expression, including LN4 and LN8. Despite following the same fixation protocol, only LN8 was deemed suitable for Visium spatial transcriptomics, whilst LN4 had to be excluded due to high RNA fragmentation. This might explain why LN8 displayed positive RNA signals for house-keeping genes while LN4 did not. The variation in RNA quality might potentially arise during the surgical procedure or in the interval between which the sample is removed and placed into fixative, which is dependent on the events that occur in the operation theatre. Nevertheless, the probe combinations successfully tested on LN8 confirmed the findings from Visium and snRNA sequencing, enabling the detection of several transcripts at higher resolution in one human sample.

The variability in fixation is a factor that may affect immunoreactivity of protein epitopes as well. Indeed, variable immunoreactivity is observed across samples labelled with anti-PI16, which might be affected not only by biological differences but by sample processing and fixation as well. For this reason, quantification of immunolabelling in human tissue is challenging. In this work, mean fluorescent intensity was used to quantify PI16 protein expression, but fluorescent intensity might be largely affected by technical factors. Alternative approaches include measuring the area of positive staining, where the establishment of a threshold for what is considered positive staining, which might vary sample to sample, presents a different challenge. In future, different quantification methods may be tested to identify which one represents more faithfully what is observed qualitatively by the investigator.

4.4.7 Conclusions and future work

In this chapter, the experiments performed with immunohistochemistry and RNAscope exploring the protein and RNA expression of a variety of targets in human lingual neuromas were described.

The targets validated with RNAscope in LN8 confirmed some of the observations from the data generated with Visium and single nuclei RNA sequencing, which can be summarised as follows:

1. SCN9A mRNA is found in the neuromas and might originate from the axons and non-myelinating Schwann cells.
2. SCN10A mRNA expression is scarcely detected in the neuromas.
3. TRPV1 mRNA expression might originate from axons or myelinating Schwann cells from injured nerves.
4. SOX10 mRNA is expressed in Schwann cells in the neuromas.
5. PTGDS mRNA is expressed to a high degree in perineurial fibroblasts, and to a lower degree in endoneurial fibroblasts and Schwann cells.
6. CD68+ mRNA is found in putative macrophages associated to nerve fascicles. A subset of macrophages express OSM mRNA.

Immunohistochemical investigation verified other observations at the protein level in a larger pool of samples:

1. PI16 is expressed in putative endoneurial fibroblasts in close association with nerve fibres. No correlation or statistical difference was identified between PI16 expression and pain VAS score reported by the patient, nor with CD45+ leukocytes infiltration.
2. NGFR is co-localised with GLUT-1 in perineurial cells in the neuromas.

This broad characterization of cell-type specific RNA and protein expression prompts follow-up questions that could be tested in future studies, for example:

1. Are SCN9A and TRPV1 translated into functional proteins in Schwann cells and what is their function?
2. Does local translation of ion channels occur in human peripheral nerves? What are the different trafficking mechanisms that drive the expression of SCN9A, TRPV1 and SCN10A?
3. How does PTGDS expression in perineurial fibroblasts affect neuroinflammation and the integrity of the blood-nerve barrier?
4. Are there sex differences in the expression of OSM and PTGDS in the neuromas?
5. Does PI16 expression in human endoneurial fibroblasts affect neuronal excitability and the integrity of the blood-nerve barrier?

6. What is the role of NGFR expression in perineurial fibroblasts following nerve injury?

These questions are relevant to the characterisation of the mechanisms that lead to neuronal sensitization and chronic neuropathic pain, in particular through the dysregulation of ion channels' expression in the axonal membrane, the integrity and function of the perineurial barrier and the interaction of the axons with the immune system and pro-inflammatory mediators.

The visualization of the transcript or protein expression of a potential pain target within human nerves, even if in a limited number of samples, is useful to assess whether to further investigate it to develop a new analgesic. Further investigations are required in *in vitro* co-culture systems of human primary cells or *in vivo* models to dissect the mechanisms that involve a molecular target and whether it contributes to neuronal sensitization.

Chapter 5. General Discussion

5.1 Summary of findings

In this thesis, the cell types and the transcriptional landscape that compose human trigeminal nerves in health and injury were characterised using single nuclei RNA sequencing, spatial transcriptomics and RNAscope. Additionally, the molecular changes linked with neuropathic pain in human injured lingual nerves were investigated using spatial transcriptomics and immunohistochemistry. A visual summary of the work presented in this thesis is shown in Figure 5.1.

In **Chapter 2**, the analysis of the transcriptome at single cell level from human lingual neuromas and healthy trigeminal nerve roots was performed, identifying several cell types that support the axons in peripheral nerves. A high degree of heterogeneity was observed in fibroblasts, where several subtypes of perineurial cells were selectively associated with healthy and injured nerves. Species differences were noted regarding fibroblast-expressed genes compared to previous reports: for example, PI16, reported to be expressed in perineural cells in mice (Singhmar et al., 2020), was found in endoneurial cells; while the NGF receptor p75, expressed in mice in endoneurial fibroblasts (Chen et al., 2021, Yim et al., 2022), was expressed in perineurial cells in the human samples examined in this thesis. The neuromas were characterised by the presence of a pro-fibrotic fibroblast cluster expressing PRRX1, which might contribute to scar formation and impair axonal regeneration (Leavitt et al., 2020, Atkins et al., 2006). Both myelinating and non-myelinating Schwann cells were identified, but myelinating Schwann cells exhibited a higher degree of heterogeneity. One subtype of myelinating Schwann cells (MSC_2) was marked by PMP2 expression, which had been previously identified as a marker for Schwann cells myelinating large-fibre neurons (Yim et al., 2022). When comparing the transcriptional profile between Schwann cells from the neuroma and the trigeminal nerve root samples, the AP-1 transcription factor family remained upregulated months after nerve injury. The AP-1 TF family was also upregulated in immune cells, as previously reported (Li et al., 2021). There was a marked increase of vascular cells in the neuromas, comprising 30% of the nuclei sequenced compared to 3% in the trigeminal nerve roots, including a cluster of

endothelial cells that highly expressed cytokine activated genes such as SELE, ICAM-1 and IL6, indicating the presence of inflammation. The cell-cell communication between trigeminal neurons, obtained from Yang et al. (2022), and the cells in the trigeminal nerve roots or neuromas was inferred computationally, focusing on chemokine signalling. The trigeminal neurons, obtained from healthy donors, expressed chemokine receptors investigated in the literature in the context of neuronal sensitisation including CXCR4, CCR5 (Oh et al., 2001), but also the atypical chemokine receptors ACKR1 and ACKR3, which have not been investigated in the context of neuronal sensitisation. Several chemokines expressed in both healthy and injured nerves displayed potential interactions with these receptors. Of particular interest, the macrophage-derived chemokine CXCL8 was expressed in the neuromas, but not in healthy trigeminal roots, where it exhibited a potential interaction with ACKR1. While the CXCL8 receptors CXCR1 and CXCR2 are usually expressed at a low level in healthy neurons, studies in animal models report that CXCR1 and CXCR2 are upregulated following injury (Nasser et al., 2009, Zhou et al., 2016, Silva et al., 2017, Piotrowska et al., 2019, Zhou et al., 2020), and CXCL8 upregulation has also been reported in the serum of patients with trigeminal neuralgia and migraines (Duarte et al., 2015, Liu et al., 2019).

In **Chapter 3**, spatial transcriptomics was used to characterise the transcriptional composition of painful and non-painful human neuromas. Clustering analysis identified several areas characterised by the enrichment of specific cell types, including Schwann cells, fibroblasts, endothelial cells and perineurial cells. A cluster characterised by the expression of activated macrophage markers, such as CHIT1 (Sklepkiewicz et al., 2023), and lysozyme activity such as LYZ and LAPTM5 (Keshav et al., 1991, Glowacka et al., 2012) was highly enriched in LN15, a sample from a patient reporting a pain VAS score of 61. LN12, another sample in the painful group with a pain VAS score of 43, exhibited a high proportion of a cluster marked by the expression of immunoglobulin genes such as IGKC, IGHG1-2, suggesting the presence of B-cell derived plasma cells (Hoffman et al., 2016). Cell-type deconvolution was performed to identify the cellular composition at a higher resolution than allowed by the Visium barcoded spots, revealing the distribution of the cell-types identified in Chapter 2. Pseudo-bulk differential expression analysis

was performed on the pathologically relevant areas by manually selecting the barcodes overlaying nerve fascicles, identified by H&E staining. The analysis highlighted 59 genes as differentially expressed in the painful and non-painful neuromas. HLA-A, an MHC class I antigen, and NLRC5, its trans-regulator (Kobayashi and van den Elsen, 2012) were highly upregulated in the painful neuromas, and genetic variants in the HLA region have previously been identified to be associated with conditions including post-herpetic neuralgia and traumatic-injury induced neuropathic pain (Sato et al., 2002, Veluchamy et al., 2018, Miclescu et al., 2023). CXCL2 and CXCL8 were also upregulated in the painful neuromas, in agreement with reports in animal studies (Kiguchi et al., 2012, Iwasa et al., 2019) and clinical samples (Duarte et al., 2015, Liu et al., 2019). Other genes differentially expressed between painful and non-painful samples include the basement membrane protein NID2 expressed in non-myelinating Schwann cells, the matrix metalloprotease MMP19 expressed in profibrotic fibroblasts and the riboflavin transporter SLC25A3, which warrant further investigation.

In **Chapter 4**, selected RNA and proteins relevant to pain development were characterised in human neuromas to confirm the data from previous chapters and visualise their expression at higher resolution. The expression of transcripts encoding the ion channels $Na_v1.7$, $Na_v1.8$ and TRPV1 recapitulated the observations from spatial transcriptomics, where $Na_v1.8$ mRNA is scarcely detected while $Na_v1.7$ and TRPV1 mRNA are detected in association with axons and non-neuronal cells, most likely Schwann cells. The presence of CD68+ macrophages was identified, confirming data from previous chapters, where a portion expressed the cytokine Oncostatin M, reported to be important in neuropathic pain development in a sex-specific manner (Ray et al., 2023). Prostaglandin D2 synthase, an enzyme involved in the conversion of PGH_2 to PGD_2, also involved in pain generation in a sex-specific manner (Ray et al., 2023), was expressed at the RNA level in cells resembling perineurial fibroblasts, confirming data from previous chapters. NGFR and GLUT-1 co-labelling with immunohistochemistry confirmed the expression of the p75 neutrophin receptor (NGFR), involved in nerve regeneration and repair, in perineurial fibroblasts. Finally, the protein expression of PI16, recently proposed as a regulator of neuropathic pain (Singhmar et al., 2020), was analysed across 10 neuroma

samples. While no significant correlations were identified between the signal intensity and symptoms of pain, it was confirmed that PI16 expression in human nerves is localised to endoneurial-like cells, supporting the single nuclei RNA-seq data and in contrast with what is reported in animal models (Singhmar et al., 2020, Garrity et al., 2023).

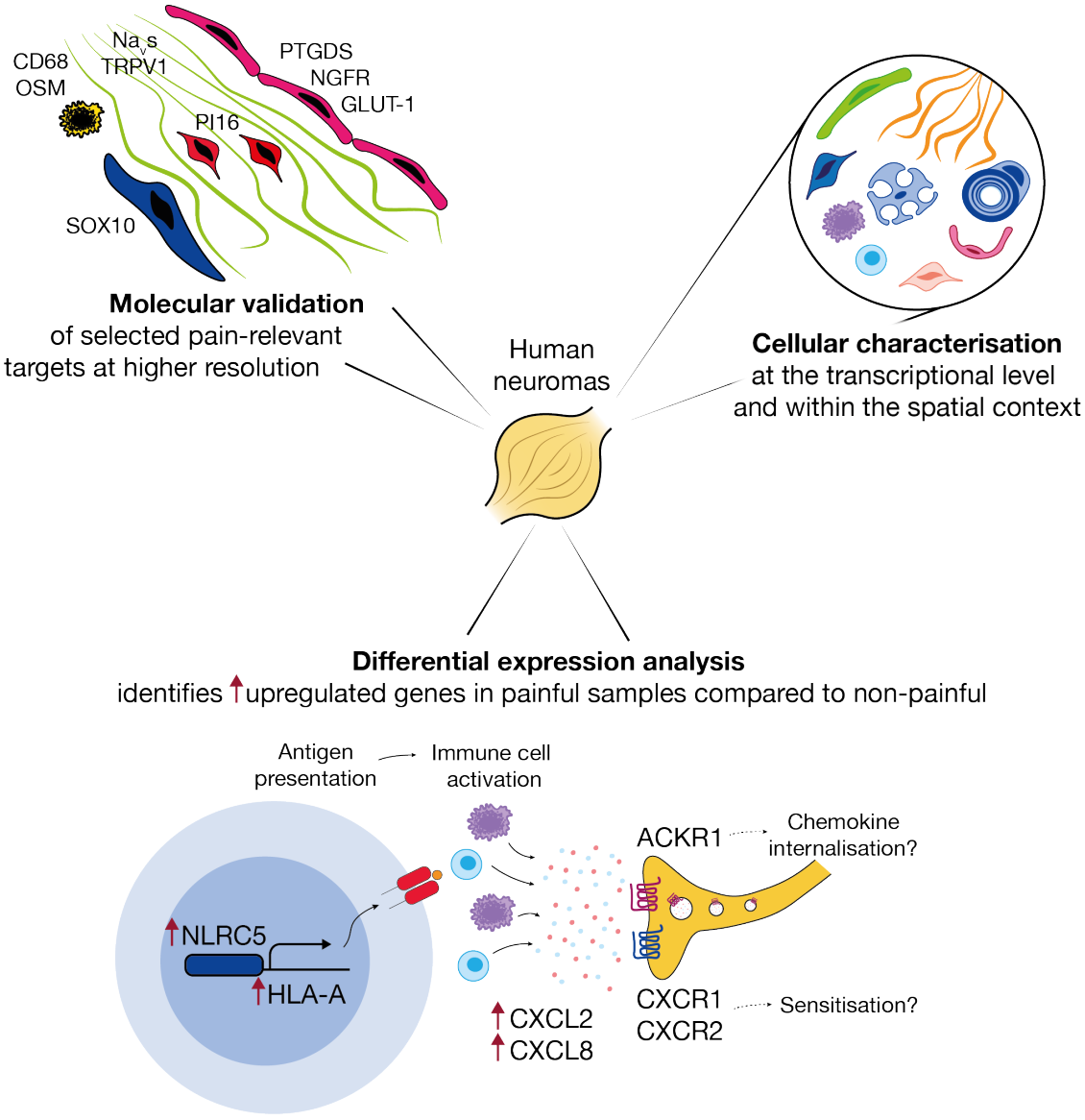

Figure 5.1 Visual summary of the main findings from this thesis.
Human neuromas were processed with spatial and single nuclei RNA sequencing to characterise the cellular and molecular composition within the spatial context. Pseudo-bulk differential expression analysis between painful and non-painful samples identified several differentially expressed genes, such as HLA-A and its transactivator NLRC5 and the chemokines CXCL2 and CXCL8, which were upregulated in the painful samples, and which might interact with the atypical chemokine receptor ACKR1 expressed in healthy trigeminal neurons (Yang et al., 2022) as well as other CXCR1 and CXCR2, upregulated in sensitised neurons and following nerve injury (Li et al., 2023a, Piotrowska et al., 2019). Molecular validation with RNAscope and immunohistochemistry was performed to validate

the expression of several molecules, including Peptidase Inhibitor 16, expressed in endoneurial fibroblasts and relevant to neuropathic pain development, the p75 neurotrophin receptor (NGFR), prostaglandin D2 synthase and glucose transporter 1 (GLUT-1) in perineurial fibroblasts, CD68+ macrophages and SOX10+ Schwann cells, as well as ion channels in axons and non-neuronal cells.

5.2 Inflammation and neuropathic pain in traumatic neuromas

Using spatial transcriptomics, areas characterised by the accumulation of inflammatory cells were identified. In LN15, a cluster characterised by the expression of lysozyme activity and activated macrophages genes was localised in close proximity to the nerve fascicles. In LN12, a cluster characterised by the expression of immunoglobulin genes, indicating the presence of B cell-derived plasma cells, was found partially overlaying the nerve fascicles. Both samples were obtained from patients displaying symptoms of pain, however in other painful neuromas examined, no visible inflammatory cell accumulation was observed. While inflammatory infiltrates could still be present in areas of the sample that weren't examined, this was in line with previous studies. Vora et al. (2007) identified the presence of mononuclear cell inflammatory infiltrate in 42% of lingual neuromas examined, and while the majority of patients with signs of inflammation reported symptoms of pain, a large group of patients with symptoms didn't display evident signs of inflammation, similar to what was found by Peszkowski and Larsson (1990) and Sist and Greene (1981).

What drives the symptoms of pain in traumatic neuromas where no inflammatory infiltrate cluster can be identified? Is it ectopic activity driven by the endogenous changes in ion channels expression and excitability? More generally, what are the main driver of symptoms of pain in neuropathic pain and how can this guide clinicians to identify the best treatments?

A critical feature of neuropathic pain has been identified in ectopic activity produced by intrinsic changes in the membrane properties due to alterations in sodium, potassium and calcium channel expression and excitability (North et al., 2018). Electrophysiological studies demonstrated spontaneous firing of both intact and axotomized fibres in animal models of traumatic neuromas (Bernal et al., 2016,

Bongenhielm and Robinson, 1996, Yates et al., 2000) and upregulation of ion channels in human painful neuromas compared to control tissue from the same patients (Black et al., 2008). A multitude of studies in animal models report accumulation of ion channels in the nerve following nerve injury associated with increased hypersensitivity to thermal and mechanical stimuli (Gold et al., 2003, Vilceanu et al., 2010, Devor et al., 1993). Crucially, a key difference between studies on clinical samples and animal models is that the control group in several animal studies consists of sham-treated animals, therefore the changes identified are linked not only with nociception, but with nerve injury as well. Instead, in humans who can communicate their levels of spontaneous pain, a distinction can be made between patients who experience pain and those who do not, given the same injury type, and a different picture emerges (Vierck et al., 2008).

In our group, the ongoing investigation of the differences between samples from patients with pain and without pain hasn't identified clear correlations between ion channels protein expression in peripheral axons and symptoms of pain, with the exception of $Na_v1.8$ expression, which was increased in neuromas from patients with pain (Bird et al., 2013). The analysis of $Na_v1.7$, $Na_v1.9$, TRPA1 and $P2X_7$ receptor expression didn't identify any significant correlation with pain (Bird et al., 2007, Morgan et al., 2009b, Bird et al., 2013, Morgan et al., 2009a). Biggs et al. (2007) identified a negative correlation between TRPV1 expression and time since injury, contributing to the idea that changes in excitability are linked with neuroma formation itself, rather than symptoms of pain. This suggests that the constitutive upregulation of ion channels' expression isn't a critical driver of symptoms of pain in traumatic neuromas.

In fact, the direct activation of nerve fibres by local inflammatory cells entrapped in the neuromas might have a more prominent role. Frisén et al. (1993) has shown a close relationship between infiltrating macrophages and unmyelinated axons found in rat sciatic nerve neuromas, observing that macrophages seem to contribute to demyelination, potentially disturbing axonal conductance and exciting C-fibres with the release of pro-inflammatory mediators. Cui et al. (2000) has shown that in rat models of mononeuropathy, only a portion of the animals develop tactile allodynia which, when compared to non-allodynic animals, display increased macrophage

infiltration, as well as increased IL6 and TNFα secretion. Several other studies since then have highlighted the importance of the interaction between axons and peripheral non-neuronal cells for neuropathic pain development, as reviewed in Ji et al. (2016). In this thesis, it was demonstrated that even in the absence of a visible inflammatory cell cluster by histological examination, painful samples are still characterised by the increased expression of inflammatory marker genes (HLA-A, CXCL2, CXCL8, NLRC5). Additionally, the removal of the neuroma is in most cases sufficient to significantly reduce symptoms of pain (Atkins and Kyriakidou, 2021). This supports the idea that spontaneous pain in traumatic neuromas is in many cases caused by the activation of nerve fibres by local inflammatory mediators and cell infiltrates; while the constitutive increase in ion channels expression in the axons, resulting in endogenous hyperexcitability and spontaneous firing, is a secondary factor which promotes the amplification and transmission of external stimuli, but doesn't itself lead to symptoms of pain.

The approach taken in studying clinical samples of neuromas is biased as the investigation focuses on peripheral tissue without cell bodies, where transcriptional changes in ion channels' expression might be more easily detected. However, even when investigating clinical tissue associated with neuropathic pain that includes neuronal cell bodies, the results also highlight the importance of inflammatory mediators and fail to identify transcriptional changes in ion channels expression. Ray et al. (2023) investigated the transcriptome of 50 human dorsal root ganglia derived from thoracic vertebrectomy, where a portion of the samples was associated with neuropathic pain, paying attention to include high quality neuronal mRNA based on the baseline expression of neuronal marker genes in all samples employed. Despite detecting increased spontaneous activity in the DRG neurons associated with pain, the transcriptional changes detected were mainly linked with inflammation but not with ion channels expression or regulation (Ray et al., 2023, North et al., 2019). In both sexes, the most highly differentially expressed genes were indeed inflammatory mediators, including Oncostatin M, CXCL2 and several other cytokines in males and genes linked with interferon signalling in females (Ray et al., 2023).

A caveat of these studies is that transcriptomic studies such as the one presented in this thesis or by Ray et al. (2023) might be missing changes at the post-translational modification level which might affect trafficking and gating properties of ion channels. Indeed, there are certainly cases where spontaneous firing in primary afferents drive pain sensation, where silencing signal transmission is successful in abolishing pain, as evidenced by the effectiveness of sodium channel blockers in the treatment of trigeminal neuralgia (Lambru et al., 2021). Indeed, trigeminal neuralgia is a unique neuropathic pain condition that seems to be driven primarily by abnormal electrical behaviour in trigeminal neurons resulting from endogenous dysregulation of ion channels expression, most likely caused by focal demyelination due to vascular compression (Devor et al., 2002). Instead, in traumatic neuromas, a primary driver of ectopic activity and pain symptoms might be inflammation at the site of injury, leading to secondary changes in excitability which promote the transmission and amplification of local nociceptive signals.

This is a reminder of the heterogeneity in pain conditions that we classify as neuropathic and the need to identify biomarkers to detect the main drivers of pain on a patient-specific basis. An important step in this direction would be to investigate whether inflammation at the site of injury can be inferred from systemic biomarkers, which might help the clinician to identify the best course of treatment.

Hypothesis: Systemic biomarkers might correlate with the inflammatory cell infiltrate in traumatic neuromas and inform surgical outcomes for pain management.

Identifying correlations between markers of inflammatory cell accumulation in patients' biofluids and the cellular composition in the neuromas might be a promising route to stratify patients which might benefit from (for example) either a) pharmacological modulation of inflammation, b) surgical removal of the neuroma and its associated inflammatory infiltrate or c) the use of ion channel blockers to reduce spontaneous activity caused by axotomy. The latter option might be beneficial in patients who don't display local cellular infiltrates or where surgical removal of the neuroma isn't sufficient to fully abolish symptoms of spontaneous pain, as reported in a case study in Sist and Greene (1981), where the treatment with phenytoin sodium, a sodium channel blocker for the treatment of epilepsy and

trigeminal neuralgia, lowered the pain symptoms to a manageable level in a patient that displayed residual pain following neuroma removal.

In our lab, we have collected the saliva, serum and whole blood from patients with lingual neuromas, where this hypothesis could be tested by investigating the correlation between different inflammatory cell markers, symptoms of pain and outcomes of surgical intervention. Analysing the expression of inflammatory markers in biofluids linked to the samples used for spatial transcriptomics could highlight whether the systemic expression of these markers is correlated with local inflammation and predictive of surgical outcomes. Experiments to test this hypothesis include:

1. Measurement of protein concentration of inflammatory markers, including CXCL2, CXCL8 and HLA-A, in the serum and saliva of patients with lingual nerve injury and correlation of their expression with symptoms of pain, surgical outcomes of neuroma removal and their relative protein expression at the site of injury.
2. In patients with linked transcriptomic data from the neuroma, explore the correlation of systemic biomarker expression in biofluids with the transcriptional profile at the local site of injury.
3. Perform whole-exome sequencing in whole blood from patients with lingual nerve injury to identify whether genetic variants, particularly in the HLA region, are correlated with the presence of pain and surgical outcomes of neuroma removal.

5.3 Considerations on chemokines and pain

In this thesis, the relevance of chemokines in nerve injury and pain generation was highlighted. Chemokines, or chemotactic cytokines, are important inflammatory mediators secreted during tissue injury and infection, creating chemical gradients that guide leucocytes to damaged tissues (Abbadie, 2005). Chemokines have long been known to directly activate sensory neurons, which express several chemokine receptors (Oh et al., 2001). Several chemokine receptors are upregulated as a result of inflammation and nerve injury, including but not limited to CXCR4, CCR2, CCR4,

CCR5, CXCR1, CXCR2 and XCR1 (Miller et al., 2009, Bird et al., 2018, Silva et al., 2017).

In human neuromas, CXCL2 and CXCL8 were found to be upregulated in the painful samples compared to non-painful using unbiased spatial transcriptomics. These chemokines might potentially interact with their receptors CXCR1 and CXCR2 as well as the atypical chemokine receptor ACKR1, whose function in sensory neurons has not been investigated yet. Here, I will discuss more in detail the potential relevance of these molecules in pain generation and future studies that might be undertaken to test these findings.

5.3.1 The Atypical Chemokine Receptor 1

ACKR1, also known as Duffy antigen receptor for chemokines (DARC), was described as a "deceptor" by Balkwill (2004) since it binds to chemokines without eliciting intracellular signalling cascades. Chemokine receptors have an extracellular N-terminal with several binding regions for CXC and CC chemokines, 7 transmembrane domains and an intracellular C terminus. ACKR1 lacks the "DRYLAIV" sequence in the intracellular loop of the third transmembrane helix, which prevents G-protein coupling and the activation of intracellular signalling cascades (Horuk, 2015).

ACKR1 was first identified as the receptor on red blood cells for entry of Plasmodium Vivax, the infectious agent for malaria. An allele of this gene prevalent in African and Arabian peninsula populations and their descendants, which contains a SNP affecting the binding region of the transcription factor GATA1, abolishes ACKR1 expression in erythrocytes conferring resistance to malaria infection (McManus et al., 2017, Oliveira et al., 2012). This genotype also results in reduced neutrophil counts in the blood stream, a condition known as benign neutropenia (Rappoport et al., 2019). While the mechanisms underlying this phenotype aren't fully understood, hypotheses include the role of ACKR1 expressed by erythrocytes in haematopoiesis (Duchene et al., 2017), as well as endothelial-expressed ACKR1 in leucocyte extravasion from the blood stream (Pruenster et al., 2009).

ACKR1 can bind to over 20 chemokines, acting as a chemokine "sink" at site of local inflammation: ACKR1-bound chemokines are scavenged and internalised, and

therefore unable to activate leucocytes (Rappoport et al., 2019). However, ACKR1 expressed on endothelial cells in blood vessels was found to actually mediate leukocyte infiltration: chemokines bound to ACKR1 at the basal surface of venular endothelial cells are transported by transcytosis to the luminal surface, where they are exposed to circulating leucocytes in the blood stream, stimulating extravasation (Pruenster et al., 2009). Interestingly, unlike other atypical receptors such as ACKR2 which result in chemokine degradation (Weber et al., 2004), only minor degradation of internalised ACKR1 is reported (Pruenster et al., 2009, Szpakowska et al., 2023).

Despite its wide expression in the central and peripheral nervous system, its role in the nervous system has only been characterised in cerebellar Purkinje cells (Schneider et al., 2014). Ackr1$^{-/-}$ mice have impaired balance, ataxia and anxiety-like behaviour (Schneider et al., 2014). ACKR1 is expressed in human trigeminal and dorsal root ganglia neurons, particularly in silent nociceptors (Yang et al., 2022, Tavares-Ferreira et al., 2022b), which warrants the investigation of its role in neuronal sensitization. Spatial transcriptomics confirms ACKR1 expression in human neuromas (Figure A1, page 206 in the appendix), likely originating from endothelial cells, as suggested from single nuclei RNA-sequencing, and potentially from axons as well.

Hypothesis: ACKR1 in sensory neurons scavenges chemokines and contributes to leucocyte infiltration in the DRG and neuronal sensitisation.

The role of ACKR1 in peripheral sensitization and neuroinflammation hasn't been investigated yet. In areas of tissue damage, ACKR1 acts as a chemokine scavenger reducing local inflammation by internalising local chemokines (Bonecchi and Graham, 2016). However, depending on the cellular context, internalization may be followed by the activation of alternative signalling pathways or transcytosis, resulting in the presentation of chemokines in areas where they can elicit an inflammatory response (Metzemaekers et al., 2020), therefore it's difficult to predict its potential role in chronic pain. Since ACKR1 hasn't been shown to lead to chemokine degradation following internalisation (Pruenster et al., 2009), one might wonder what happens to the internalised chemokines in sensory neurons. Are internalised chemokines transported as observed in endothelial cells and presented elsewhere, such as in the DRG or spinal cord, eliciting leucocyte infiltration or

microglial activation? Do they activate any alternative signalling pathways? Additionally, ACKR1 is expressed in the blood brain barrier where it promotes neuroinflammation (Marchetti et al., 2022), potentially playing a role in migraines (DosSantos et al., 2014).

To begin elucidating the potential role of ACKR1 in chronic pain, the following experiments should be considered:

1. Validation of ACKR1 expression in peripheral axons in human neuromas with immunohistochemistry by co-labelling with TUJ1 and investigation of any correlations with symptoms of pain and time since injury.
2. Assessment of behavioural responses to pain in animal models of inflammatory and neuropathic pain in Ackr1$^{-/-}$ mice.
3. Investigation of the extent of infiltration of leucocytes in the DRG of inflammatory and neuropathic pain animal models in Ackr1$^{-/-}$ mice.
4. Assessment of sensitization following chemokine administration in primary sensory neurons from naïve and Ackr1$^{-/-}$ mice using calcium imaging and electrophysiology.

5.3.2 CXCR2 signalling in neuropathic pain.

CXCR2, the receptor for CXCL2 and CXCL8, has been associated with peripheral neuronal sensitization (Silva et al., 2017). CXCR2 is a 7 transmembrane receptor that when activated triggers intracellular signalling pathways mostly involving G-protein activation. Kiguchi et al. (2012) have shown that perineurial injection of CXCR2 antagonist reduces mechanical and thermal hyperalgesia following nerve injury. Piotrowska et al. (2019) demonstrated the upregulation of CXCR2 in dorsal horn neurons following nerve injury, while its inhibition with an antagonist alleviated mechanical and thermal hyperalgesia following nerve injury. Zhou et al. (2020) confirmed this finding, showing that CXCR2 inhibition with another antagonist induces reduced microglial activation and proliferation in the spinal cord. CXCR2 is endogenously modulated by the interaction with G-protein kinase 6 (GRK6), which mediates β-arrestin-mediated receptor desensitization and internalisation: when GRK6 is over-expressed, CXCR2 expression in DRG neurons is reduced, together with neuronal hyperexcitability and mechanical and thermal hyperalgesia following

CCI (Zhou et al., 2016). In the trigeminal system, neuronal sensitization by pruritogens was shown to be mediated by CXCR2 upregulation, whilst its inhibition reversed itch behaviour (Li et al., 2023a). In summary, several studies have demonstrated CXCR2 upregulation following nerve injury and how its inhibition leads to the attenuation of behavioural responses to pain.

Hypothesis: CXCL2 and CXCL8 produce peripheral sensitization in human trigeminal neurons via CXCR2 activation

Cell-cell communication inference indicated that macrophage-derived CXCL8 in neuromas, and not healthy trigeminal nerve roots, may interact with ACKR1 expressed in sensory neurons. Spatial transcriptomics identified the upregulation of CXCL2 and CXCL8 mRNA in painful neuromas compared to non-painful, both ligands for CXCR2. Several studies evidence CXCR2 upregulation in neurons of rat and mice DRG and spinal cord following nerve injury, while its inhibition is shown to attenuate neuronal hyperexcitability and behavioural responses to pain (Kiguchi et al., 2012, Zhou et al., 2016, Silva et al., 2017, Piotrowska et al., 2019, Zhou et al., 2020, Li et al., 2023a). The role of CXCL8-mediated activation of CXCR2 is particularly interesting for further investigation due the evidence of CXCL8 upregulation in the serum of patients suffering from neuropathic pain conditions affecting the trigeminal system, such as migraines (Duarte et al., 2015) and trigeminal neuralgia (Liu et al., 2019)

The Involvement of CXCR2 activation by CXCL2 and CXCL8 in neuromas should be further investigated, as well as further dissecting its signalling mechanisms in human neurons. Future lines of investigation to elucidate the role of CXCR2 activation in neuropathic pain generation involve the following experiments:

1. Validate CXCL2 and CXCL8 upregulation in human neuromas classified as painful at the protein level with immunohistochemistry.
2. Investigate the expression of CXCR2 in the axons by TUJ1 co-labelling in human neuromas in painful and non-painful samples.
3. Further elucidate the mechanisms underlying CXCR2-mediated sensitization in human sensory neurons (either from primary tissue or derived from induced pluripotent stem cells):

a. Assess CXCR2 expression following chemokine administration and other sensitising factors (ATP, bradykinin, capsaicin).
b. Assess neuronal excitability with and without pharmacological inhibition of CXCR2 with calcium imaging and/or electrophysiology.
c. Assess neuronal excitability with and without CRISPRi knockdown of CXCR2 with calcium imaging and/or electrophysiology.
d. Analyse transcriptomic and proteomic changes between human sensory neurons treated with vehicle and human sensory neurons treated with CXCR2 inhibitor and/or CRISPi CXCR2$^{-/-}$ human sensory neurons following sensitization to identify changes associated by CXCR2 expression and activation.

5.4 The role of endothelial cells in neuropathic pain

Angiogenesis and blood vessels integrity are increasingly recognised as an important factor in neuropathic pain development: diabetes, chemotherapy or traumatic nerve injury may lead to alterations in the blood-nerve barrier, leading to ischaemia and neuropathy (Sharma et al., 2023).

The single cell RNA sequencing dataset presented in this thesis highlighted an expansion of the endothelial cells in the neuroma samples, where 30% of the sequenced nuclei were identified as endothelial, compared to 3% of the nuclei from the trigeminal nerve roots. Additionally, one cluster (Endo_1) found only in the neuromas was characterised by the expression of pro-inflammatory genes such as SELE, ICAM-1 and IL-6 which play a role in leukocyte infiltration. Tissue injury and inflammation are linked with angiogenesis, however in recent years the role of endothelial activation in neuropathic pain has been highlighted, particularly through the study of the pro-angiogenic VEGF family.

VEGF is a potent stimulator of angiogenesis and has a dual role in the nervous system, providing neuroprotective effects but also enhancing neuroinflammation through the increase of blood vessels permeability (Lange et al., 2016). The most studied VEGF family member is VEGF-A, which binds to the tyrosine kinase receptors VEGFR1 and VEGFR2, expressed in nociceptors, as well as the co-receptors NRP-1 and NRP-2 (Llorián-Salvador and González-Rodríguez, 2018).

Studies on VEGF-A have highlighted both anti- and pro-nociceptive effects (Matsuoka et al., 2016, Kiguchi et al., 2014, Llorián-Salvador and González-Rodríguez, 2018). Paclitaxel as a chemotherapeutic agent is enhanced with the use of bevacizumab, a monoclonal antibody against VEGF-A; however, in a cohort with the combined treatment of paclitaxel and bevacizumab, more patients experienced chemotherapy induced peripheral neuropathy compared to paclitaxel alone (Matsuoka et al., 2016). On the other hand, in animal models, inhibition of VEGF-A and VEGFR2 prevented the development of mechanical allodynia in a model of partial sciatic nerve ligation (Kiguchi et al., 2014). Hulse et al. (2014) identified that alternative splicing of VEGF-A might affect its dual role in nociception. VEGF-A has two splicing isoforms which vary by the alternative splicing of exon 8 and are both 165 amino acids in length: $VEGFA_{165}a$ is thought to mediate pro-nociceptive effects while $VEGFA_{165}b$ mediates the anti-nociceptive effects (Hulse et al., 2014). $VEGFA_{165}a$ binds to VEGFR2 and activates PLC/PKC intracellular signalling pathways leading to increased TRPV1-mediated currents, while $VEGFA_{165}b$ acts as its competitive inhibitor (Hulse et al., 2014). Indeed, further studies on animal models confirmed the analgesic effect of $VEGFA_{165}b$, but proposed its action through VEGFR1 activation, suggesting selective VEGFR1 inhibition as a potential route to treat neuropathies without interfering with the neuroprotective roles of VEGFR2 activation (Micheli et al., 2021). In contrast, in an osteoarthritis model, $VEGFA_{165}a$-mediated activation of VEGFR2 was shown to drive nociception, increasing endothelial cell activation and leucocyte transmigration through the expression of the adhesion molecule ICAM-1 (Beazley-Long et al., 2018). While more research is needed to identify the specific receptors and intracellular pathways that drive the pro- and anti-nociceptive effects of VEGF-A, VEGF clearly modulates chronic pain development acting by inducing angiogenesis and altering blood vessel permeability.

The expansion of endothelial cells with an activated pro-inflammatory phenotype in human lingual neuromas identified by single nuclei RNA sequencing in this thesis is further evidence of the role of vascularisation and blood vessel permeability in nerve injury-induced neuropathic pain. The over-expression of immune cell-derived pro-inflammatory cytokines (CXCL2 and CXCL8) in samples associated with

neuropathic pain indicates increased immune cell infiltration, which is likely to be influenced by increased vascularisation and altered blood vessel permeability. In future, identifying the proportion of VEGF-A isoforms present in the samples might indicate whether the pro-inflammatory gene expression associated with neuropathic pain in the neuromas might be linked with the expression of a specific VEGF-A isoform.

5.5 General Approach and Study Limitations

The work conducted in this thesis aimed to characterise the cellular and transcriptional composition of healthy and injured trigeminal nerves, as well as identify molecular changes linked with symptoms of pain reported by the patients. High-throughput techniques including spatial transcriptomics and single nuclei RNA sequencing were employed to characterise in an unbiased manner neuromas at transcriptome-wide level with detailed information on the cellular sources and spatial location of each transcript. This approach enabled the capture of a large amount of information from a small amount of tissue, providing data to generate new hypotheses on neuropathic pain maintenance and develop new treatment options.

The techniques used in this thesis, i.e. spatial transcriptomics and single nuclei RNA sequencing, are highly validated despite their recent emergence (Yue et al., 2023, Heumos et al., 2023) and provide the benefit of profiling the whole transcriptome without bias. They have downsides: Visium-based spatial transcriptomics limits the resolution at 55 µm, while single nuclei RNA sequencing doesn't enable the detection of cytoplasmic RNA. However, when used in combination, as performed in this thesis, they successfully provided complementary answers.

One caveat of this study is that due to the rarity of the samples, only a small number of samples could be analysed. Further analysis of a larger group of samples with complementary and alternative methodologies such as imaging based spatial transcriptomics with the 10X platform Xenium (Ke et al., 2013) or MERfish (Xia et al.,

2019) will be important to validate these results and identify more statistically significant changes correlated with symptoms of pain.

Nevertheless, the information obtained even from a small number of human samples is beneficial, especially due to the availability of both painful and non-painful samples, providing a control group which experienced the same type of injury but does not display symptoms of pain. Targets identified from these studies should be further validated in a larger pool of samples with immunohistochemistry, while in vitro assays with human sensory neurons should be employed to further dissect the mechanisms. Additionally, the comparison of the molecular and cellular composition of human peripheral nerves to that found in a relevant animal model would be beneficial to establish their reliability and further investigate the physiological relevance of these findings *in vivo*. On this aim, the integration of single nuclei data from this thesis with the data generated from peripheral nerves in animal models (Chen et al., 2021, Yim et al., 2022, Lovatt et al., 2022) should be performed, in order to more accurately identify and quantify the discrepancies between animal models and human tissue.

5.6 Conclusion

The cellular and transcriptional landscape characterising human trigeminal nerves was presented in this thesis, where the heterogenous cell types that support and interact with the axons, sustaining them in health, guiding them during nerve regeneration and promoting maladaptive changes during neuropathic pain generation, were investigated. Using spatial transcriptomics and single nuclei RNA sequencing, the cellular composition of painful and non-painful neuromas was characterised and several differentially expressed genes associated with neuropathic pain were identified. Immunohistochemistry and RNAscope were employed to visualise molecules relevant to neuropathic pain at higher resolution, including ion channels, pro-inflammatory mediators and fibroblast-derived molecules. Overall, this work confirmed the importance of the interaction with inflammatory cells for the development of pain following neuroma formation, evidenced by the upregulation of inflammatory mediators, including CXCL2, CXCL8 and HLA-A in painful samples compared to non-painful.

The data generated from this study will benefit the wider research community by providing an atlas that reports the expression of thousands of genes in disease-relevant human tissue, a precious resource for the development of novel pain treatments and for the translation of mechanisms identified in animal models.

Outputs

Publications

- Morchio, M., Sher, E., Collier, D.A., Lambert, D.W., Boissonade, F.M. (2023) The Role of miRNAs in Neuropathic Pain. Biomedicines, 11, 775. https://doi.org/10.3390/biomedicines11030775

Conferences

- Selected talk presented at "The challenge of Chronic Pain: from Genomics to Therapy", Wellcome Genome Campus, Cambridge, UK (2023) titled "*Investigating the cellular composition of healthy and injured human trigeminal nerves with single nuclei RNA sequencing*".
- Selected talk presented at the Peripheral Nerve Society Meeting, Copenhagen, Denmark (2023) titled: "*Investigating the gene expression of human lingual nerve neuromas with spatial transcriptomics*".
- Poster presentation at the European Pain Federation EFIC Conference, Dublin, Ireland (2022) titled "*Investigating the gene expression of lingual nerve neuromas with spatial transcriptomics*".

Scholarship, funding and awards

- Wellcome Connecting Science Bursary to fund attendance at "The Challenge of Chronic Pain: from Genomics to Therapy" conference (2023)
- Wellcome Trust Biomedical Vacation Scholarship to provide stipend and consumables for a vacation student under my supervision during a 6-week project (2023)
- Dr Jeff Wadsworth – Battelle Knowledge Exchange Scheme Award (£15,917) to support a six-month knowledge exchange project with Prof Theodore Price, University of Texas.
- BBSRC IAA Knowledge exchange funding (£10,000) to further support the costs of the spatial transcriptomics work.

Outreach

- PhD Tutor at the Brilliant Club at Meadowhead School (key stage 5) to design and deliver university-style tutorials to A-levels students titled: "*A painful challenge: why do we feel pain and how can we stop it?*"

Appendix

Appendix 1: Single nuclei RNA-sequencing

Appendix 1.a. Cellranger output

Table A1 Output of CellRanger count function.
Table showing the UMIs and cells detected per barcode following processing with Cellranger count (10X Genomics)

Barcode	*ID*	*UMIs per probe barcode*	*Cells per probe barcode*
BC013	N1	9,531,621 (1.90%)	5,162 (4.64%)
BC014	N1	7,421,012 (1.48%)	3,965 (3.57%)
BC015	N2	15,346,227 (3.06%)	4,843 (4.35%)
BC016	N2	15,586,305 (3.11%)	4,840 (4.35%)
BC009	TG1	58,830,859 (11.72%)	11,992 (10.78%)
BC010	TG1	39,028,397 (7.78%)	7,883 (7.09%)
BC011	TG2	47,102,012 (9.39%)	11,150 (10.03%)
BC012	TG2	42,267,865 (8.42%)	10,223 (9.19%)

Appendix 1.b. QC and filtering parameters

Table A2 Parameters used for analysis of snRNA-seq data
Parameters used for the clean-up of ambient RNA signal with Cellbender, removal of doublets with scDblFinder and filtering of good quality nuclei with Seurat.

	N1	**N2**	**TG1**	**TG2**
			Cellbender	
expected-cells	8000	7000	10000	10000
total droplets included	60000	40000	60000	60000
fpr	0.01			
learning-rate	N/A	N/A	0.00005	N/A
epochs	150		200	
			scDblFinder	
set.seed			123	
			Seurat	
nCount >=			500	
nFeature >=			250	
log10GenesperUMI			0.8	
% mito <			5	

Appendix 1.c. Number of nuclei annotated in each cluster grouped by sample ID

Table A3 Table displaying the absolute and relative frequency of the annotation of cell types in each sample.
The table displays the absolute and relative (% in each sample) frequency of each cell type in each of the four samples. N1 (LN14) is non-painful, N2 (LN13) is painful.

	n1	*% n1*	*n2*	*% n2*	*tg1*	*%tg1*	*tg2*	*%tg2*
MSC_1	14	0.17%	112	1.18%	2961	17.43%	4167	21.76%
MSC_2	44	0.54%	154	1.62%	2417	14.23%	2082	10.87%
MSC_3	659	8.14%	438	4.61%	0	0.00%	0	0.00%
NMSC	95	1.17%	182	1.92%	2706	15.93%	2745	14.33%
Astro	0	0.00%	0	0.00%	1	0.01%	271	1.42%
Oligo	0	0.00%	0	0.00%	0	0.00%	200	1.04%
EndoF	252	3.11%	528	5.56%	1345	7.92%	1453	7.59%
PeriF_1	0	0.00%	45	0.47%	1157	6.81%	2337	12.20%
PeriF_2	18	0.22%	10	0.11%	3358	19.77%	59	0.31%
PeriF_3	3	0.04%	43	0.45%	44	0.26%	2787	14.55%
PeriF_4	188	2.32%	1944	20.47%	12	0.07%	103	0.54%
MenF_1	0	0.00%	0	0.00%	482	2.84%	381	1.99%
MenF_2	0	0.00%	0	0.00%	479	2.82%	724	3.78%
Fibro_PRRX1+	1712	21.15%	812	8.55%	8	0.05%	48	0.25%
Endo_1	1297	16.02%	2345	24.69%	11	0.06%	14	0.07%
Endo_2	444	5.48%	1158	12.19%	32	0.19%	46	0.24%
Endo_3	8	0.10%	28	0.29%	421	2.48%	441	2.30%
Mural	350	4.32%	1132	11.92%	249	1.47%	266	1.39%
Myeloid	84	1.04%	41	0.43%	1111	6.54%	871	4.55%
Lymphocytes	66	0.82%	56	0.59%	193	1.14%	156	0.81%
SGC_1	1662	20.53%	193	2.03%	0	0.00%	0	0.00%
SGC_2	614	7.58%	37	0.39%	0	0.00%	0	0.00%
SGC_3	272	3.36%	68	0.72%	0	0.00%	0	0.00%
Myo	313	3.87%	170	1.79%	0	0.00%	0	0.00%
total	8095	100.00%	9496	100.00%	16987	100.00%	19151	100.00%

Appendix 1.d Number of nuclei annotated in each cluster grouped by sample type

Table A4 Table displaying the absolute and relative frequency of the annotation of cell types in each sample type.
The table displays the absolute and relative (% in each sample) frequency of each cell type in each of the four samples.

	neuromas	*% neuromas*	*tgs*	*% tgs*
MSC_1	126	0.72%	7128	19.72%
MSC_2	198	1.13%	4499	12.45%
MSC_3	1097	6.24%	0	0.00%
NMSC	277	1.57%	5451	15.08%
Astro	0	0.00%	272	0.75%
Oligo	0	0.00%	200	0.55%
EndoF	780	4.43%	2798	7.74%
PeriF_1	45	0.26%	3494	9.67%
PeriF_2	28	0.16%	3417	9.46%
PeriF_3	46	0.26%	2831	7.83%
PeriF_4	2132	12.12%	115	0.32%
MenF_1	0	0.00%	863	2.39%
MenF_2	0	0.00%	1203	3.33%
Fibro_PRRX1+	2524	14.35%	56	0.15%
Endo_1	3642	20.70%	25	0.07%
Endo_2	1602	9.11%	78	0.22%
Endo_3	36	0.20%	862	2.39%
Mural	1482	8.42%	515	1.43%
Myeloid	125	0.71%	1982	5.48%
Lymphocytes	122	0.69%	349	0.97%
SGC_1	1855	10.55%	0	0.00%
SGC_2	651	3.70%	0	0.00%
SGC_3	340	1.93%	0	0.00%
Myo	483	2.75%	0	0.00%
total	17591	100.00%	36138	100.00%

Appendix 2: Spatial transcriptomics

Appendix 2.a Differentially expressed genes.

Table A5 Differentially expressed genes in pseudo-bulk analysis
List of significantly DE genes in painful versus non-painful group calculated with DEseq2 discussed in Chapter 3.

gene	baseMean	log2FoldChange	lfcSE	pvalue	padj
HLA-A	3732.98308	3.96209025	0.63700645	3.93E-12	6.01E-08
CXCL2	945.271064	2.07691729	0.3741736	6.87E-10	3.49E-06
NID2	1138.85425	2.10234897	0.37776821	5.89E-10	3.49E-06
SLC52A3	176.045174	2.81958663	0.5304935	6.22E-09	2.37E-05
MTLN	658.556939	-1.2737827	0.2698749	1.91E-07	0.00058306

MMP19	2059.79265	1.8481752	0.44940288	8.28E-07	0.00210622
ADGRG1	497.68488	1.82257403	0.44849106	1.17E-06	0.00254832
CXCL8	437.374605	3.1318051	0.81789978	1.74E-06	0.002944
JMJD1C	1908.78945	2.22327595	0.57008455	1.54E-06	0.002944
PUS7L	153.274003	2.24478893	0.55741114	1.93E-06	0.00294481
TNFAIP3	1759.3612	2.05520455	0.56336315	4.34E-06	0.0060255
IGFBP2	1040.94854	1.43915656	0.38565648	4.82E-06	0.00613074
GLRX5	1287.83774	-1.2193629	0.306225	5.26E-06	0.00618238
GSTM3	2776.47552	-0.9720634	0.25031004	8.10E-06	0.00824117
ZNF775	209.644591	-1.552507	0.3992998	7.92E-06	0.00824117
NLRC5	157.603886	2.18704394	0.61097833	9.41E-06	0.00897992
SLC20A1	1299.2717	1.36795691	0.39524334	1.34E-05	0.01102222
RBMS1	459.370346	1.72198656	0.51016012	1.50E-05	0.01102222
NOTCH1	1179.15101	1.67106113	0.4928374	1.52E-05	0.01102222
ADD3	4205.64898	0.92236035	0.2606074	1.40E-05	0.01102222
PUDP	195.244193	2.67534622	0.79907443	1.38E-05	0.01102222
PELI1	1247.56461	1.72647922	0.51814784	1.62E-05	0.01110569
ABCB1	359.698359	1.83943152	0.55181988	1.77E-05	0.01110569
SLITRK5	653.734153	2.41602871	0.75499711	1.79E-05	0.01110569
SGF29	365.176944	-0.9889459	0.27040287	1.82E-05	0.01110569
EIF2S3B	331.268048	2.26155264	0.71210818	2.30E-05	0.01350386
TCF7L1	674.214305	1.24222883	0.38371083	3.15E-05	0.0167372
GLT8D1	713.865049	1.51004789	0.47850939	3.23E-05	0.0167372
FOSL1	243.028072	3.81975251	1.29785346	3.29E-05	0.0167372
CNN2	863.816535	1.1608777	0.35473223	3.05E-05	0.0167372
NTM	388.618431	1.53066266	0.48041373	3.54E-05	0.01745794
ATAD3C	125.406328	3.16319256	0.97606106	3.83E-05	0.0182693
RAD21	765.524404	1.36991311	0.43731129	4.00E-05	0.01852264
ZNF138	199.40551	1.47995215	0.46378888	4.49E-05	0.01902911
CCND1	1052.48405	2.03607216	0.6903246	4.35E-05	0.01902911
MPDU1	572.599457	1.52956972	0.50100906	4.45E-05	0.01902911
CAVIN3	8662.81582	-0.9131125	0.26769627	5.21E-05	0.02149722
ADCY3	1981.06614	0.84516932	0.26666399	6.02E-05	0.02417095
BRF2	364.567016	-0.9625514	0.29392665	7.34E-05	0.02871587
ECH1	3109.56951	-0.7754682	0.23722476	7.76E-05	0.02962413
EFCAB11	157.624384	1.76317501	0.60703757	8.84E-05	0.0329048
TMEM14B	89.8909117	2.2141205	0.74062097	9.12E-05	0.03316394
HIST1H3A	497.500117	1.23778007	0.43286697	0.00010558	0.03684007
HRCT1	129.81849	2.28157733	0.82228196	0.00010617	0.03684007
KIAA0040	525.718174	1.46805385	0.52753678	0.00011011	0.03697875
TIMM29	1041.19759	-0.7875063	0.24750282	0.00011141	0.03697875
ANXA2	8424.74011	1.36559303	0.49835581	0.00011677	0.03793295
IFITM1	2995.65628	1.10081069	0.39319602	0.00012714	0.04044037

ARHGAP5	986.71202	1.5968426	0.60164865	0.00013898	0.04243918
ZNF500	153.368856	3.68784814	1.46197241	0.00013885	0.04243918
SLC25A2	106.355486	2.47130573	0.90411398	0.00015407	0.0436426
SRI	588.041851	1.50946606	0.57580324	0.00015298	0.0436426
LPAR5	170.707384	-1.2531244	0.4125944	0.00015721	0.0436426
IGHG2	806.678448	0.01298874	0.1796055	0.00015087	0.0436426
BCAR1	1561.73031	0.88887285	0.31429284	0.00015638	0.0436426
MESD	1983.48939	-0.7077342	0.22951255	0.00016636	0.04535743
ABCF3	1467.63688	-0.6885055	0.22706995	0.00017405	0.04662092
RRP12	467.050876	1.40913778	0.53773823	0.00018147	0.04777052
KLF4	9209.98209	1.52113724	0.6073504	0.00018901	0.04891192

Appendix 2.b CXCL2, CXCL8, ACKR1, CXCR1 and CXCR2 expression detected by spatial transcriptomics

Figure A1 Expression of chemokines and chemokine receptors in samples of human neuromas detected by spatial transcriptomics.
The images show the expression of the chemokines and chemokine receptors discussed in Chapter 3 and Chapter 5. From top to bottom row: CXCL2, CXCL8, ACKR1, CXCR2, CXCR1. The samples shown are, from left to right, LN1 (painful), LN15 (painful), LN2 (non-painful) and LN8 (non-painful). The expression level of each gene in each barcode is indicated on a colour scale where blue indicates the lowest level of expression and yellow indicates the highest. In each sample, an associated scale bar indicating the range of expression is shown. Samples which appear in a shade of teal display no expression of the gene in question.

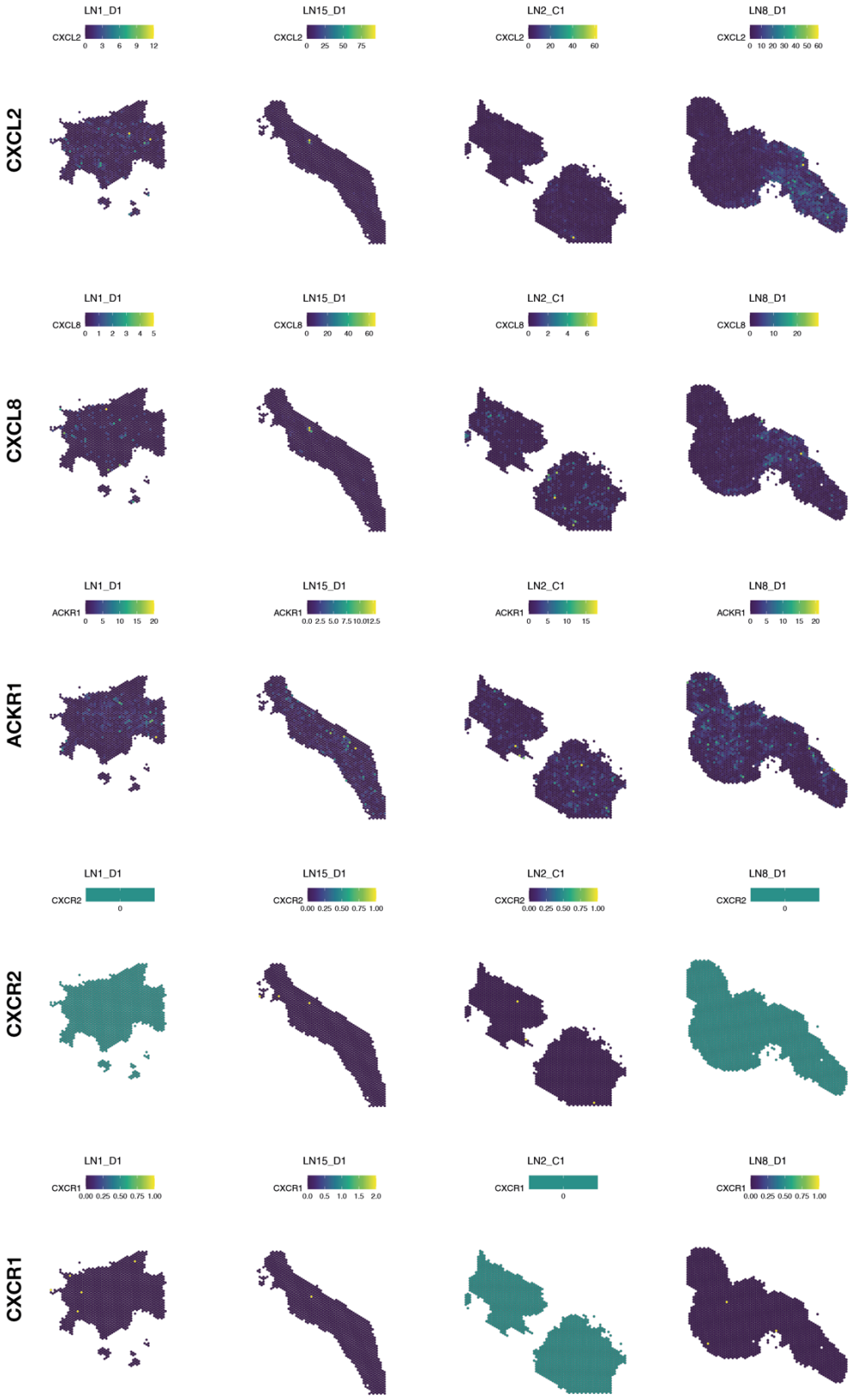
LN1_D1
LN15_D1
LN2_C1
LN8_D1
CXCL2
CXCL8
ACKR1
CXCR2
CXCR1

References

2020. International Classification of Orofacial Pain, 1st edition (ICOP). *Cephalalgia,* 40**,** 129-221.

2022. Visium Spatial Gene Expression for FFPE – Deparaffinization, H&E Staining, Imaging & Decrosslinking, CG000409. 10X Genomics.

2023. Chromium Fixed RNA Profiling Reagent Kits for Multiplexed Samples, CG000527. 10X Genomics.

ABBADIE, C. 2005. Chemokines, chemokine receptors and pain. *Trends in Immunology,* 26**,** 529-534.

ACKERMAN, S. D., LUO, R., POITELON, Y., MOGHA, A., HARTY, B. L., D'ROZARIO, M., SANCHEZ, N. E., LAKKARAJU, A. K. K., GAMBLE, P., LI, J., QU, J., MACEWAN, M. R., RAY, W. Z., AGUZZI, A., FELTRI, M. L., PIAO, X. & MONK, K. R. 2018. GPR56/ADGRG1 regulates development and maintenance of peripheral myelin. *J Exp Med,* 215**,** 941-961.

AKIN, E. J., HIGERD-RUSLI, G. P., MIS, M. A., TANAKA, B. S., ADI, T., LIU, S., DIB-HAJJ, F. B., WAXMAN, S. G. & DIB-HAJJ, S. D. 2019. Building sensory axons: Delivery and distribution of NaV1.7 channels and effects of inflammatory mediators. *Science Advances,* 5.

ARVIDSON, B. 1977. Cellular uptake of exogenous horseradish peroxidase in mouse peripheral nerve. *Acta Neuropathologica,* 37**,** 35-41.

ATKINS, S. & KYRIAKIDOU, E. 2021. Clinical outcomes of lingual nerve repair. *Br J Oral Maxillofac Surg,* 59**,** 39-45.

ATKINS, S., SMITH, K. G., LOESCHER, A. R., BOISSONADE, F. M., O'KANE, S., FERGUSON, M. W. J. & ROBINSON, P. P. 2006. Scarring impedes regeneration at sites of peripheral nerve repair. *NeuroReport,* 17.

AVILA COBOS, F., ALQUICIRA-HERNANDEZ, J., POWELL, J. E., MESTDAGH, P. & DE PRETER, K. 2020. Benchmarking of cell type deconvolution pipelines for transcriptomics data. *Nature Communications,* 11**,** 5650.

BAI, Y., HU, M., CHEN, Z., WEI, J. & DU, H. 2021. Single-Cell Transcriptome Analysis Reveals RGS1 as a New Marker and Promoting Factor for T-Cell Exhaustion in Multiple Cancers. *Front Immunol,* 12**,** 767070.

BALAKRISHNAN, A., BELFIORE, L., CHU, T.-H., FLEMING, T., MIDHA, R., BIERNASKIE, J. & SCHUURMANS, C. 2021. Insights Into the Role and Potential of Schwann Cells for Peripheral Nerve Repair From Studies of Development and Injury. *Frontiers in Molecular Neuroscience,* 13.

BALKWILL, F. 2004. Cancer and the chemokine network. *Nature Reviews Cancer,* 4**,** 540-550.

BALL, J. B., MCNULTY, C. J., GREEN-FULGHAM, S. M., DRAGAVON, J. M., CORREIA ROCHA, I. R., FINCH, M. R., PRÉVOST, E. D., SIDDIQUE, I. I., WOODALL, B. J., WATKINS, L. R., BARATTA, M. V. & ROOT, D. H. 2023. Combining RNAscope and immunohistochemistry to visualize inflammatory

gene products in neurons and microglia. *Frontiers in Molecular Neuroscience,* 16.

BARGAGNA-MOHAN, P., SCHULTZ, G., RHEAUME, B., TRAKHTENBERG, E. F., ROBSON, P., PAL-GHOSH, S., STEPP, M. A., GIVEN, K. S., MACKLIN, W. B. & MOHAN, R. 2021. Corneal nonmyelinating Schwann cells illuminated by single-cell transcriptomics and visualized by protein biomarkers. *J Neurosci Res,* 99**,** 731-749.

BASBAUM, A. I., BAUTISTA, D. M., SCHERRER, G. & JULIUS, D. 2009. Cellular and molecular mechanisms of pain. *Cell,* 139**,** 267-284.

BASSO, L. & ALTIER, C. 2017. Transient Receptor Potential Channels in neuropathic pain. *Current Opinion in Pharmacology,* 32**,** 9-15.

BEAZLEY-LONG, N., HODGE, D., ASHBY, W. R., BESTALL, S. M., ALMAHASNEH, F., DURRANT, A. M., BENEST, A. V., BLACKLEY, Z., BALLMER-HOFER, K., HIRASHIMA, M., HULSE, R. P., BATES, D. O. & DONALDSON, L. F. 2018. VEGFR2 promotes central endothelial activation and the spread of pain in inflammatory arthritis. *Brain, Behavior, and Immunity,* 74**,** 49-67.

BENEDETTI, S., BERTINI, E., IANNACCONE, S., ANGELINI, C., TRISCIANI, M., TONIOLO, D., SFERRAZZA, B., CARRERA, P., COMI, G., FERRARI, M., QUATTRINI, A. & PREVITALI, S. C. 2005. Dominant LMNA mutations can cause combined muscular dystrophy and peripheral neuropathy. *J Neurol Neurosurg Psychiatry,* 76**,** 1019-21.

BENNETT, D. L., CLARK, A. J., HUANG, J., WAXMAN, S. G. & DIB-HAJJ, S. D. 2019. The Role of Voltage-Gated Sodium Channels in Pain Signaling. *Physiological Reviews,* 99**,** 1079-1151.

BERNAL, L., LOPEZ-GARCIA, J. A. & ROZA, C. 2016. Spontaneous activity in C-fibres after partial damage to the saphenous nerve in mice: Effects of retigabine. *European Journal of Pain,* 20**,** 1335-1345.

BERNIER, L. P., ASE, A. R. & SÉGUÉLA, P. 2018. P2X receptor channels in chronic pain pathways. *Br J Pharmacol,* 175**,** 2219-2230.

BESTER, H., BEGGS, S. & WOOLF, C. J. 2000. Changes in tactile stimuli-induced behavior and c-Fos expression in the superficial dorsal horn and in parabrachial nuclei after sciatic nerve crush. *Journal of Comparative Neurology,* 428**,** 45-61.

BEUCKMANN, C. T., FUJIMORI, K., URADE, Y. & HAYAISHI, O. 2000. Identification of Mu-Class Glutathione Transferases M2-2 and M3-3 as Cytosolic Prostaglandin E Synthases in the Human Brain. *Neurochemical Research,* 25**,** 733-738.

BHUIYAN, S. A., XU, M., YANG, L., SEMIZOGLOU, E., BHATIA, P., PANTALEO, K. I., TOCHITSKY, I., JAIN, A., ERDOGAN, B., BLAIR, S., CAT, V., MWIRIGI, J. M., SANKARANARAYANAN, I., TAVARES-FERREIRA, D., GREEN, U., MCILVRIED, L. A., COPITS, B. A., BERTELS, Z., DEL ROSARIO, J. S., WIDMAN, A. J., SLIVICKI, R. A., YI, J., WOOLF, C. J., LENNERZ, J. K., WHITED, J. L., PRICE, T. J., GEREAU, R. W. T. & RENTHAL, W. 2023.

Harmonized cross-species cell atlases of trigeminal and dorsal root ganglia. *bioRxiv*.

BIGGS, J. E., YATES, J. M., LOESCHER, A. R., CLAYTON, N. M., BOISSONADE, F. M. & ROBINSON, P. P. 2007. Vanilloid receptor 1 (TRPV1) expression in lingual nerve neuromas from patients with or without symptoms of burning pain. *Brain Research,* 1127**,** 59-65.

BIRD, E. V., CHRISTMAS, C. R., LOESCHER, A. R., SMITH, K. G., ROBINSON, P. P., BLACK, J. A., WAXMAN, S. G. & BOISSONADE, F. M. 2013. Correlation of Nav1.8 and Nav1.9 sodium channel expression with neuropathic pain in human subjects with lingual nerve neuromas. *Molecular pain,* 9**,** 52-52.

BIRD, E. V., IANNITTI, T., CHRISTMAS, C. R., OBARA, I., ANDREEV, V. I., KING, A. E. & BOISSONADE, F. M. 2018. A Novel Role for Lymphotactin (XCL1) Signaling in the Nervous System: XCL1 Acts via its Receptor XCR1 to Increase Trigeminal Neuronal Excitability. *Neuroscience,* 379**,** 334-349.

BIRD, E. V., ROBINSON, P. P. & BOISSONADE, F. M. 2007. Nav1.7 sodium channel expression in human lingual nerve neuromas. *Archives of Oral Biology,* 52**,** 494-502.

BLACK, J. A., NIKOLAJSEN, L., KRONER, K., JENSEN, T. S. & WAXMAN, S. G. 2008. Multiple sodium channel isoforms and mitogen-activated protein kinases are present in painful human neuromas. *Annals of Neurology,* 64**,** 644-653.

BLIGHE, K. L., A. 2019. *PCAtools: everything Principal Components Analysis.* [Online]. Available: https://github.com/kevinblighe/PCAtools. [Accessed].

BONECCHI, R. & GRAHAM, G. J. 2016. Atypical Chemokine Receptors and Their Roles in the Resolution of the Inflammatory Response. *Front Immunol,* 7**,** 224.

BONEZZI, C., COSTANTINI, A., CRUCCU, G., FORNASARI, D. M., GUARDAMAGNA, V., PALMIERI, V., POLATI, E., ZINI, P. & DICKENSON, A. H. 2020. Capsaicin 8% dermal patch in clinical practice: an expert opinion. *Expert opinion on pharmacotherapy,* 21**,** 1377-1387.

BONGENHIELM, U. & ROBINSON, P. P. 1996. Spontaneous and mechanically evoked afferent activity originating from myelinated fibres in ferret inferior alveolar nerve neuromas. *Pain,* 67**,** 399-406.

BORNSTEIN, P. 2009. Matricellular proteins: an overview. *J Cell Commun Signal,* 3**,** 163-5.

BOUHASSIRA, D. & ATTAL, N. 2016. Translational neuropathic pain research: A clinical perspective. *Neuroscience,* 338**,** 27-35.

BRANDOLINI, L., CASTELLI, V., ARAMINI, A., GIORGIO, C., BIANCHINI, G., RUSSO, R., DE CARO, C., D'ANGELO, M., CATANESI, M., BENEDETTI, E., GIORDANO, A., CIMINI, A. & ALLEGRETTI, M. 2019. DF2726A, a new IL-8 signalling inhibitor, is able to counteract chemotherapy-induced neuropathic pain. *Scientific Reports,* 9**,** 11729.

BREIVIK, H., COLLETT, B., VENTAFRIDDA, V., COHEN, R. & GALLACHER, D. 2006. Survey of chronic pain in Europe: Prevalence, impact on daily life, and treatment. *European Journal of Pain,* 10**,** 287-333.

BREMER, M., FRÖB, F., KICHKO, T., REEH, P., TAMM, E. R., SUTER, U. & WEGNER, M. 2011. Sox10 is required for Schwann-cell homeostasis and myelin maintenance in the adult peripheral nerve. *Glia,* 59**,** 1022-32.

BROWN, V. M., OSSADTCHI, A., KHAN, A. H., YEE, S., LACAN, G., MELEGA, W. P., CHERRY, S. R., LEAHY, R. M. & SMITH, D. J. 2002. Multiplex three-dimensional brain gene expression mapping in a mouse model of Parkinson's disease. *Genome Res,* 12**,** 868-84.

BRÜCK, W. 1997. The role of macrophages in Wallerian degeneration. *Brain Pathol,* 7**,** 741-52.

BRUNO, F., ABONDIO, P., MONTESANTO, A., LUISELLI, D., BRUNI, A. C. & MALETTA, R. 2023. The Nerve Growth Factor Receptor (NGFR/p75(NTR)): A Major Player in Alzheimer's Disease. *Int J Mol Sci,* 24.

BUESING, S., COSTA, M., SCHILLING, J. M. & MOELLER-BERTRAM, T. 2019. Vitamin B12 as a treatment for pain. *Pain physician,* 22**,** E45.

BUI, T. M., WIESOLEK, H. L. & SUMAGIN, R. 2020. ICAM-1: A master regulator of cellular responses in inflammation, injury resolution, and tumorigenesis. *J Leukoc Biol,* 108**,** 787-799.

BUNGE, M. B., WOOD, P. M., TYNAN, L. B., BATES, M. L. & SANES, J. R. 1989. Perineurium Originates from Fibroblasts: Demonstration in vitro with a Retroviral Marker. *Science,* 243**,** 229-231.

BURCHIEL, K. J. 1988. Carbamazepine inhibits spontaneous activity in experimental neuromas. *Experimental neurology,* 102**,** 249-253.

BURGY, O. & KÖNIGSHOFF, M. 2018. The WNT signaling pathways in wound healing and fibrosis. *Matrix Biology,* 68-69**,** 67-80.

BYERS, M. R. 1990. Segregation of NGF receptor in sensory receptors, nerves and local cells of teeth and periodontium demonstrated by EM immunocytochemistry. *J Neurocytol,* 19**,** 765-75.

CAMBIER, S., GOUWY, M. & PROOST, P. 2023. The chemokines CXCL8 and CXCL12: molecular and functional properties, role in disease and efforts towards pharmacological intervention. *Cellular & Molecular Immunology,* 20**,** 217-251.

CAREY, B. S., POULTON, K. V. & POLES, A. 2019. Factors affecting HLA expression: A review. *International Journal of Immunogenetics,* 46**,** 307-320.

CARR, M. J., TOMA, J. S., JOHNSTON, A. P. W., STEADMAN, P. E., YUZWA, S. A., MAHMUD, N., FRANKLAND, P. W., KAPLAN, D. R. & MILLER, F. D. 2019. Mesenchymal Precursor Cells in Adult Nerves Contribute to Mammalian Tissue Repair and Regeneration. *Cell Stem Cell,* 24.

CATERINA, M. J., LEFFLER, A., MALMBERG, A. B., MARTIN, W. J., TRAFTON, J., PETERSEN-ZEITZ, K. R., KOLTZENBURG, M., BASBAUM, A. I. & JULIUS, D.

2000. Impaired Nociception and Pain Sensation in Mice Lacking the Capsaicin Receptor. *Science,* 288**,** 306-313.

CAUSEY, G. & BARTON, A. A. 1959. The cellular content of the endoneurium of peripheral nerve. *Brain,* 82**,** 594-8.

CAVALLI, E., MAMMANA, S., NICOLETTI, F., BRAMANTI, P. & MAZZON, E. 2019. The neuropathic pain: An overview of the current treatment and future therapeutic approaches. *Int J Immunopathol Pharmacol,* 33.

CERVERO, F. & WOOD, J. N. 2020. History of Pain Research. *In:* WOOD, J. N. (ed.) *The Oxford Handbook of the Neurobiology of Pain.* Oxford University Press.

CHAU, M. J., QUINTERO, J. E., MONJE, P. V., VOSS, S. R., WELLEFORD, A. S., GERHARDT, G. A. & VAN HORNE, C. G. 2022. Using a Transection Paradigm to Enhance the Repair Mechanisms of an Investigational Human Cell Therapy. *Cell Transplant,* 31.

CHEN, A., LIAO, S., CHENG, M., MA, K., WU, L., LAI, Y., QIU, X., YANG, J., XU, J. & HAO, S. 2022. Spatiotemporal transcriptomic atlas of mouse organogenesis using DNA nanoball-patterned arrays. *Cell,* 185**,** 1777-1792.

CHEN, B., BANTON, M. C., SINGH, L., PARKINSON, D. B. & DUN, X. P. 2021. Single Cell Transcriptome Data Analysis Defines the Heterogeneity of Peripheral Nerve Cells in Homeostasis and Regeneration. *Front Cell Neurosci,* 15.

CHEN, K. H., BOETTIGER, A. N., MOFFITT, J. R., WANG, S. & ZHUANG, X. 2015. Spatially resolved, highly multiplexed RNA profiling in single cells. *Science,* 348.

CHEN, L., YANG, G. & GROSSER, T. 2013. Prostanoids and inflammatory pain. *Prostaglandins & Other Lipid Mediators,* 104-105**,** 58-66.

CHENG, T., XU, Z. & MA, X. 2022. The role of astrocytes in neuropathic pain. *Frontiers in Molecular Neuroscience,* 15.

CHENG, Z., ZHANG, Y., TIAN, Y., CHEN, Y., DING, F., WU, H., JI, Y. & SHEN, M. 2021. Cyr61 promotes Schwann cell proliferation and migration via α v β 3 integrin. *BMC Mol Cell Biol,* 22**,** 21.

CHINCHOLKAR, M. 2020. Gabapentinoids: pharmacokinetics, pharmacodynamics and considerations for clinical practice. *Br J Pain,* 14**,** 104-114.

CHISTIAKOV, D. A., KILLINGSWORTH, M. C., MYASOEDOVA, V. A., OREKHOV, A. N. & BOBRYSHEV, Y. V. 2017. CD68/macrosialin: not just a histochemical marker. *Laboratory Investigation,* 97**,** 4-13.

CHRISTENSEN, B. N. & PERL, E. R. 1970. Spinal neurons specifically excited by noxious or thermal stimuli: marginal zone of the dorsal horn. *J Neurophysiol,* 33**,** 293-307.

COLIN, W. & DONOFF, R. B. 1992. RESTORING SENSATION AFTER TRIGEMINAL NERVE INJURY - A REVIEW OF CURRENT MANAGEMENT. *Journal of the American Dental Association,* 123**,** 80-85.

COSGAYA, J. M., CHAN, J. R. & SHOOTER, E. M. 2002. The Neurotrophin Receptor p75NTR as a Positive Modulator of Myelination. *Science,* 298**,** 1245-1248.

COSTIGAN, M., SCHOLZ, J. & WOOLF, C. J. 2009. Neuropathic Pain: A Maladaptive Response of the Nervous System to Damage. *Annual Review of Neuroscience,* 32**,** 1-32.

CUI, J.-G., HOLMIN, S., MATHIESEN, T., MEYERSON, B. A. & LINDEROTH, B. 2000. Possible role of inflammatory mediators in tactile hypersensitivity in rat models of mononeuropathy. *PAIN,* 88**,** 239-248.

CUI, L., CHEN, S.-Y., LERBS, T., LEE, J.-W., DOMIZI, P., GORDON, S., KIM, Y.-H., NOLAN, G., BETANCUR, P. & WERNIG, G. 2020. Activation of JUN in fibroblasts promotes pro-fibrotic programme and modulates protective immunity. *Nature Communications,* 11**,** 2795.

DAVIES, S. L., LOESCHER, A. R., CLAYTON, N. M., BOUNTRA, C., ROBINSON, P. P. & BOISSONADE, F. M. 2006. Changes in sodium channel expression following trigeminal nerve injury. *Exp Neurol,* 202**,** 207-16.

DE ROOIJ, A. M., FLORENCIA GOSSO, M., HAASNOOT, G. W., MARINUS, J., VERDUIJN, W., CLAAS, F. H., VAN DEN MAAGDENBERG, A. M. & VAN HILTEN, J. J. 2009. HLA-B62 and HLA-DQ8 are associated with Complex Regional Pain Syndrome with fixed dystonia. *Pain,* 145**,** 82-5.

DECHANT, G. & BARDE, Y.-A. 2002. The neurotrophin receptor p75NTR: novel functions and implications for diseases of the nervous system. *Nature Neuroscience,* 5**,** 1131-1136.

DENDROU, C. A., PETERSEN, J., ROSSJOHN, J. & FUGGER, L. 2018. HLA variation and disease. *Nature Reviews Immunology,* 18**,** 325-339.

DERRY, S., BELL, R. F., STRAUBE, S., WIFFEN, P. J., ALDINGTON, D. & MOORE, R. A. 2019. Pregabalin for neuropathic pain in adults. *Cochrane Database Syst Rev,* 1.

DESISTO, J., O'ROURKE, R., JONES, H. E., PAWLIKOWSKI, B., MALEK, A. D., BONNEY, S., GUIMIOT, F., JONES, K. L. & SIEGENTHALER, J. A. 2020. Single-Cell Transcriptomic Analyses of the Developing Meninges Reveal Meningeal Fibroblast Diversity and Function. *Dev Cell,* 54**,** 43-59.

DEVOR, M., AMIR, R. & RAPPAPORT, Z. H. 2002. Pathophysiology of Trigeminal Neuralgia: The Ignition Hypothesis. *The Clinical Journal of Pain,* 18.

DEVOR, M., GOVRIN-LIPPMANN, R. & ANGELIDES, K. 1993. Na+ channel immunolocalization in peripheral mammalian axons and changes following nerve injury and neuroma formation. *Journal of Neuroscience,* 13**,** 1976-1992.

DHAKA, A., VISWANATH, V. & PATAPOUTIAN, A. 2006. TRP ION CHANNELS AND TEMPERATURE SENSATION. *Annual Review of Neuroscience,* 29**,** 135-161.

DIATCHENKO, L., PARISIEN, M., JAHANGIRI ESFAHANI, S. & MOGIL, J. S. 2022. Omics approaches to discover pathophysiological pathways contributing to human pain. *Pain,* 163.

DIPIETRO, L. A. 2016. Angiogenesis and wound repair: when enough is enough. *Journal of Leukocyte Biology,* 100**,** 979-984.

DJOUHRI, L. & LAWSON, S. N. 2004. A β -fiber nociceptive primary afferent neurons: a review of incidence and properties in relation to other afferent A-fiber neurons in mammals. *Brain Research Reviews,* 46**,** 131-145.

DOMINGUEZ, C. A., KALLIOMÄKI, M., GUNNARSSON, U., MOEN, A., SANDBLOM, G., KOCKUM, I., LAVANT, E., OLSSON, T., NYBERG, F., RYGH, L. J., RØE, C., GJERSTAD, J., GORDH, T. & PIEHL, F. 2013. The DQB1*03:02 HLA haplotype is associated with increased risk of chronic pain after inguinal hernia surgery and lumbar disc herniation. *PAIN,* 154.

DOMINGUEZ, C. A., LIDMAN, O., HAO, J.-X., DIEZ, M., TUNCEL, J., OLSSON, T., WIESENFELD-HALLIN, Z., PIEHL, F. & XU, X.-J. 2008. Genetic analysis of neuropathic pain-like behavior following peripheral nerve injury suggests a role of the major histocompatibility complex in development of allodynia. *PAIN,* 136.

DOMOTO, R., SEKIGUCHI, F., TSUBOTA, M. & KAWABATA, A. 2021. Macrophage as a Peripheral Pain Regulator. *Cells,* 10.

DONG, B., WU, C., HUANG, L. & QI, Y. 2021. Macrophage-Related SPP1 as a Potential Biomarker for Early Lymph Node Metastasis in Lung Adenocarcinoma. *Front Cell Dev Biol,* 9.

DONG, F., DU, Y.-R., XIE, W., STRONG, J. A., HE, X.-J. & ZHANG, J.-M. 2012. Increased function of the TRPV1 channel in small sensory neurons after local inflammation or in vitro exposure to the pro-inflammatory cytokine GRO/KC. *Neuroscience bulletin,* 28**,** 155-164.

DONG, R. & YUAN, G.-C. 2021. SpatialDWLS: accurate deconvolution of spatial transcriptomic data. *Genome Biology,* 22**,** 145.

DOSSANTOS, M. F., HOLANDA-AFONSO, R. C., LIMA, R. L., DASILVA, A. F. & MOURA-NETO, V. 2014. The role of the blood-brain barrier in the development and treatment of migraine and other pain disorders. *Front Cell Neurosci,* 8**,** 302.

DRIES, R., ZHU, Q., DONG, R., ENG, C.-H. L., LI, H., LIU, K., FU, Y., ZHAO, T., SARKAR, A., BAO, F., GEORGE, R. E., PIERSON, N., CAI, L. & YUAN, G.-C. 2021. Giotto: a toolbox for integrative analysis and visualization of spatial expression data. *Genome Biology,* 22**,** 78.

DRISSI, I., WOODS, W. A. & WOODS, C. G. 2020. Understanding the genetic basis of congenital insensitivity to pain. *Br Med Bull,* 133**,** 65-78.

DU, B., DING, Y.-Q., XIAO, X., REN, H.-Y., SU, B.-Y. & QI, J.-G. 2018. CD4+ α β T cell infiltration into the leptomeninges of lumbar dorsal roots contributes to the transition from acute to chronic mechanical allodynia after adult rat tibial nerve injuries. *Journal of Neuroinflammation,* 15**,** 81.

DUAN, B., CHENG, L., BOURANE, S., BRITZ, O., PADILLA, C., GARCIA-CAMPMANY, L., KRASHES, M., KNOWLTON, W., VELASQUEZ, T., REN, X., ROSS, S., LOWELL, B. B., WANG, Y., GOULDING, M. & MA, Q. 2014.

Identification of spinal circuits transmitting and gating mechanical pain. *Cell,* 159**,** 1417-1432.

DUARTE, H., TEIXEIRA, A. L., ROCHA, N. P. & DOMINGUES, R. B. 2015. Increased interictal serum levels of CXCL8/IL-8 and CCL3/MIP-1 α in migraine. *Neurological Sciences,* 36**,** 203-208.

DUCHENE, J., NOVITZKY-BASSO, I., THIRIOT, A., CASANOVA-ACEBES, M., BIANCHINI, M., ETHERIDGE, S. L., HUB, E., NITZ, K., ARTINGER, K., ELLER, K., CAAMAÑO, J., RÜLICKE, T., MOSS, P., MEGENS, R. T. A., VON ANDRIAN, U. H., HIDALGO, A., WEBER, C. & ROT, A. 2017. Atypical chemokine receptor 1 on nucleated erythroid cells regulates hematopoiesis. *Nat Immunol,* 18**,** 753-761.

DUCLOT, F. & KABBAJ, M. 2017. The Role of Early Growth Response 1 (EGR1) in Brain Plasticity and Neuropsychiatric Disorders. *Frontiers in Behavioral Neuroscience,* 11.

EDVINSSON, J. C. A., VIGANÒ, A., ALEKSEEVA, A., ALIEVA, E., ARRUDA, R., DE LUCA, C., D'ETTORE, N., FRATTALE, I., KURNUKHINA, M., MACEROLA, N., MALENKOVA, E., MAIOROVA, M., NOVIKOVA, A., ŘEHULKA, P., RAPACCINI, V., ROSHCHINA, O., VANDERSCHUEREN, G., ZVAUNE, L., ANDREOU, A. P., HAANES, K. A. & ON BEHALF OF THE EUROPEAN HEADACHE FEDERATION SCHOOL OF ADVANCED, S. 2020. The fifth cranial nerve in headaches. *The Journal of Headache and Pain,* 21**,** 65.

EMRE, Y. & IMHOF, B. A. 2014. Matricellular protein CCN1/CYR61: a new player in inflammation and leukocyte trafficking. *Semin Immunopathol,* 36**,** 253-9.

ENG, C.-H. L., LAWSON, M., ZHU, Q., DRIES, R., KOULENA, N., TAKEI, Y., YUN, J., CRONIN, C., KARP, C. & YUAN, G.-C. 2019. Transcriptome-scale super-resolved imaging in tissues by RNA seqFISH+. *Nature,* 568**,** 235-239.

FAYAZ, A., CROFT, P., LANGFORD, R. M., DONALDSON, L. J. & JONES, G. T. 2016. Prevalence of chronic pain in the UK: a systematic review and meta-analysis of population studies. *BMJ Open,* 6.

FELLER, L., KHAMMISSA, R. A. G., FOURIE, J., BOUCKAERT, M. & LEMMER, J. 2017. Postherpetic Neuralgia and Trigeminal Neuralgia. *Pain Res Treat,* 2017.

FENG, D., YU, J., BAO, L., FAN, D. & ZHANG, B. 2022. Inhibiting RGS1 attenuates secondary inflammation response and tissue degradation via the TLR/TRIF/NF- κ B pathway in macrophage post spinal cord injury. *Neurosci Lett,* 768.

FERREIRA, G. E., ABDEL-SHAHEED, C., UNDERWOOD, M., FINNERUP, N. B., DAY, R. O., MCLACHLAN, A., ELDABE, S., ZADRO, J. R. & MAHER, C. G. 2023. Efficacy, safety, and tolerability of antidepressants for pain in adults: overview of systematic reviews. *BMJ,* 380.

FINAK, G., MCDAVID, A., YAJIMA, M., DENG, J., GERSUK, V., SHALEK, A. K., SLICHTER, C. K., MILLER, H. W., MCELRATH, M. J., PRLIC, M., LINSLEY, P. S. & GOTTARDO, R. 2015. MAST: a flexible statistical framework for assessing transcriptional changes and characterizing heterogeneity in single-cell RNA sequencing data. *Genome Biol,* 16**,** 278.

FINNERUP, N. B., ATTAL, N., HAROUTOUNIAN, S., MCNICOL, E., BARON, R., DWORKIN, R. H., GILRON, I., HAANPAA, M., HANSSON, P., JENSEN, T. S., KAMERMAN, P. R., LUND, K., MOORE, A., RAJA, S. N., RICE, A. S. C., ROWBOTHAM, M., SENA, E., SIDDALL, P., SMITH, B. H. & WALLACE, M. 2015. Pharmacotherapy for neuropathic pain in adults: a systematic review and meta-analysis. *Lancet Neurology,* 14**,** 162-173.

FINNERUP, N. B., KUNER, R. & JENSEN, T. S. 2021. Neuropathic Pain: From Mechanisms to Treatment. *Physiol Rev,* 101**,** 259-301.

FINZSCH, M., SCHREINER, S., KICHKO, T., REEH, P., TAMM, E. R., BÖSL, M. R., MEIJER, D. & WEGNER, M. 2010. Sox10 is required for Schwann cell identity and progression beyond the immature Schwann cell stage. *J Cell Biol,* 189**,** 701-12.

FLEMING, S. J., CHAFFIN, M. D., ARDUINI, A., AKKAD, A.-D., BANKS, E., MARIONI, J. C., PHILIPPAKIS, A. A., ELLINOR, P. T. & BABADI, M. 2023. Unsupervised removal of systematic background noise from droplet-based single-cell experiments using CellBender. *Nature Methods,* 20**,** 1323-1335.

FOLEY, A. R., MENEZES, M. P., PANDRAUD, A., GONZALEZ, M. A., AL-ODAIB, A., ABRAMS, A. J., SUGANO, K., YONEZAWA, A., MANZUR, A. Y. & BURNS, J. 2014. Treatable childhood neuronopathy caused by mutations in riboflavin transporter RFVT2. *Brain,* 137**,** 44-56.

FRISÉN, J., RISLING, M. & FRIED, K. 1993. Distribution and axonal relations of macrophages in a neuroma. *Neuroscience,* 55**,** 1003-1013.

FUJITA, S., MIZOBATA, N., NAKANISHI, T. & TOJYO, I. 2019. A case report of a long-term abandoned torn lingual nerve injury repaired by collagen nerve graft induced by lower third molar extraction. *Maxillofacial Plastic and Reconstructive Surgery,* 41**,** 60.

GALE, J. R., GEDEON, J. Y., DONNELLY, C. J. & GOLD, M. S. 2022. Local translation in primary afferents and its contribution to pain. *Pain,* 163**,** 2302-2314.

GALVIN, D. A. & C, M. 2021. The role of T-lymphocytes in neuropathic pain initiation, development of chronicity and treatment. *Brain Behav Immun Health,* 18**,** 100371.

GAMBLE, H. J. & EAMES, R. A. 1964. An electron microscopy study of the connective tissues of human peripheral nerves. *J Anat,* 98**,** 655-63.

GARRITY, R., ARORA, N., HAQUE, M. A., WEIS, D., TRINH, R. T., NEERUKONDA, S. V., KUMARI, S., CORTEZ, I., UBOGU, E. E., MAHALINGAM, R., TAVARES-FERREIRA, D., PRICE, T. J., KAVELAARS, A., HEIJNEN, C. J. & SHEPHERD, A. J. 2023. Fibroblast-derived PI16 sustains inflammatory pain via regulation of CD206+ myeloid cells. *Brain, Behavior, and Immunity,* 112**,** 220-234.

GAUDET, A. D., POPOVICH, P. G. & RAMER, M. S. 2011. Wallerian degeneration: gaining perspective on inflammatory events after peripheral nerve injury. *Journal of Neuroinflammation,* 8**,** 110.

GEISERT, E. E., JR. & FRANKFURTER, A. 1989. The neuronal response to injury as visualized by immunostaining of class III beta-tubulin in the rat. *Neurosci Lett,* 102**,** 137-41.

GERBER, D., PEREIRA, J. A., GERBER, J., TAN, G., DIMITRIEVA, S., YÁNGÜEZ, E. & SUTER, U. 2021. Transcriptional profiling of mouse peripheral nerves to the single-cell level to build a sciatic nerve ATlas (SNAT). *eLife,* 10.

GERMAIN, P., LUN, A., MACNAIR, W. & ROBINSON, M. 2021. Doublet identification in single-cell sequencing data using scDblFinder [version 1; peer review: 1 approved, 1 approved with reservations]. *F1000Research,* 10.

GIANNINI, C. & DYCK, P. J. 1994. Ultrastructural morphometric abnormalities of sural nerve endoneurial microvessels in diabetes mellitus. *Annals of Neurology,* 36**,** 408-415.

GLOWACKA, W. K., ALBERTS, P., OUCHIDA, R., WANG, J. Y. & ROTIN, D. 2012. LAPTM5 protein is a positive regulator of proinflammatory signaling pathways in macrophages. *J Biol Chem,* 287**,** 27691-702.

GOLD, M. S., WEINREICH, D., KIM, C.-S., WANG, R., TREANOR, J., PORRECA, F. & LAI, J. 2003. Redistribution of Na_V1.8 in Uninjured Axons Enables Neuropathic Pain. *The Journal of Neuroscience,* 23**,** 158-166.

GONÇALVES, N. P., MOHSENI, S., EL SOURY, M., ULRICHSEN, M., RICHNER, M., XIAO, J., WOOD, R. J., ANDERSEN, O. M., COULSON, E. J., RAIMONDO, S., MURRAY, S. S. & VÆGTER, C. B. 2019. Peripheral Nerve Regeneration Is Independent From Schwann Cell p75(NTR) Expression. *Front Cell Neurosci,* 13**,** 235.

GONG, T., WANG, Y., DONG, S., MA, X., DU, D., ZOU, C., ZHENG, Q. & WEN, Z. 2022. Single-cell RNA-seq reveals the communications between extracellular matrix-related components and Schwann cells contributing to the earlobe keloid formation. *Front Med (Lausanne),* 9.

GOODWIN, G. & MCMAHON, S. B. 2021. The physiological function of different voltage-gated sodium channels in pain. *Nature Reviews Neuroscience,* 22**,** 263-274.

GORDON, T., WOOD, P. & SULAIMAN, O. A. R. 2019. Long-Term Denervated Rat Schwann Cells Retain Their Capacity to Proliferate and to Myelinate Axons in vitro. *Frontiers in Cellular Neuroscience,* 12.

GRACIA VILLACAMPA, E., LARSSON, L., MIRZAZADEH, R., KVASTAD, L., ANDERSSON, A., MOLLBRINK, A., KOKARAKI, G., MONTEIL, V., SCHULTZ, N., APPELBERG, K. S., MONTSERRAT, N., ZHANG, H., PENNINGER, J. M., MIESBACH, W., MIRAZIMI, A., CARLSON, J. & LUNDEBERG, J. 2021. Genome-wide spatial expression profiling in formalin-fixed tissues. *Cell Genomics,* 1.

GRIFFIN, J. W., GEORGE, R. & HO, T. 1993. Macrophage Systems in Peripheral Nerves. A Review. *Journal of Neuropathology & Experimental Neurology,* 52**,** 553-560.

GROSSMANN, L., GORODETSKAYA, N., BARON, R. & JÄNIG, W. 2009. Enhancement of Ectopic Discharge in Regenerating A- and C-Fibers by Inflammatory Mediators. *Journal of Neurophysiology,* 101**,** 2762-2774.

GRÜTER, T., BLUSCH, A., MOTTE, J., SGODZAI, M., BACHIR, H., KLIMAS, R., AMBROSIUS, B., GOLD, R., ELLRICHMANN, G. & PITAROKOILI, K. 2020. Immunomodulatory and anti-oxidative effect of the direct TRPV1 receptor agonist capsaicin on Schwann cells. *J Neuroinflammation,* 17**,** 145.

GU, Q. & LEE, L. Y. 2010. Acid-Sensing Ion Channels and Pain. *Pharmaceuticals (Basel),* 3**,** 1411-1425.

GU, Y., LI, X., BI, Y., ZHENG, Y., WANG, J., LI, X., HUANG, Z., CHEN, L., HUANG, Y. & HUANG, Y. 2020. CCL14 is a prognostic biomarker and correlates with immune infiltrates in hepatocellular carcinoma. *Aging (Albany NY),* 12**,** 784-807.

GUO, F., DU, Y., QU, F.-H., LIN, S.-D., CHEN, Z. & ZHANG, S.-H. 2022. Dissecting the Neural Circuitry for Pain Modulation and Chronic Pain: Insights from Optogenetics. *Neuroscience Bulletin,* 38**,** 440-452.

HAO, Y., STUART, T., KOWALSKI, M., CHOUDHARY, S., HOFFMAN, P., HARTMAN, A., SRIVASTAVA, A., MOLLA, G., MADAD, S., FERNANDEZ-GRANDA, C. & SATIJA, R. 2022. Dictionary learning for integrative, multimodal, and scalable single-cell analysis. *bioRxiv***,** 2022.02.24.481684.

HARA, M., KADOYA, K., ENDO, T. & IWASAKI, N. 2023. Peripheral nerve-derived fibroblasts promote neurite outgrowth in adult dorsal root ganglion neurons more effectively than skin-derived fibroblasts. *Experimental Physiology,* 108**,** 621-635.

HARTLEHNERT, M., DERKSEN, A., HAGENACKER, T., KINDERMANN, D., SCHÄFERS, M., PAWLAK, M., KIESEIER, B. C. & MEYER ZU HORSTE, G. 2017. Schwann cells promote post-traumatic nerve inflammation and neuropathic pain through MHC class II. *Scientific Reports,* 7.

HÉBERT, H. L., PASCAL, M. M. V., SMITH, B. H., WYNICK, D. & BENNETT, D. L. H. 2023. Big data, big consortia, and pain: UK Biobank, PAINSTORM, and DOLORisk. *PAIN Reports,* 8.

HENSSEN, D. J. H. A., KURT, E., KOZICZ, T., VAN DONGEN, R., BARTELS, R. H. M. A. & VAN CAPPELLEN VAN WALSUM, A.-M. 2016. New Insights in Trigeminal Anatomy: A Double Orofacial Tract for Nociceptive Input. *Frontiers in Neuroanatomy,* 10.

HEUMOS, L., SCHAAR, A. C., LANCE, C., LITINETSKAYA, A., DROST, F., ZAPPIA, L., LÜCKEN, M. D., STROBL, D. C., HENAO, J., CURION, F., ALIEE, H., ANSARI, M., BADIA-I-MOMPEL, P., BÜTTNER, M., DANN, E., DIMITROV, D., DONY, L., FRISHBERG, A., HE, D., HEDIYEH-ZADEH, S., HETZEL, L., IBARRA, I. L., JONES, M. G., LOTFOLLAHI, M., MARTENS, L. D., MÜLLER, C. L., NITZAN, M., OSTNER, J., PALLA, G., PATRO, R., PIRAN, Z., RAMÍREZ-SUÁSTEGUI, C., SAEZ-RODRIGUEZ, J., SARKAR, H., SCHUBERT, B., SIKKEMA, L., SRIVASTAVA, A., TANEVSKI, J., VIRSHUP, I., WEILER, P., SCHILLER, H. B., THEIS, F. J. & SINGLE-CELL BEST

PRACTICES, C. 2023. Best practices for single-cell analysis across modalities. *Nature Reviews Genetics,* 24**,** 550-572.

HIGERD-RUSLI, G. P., TYAGI, S., BAKER, C. A., LIU, S., DIB-HAJJ, F. B., DIB-HAJJ, S. D. & WAXMAN, S. G. 2023. Inflammation differentially controls transport of depolarizing Nav versus hyperpolarizing Kv channels to drive rat nociceptor activity. *Proceedings of the National Academy of Sciences,* 120.

HIGHET, B., VIKAS ANEKAL, P., RYAN, B., MURRAY, H., COPPIETERS, N., VICTOR DIERIKS, B., SINGH-BAINS, M. K., MEHRABI, N. F., FAULL, R. L. M., DRAGUNOW, M. & CURTIS, M. A. 2021. fISHing with immunohistochemistry for housekeeping gene changes in Alzheimer's disease using an automated quantitative analysis workflow. *J Neurochem,* 157**,** 1270-1283.

HILL, R. 2000. NK1 (substance P) receptor antagonists; why are they not analgesic in humans? *Trends in Pharmacological Sciences,* 21**,** 244-246.

HILLA, A. M., BAEHR, A., LEIBINGER, M., ANDREADAKI, A. & FISCHER, D. 2021. CXCR4/CXCL12-mediated entrapment of axons at the injury site compromises optic nerve regeneration. *Proceedings of the National Academy of Sciences,* 118.

HIRAI, T., MULPURI, Y., CHENG, Y., XIA, Z., LI, W., RUANGSRI, S., SPIGELMAN, I. & NISHIMURA, I. 2017a. Aberrant plasticity of peripheral sensory axons in a painful neuropathy. *Scientific Reports,* 7**,** 3407.

HIRAI, T., MULPURI, Y., CHENG, Y. B., XIA, Z., LI, W., RUANGSRI, S., SPIGELMAN, I. & NISHIMURA, I. 2017b. Aberrant plasticity of peripheral sensory axons in a painful neuropathy. *Scientific Reports,* 7.

HOFFMAN, W., LAKKIS, F. G. & CHALASANI, G. 2016. B Cells, Antibodies, and More. *Clin J Am Soc Nephrol,* 11**,** 137-54.

HOLT, C. E., MARTIN, K. C. & SCHUMAN, E. M. 2019. Local translation in neurons: visualization and function. *Nature Structural & Molecular Biology,* 26**,** 557-566.

HONG, J., WONG, B., HUYNH, C., TANG, B., RUFFENACH, G., LI, M., UMAR, S., YANG, X. & EGHBALI, M. 2023. Tm4sf1-marked Endothelial Subpopulation Is Dysregulated in Pulmonary Arterial Hypertension. *Am J Respir Cell Mol Biol,* 68**,** 381-394.

HORUK, R. 2015. The Duffy Antigen Receptor for Chemokines DARC/ACKR1. *Frontiers in Immunology,* 6.

HU, H.-J., CARRASQUILLO, Y., KARIM, F., JUNG, W. E., NERBONNE, J. M., SCHWARZ, T. L. & GEREAU, R. W. 2006. The Kv4.2 Potassium Channel Subunit Is Required for Pain Plasticity. *Neuron,* 50**,** 89-100.

HU, J. M., LIU, K., LIU, J. H., JIANG, X. L., WANG, X. L., CHEN, Y. Z., LI, S. G., ZOU, H., PANG, L. J., LIU, C. X., CUI, X. B., YANG, L., ZHAO, J., SHEN, X. H., JIANG, J. F., LIANG, W. H., YUAN, X. L. & LI, F. 2017. CD163 as a marker of M2 macrophage, contribute to predicte aggressiveness and prognosis of Kazakh esophageal squamous cell carcinoma. *Oncotarget,* 8**,** 21526-21538.

HUASHENG, Y., DMITRY, U., SAAD, S. N., YIZHOU, H., JUSSI, K., OTMANE, B., SUNA LI, C., MAYANK, G., YIJING, S., YOU, L., JAMES, W., MAX, G., PHILLIP, A., HONGJUN, S., GUO-LI, M., STEPHEN, P., JOHN, S., HAO, W., MINGHONG, M., FRANK, L. R., HÅKAN, O., PATRIK, E. & WENQIN, L. 2023. Single-Soma Deep RNA Sequencing of Human Dorsal Root Ganglion Neurons Reveals Novel Molecular and Cellular Mechanisms Underlying Somatosensation. *bioRxiv*.

HULSE, R. P., BEAZLEY-LONG, N., HUA, J., KENNEDY, H., PRAGER, J., BEVAN, H., QIU, Y., FERNANDES, E. S., GAMMONS, M. V., BALLMER-HOFER, K., GITTENBERGER DE GROOT, A. C., CHURCHILL, A. J., HARPER, S. J., BRAIN, S. D., BATES, D. O. & DONALDSON, L. F. 2014. Regulation of alternative VEGF-A mRNA splicing is a therapeutic target for analgesia. *Neurobiology of Disease,* 71**,** 245-259.

HWANG, B., LEE, J. H. & BANG, D. 2018. Single-cell RNA sequencing technologies and bioinformatics pipelines. *Experimental & Molecular Medicine,* 50**,** 96.

IBRAHIM, T., WU, P., WANG, L.-J., FANG-MEI, C., MURILLO, J., MERLO, J., SHEIN, S. S., TUMANOV, A. V., LAI, Z., WELDON, K., CHEN, Y. & RUPAREL, S. 2023. Sex-dependent differences in the genomic profile of lingual sensory neurons in naïve and tongue-tumor bearing mice. *Scientific Reports,* 13.

IKEDA, H., HEINKE, B., RUSCHEWEYH, R. & SANDKÜHLER, J. 2003. Synaptic Plasticity in Spinal Lamina I Projection Neurons That Mediate Hyperalgesia. *Science,* 299**,** 1237-1240.

IWANAGA, T., TAKAHASHI-IWANAGA, H., NIO-KOBAYASHI, J. & EBARA, S. 2022. Structure and barrier functions of the perineurium and its relationship with associated sensory corpuscles: A review. *Biomed Res,* 43**,** 145-159.

IWASA, T., AFROZ, S., INOUE, M., ARAKAKI, R., OSHIMA, M., RAJU, R., WASKITHO, A., INOUE, M., BABA, O. & MATSUKA, Y. 2019. IL-10 and CXCL2 in trigeminal ganglia in neuropathic pain. *Neuroscience Letters,* 703**,** 132-138.

JANG, Y., KIM, M. & HWANG, S. W. 2020. Molecular mechanisms underlying the actions of arachidonic acid-derived prostaglandins on peripheral nociception. *Journal of Neuroinflammation,* 17**,** 30.

JESSEN, K. R. & ARTHUR-FARRAJ, P. 2019. Repair Schwann cell update: Adaptive reprogramming, EMT, and stemness in regenerating nerves. *Glia,* 67**,** 421-437.

JESSEN, K. R. & MIRSKY, R. 2016. The repair Schwann cell and its function in regenerating nerves. *J Physiol,* 594**,** 3521-31.

JESSEN, K. R. & MIRSKY, R. 2019. The Success and Failure of the Schwann Cell Response to Nerve Injury. *Front Cell Neurosci,* 13**,** 33.

JESSEN, K. R., MIRSKY, R. & LLOYD, A. C. 2015. Schwann Cells: Development and Role in Nerve Repair. *Cold Spring Harb Perspect Biol,* 7**,** a020487.

JI, R.-R., BABA, H., BRENNER, G. J. & WOOLF, C. J. 1999. Nociceptive-specific activation of ERK in spinal neurons contributes to pain hypersensitivity. *Nature Neuroscience,* 2**,** 1114-1119.

JI, R.-R., CHAMESSIAN, A. & ZHANG, Y.-Q. 2016. Pain regulation by non-neuronal cells and inflammation. *Science,* 354**,** 572-577.

JI, R. R., XU, Z. Z., WANG, X. & LO, E. H. 2009. Matrix metalloprotease regulation of neuropathic pain. *Trends Pharmacol Sci,* 30**,** 336-40.

JIANG, B.-C., LIU, T. & GAO, Y.-J. 2020. Chemokines in chronic pain: cellular and molecular mechanisms and therapeutic potential. *Pharmacology & Therapeutics,* 212.

JIN, S., GUERRERO-JUAREZ, C. F., ZHANG, L., CHANG, I., RAMOS, R., KUAN, C.-H., MYUNG, P., PLIKUS, M. V. & NIE, Q. 2021. Inference and analysis of cell-cell communication using CellChat. *Nature Communications,* 12**,** 1088.

JONES, R. H. B. 2010. Repair of the trigeminal nerve: a review. *Australian Dental Journal,* 55**,** 112-119.

JOSEPH, N. M., MUKOUYAMA, Y.-S., MOSHER, J. T., JAEGLE, M., CRONE, S. A., DORMAND, E.-L., LEE, K.-F., MEIJER, D., ANDERSON, D. J. & MORRISON, S. J. 2004. Neural crest stem cells undergo multilineage differentiation in developing peripheral nerves to generate endoneurial fibroblasts in addition to Schwann cells. *Development,* 131**,** 5599-5612.

KARAKAS, P., ÜZEL, M. & KOEBKE, J. 2007. The relationship of the lingual nerve to the third molar region using radiographic imaging. *British Dental Journal,* 203**,** 29-31.

KATO, G., YASAKA, T., KATAFUCHI, T., FURUE, H., MIZUNO, M., IWAMOTO, Y. & YOSHIMURA, M. 2006. Direct GABAergic and glycinergic inhibition of the substantia gelatinosa from the rostral ventromedial medulla revealed by in vivo patch-clamp analysis in rats. *J Neurosci,* 26**,** 1787-94.

KATZ, B., ZAGURI, R., EDVARDSON, S., MAAYAN, C., ELPELEG, O., LEV, S., DAVIDSON, E., PETERS, M., KFIR-ERENFELD, S., BERGER, E., GHAZALIN, S., BINSHTOK, A. M. & MINKE, B. 2023. Nociception and pain in humans lacking a functional TRPV1 channel. *J Clin Invest,* 133.

KE, R., MIGNARDI, M., PACUREANU, A., SVEDLUND, J., BOTLING, J., WÄHLBY, C. & NILSSON, M. 2013. In situ sequencing for RNA analysis in preserved tissue and cells. *Nature methods,* 10**,** 857-860.

KESHAV, S., CHUNG, P., MILON, G. & GORDON, S. 1991. Lysozyme is an inducible marker of macrophage activation in murine tissues as demonstrated by in situ hybridization. *J Exp Med,* 174**,** 1049-58.

KHAN, J., NOBORU, N., YOUNG, A. & THOMAS, D. 2017. Pro and anti-inflammatory cytokine levels (TNF- α , IL-1 β , IL-6 and IL-10) in rat model of neuroma. *Pathophysiology,* 24**,** 155-159.

KIGUCHI, N., KOBAYASHI, Y., KADOWAKI, Y., FUKAZAWA, Y., SAIKA, F. & KISHIOKA, S. 2014. Vascular endothelial growth factor signaling in injured nerves underlies peripheral sensitization in neuropathic pain. *Journal of Neurochemistry,* 129**,** 169-178.

KIGUCHI, N., KOBAYASHI, Y., MAEDA, T., FUKAZAWA, Y., TOHYA, K., KIMURA, M. & KISHIOKA, S. 2012. Epigenetic augmentation of the macrophage

inflammatory protein 2/C-X-C chemokine receptor type 2 axis through histone H3 acetylation in injured peripheral nerves elicits neuropathic pain. *J Pharmacol Exp Ther,* 340**,** 577-87.

KIM, G. D., DAS, R., GODUNI, L., MCCLELLAN, S., HAZLETT, L. D. & MAHABELESHWAR, G. H. 2016. Kruppel-like Factor 6 Promotes Macrophage-mediated Inflammation by Suppressing B Cell Leukemia/Lymphoma 6 Expression. *J Biol Chem,* 291**,** 21271-21282.

KOBAYASHI, H., CHATTOPADHYAY, S., KATO, K., DOLKAS, J., KIKUCHI, S.-I., MYERS, R. R. & SHUBAYEV, V. I. 2008. MMPs initiate Schwann cell-mediated MBP degradation and mechanical nociception after nerve damage. *Molecular and Cellular Neuroscience,* 39**,** 619-627.

KOBAYASHI, K. S. & VAN DEN ELSEN, P. J. 2012. NLRC5: a key regulator of MHC class I-dependent immune responses. *Nature Reviews Immunology,* 12**,** 813-820.

KREMER, M., SALVAT, E., MULLER, A., YALCIN, I. & BARROT, M. 2016. Antidepressants and gabapentinoids in neuropathic pain: Mechanistic insights. *Neuroscience,* 338**,** 183-206.

KRISHNAN, A. V., LIN, C. S. Y., PARK, S. B. & KIERNAN, M. C. 2009. Axonal ion channels from bench to bedside: A translational neuroscience perspective. *Progress in Neurobiology,* 89**,** 288-313.

KUKKAR, A., BALI, A., SINGH, N. & JAGGI, A. S. 2013. Implications and mechanism of action of gabapentin in neuropathic pain. *Archives of Pharmacal Research,* 36**,** 237-251.

LA MONACA, G., VOZZA, I., GIARDINO, R., ANNIBALI, S., PRANNO, N. & CRISTALLI, M. P. 2017. Prevention of neurological injuries during mandibular third molar surgery: technical notes. *Ann Stomatol (Roma),* 8**,** 45-52.

LAEDERMANN, C. J., ABRIEL, H. & DECOSTERD, I. 2015. Post-translational modifications of voltage-gated sodium channels in chronic pain syndromes. *Front Pharmacol,* 6**,** 263.

LAKHAN, S. E. & AVRAMUT, M. 2012. Matrix metalloproteinases in neuropathic pain and migraine: friends, enemies, and therapeutic targets. *Pain Res Treat,* 2012**,** 952906.

LAMBRU, G., ZAKRZEWSKA, J. & MATHARU, M. 2021. Trigeminal neuralgia: a practical guide. *Pract Neurol,* 21**,** 392-402.

LANGE, C., STORKEBAUM, E., DE ALMODÓVAR, C. R., DEWERCHIN, M. & CARMELIET, P. 2016. Vascular endothelial growth factor: a neurovascular target in neurological diseases. *Nature Reviews Neurology,* 12**,** 439-454.

LAUMET, G., MA, J., ROBISON, A. J., KUMARI, S., HEIJNEN, C. J. & KAVELAARS, A. 2019. T Cells as an Emerging Target for Chronic Pain Therapy. *Frontiers in Molecular Neuroscience,* 12.

LE, N. P., CHANNABASAPPA, S., HOSSAIN, M., LIU, L. & SINGH, B. 2015. Leukocyte-specific protein 1 regulates neutrophil recruitment in acute lung inflammation. *Am J Physiol Lung Cell Mol Physiol,* 309.

LEAVITT, T., HU, M. S., BORRELLI, M. R., JANUSZYK, M., GARCIA, J. T., RANSOM, R. C., MASCHARAK, S., DESJARDINS-PARK, H. E., LITZENBURGER, U. M., WALMSLEY, G. G., MARSHALL, C. D., MOORE, A. L., DUOTO, B., ADEM, S., FOSTER, D. S., SALHOTRA, A., SHEN, A. H., GRIFFIN, M., SHEN, E. Z., BARNES, L. A., ZIELINS, E. R., MAAN, Z. N., WEI, Y., CHAN, C. K. F., WAN, D. C., LORENZ, H. P., CHANG, H. Y., GURTNER, G. C. & LONGAKER, M. T. 2020. Prrx1 Fibroblasts Represent a Pro-fibrotic Lineage in the Mouse Ventral Dermis. *Cell Rep,* 33**,** 108356.

LEE, H. K., SEO, I. A., PARK, H. K., PARK, Y. M., AHN, K. J., YOO, Y. H. & PARK, H. T. 2007. Nidogen is a prosurvival and promigratory factor for adult Schwann cells. *Journal of Neurochemistry,* 102**,** 686-698.

LEE, P. R., KIM, J., ROSSI, H. L., CHUNG, S., HAN, S. Y., KIM, J. & OH, S. B. 2023. Transcriptional profiling of dental sensory and proprioceptive trigeminal neurons using single-cell RNA sequencing. *International Journal of Oral Science,* 15**,** 45.

LEVER, J., KRZYWINSKI, M. & ALTMAN, N. 2017. Principal component analysis. *Nature Methods,* 14**,** 641-642.

LI, B., ZHANG, W., GUO, C., XU, H., LI, L., FANG, M., HU, Y., ZHANG, X., YAO, X., TANG, M., LIU, K., ZHAO, X., LIN, J., CHENG, L., CHEN, F., XUE, T. & QU, K. 2022a. Benchmarking spatial and single-cell transcriptomics integration methods for transcript distribution prediction and cell type deconvolution. *Nature Methods,* 19**,** 662-670.

LI, D.-J., ZHONG, Z.-J., WANG, X.-L., WEI, N., ZHAO, S.-J., SHAN, T.-T., LIU, Y.-P. & YU, Y.-Q. 2023a. Chemokine receptor CXCR2 in primary sensory neurons of trigeminal ganglion mediates orofacial itch. *Frontiers in Molecular Neuroscience,* 16.

LI, H., ZHOU, J., LI, Z., CHEN, S., LIAO, X., ZHANG, B., ZHANG, R., WANG, Y., SUN, S. & GAO, X. 2023b. A comprehensive benchmarking with practical guidelines for cellular deconvolution of spatial transcriptomics. *Nature Communications,* 14**,** 1548.

LI, M., BANTON, M. C., MIN, Q., PARKINSON, D. B. & DUN, X. 2021. Meta-Analysis Reveals Transcription Factor Upregulation in Cells of Injured Mouse Sciatic Nerve. *Front Cell Neurosci,* 15.

LI, W., LIANG, J., LI, S., WANG, L., XU, S., JIANG, S., SONG, M., MENG, H., ZHAI, D., TANG, L., YANG, Y., ZHANG, L. & ZHANG, B. 2022b. Research progress of targeting NLRP3 inflammasome in peripheral nerve injury and pain. *International Immunopharmacology,* 110.

LI, Y., ZHANG, Y., ZHOU, Z., YI, L., JI, F., ZHANG, K., ZHANG, Y. & XU, H. 2023c. JMJD8 regulates neuropathic pain by affecting spinal cord astrocyte differentiation. *Neuroscience Letters,* 809.

LIM, E.-M. F., HOGHOOGHI, V., HAGEN, K. M., KAPOOR, K., FREDERICK, A., FINLAY, T. M. & OUSMAN, S. S. 2021. Presence and activation of pro-inflammatory macrophages are associated with CRYAB expression in vitro and after peripheral nerve injury. *Journal of Neuroinflammation,* 18**,** 82.

LIM, T. K. Y., SHI, X. Q., JOHNSON, J. M., RONE, M. B., ANTEL, J. P., DAVID, S. & ZHANG, J. 2015. Peripheral Nerve Injury Induces Persistent Vascular Dysfunction and Endoneurial Hypoxia, Contributing to the Genesis of Neuropathic Pain. *The Journal of Neuroscience,* 35**,** 3346-3359.

LINDBORG, J. A., MACK, M. & ZIGMOND, R. E. 2017. Neutrophils Are Critical for Myelin Removal in a Peripheral Nerve Injury Model of Wallerian Degeneration. *J Neurosci,* 37**,** 10258-10277.

LIU, M.-X., ZHONG, J., XIA, L., DOU, N.-N. & LI, S.-T. 2019. A correlative analysis between inflammatory cytokines and trigeminal neuralgia or hemifacial spasm. *Neurological Research,* 41**,** 335-340.

LIU, Z., JIN, Y. Q., CHEN, L., WANG, Y., YANG, X., CHENG, J., WU, W., QI, Z. & SHEN, Z. 2015. Specific marker expression and cell state of Schwann cells during culture in vitro. *PLoS One,* 10.

LLORIÁN-SALVADOR, M. & GONZÁLEZ-RODRÍGUEZ, S. 2018. Painful Understanding of VEGF. *Front Pharmacol,* 9**,** 1267.

LOESER, J. D. & TREEDE, R.-D. 2008. The Kyoto protocol of IASP Basic Pain Terminology. *PAIN®,* 137**,** 473-477.

LOPES, D. M., DENK, F. & MCMAHON, S. B. 2017. The Molecular Fingerprint of Dorsal Root and Trigeminal Ganglion Neurons. *Frontiers in Molecular Neuroscience*.

LOPEZ-DEE, Z., PIDCOCK, K. & GUTIERREZ, L. S. 2011. Thrombospondin-1: Multiple Paths to Inflammation. *Mediators of Inflammation,* 2011.

LOVATT, D., TAMBURINO, A., KRASOWSKA-ZOLADEK, A., SANOJA, R., LI, L., PETERSON, V., WANG, X. & USLANER, J. 2022. scRNA-seq generates a molecular map of emerging cell subtypes after sciatic nerve injury in rats. *Communications Biology,* 5**,** 1105.

LOVE, M. I., HUBER, W. & ANDERS, S. 2014. Moderated estimation of fold change and dispersion for RNA-seq data with DESeq2. *Genome Biology,* 15**,** 550.

LUECKEN, M. D., BÜTTNER, M., CHAICHOOMPU, K., DANESE, A., INTERLANDI, M., MUELLER, M. F., STROBL, D. C., ZAPPIA, L., DUGAS, M., COLOMÉ-TATCHÉ, M. & THEIS, F. J. 2022. Benchmarking atlas-level data integration in single-cell genomics. *Nature Methods,* 19**,** 41-50.

LUO, D., LI, X., TANG, S., SONG, F., LI, W., XIE, G., LIANG, J. & ZHOU, J. 2021. Epigenetic modifications in neuropathic pain. *Mol Pain,* 17.

MACIOCIA, P. M., WAWRZYNIECKA, P. A., PHILIP, B., RICCIARDELLI, I., AKARCA, A. U., ONUOHA, S. C., LEGUT, M., COLE, D. K., SEWELL, A. K., GRITTI, G., SOMJA, J., PIRIS, M. A., PEGGS, K. S., LINCH, D. C., MARAFIOTI, T. & PULE, M. A. 2017. Targeting the T cell receptor β -chain constant region for immunotherapy of T cell malignancies. *Nature Medicine,* 23**,** 1416-1423.

MANOLE, A., JAUNMUKTANE, Z., HARGREAVES, I., LUDTMANN, M. H. R., SALPIETRO, V., BELLO, O. D., POPE, S., PANDRAUD, A., HORGA, A., SCALCO, R. S., LI, A., ASHOKKUMAR, B., LOURENÇO, C. M., HEALES, S., HORVATH, R., CHINNERY, P. F., TORO, C., SINGLETON, A. B., JACQUES,

T. S., ABRAMOV, A. Y., MUNTONI, F., HANNA, M. G., REILLY, M. M., REVESZ, T., KULLMANN, D. M., JEPSON, J. E. C. & HOULDEN, H. 2017. Clinical, pathological and functional characterization of riboflavin-responsive neuropathy. *Brain,* 140**,** 2820-2837.

MANTYH, P. W., ROGERS, S. D., HONORE, P., ALLEN, B. J., GHILARDI, J. R., LI, J., DAUGHTERS, R. S., LAPPI, D. A., WILEY, R. G. & SIMONE, D. A. 1997. Inhibition of Hyperalgesia by Ablation of Lamina I Spinal Neurons Expressing the Substance P Receptor. *Science,* 278**,** 275-279.

MARCHETTI, L., FRANCISCO, D., SOLDATI, S., HAGHAYEGH JAHROMI, N., BARCOS, S., GRUBER, I., PAREJA, J. R., THIRIOT, A., VON ANDRIAN, U., DEUTSCH, U., LYCK, R., BRUGGMANN, R. & ENGELHARDT, B. 2022. ACKR1 favors transcellular over paracellular T-cell diapedesis across the blood-brain barrier in neuroinflammation in vitro. *Eur J Immunol,* 52**,** 161-177.

MARCIANÒ, G., VOCCA, C., RANIA, V., CITRARO, R., DE SARRO, G. & GALLELLI, L. 2023. Metalloproteases in Pain Generation and Persistence: A Possible Target? *Biomolecules,* 13.

MARTINI, R., FISCHER, S., LÓPEZ-VALES, R. & DAVID, S. 2008. Interactions between Schwann cells and macrophages in injury and inherited demyelinating disease. *Glia,* 56**,** 1566-1577.

MARTINI, R., SCHACHNER, M. & BRUSHART, T. M. 1994. The L2/HNK-1 carbohydrate is preferentially expressed by previously motor axon-associated Schwann cells in reinnervated peripheral nerves. *The Journal of Neuroscience,* 14**,** 7180.

MARZBAN, A., KIANI, J., HAJILOOI, M., REZAEI, H., KAHRAMFAR, Z. & SOLGI, G. 2016. HLA class II alleles and risk for peripheral neuropathy in type 2 diabetes patients. *Neural Regen Res,* 11**,** 1839-1844.

MATSUOKA, A., MAEDA, O., MIZUTANI, T., NAKANO, Y., TSUNODA, N., KIKUMORI, T., GOTO, H. & ANDO, Y. 2016. Bevacizumab Exacerbates Paclitaxel-Induced Neuropathy: A Retrospective Cohort Study. *PLOS ONE,* 11.

MÄURER, M., MÜLLER, M., KOBSAR, I., LEONHARD, C., MARTINI, R. & KIEFER, R. 2003. Origin of pathogenic macrophages and endoneurial fibroblast-like cells in an animal model of inherited neuropathy. *Molecular and Cellular Neuroscience,* 23**,** 351-359.

MCMANUS, K. F., TARAVELLA, A. M., HENN, B. M., BUSTAMANTE, C. D., SIKORA, M. & CORNEJO, O. E. 2017. Population genetic analysis of the DARC locus (Duffy) reveals adaptation from standing variation associated with malaria resistance in humans. *PLoS Genet,* 13.

MCWILLIAMS, D. F. & WALSH, D. A. 2017. Pain mechanisms in rheumatoid arthritis. *Clin Exp Rheumatol,* 35**,** 94-101.

MEACHAM, K., SHEPHERD, A., MOHAPATRA, D. P. & HAROUTOUNIAN, S. 2017. Neuropathic Pain: Central vs. Peripheral Mechanisms. *Curr Pain Headache Rep,* 21**,** 28-28.

MEAD, T. J. & APTE, S. S. 2018. ADAMTS proteins in human disorders. *Matrix Biol,* 71-72**,** 225-239.

MEGAT, S., RAY, P. R., TAVARES-FERREIRA, D., MOY, J. K., SANKARANARAYANAN, I., WANGHZOU, A., FANG LOU, T., BARRAGAN-IGLESIAS, P., CAMPBELL, Z. T., DUSSOR, G. & PRICE, T. J. 2019. Differences between Dorsal Root and Trigeminal Ganglion Nociceptors in Mice Revealed by Translational Profiling. *The Journal of neuroscience : the official journal of the Society for Neuroscience,* 39**,** 6829-6847.

MEISSNER, T. B., LI, A., BISWAS, A., LEE, K.-H., LIU, Y.-J., BAYIR, E., ILIOPOULOS, D., VAN DEN ELSEN, P. J. & KOBAYASHI, K. S. 2010. NLR family member NLRC5 is a transcriptional regulator of MHC class I genes. *Proceedings of the National Academy of Sciences,* 107**,** 13794-13799.

MEISSNER, T. B., LIU, Y. J., LEE, K. H., LI, A., BISWAS, A., VAN EGGERMOND, M. C., VAN DEN ELSEN, P. J. & KOBAYASHI, K. S. 2012. NLRC5 cooperates with the RFX transcription factor complex to induce MHC class I gene expression. *J Immunol,* 188**,** 4951-8.

MELOTO, C. B., BENAVIDES, R., LICHTENWALTER, R. N., WEN, X., TUGARINOV, N., ZORINA-LICHTENWALTER, K., CHABOT-DORÉ, A.-J., PILTONEN, M. H., CATTANEO, S., VERMA, V., KLARES, R. I., KHOURY, S., PARISIEN, M. & DIATCHENKO, L. 2018. Human pain genetics database: a resource dedicated to human pain genetics research. *PAIN,* 159**,** 749-763.

MELZACK, R. & WALL, P. D. 1965. Pain Mechanisms: A New Theory. *Science,* 150**,** 971-979.

MERRITT, C. R., ONG, G. T., CHURCH, S. E., BARKER, K., DANAHER, P., GEISS, G., HOANG, M., JUNG, J., LIANG, Y., MCKAY-FLEISCH, J., NGUYEN, K., NORGAARD, Z., SORG, K., SPRAGUE, I., WARREN, C., WARREN, S., WEBSTER, P. J., ZHOU, Z., ZOLLINGER, D. R., DUNAWAY, D. L., MILLS, G. B. & BEECHEM, J. M. 2020. Multiplex digital spatial profiling of proteins and RNA in fixed tissue. *Nat Biotechnol,* 38**,** 586-599.

METZEMAEKERS, M., GOUWY, M. & PROOST, P. 2020. Neutrophil chemoattractant receptors in health and disease: double-edged swords. *Cellular & Molecular Immunology,* 17**,** 433-450.

MICHELI, L., PARISIO, C., LUCARINI, E., VONA, A., TOTI, A., PACINI, A., MELLO, T., BOCCELLA, S., RICCIARDI, F., MAIONE, S., GRAZIANI, G., LACAL, P. M., FAILLI, P., GHELARDINI, C. & DI CESARE MANNELLI, L. 2021. VEGF-A/VEGFR-1 signalling and chemotherapy-induced neuropathic pain: therapeutic potential of a novel anti-VEGFR-1 monoclonal antibody. *Journal of Experimental & Clinical Cancer Research,* 40**,** 320.

MICLESCU, A., RÖNNGREN, C., BENGTSSON, M., GORDH, T. & HEDIN, A. 2023. Increased risk of persistent neuropathic pain after traumatic nerve injury and surgery for carriers of a human leukocyte antigen haplotype. *PAIN*.

MIDDLETON, S. J., BARRY, A. M., COMINI, M., LI, Y., RAY, P. R., SHIERS, S., THEMISTOCLEOUS, A. C., UHELSKI, M. L., YANG, X., DOUGHERTY, P. M., PRICE, T. J. & BENNETT, D. L. 2021. Studying human nociceptors: from fundamentals to clinic. *Brain*.

MILLER, R. J., JUNG, H., BHANGOO, S. K. & WHITE, F. A. 2009. Cytokine and chemokine regulation of sensory neuron function. *Handb Exp Pharmacol***,** 417-49.

MILORO, M., RUCKMAN, P. & KOLOKYTHAS, A. 2015. Lingual Nerve Repair: To Graft or Not to Graft? *Journal of Oral and Maxillofacial Surgery,* 73**,** 1844-1850.

MIURA, M., SASAKI, M., MIZUKOSHI, K., SHIBASAKI, M., IZUMI, Y., SHIMOSATO, G. & AMAYA, F. 2011. Peripheral sensitization caused by insulin-like growth factor 1 contributes to pain hypersensitivity after tissue injury. *PAIN®,* 152**,** 888-895.

MOAYEDI, M., WEISSMAN-FOGEL, I., SALOMONS, T. V., CRAWLEY, A. P., GOLDBERG, M. B., FREEMAN, B. V., TENENBAUM, H. C. & DAVIS, K. D. 2012. White matter brain and trigeminal nerve abnormalities in temporomandibular disorder. *PAIN®,* 153**,** 1467-1477.

MOORE, K. A., KOHNO, T., KARCHEWSKI, L. A., SCHOLZ, J., BABA, H. & WOOLF, C. J. 2002. Partial peripheral nerve injury promotes a selective loss of GABAergic inhibition in the superficial dorsal horn of the spinal cord. *J Neurosci,* 22**,** 6724-31.

MOPARTHI, L., KICHKO, T. I., EBERHARDT, M., HÖGESTÄTT, E. D., KJELLBOM, P., JOHANSON, U., REEH, P. W., LEFFLER, A., FILIPOVIC, M. R. & ZYGMUNT, P. M. 2016. Human TRPA1 is a heat sensor displaying intrinsic U-shaped thermosensitivity. *Scientific Reports,* 6**,** 28763.

MORCHIO, M., SHER, E., COLLIER, D. A., LAMBERT, D. W. & BOISSONADE, F. M. 2023. The Role of miRNAs in Neuropathic Pain. *Biomedicines,* 11**,** 775.

MORGAN, C. R., BIRD, E. V., ROBINSON, P. P. & BOISSONADE, F. M. 2009a. Immunohistochemical analysis of the purinoceptor P2X7 in human lingual nerve neuromas. *J Orofac Pain,* 23**,** 65-72.

MORGAN, C. R., BIRD, E. V., ROBINSON, P. P. & BOISSONADE, F. M. 2009b. TRPA1 expression in human lingual nerve neuromas in patients with and without symptoms of dysaesthesia. *Neuroscience Letters,* 465**,** 189-193.

MORGAN, C. R., RODD, H. D., CLAYTON, N., DAVIS, J. B. & BOISSONADE, F. M. 2005. Vanilloid receptor 1 expression in human tooth pulp in relation to caries and pain. *J Orofac Pain,* 19**,** 248-60.

MORIKAWA, Y., TAMURA, S., MINEHATA, K., DONOVAN, P. J., MIYAJIMA, A. & SENBA, E. 2004. Essential function of oncostatin m in nociceptive neurons of dorsal root ganglia. *J Neurosci,* 24**,** 1941-7.

MORIYAMA, T., HIGASHI, T., TOGASHI, K., IIDA, T., SEGI, E., SUGIMOTO, Y., TOMINAGA, T., NARUMIYA, S. & TOMINAGA, M. 2005. Sensitization of TRPV1 by EP1 and IP Reveals Peripheral Nociceptive Mechanism of Prostaglandins. *Molecular Pain,* 1.

MOSES, L. & PACHTER, L. 2022. Museum of spatial transcriptomics. *Nature Methods,* 19**,** 534-546.

MOSTEGL, M. M., RICHTER, B., DINHOPL, N. & WEISSENBÖCK, H. 2011. Influence of prolonged formalin fixation of tissue samples on the sensitivity of chromogenic in situ hybridization. *Journal of Veterinary Diagnostic Investigation,* 23**,** 1212-1216.

MOULTON, E. A., PENDSE, G., MORRIS, S., AIELLO-LAMMENS, M., BECERRA, L. & BORSOOK, D. 2009. Segmentally arranged somatotopy within the face representation of human primary somatosensory cortex. *Hum Brain Mapp,* 30**,** 757-65.

MOUSSET, C. M., HOBO, W., WOESTENENK, R., PREIJERS, F., DOLSTRA, H. & VAN DER WAART, A. B. 2019. Comprehensive Phenotyping of T Cells Using Flow Cytometry. *Cytometry A,* 95**,** 647-654.

MUELLER, M., WACKER, K., RINGELSTEIN, E. B., HICKEY, W. F., IMAI, Y. & KIEFER, R. 2001. Rapid response of identified resident endoneurial macrophages to nerve injury. *Am J Pathol,* 159**,** 2187-97.

MUHL, L., GENOVÉ, G., LEPTIDIS, S., LIU, J., HE, L., MOCCI, G., SUN, Y., GUSTAFSSON, S., BUYANDELGER, B., CHIVUKULA, I. V., SEGERSTOLPE, Å., RASCHPERGER, E., HANSSON, E. M., BJÖRKEGREN, J. L. M., PENG, X.-R., VANLANDEWIJCK, M., LENDAHL, U. & BETSHOLTZ, C. 2020. Single-cell analysis uncovers fibroblast heterogeneity and criteria for fibroblast and mural cell identification and discrimination. *Nature Communications,* 11**,** 3953.

MYCKATYN, T. M. & MACKINNON, S. E. 2004. A review of research endeavors to optimize peripheral nerve reconstruction. *Neurol Res,* 26**,** 124-38.

NAGI, S. S., MARSHALL, A. G., MAKDANI, A., JAROCKA, E., LILJENCRANTZ, J., RIDDERSTRÖM, M., SHAIKH, S., O'NEILL, F., SAADE, D., DONKERVOORT, S., FOLEY, A. R., MINDE, J., TRULSSON, M., COLE, J., BÖNNEMANN, C. G., CHESLER, A. T., BUSHNELL, M. C., MCGLONE, F. & OLAUSSON, H. 2019. An ultrafast system for signaling mechanical pain in human skin. *Sci Adv,* 5.

NAKASHIMA, C., ISHIDA, Y., KITOH, A., OTSUKA, A. & KABASHIMA, K. 2019. Interaction of peripheral nerves and mast cells, eosinophils, and basophils in the development of pruritus. *Experimental Dermatology,* 28**,** 1405-1411.

NASSER, M. W., RAGHUWANSHI, S. K., GRANT, D. J., JALA, V. R., RAJARATHNAM, K. & RICHARDSON, R. M. 2009. Differential activation and regulation of CXCR1 and CXCR2 by CXCL8 monomer and dimer. *J Immunol,* 183**,** 3425-32.

NEOGI, T. 2013. The epidemiology and impact of pain in osteoarthritis. *Osteoarthritis and Cartilage,* 21**,** 1145-1153.

NICHOLAS, M., VLAEYEN, J. W. S., RIEF, W., BARKE, A., AZIZ, Q., BENOLIEL, R., COHEN, M., EVERS, S., GIAMBERARDINO, M. A., GOEBEL, A., KORWISI, B., PERROT, S., SVENSSON, P., WANG, S. J. & TREEDE, R. D. 2019. The IASP classification of chronic pain for ICD-11: chronic primary pain. *Pain,* 160**,** 28-37.

NORTH, R. Y., LAZARO, T. T. & DOUGHERTY, P. M. 2018. Ectopic Spontaneous Afferent Activity and Neuropathic Pain. *Neurosurgery,* 65.

NORTH, R. Y., LI, Y., RAY, P., RHINES, L. D., TATSUI, C. E., RAO, G., JOHANSSON, C. A., ZHANG, H. M., KIM, Y. H., ZHANG, B., DUSSOR, G., KIM, T. H., PRICE, T. J. & DOUGHERTY, P. M. 2019. Electrophysiological and transcriptomic correlates of neuropathic pain in human dorsal root ganglion neurons. *Brain,* 142**,** 1215-1226.

O'SHEA, K. S., LIU, L. H. & DIXIT, V. M. 1991. Thrombospondin and a 140 kd fragment promote adhesion and neurite outgrowth from embryonic central and peripheral neurons and from PC12 cells. *Neuron,* 7**,** 231-7.

OBARA, I., GÉRANTON, S. M. & HUNT, S. P. 2012. Axonal protein synthesis: a potential target for pain relief? *Current Opinion in Pharmacology,* 12**,** 42-48.

ODIER, L. 1811. *Manuel de médecine-pratique: ou, Sommaire d'un cours gratuit, donné en 1800, 1801 et 1804 aux officiers de santé du département du Léman, avec une petite pharmacopée à leur usage*, Paschoud.

OH, S. B., TRAN, P. B., GILLARD, S. E., HURLEY, R. W., HAMMOND, D. L. & MILLER, R. J. 2001. Chemokines and glycoprotein120 produce pain hypersensitivity by directly exciting primary nociceptive neurons. *J Neurosci,* 21**,** 5027-35.

OLD, E. A., CLARK, A. K. & MALCANGIO, M. 2015. The Role of Glia in the Spinal Cord in Neuropathic and Inflammatory Pain. *In:* SCHAIBLE, H.-G. (ed.) *Pain Control.* Berlin, Heidelberg: Springer Berlin Heidelberg.

OLIVEIRA, T. Y. K., HARRIS, E. E., MEYER, D., JUE, C. K. & SILVA, W. A. 2012. Molecular evolution of a malaria resistance gene (DARC) in primates. *Immunogenetics,* 64**,** 497-505.

PARISIEN, M., LIMA, L. V., DAGOSTINO, C., EL-HACHEM, N., DRURY, G. L., GRANT, A. V., HUISING, J., VERMA, V., MELOTO, C. B., SILVA, J. R., DUTRA, G. G. S., MARKOVA, T., DANG, H., TESSIER, P. A., SLADE, G. D., NACKLEY, A. G., GHASEMLOU, N., MOGIL, J. S., ALLEGRI, M. & DIATCHENKO, L. 2022. Acute inflammatory response via neutrophil activation protects against the development of chronic pain. *Sci Transl Med,* 14.

PARMANTIER, E., LYNN, B., LAWSON, D., TURMAINE, M., NAMINI, S. S., CHAKRABARTI, L., MCMAHON, A. P., JESSEN, K. R. & MIRSKY, R. 1999. Schwann Cell–Derived Desert Hedgehog Controls the Development of Peripheral Nerve Sheaths. *Neuron,* 23**,** 713-724.

PARPAITE, T., BROSSE, L., SÉJOURNÉ, N., LAUR, A., MECHIOUKHI, Y., DELMAS, P. & COSTE, B. 2021. Patch-seq of mouse DRG neurons reveals candidate genes for specific mechanosensory functions. *Cell Rep,* 37**,** 109914.

PEKER, S., KURTKAYA, O., UZÜN, I. & PAMIR, M. N. 2006. Microanatomy of the central myelin-peripheral myelin transition zone of the trigeminal nerve. *Neurosurgery,* 59**,** 354-9.

PEREZ-SANCHEZ, J., MIDDLETON, S. J., PATTISON, L. A., HILTON, H., ALI AWADELKAREEM, M., ZUBERI, S. R., RENKE, M. B., HU, H., YANG, X.,

CLARK, A. J., ST. JOHN SMITH, E. & BENNETT, D. L. 2023. A humanized chemogenetic system inhibits murine pain-related behavior and hyperactivity in human sensory neurons. *Science Translational Medicine,* 15.

PESZKOWSKI, M. J. & LARSSON, A. 1990. Extraosseous and intraosseous oral traumatic neuromas and their association with tooth extraction. *J Oral Maxillofac Surg,* 48**,** 963-7.

PICHLER, J. W. & BEIRNE, O. R. 2001. Lingual flap retraction and prevention of lingual nerve damage associated with third molar surgery: A systematic review of the literature. *Oral Surgery, Oral Medicine, Oral Pathology, Oral Radiology, and Endodontology,* 91**,** 395-401.

PIÑA, A. R., MARTÍNEZ, M. M. & DE ALMEIDA, O. P. 2015. Glut-1, best immunohistochemical marker for perineurial cells. *Head Neck Pathol,* 9**,** 104-6.

PINGAULT, V., ZERAD, L., BERTANI-TORRES, W. & BONDURAND, N. 2022. SOX10: 20 years of phenotypic plurality and current understanding of its developmental function. *J Med Genet,* 59**,** 105-114.

PIOTROWSKA, A., ROJEWSKA, E., PAWLIK, K., KREINER, G., CIECHANOWSKA, A., MAKUCH, W., NALEPA, I. & MIKA, J. 2019. Pharmacological Blockade of Spinal CXCL3/CXCR2 Signaling by NVP CXCR2 20, a Selective CXCR2 Antagonist, Reduces Neuropathic Pain Following Peripheral Nerve Injury. *Frontiers in Immunology,* 10.

POLGÁR, E., GRAY, S., RIDDELL, J. S. & TODD, A. J. 2004. Lack of evidence for significant neuronal loss in laminae I-III of the spinal dorsal horn of the rat in the chronic constriction injury model. *Pain,* 111**,** 144-50.

POPE, J. E. & DEER, T. R. 2017. *Treatment of Chronic Pain Conditions: A Comprehensive Handbook,* New York, NY, New York, NY : Springer New York : Imprint: Springer, 2017.

POPPLER, L. H., DAVIDGE, K., LU, J. C., ARMSTRONG, J., FOX, I. K. & MACKINNON, S. E. 2015. Alternatives to sural nerve grafts in the upper extremity. *Hand (N Y),* 10**,** 68-75.

PRATO, V., TABERNER, F. J., HOCKLEY, J. R. F., CALLEJO, G., ARCOURT, A., TAZIR, B., HAMMER, L., SCHAD, P., HEPPENSTALL, P. A., SMITH, E. S. & LECHNER, S. G. 2017. Functional and Molecular Characterization of Mechanoinsensitive "Silent" Nociceptors. *Cell Rep,* 21**,** 3102-3115.

PRESS, R., NENNESMO, I., KOUWENHOVEN, M., HUANG, Y. M., LINK, H. & PASHENKOV, M. 2005. Dendritic cells in the cerebrospinal fluid and peripheral nerves in Guillain-Barré syndrome and chronic inflammatory demyelinating polyradiculoneuropathy. *Journal of Neuroimmunology,* 159**,** 165-176.

PRICE, D. D. & DUBNER, R. 1977. MECHANISMS OF FIRST AND SECOND PAIN IN THE PERIPHERAL AND CENTRAL NERVOUS SYSTEMS. *Journal of Investigative Dermatology,* 69**,** 167-171.

PRUENSTER, M., MUDDE, L., BOMBOSI, P., DIMITROVA, S., ZSAK, M., MIDDLETON, J., RICHMOND, A., GRAHAM, G. J., SEGERER, S., NIBBS, R.

J. B. & ROT, A. 2009. The Duffy antigen receptor for chemokines transports chemokines and supports their promigratory activity. *Nature Immunology,* 10**,** 101-108.

QIN, S., ZOU, Y. & ZHANG, C.-L. 2013. Cross-talk between KLF4 and STAT3 regulates axon regeneration. *Nature Communications,* 4**,** 2633.

QUEIROZ, R. M. L., PIPER, S. C., REES, J. S., STRICKSON, S., BRIEND, E., LOW, C. P., FERGUSON, G. J., LILLEY, K. S., JACKSON, A. P. & FINCH, D. K. 2022. Proteomic analysis in primary T cells reveals IL-7 alters T cell receptor thresholding via CYTIP/cytohesin/LFA-1 localisation and activation. *Biochem J,* 479**,** 225-243.

QUERAL-GODOY, E., FIGUEIREDO, R., VALMASEDA-CASTELLÓN, E., BERINI-AYTÉS, L. & GAY-ESCODA, C. 2006. Frequency and Evolution of Lingual Nerve Lesions Following Lower Third Molar Extraction. *Journal of Oral and Maxillofacial Surgery,* 64**,** 402-407.

RAJA, S. N., CARR, D. B., COHEN, M., FINNERUP, N. B., FLOR, H., GIBSON, S., KEEFE, F. J., MOGIL, J. S., RINGKAMP, M., SLUKA, K. A., SONG, X. J., STEVENS, B., SULLIVAN, M. D., TUTELMAN, P. R., USHIDA, T. & VADER, K. 2020. The revised International Association for the Study of Pain definition of pain: concepts, challenges, and compromises. *Pain,* 161**,** 1976-1982.

RAPPOPORT, N., SIMON, A. J., AMARIGLIO, N. & RECHAVI, G. 2019. The Duffy antigen receptor for chemokines, ACKR 1,–'Jeanne DARC'of benign neutropenia. *British journal of haematology,* 184**,** 497-507.

RAWAT, A. & MORRISON, B. M. 2021. Metabolic Transporters in the Peripheral Nerve-What, Where, and Why? *Neurotherapeutics,* 18**,** 2185-2199.

RAY, P. R., SHIERS, S., CARUSO, J. P., TAVARES-FERREIRA, D., SANKARANARAYANAN, I., UHELSKI, M. L., LI, Y., NORTH, R. Y., TATSUI, C., DUSSOR, G., BURTON, M. D., DOUGHERTY, P. M. & PRICE, T. J. 2023. RNA profiling of human dorsal root ganglia reveals sex differences in mechanisms promoting neuropathic pain. *Brain,* 146**,** 749-766.

REMACLE, A. G., HULLUGUNDI, S. K., DOLKAS, J., ANGERT, M., CHERNOV, A. V., STRONGIN, A. Y. & SHUBAYEV, V. I. 2018. Acute- and late-phase matrix metalloproteinase (MMP)-9 activity is comparable in female and male rats after peripheral nerve injury. *Journal of Neuroinflammation,* 15**,** 89.

REPOVIC, P. & BENVENISTE, E. N. 2002. Prostaglandin E2 is a novel inducer of oncostatin-M expression in macrophages and microglia. *J Neurosci,* 22**,** 5334-43.

REXED, B. 1954. A cytoarchitectonic atlas of the spinal cord in the cat. *J Comp Neurol,* 100**,** 297-379.

RICHARD, L., TOPILKO, P., MAGY, L., DECOUVELAERE, A.-V., CHARNAY, P., FUNALOT, B. & VALLAT, J.-M. 2012. Endoneurial Fibroblast-Like Cells. *Journal of Neuropathology & Experimental Neurology,* 71**,** 938-947.

RICHARD, L., VÉDRENNE, N., VALLAT, J. M. & FUNALOT, B. 2014. Characterization of Endoneurial Fibroblast-like Cells from Human and Rat Peripheral Nerves. *J Histochem Cytochem,* 62**,** 424-435.

RIVERS, W. H. R. & HEAD, H. 1908. A HUMAN EXPERIMENT IN NERVE DIVISION. *Brain,* 31**,** 323-450.

ROBERT, R. C., BACCHETTI, P. & POGREL, M. A. 2005. Frequency of trigeminal nerve injuries following third molar removal. *Journal of oral and maxillofacial surgery,* 63**,** 732-735.

ROBINSON, L. R. 2000. Traumatic injury to peripheral nerves. *Muscle & Nerve,* 23**,** 863-873.

ROBINSON, P. P., BOISSONADE, F. M., LOESCHER, A. R., SMITH, K. G., YATES, J. M., ELCOCK, C., BIRD, E. V., DAVIES, S. L., SMITH, P. L. & VORA, A. R. 2004. Peripheral mechanisms for the initiation of pain following trigeminal nerve injury. *Journal of Orofacial Pain,* 18**,** 287-292.

RODELLA, L. F., BUFFOLI, B., LABANCA, M. & REZZANI, R. 2012. A review of the mandibular and maxillary nerve supplies and their clinical relevance. *Arch Oral Biol,* 57**,** 323-34.

RODRIGUEZ, E., SAKURAI, K., XU, J., CHEN, Y., TODA, K., ZHAO, S., HAN, B. X., RYU, D., YIN, H., LIEDTKE, W. & WANG, F. 2017. A craniofacial-specific monosynaptic circuit enables heightened affective pain. *Nat Neurosci,* 20**,** 1734-1743.

RONNI, T., PAYNE, K. J., HO, S., BRADLEY, M. N., DORSAM, G. & DOVAT, S. 2007. Human Ikaros function in activated T cells is regulated by coordinated expression of its largest isoforms. *J Biol Chem,* 282**,** 2538-47.

ROUX, P. P. & BARKER, P. A. 2002. Neurotrophin signaling through the p75 neurotrophin receptor. *Progress in Neurobiology,* 67**,** 203-233.

RUANGSRI, S., LIN, A., MULPURI, Y., LEE, K., SPIGELMAN, I. & NISHIMURA, I. 2011. Relationship of axonal voltage-gated sodium channel 1.8 (NaV1.8) mRNA accumulation to sciatic nerve injury-induced painful neuropathy in rats. *J Biol Chem,* 286**,** 39836-47.

SAKKA, L., GABRILLARGUES, J. & COLL, G. 2016. Anatomy of the Spinal Meninges. *Operative Neurosurgery,* 12.

SANDY-HINDMARCH, O., BENNETT, D. L., WIBERG, A., FURNISS, D., BASKOZOS, G. & SCHMID, A. B. 2022. Systemic inflammatory markers in neuropathic pain, nerve injury, and recovery. *Pain,* 163**,** 526-537.

SATO, M., OHASHI, J., TSUCHIYA, N., KASHIWASE, K., ISHIKAWA, Y., ARITA, H., HANAOKA, K., TOKUNAGA, K. & YABE, T. 2002. Association of HLA-A*3303-B*4403-DRB1*1302 haplotype, but not of TNFA promoter and NKp30 polymorphism, with postherpetic neuralgia (PHN) in the Japanese population. *Genes & Immunity,* 3**,** 477-481.

SATO-TAKEDA, M., IHN, H., OHASHI, J., TSUCHIYA, N., SATAKE, M., ARITA, H., TAMAKI, K., HANAOKA, K., TOKUNAGA, K. & YABE, T. 2004. The human histocompatibility leukocyte antigen (HLA) haplotype is associated with the onset of postherpetic neuralgia after herpes zoster. *Pain,* 110**,** 329-336.

SCHINDELIN, J., ARGANDA-CARRERAS, I., FRISE, E., KAYNIG, V., LONGAIR, M., PIETZSCH, T., PREIBISCH, S., RUEDEN, C., SAALFELD, S., SCHMID, B.,

TINEVEZ, J.-Y., WHITE, D. J., HARTENSTEIN, V., ELICEIRI, K., TOMANCAK, P. & CARDONA, A. 2012. Fiji: an open-source platform for biological-image analysis. *Nature Methods,* 9**,** 676-682.

SCHMIDT, K., FORKMANN, K., SINKE, C., GRATZ, M., BITZ, A. & BINGEL, U. 2016. The differential effect of trigeminal vs. peripheral pain stimulation on visual processing and memory encoding is influenced by pain-related fear. *NeuroImage,* 134**,** 386-395.

SCHMIDT, K., SCHUNKE, O., FORKMANN, K. & BINGEL, U. 2015. Enhanced Short-Term Sensitization of Facial Compared With Limb Heat Pain. *The Journal of Pain,* 16**,** 781-790.

SCHNEIDER, E. H., FOWLER, S. C., LIONAKIS, M. S., SWAMYDAS, M., HOLMES, G., DIAZ, V., MUNASINGHE, J., PEIPER, S. C., GAO, J.-L. & MURPHY, P. M. 2014. Regulation of Motor Function and Behavior by Atypical Chemokine Receptor 1. *Behavior Genetics,* 44**,** 498-515.

SCHOLZ, J., FINNERUP, N. B., ATTAL, N., AZIZ, Q., BARON, R., BENNETT, M. I., BENOLIEL, R., COHEN, M., CRUCCU, G., DAVIS, K. D., EVERS, S., FIRST, M., GIAMBERARDINO, M. A., HANSSON, P., KAASA, S., KORWISI, B., KOSEK, E., LAVAND'HOMME, P., NICHOLAS, M., NURMIKKO, T., PERROT, S., RAJA, S. N., RICE, A. S. C., ROWBOTHAM, M. C., SCHUG, S., SIMPSON, D. M., SMITH, B. H., SVENSSON, P., VLAEYEN, J. W. S., WANG, S. J., BARKE, A., RIEF, W. & TREEDE, R. D. 2019. The IASP classification of chronic pain for ICD-11: chronic neuropathic pain. *Pain,* 160**,** 53-59.

SCHOLZ, J. & WOOLF, C. J. 2007. The neuropathic pain triad: Neurons, immune cells and glia. *Nature Neuroscience,* 10**,** 1361-1368.

SEDDON, H. J. 1943. THREE TYPES OF NERVE INJURY. *Brain,* 66**,** 237-288.

SESSLE, B. J. 2000. Acute and chronic craniofacial pain: brainstem mechanisms of nociceptive transmission and neuroplasticity, and their clinical correlates. *Crit Rev Oral Biol Med,* 11**,** 57-91.

SESSLE, B. J. 2005. Peripheral and central mechanisms of orofacial pain and their clinical correlates. *Minerva Anestesiol,* 71**,** 117-36.

SHARGHI-NAMINI, S., TURMAINE, M., MEIER, C., SAHNI, V., UMEHARA, F., JESSEN, K. R. & MIRSKY, R. 2006. The structural and functional integrity of peripheral nerves depends on the glial-derived signal desert hedgehog. *J Neurosci,* 26**,** 6364-76.

SHARMA, A., BEHL, T., SHARMA, L., SHAH, O. P., YADAV, S., SACHDEVA, M., RASHID, S., BUNGAU, S. G. & BUSTEA, C. 2023. Exploring the molecular pathways and therapeutic implications of angiogenesis in neuropathic pain. *Biomedicine & Pharmacotherapy,* 162.

SHEN, B. Q., SANKARANARAYANAN, I., PRICE, T. J. & TAVARES-FERREIRA, D. 2023. Sex-differences in prostaglandin signaling: a semi-systematic review and characterization of PTGDS expression in human sensory neurons. *Scientific Reports,* 13**,** 4670.

SHEPHERD, A. J., MICKLE, A. D., GOLDEN, J. P., MACK, M. R., HALABI, C. M., DE KLOET, A. D., SAMINENI, V. K., KIM, B. S., KRAUSE, E. G., GEREAU, R. W.

T. & MOHAPATRA, D. P. 2018. Macrophage angiotensin II type 2 receptor triggers neuropathic pain. *Proc Natl Acad Sci U S A,* 115**,** 8057-8066.

SHI, J., LU, D., GU, R., XU, Y., PAN, R., BO, F. & ZHANG, Y. 2022. Identification of Key Biomarkers and Immune Infiltration in Sporadic Vestibular Schwannoma Basing Transcriptome-Wide Profiling. *World Neurosurgery,* 160**,** 591-600.

SHIERS, S., KLEIN, R. M. & PRICE, T. J. 2020. Quantitative differences in neuronal subpopulations between mouse and human dorsal root ganglia demonstrated with RNAscope in situ hybridization. *Pain,* 161**,** 2410-2424.

SHIERS, S. I., SANKARANARAYANAN, I., JEEVAKUMAR, V., CERVANTES, A., REESE, J. C. & PRICE, T. J. 2021. Convergence of peptidergic and non-peptidergic protein markers in the human dorsal root ganglion and spinal dorsal horn. *J Comp Neurol,* 529**,** 2771-2788.

SILETTI, K., HODGE, R., MOSSI ALBIACH, A., LEE, K. W., DING, S.-L., HU, L., LÖNNERBERG, P., BAKKEN, T., CASPER, T., CLARK, M., DEE, N., GLOE, J., HIRSCHSTEIN, D., SHAPOVALOVA, N. V., KEENE, C. D., NYHUS, J., TUNG, H., YANNY, A. M., ARENAS, E., LEIN, E. S. & LINNARSSON, S. 2023. Transcriptomic diversity of cell types across the adult human brain. *Science,* 382.

SILVA, C. E. A., GUIMARÃES, R. M. & CUNHA, T. M. 2021. Sensory neuron–associated macrophages as novel modulators of neuropathic pain. *PAIN Reports,* 6.

SILVA, R. & MALCANGIO, M. 2021. Fractalkine/CX3CR1 Pathway in Neuropathic Pain: An Update. *Frontiers in Pain Research,* 2.

SILVA, R. L., LOPES, A. H., GUIMARÃES, R. M. & CUNHA, T. M. 2017. CXCL1/CXCR2 signaling in pathological pain: Role in peripheral and central sensitization. *Neurobiology of Disease,* 105**,** 109-116.

SINGHMAR, P., TRINH, R. T. P., MA, J., HUO, X., PENG, B., HEIJNEN, C. J. & KAVELAARS, A. 2020. The fibroblast-derived protein PI16 controls neuropathic pain. *Proc Natl Acad Sci U S A,* 117**,** 5463-5471.

SIQUEIRA, S. R. D. T., ALVES, B., MALPARTIDA, H. M. G., TEIXEIRA, M. J. & SIQUEIRA, J. T. T. 2009. Abnormal expression of voltage-gated sodium channels Nav1.7, Nav1.3 and Nav1.8 in trigeminal neuralgia. *Neuroscience,* 164**,** 573-577.

SIST, T. C. & GREENE, G. W. 1981. Traumatic neuroma of the oral cavity: Report of thirty-one new cases and review of the literature. *Oral Surgery, Oral Medicine, Oral Pathology,* 51**,** 394-402.

SITTITAVORNWONG, S., BABSTON, M., DENSON, D., ZEHREN, S. & FRIEND, J. 2017. Clinical Anatomy of the Lingual Nerve: A Review. *Journal of Oral and Maxillofacial Surgery,* 75.

SKLEPKIEWICZ, P., DYMEK, B., MLACKI, M., ZAGOZDZON, A., SALAMON, M., SIWIŃSKA, A. M., MAZURKIEWICZ, M. P., DE SOUZA XAVIER COSTA, N., MAZUR, M., MAUAD, T., GOŁĘBIOWSKI, A., DZWONEK, K., GOŁĄB, J. & ZASŁONA, Z. 2023. Inhibition of Macrophage-Specific CHIT1 as an Approach to Treat Airway Remodeling in Severe Asthma. *Int J Mol Sci,* 24.

SOBAH, M. L., LIONGUE, C. & WARD, A. C. 2021. SOCS Proteins in Immunity, Inflammatory Diseases, and Immune-Related Cancer. *Frontiers in Medicine,* 8.

SOLIS-CASTRO, O. O., WONG, N. & BOISSONADE, F. M. 2021. Chemokines and Pain in the Trigeminal System. *Front Pain Res (Lausanne),* 2.

ST. JOHN SMITH, E. 2018. Advances in understanding nociception and neuropathic pain. *Journal of Neurology,* 265**,** 231-238.

STÅHL, P. L., SALMÉN, F., VICKOVIC, S., LUNDMARK, A., NAVARRO, J. F., MAGNUSSON, J., GIACOMELLO, S., ASP, M., WESTHOLM, J. O. & HUSS, M. 2016. Visualization and analysis of gene expression in tissue sections by spatial transcriptomics. *Science,* 353**,** 78-82.

STARK, R., GRZELAK, M. & HADFIELD, J. 2019. RNA sequencing: the teenage years. *Nature Reviews Genetics,* 20**,** 631-656.

STICKELS, R. R., MURRAY, E., KUMAR, P., LI, J., MARSHALL, J. L., DI BELLA, D. J., ARLOTTA, P., MACOSKO, E. Z. & CHEN, F. 2021. Highly sensitive spatial transcriptomics at near-cellular resolution with Slide-seqV2. *Nature biotechnology,* 39**,** 313-319.

STIERLI, S., NAPOLI, I., WHITE, I. J., CATTIN, A. L., MONTEZA CABREJOS, A., GARCIA CALAVIA, N., MALONG, L., RIBEIRO, S., NIHOUARN, J., WILLIAMS, R., YOUNG, K. M., RICHARDSON, W. D. & LLOYD, A. C. 2018. The regulation of the homeostasis and regeneration of peripheral nerve is distinct from the CNS and independent of a stem cell population. *Development,* 145.

STOLL, G. & MÜLLER, H. W. 1999. Nerve Injury, Axonal Degeneration and Neural Regeneration: Basic Insights. *Brain Pathology,* 9**,** 313-325.

SUGAWARA, S., SHINODA, M., HAYASHI, Y., SAITO, H., ASANO, S., KUBO, A., SHIBUTA, I., FURUKAWA, A., TOYOFUKU, A. & IWATA, K. 2019. Increase in IGF-1 Expression in the Injured Infraorbital Nerve and Possible Implications for Orofacial Neuropathic Pain. *International Journal of Molecular Sciences,* 20**,** 6360.

SUNDERLAND, S. 1951. A CLASSIFICATION OF PERIPHERAL NERVE INJURIES PRODUCING LOSS OF FUNCTION. *Brain,* 74**,** 491-516.

SUNDERLAND, S. S. 1990. The anatomy and physiology of nerve injury. *Muscle & Nerve,* 13**,** 771-784.

SWANSON, H. H. 1961. Traumatic neuromas. A review of the literature. *Oral Surg Oral Med Oral Pathol,* 14**,** 317-26.

SZPAKOWSKA, M., D'UONNOLO, G., LUÍS, R., ALONSO BARTOLOMÉ, A., THELEN, M., LEGLER, D. F. & CHEVIGNÉ, A. 2023. New pairings and deorphanization among the atypical chemokine receptor family - physiological and clinical relevance. *Front Immunol,* 14.

TAFOYA, L. C. R., SHUTTLEWORTH, C. W., YANAGAWA, Y., OBATA, K. & WILSON, M. C. 2008. The role of the t-SNARE SNAP-25 in action potential-dependent calcium signaling and expression in GABAergic and glutamatergic neurons. *BMC Neuroscience,* 9**,** 105.

TAL, M. & DEVOR, M. 1992. Ectopic discharge in injured nerves: comparison of trigeminal and somatic afferent. *Brain Research,* 579**,** 148-151.

TANAKA, T., NARAZAKI, M. & KISHIMOTO, T. 2014. IL-6 in inflammation, immunity, and disease. *Cold Spring Harb Perspect Biol,* 6.

TANG, X., LI, Q., HUANG, T., ZHANG, H., CHEN, X., LING, J. & YANG, Y. 2022. Regenerative Role of T Cells in Nerve Repair and Functional Recovery. *Frontiers in Immunology,* 13.

TAVARES-FERREIRA, D., LAWLESS, N., BIRD, E. V., ATKINS, S., COLLIER, D., SHER, E., MALKI, K., LAMBERT, D. W. & BOISSONADE, F. M. 2019. Correlation of miRNA expression with intensity of neuropathic pain in man. *Mol Pain,* 15.

TAVARES-FERREIRA, D., RAY, P. R., SANKARANARAYANAN, I., MEJIA, G. L., WANGZHOU, A., SHIERS, S., UTTARKAR, R., MEGAT, S., BARRAGAN-IGLESIAS, P., DUSSOR, G., AKOPIAN, A. N. & PRICE, T. J. 2022a. Sex Differences in Nociceptor Translatomes Contribute to Divergent Prostaglandin Signaling in Male and Female Mice. *Biological Psychiatry,* 91**,** 129-140.

TAVARES-FERREIRA, D., SHIERS, S., RAY, P. R., WANGZHOU, A., JEEVAKUMAR, V., SANKARANARAYANAN, I., CERVANTES, A. M., REESE, J. C., CHAMESSIAN, A., COPITS, B. A., DOUGHERTY, P. M., GEREAU, R. W. T., BURTON, M. D., DUSSOR, G. & PRICE, T. J. 2022b. Spatial transcriptomics of dorsal root ganglia identifies molecular signatures of human nociceptors. *Sci Transl Med,* 14.

TAY, T. L., SAVAGE, J. C., HUI, C. W., BISHT, K. & TREMBLAY, M.-È. 2017. Microglia across the lifespan: from origin to function in brain development, plasticity and cognition. *The Journal of Physiology,* 595**,** 1929-1945.

TERRIER, L.-M., HADJIKHANI, N. & DESTRIEUX, C. 2022. The trigeminal pathways. *Journal of Neurology,* 269**,** 3443-3460.

THAKOR, D. K., LIN, A., MATSUKA, Y., MEYER, E. M., RUANGSRI, S., NISHIMURA, I. & SPIGELMAN, I. 2009. Increased peripheral nerve excitability and local NaV1.8 mRNA up-regulation in painful neuropathy. *Mol Pain,* 5**,** 14.

THULASI, V., VEERAPANDIYAN, A., PLETCHER, B. A., TONG, C. M. & MING, X. 2017. A Case of Brown-Vialetto-Van Laere Syndrome Due To a Novel Mutation in SLC52A3 Gene: Clinical Course and Response to Riboflavin. *Child Neurol Open,* 4.

TODD, A. J. 2010. Neuronal circuitry for pain processing in the dorsal horn. *Nature Reviews Neuroscience,* 11**,** 823-836.

TODD, A. J., PUSKAR, Z., SPIKE, R. C., HUGHES, C., WATT, C. & FORREST, L. 2002. Projection Neurons in Lamina I of Rat Spinal Cord with the Neurokinin 1 Receptor Are Selectively Innervated by Substance P-Containing Afferents and Respond to Noxious Stimulation. *J Neurosci,* 22**,** 4103-4113.

TOHDA, C., SASAKI, M., KONEMURA, T., SASAMURA, T., ITOH, M. & KURAISHI, Y. 2001. Axonal transport of VR1 capsaicin receptor mRNA in primary

afferents and its participation in inflammation-induced increase in capsaicin sensitivity. *Journal of Neurochemistry,* 76**,** 1628-1635.

TOMA, J. S., KARAMBOULAS, K., CARR, M. J., KOLAJ, A., YUZWA, S. A., MAHMUD, N., STORER, M. A., KAPLAN, D. R. & MILLER, F. D. 2020. Peripheral Nerve Single-Cell Analysis Identifies Mesenchymal Ligands that Promote Axonal Growth. *eNeuro,* 7.

TOMINAGA, M. & TOMINAGA, T. 2005. Structure and function of TRPV1. *Pflügers Archiv,* 451**,** 143-150.

TÓTH, A., CZIKORA, Á., PÁSZTOR, E. T., DIENES, B., BAI, P., CSERNOCH, L., RUTKAI, I., CSATÓ, V., MÁNYINÉ, I. S., PÓRSZÁSZ, R., ÉDES, I., PAPP, Z. & BOCZÁN, J. 2014. Vanilloid Receptor-1 (TRPV1) Expression and Function in the Vasculature of the Rat. *Journal of Histochemistry & Cytochemistry,* 62**,** 129-144.

TOTSCH, S. K. & SORGE, R. E. 2017. Immune System Involvement in Specific Pain Conditions. *Mol Pain,* 13.

TRAAG, V. A., WALTMAN, L. & VAN ECK, N. J. 2019. From Louvain to Leiden: guaranteeing well-connected communities. *Scientific Reports,* 9**,** 5233.

TSANTOULAS, C. & MCMAHON, S. B. 2014. Opening paths to novel analgesics: the role of potassium channels in chronic pain. *Trends in Neurosciences,* 37**,** 146-158.

TSOUCAS, D., DONG, R., CHEN, H., ZHU, Q., GUO, G. & YUAN, G.-C. 2019. Accurate estimation of cell-type composition from gene expression data. *Nature Communications,* 10**,** 2975.

VAN HECKE, O., AUSTIN, S. K., KHAN, R. A., SMITH, B. H. & TORRANCE, N. 2014. Neuropathic pain in the general population: A systematic review of epidemiological studies. *PAIN,* 155**,** 654-662.

VAN STEENWINCKEL, J., REAUX-LE GOAZIGO, A., POMMIER, B., MAUBORGNE, A., DANSEREAU, M. A., KITABGI, P., SARRET, P., POHL, M. & MÉLIK PARSADANIANTZ, S. 2011. CCL2 released from neuronal synaptic vesicles in the spinal cord is a major mediator of local inflammation and pain after peripheral nerve injury. *J Neurosci,* 31**,** 5865-75.

VAN VLIET, A. C., LEE, J., VAN DER POEL, M., MASON, M. R. J., NOORDERMEER, J. N., FRADKIN, L. G., TANNEMAAT, M. R., MALESSY, M. J. A., VERHAAGEN, J. & DE WINTER, F. 2021. Coordinated changes in the expression of Wnt pathway genes following human and rat peripheral nerve injury. *PLoS One,* 16.

VELUCHAMY, A., HÉBERT, H. L., MENG, W., PALMER, C. N. A. & SMITH, B. H. 2018. Systematic review and meta-analysis of genetic risk factors for neuropathic pain. *Pain,* 159**,** 825-848.

VERKMAN, A. S. 2002. Aquaporin water channels and endothelial cell function. *J Anat,* 200**,** 617-27.

VIERCK, C. J., HANSSON, P. T. & YEZIERSKI, R. P. 2008. Clinical and pre-clinical pain assessment: Are we measuring the same thing? *PAIN®,* 135**,** 7-10.

VILCEANU, D., HONORE, P., HOGAN, Q. H. & STUCKY, C. L. 2010. Spinal nerve ligation in mouse upregulates TRPV1 heat function in injured IB4-positive nociceptors. *The Journal of Pain,* 11**,** 588-599.

VISCARRA, J. A., WANG, Y., NGUYEN, H. P., CHOI, Y. G. & SUL, H. S. 2020. Histone demethylase JMJD1C is phosphorylated by mTOR to activate de novo lipogenesis. *Nature communications,* 11**,** 796.

VITAL, A., FERRER, X., GOIZET, C., ROUANET-LARRIVIÈRE, M., EIMER, S., BONNE, G. & VITAL, C. 2005. Peripheral nerve lesions associated with a dominant missense mutation, E33D, of the lamin A/C gene. *Neuromuscular Disorders,* 15**,** 618-621.

VORA, A. R., BODELL, S. M., LOESCHER, A. R., SMITH, K. G., ROBINSON, P. P. & BOISSONADE, F. M. 2007. Inflammatory cell accumulation in traumatic neuromas of the human lingual nerve. *Archives of Oral Biology,* 52**,** 74-82.

WAGSTAFF, L. J., GOMEZ-SANCHEZ, J. A., FAZAL, S. V., OTTO, G. W., KILPATRICK, A. M., MICHAEL, K., WONG, L. Y. N., MA, K. H., TURMAINE, M., SVAREN, J., GORDON, T., ARTHUR-FARRAJ, P., VELASCO-AVILES, S., CABEDO, H., BENITO, C., MIRSKY, R. & JESSEN, K. R. 2021. Failures of nerve regeneration caused by aging or chronic denervation are rescued by restoring Schwann cell c-Jun. *Elife,* 10.

WALSH, D. A. & MCWILLIAMS, D. F. 2012. Pain in Rheumatoid Arthritis. *Current Pain and Headache Reports,* 16**,** 509-517.

WANG, P. L., YIM, A. K. Y., KIM, K.-W., AVEY, D., CZEPIELEWSKI, R. S., COLONNA, M., MILBRANDT, J. & RANDOLPH, G. J. 2020. Peripheral nerve resident macrophages share tissue-specific programming and features of activated microglia. *Nature Communications,* 11**,** 2552.

WANG, Y., LEUNG, V. H., ZHANG, Y., NUDELL, V. S., LOUD, M., SERVIN-VENCES, M. R., YANG, D., WANG, K., MOYA-GARZON, M. D., LI, V. L., LONG, J. Z., PATAPOUTIAN, A. & YE, L. 2022a. The role of somatosensory innervation of adipose tissues. *Nature,* 609**,** 569-574.

WANG, Y., LI, X., XU, X., YU, J., CHEN, X., CAO, X., ZOU, J., SHEN, B. & DING, X. 2022b. Clec7a expression in inflammatory macrophages orchestrates progression of acute kidney injury. *Frontiers in Immunology,* 13.

WAWRZAK, D., MÉTIOUI, M., WILLEMS, E., HENDRICKX, M., DE GENST, E. & LEYNS, L. 2007. Wnt3a binds to several sFRPs in the nanomolar range. *Biochem Biophys Res Commun,* 357**,** 1119-23.

WEBER, M., BLAIR, E., SIMPSON, C. V., O'HARA, M., BLACKBURN, P. E., ROT, A., GRAHAM, G. J. & NIBBS, R. J. 2004. The chemokine receptor D6 constitutively traffics to and from the cell surface to internalize and degrade chemokines. *Mol Biol Cell,* 15**,** 2492-508.

WEERASURIYA, A. & MIZISIN, A. P. 2011. The Blood-Nerve Barrier: Structure and Functional Significance. *In:* NAG, S. (ed.) *The Blood-Brain and Other Neural Barriers: Reviews and Protocols.* Totowa, NJ: Humana Press.

WEN, C., XU, M., MO, C., CHENG, Z., GUO, Q. & ZHU, X. 2018. JMJD6 exerts function in neuropathic pain by regulating NF- κ B following peripheral nerve injury in rats. *Int J Mol Med,* 42**,** 633-642.

WHITE, F. A., JUNG, H. & MILLER, R. J. 2007. Chemokines and the pathophysiology of neuropathic pain. *Proceedings of the National Academy of Sciences,* 104**,** 20151-20158.

WIFFEN, P. J., DERRY, S., BELL, R. F., RICE, A. S., TÖLLE, T. R., PHILLIPS, T. & MOORE, R. A. 2017. Gabapentin for chronic neuropathic pain in adults. *Cochrane Database Syst Rev,* 6.

WIFFEN, P. J., DERRY, S., MOORE, R. A. & MCQUAY, H. J. 2011. Carbamazepine for acute and chronic pain in adults. *Cochrane Database Syst Rev*.

WILCOX, M. B., LARANJEIRA, S. G., ERIKSSON, T. M., JESSEN, K. R., MIRSKY, R., QUICK, T. J. & PHILLIPS, J. B. 2020. Characterising cellular and molecular features of human peripheral nerve degeneration. *Acta Neuropathologica Communications,* 8**,** 51.

WILLIAMS, C. D., AL-JAMMALI, Z. & HERINK, M. C. 2023. Gabapentinoids for Pain: A Review of Published Comparative Effectiveness Trials and Data Submitted to the FDA for Approval. *Drugs,* 83**,** 37-53.

WITTE, K. E., SLOTTA, C., LÜTKEMEYER, M., KITKE, A., CORAS, R., SIMON, M., KALTSCHMIDT, C. & KALTSCHMIDT, B. 2020. PLEKHG5 regulates autophagy, survival and MGMT expression in U251-MG glioblastoma cells. *Sci Rep,* 10.

WOLBERT, J., LI, X., HEMING, M., MAUSBERG, A. K., AKKERMANN, D., FRYDRYCHOWICZ, C., FLEDRICH, R., GROENEWEG, L., SCHULZ, C., STETTNER, M., ALONSO GONZALEZ, N., WIENDL, H., STASSART, R. & MEYER ZU HÖRSTE, G. 2020. Redefining the heterogeneity of peripheral nerve cells in health and autoimmunity. *Proc Natl Acad Sci U S A,* 117**,** 9466-9476.

WOLF, G., GABAY, E., TAL, M., YIRMIYA, R. & SHAVIT, Y. 2006. Genetic impairment of interleukin-1 signaling attenuates neuropathic pain, autotomy, and spontaneous ectopic neuronal activity, following nerve injury in mice. *Pain,* 120**,** 315-324.

WOOD, W. 1829. Observations on Neuroma, with Cases and Histories of the Disease. *Trans Med Chir Soc Edinb,* 3**,** 367-433.

WOOLF, C. J. 1983. Evidence for a central component of post-injury pain hypersensitivity. *Nature,* 306**,** 686-8.

WOOLF, C. J. 2011. Central sensitization: Implications for the diagnosis and treatment of pain. *PAIN,* 152**,** S2-S15.

WOOLF, C. J., SHORTLAND, P. & COGGESHALL, R. E. 1992. Peripheral nerve injury triggers central sprouting of myelinated afferents. *Nature,* 355**,** 75-78.

WRIGHT, M. C., MI, R., CONNOR, E., REED, N., VYAS, A., ALSPALTER, M., COPPOLA, G., GESCHWIND, D. H., BRUSHART, T. M. & HÖKE, A. 2014.

Novel roles for osteopontin and clusterin in peripheral motor and sensory axon regeneration. *J Neurosci,* 34**,** 1689-700.

WU, F., LIU, L. & ZHOU, H. 2017. Endothelial cell activation in central nervous system inflammation. *Journal of Leukocyte Biology,* 101**,** 1119-1132.

WU, P., ARRIS, D., GRAYSON, M., HUNG, C.-N. & RUPAREL, S. 2018. Characterization of sensory neuronal subtypes innervating mouse tongue. *PLOS ONE,* 13.

WYATT, S., SHOOTER, E. M. & DAVIES, A. M. 1990. Expression of the NGF receptor gene in sensory neurons and their cutaneous targets prior to and during innervation. *Neuron,* 4**,** 421-427.

XIA, C., BABCOCK, H. P., MOFFITT, J. R. & ZHUANG, X. 2019. Multiplexed detection of RNA using MERFISH and branched DNA amplification. *Sci Rep,* 9**,** 7721.

XIE, K., QIAO, F., SUN, Y., WANG, G. & HOU, L. 2015. Notch signaling activation is critical to the development of neuropathic pain. *BMC Anesthesiology,* 15**,** 41.

XIE, L., YIN, Y. & BENOWITZ, L. 2021. Chemokine CCL5 promotes robust optic nerve regeneration and mediates many of the effects of CNTF gene therapy. *Proceedings of the National Academy of Sciences,* 118.

XING, T., WANG, Y., DING, W. J., LI, Y. L., HU, X. D., WANG, C., DING, A. & SHEN, J. L. 2017. Thrombospondin-1 Production Regulates the Inflammatory Cytokine Secretion in THP-1 Cells Through NF- κ B Signaling Pathway. *Inflammation,* 40**,** 1606-1621.

XU, J. H., QIN, X. Z., ZHANG, H. N., MA, Y. X., QI, S. B., ZHANG, H. C., MA, J. J., FU, X. Y., XIE, J. L. & SAIJILAFU 2021. Deletion of Krüppel-like factor-4 promotes axonal regeneration in mammals. *Neural Regen Res,* 16**,** 166-171.

XU, M., BENNETT, D. L., QUEROL, L. A., WU, L.-J., IRANI, S. R., WATSON, J. C., PITTOCK, S. J. & KLEIN, C. J. 2018. Pain and the immune system: emerging concepts of IgG-mediated autoimmune pain and immunotherapies. *J Neurol Neurosurg Psychiatry*.

YADAV, A., MATSON, K. J. E., LI, L., HUA, I., PETRESCU, J., KANG, K., ALKASLASI, M. R., LEE, D. I., HASAN, S., GALUTA, A., DEDEK, A., AMERI, S., PARNELL, J., ALSHARDAN, M. M., QUMQUMJI, F. A., ALHAMAD, S. M., WANG, A. P., POULEN, G., LONJON, N., VACHIERY-LAHAYE, F., GAUR, P., NALLS, M. A., QI, Y. A., MARIC, D., WARD, M. E., HILDEBRAND, M. E., MERY, P. F., BOURINET, E., BAUCHET, L., TSAI, E. C., PHATNANI, H., LE PICHON, C. E., MENON, V. & LEVINE, A. J. 2023a. A cellular taxonomy of the adult human spinal cord. *Neuron,* 111**,** 328-344.

YADAV, S., SINGH, A., KANT, R. & SUROLIA, A. 2023b. TLR4 activation by lysozyme induces pain without inflammation. *Frontiers in Immunology,* 14.

YADAV, S. & SUROLIA, A. 2019. Lysozyme elicits pain during nerve injury by neuronal Toll-like receptor 4 activation and has therapeutic potential in neuropathic pain. *Science Translational Medicine,* 11.

YAMAMOTO, M., KONDO, H. & ISEKI, S. 1992. Nerve growth factor receptor (NGFR)-like immunoreactivity in the perineurial cell in normal and sectioned peripheral nerves of rats. *Anat Rec,* 233**,** 301-8.

YANG, H., DONG, Y., WANG, Z., LAI, J., YAO, C., ZHOU, H., ALHASKAWI, A., HASAN ABDULLAH EZZI, S., KOTA, V. G., HASAN ABDULLA HASAN ABDULLA, M. & LU, H. 2023. Traumatic neuromas of peripheral nerves: Diagnosis, management and future perspectives. *Frontiers in Neurology,* 13.

YANG, L., XU, M., BHUIYAN, S. A., LI, J., ZHAO, J., COHRS, R. J., SUSTERICH, J. T., SIGNORELLI, S., GREEN, U., STONE, J. R., LEVY, D., LENNERZ, J. K. & RENTHAL, W. Human and mouse trigeminal ganglia cell atlas implicates multiple cell types in migraine. *Neuron*.

YANG, L., XU, M., BHUIYAN, S. A., LI, J., ZHAO, J., COHRS, R. J., SUSTERICH, J. T., SIGNORELLI, S., GREEN, U., STONE, J. R., LEVY, D., LENNERZ, J. K. & RENTHAL, W. 2022. Human and mouse trigeminal ganglia cell atlas implicates multiple cell types in migraine. *Neuron,* 110**,** 1806-1821.

YAO, Z., VAN VELTHOVEN, C. T. J., KUNST, M., ZHANG, M., MCMILLEN, D., LEE, C., JUNG, W., GOLDY, J., ABDELHAK, A., AITKEN, M., BAKER, K., BAKER, P., BARKAN, E., BERTAGNOLLI, D., BHANDIWAD, A., BIELSTEIN, C., BISHWAKARMA, P., CAMPOS, J., CAREY, D., CASPER, T., CHAKKA, A. B., CHAKRABARTY, R., CHAVAN, S., CHEN, M., CLARK, M., CLOSE, J., CRICHTON, K., DANIEL, S., DIVALENTIN, P., DOLBEARE, T., ELLINGWOOD, L., FIABANE, E., FLISS, T., GEE, J., GERSTENBERGER, J., GLANDON, A., GLOE, J., GOULD, J., GRAY, J., GUILFORD, N., GUZMAN, J., HIRSCHSTEIN, D., HO, W., HOOPER, M., HUANG, M., HUPP, M., JIN, K., KROLL, M., LATHIA, K., LEON, A., LI, S., LONG, B., MADIGAN, Z., MALLOY, J., MALONE, J., MALTZER, Z., MARTIN, N., MCCUE, R., MCGINTY, R., MEI, N., MELCHOR, J., MEYERDIERKS, E., MOLLENKOPF, T., MOONSMAN, S., NGUYEN, T. N., OTTO, S., PHAM, T., RIMORIN, C., RUIZ, A., SANCHEZ, R., SAWYER, L., SHAPOVALOVA, N., SHEPARD, N., SLAUGHTERBECK, C., SULC, J., TIEU, M., TORKELSON, A., TUNG, H., VALERA CUEVAS, N., VANCE, S., WADHWANI, K., WARD, K., LEVI, B., FARRELL, C., YOUNG, R., STAATS, B., WANG, M.-Q. M., THOMPSON, C. L., MUFTI, S., PAGAN, C. M., KRUSE, L., DEE, N., SUNKIN, S. M., ESPOSITO, L., HAWRYLYCZ, M. J., WATERS, J., NG, L., SMITH, K., TASIC, B., ZHUANG, X., et al. 2023. A high-resolution transcriptomic and spatial atlas of cell types in the whole mouse brain. *Nature,* 624**,** 317-332.

YATES, J. M., SMITH, K. G. & ROBINSON, P. P. 2000. Ectopic neural activity from myelinated afferent fibres in the lingual nerve of the ferret following three types of injury. *Brain Research,* 874**,** 37-47.

YDENS, E., AMANN, L., ASSELBERGH, B., SCOTT, C. L., MARTENS, L., SICHIEN, D., MOSSAD, O., BLANK, T., DE PRIJCK, S., LOW, D., MASUDA, T., SAEYS, Y., TIMMERMAN, V., STUMM, R., GINHOUX, F., PRINZ, M., JANSSENS, S. & GUILLIAMS, M. 2020. Profiling peripheral nerve macrophages reveals two macrophage subsets with distinct localization, transcriptome and response to injury. *Nature Neuroscience,* 23**,** 676-689.

YIM, A. K. Y., WANG, P. L., BERMINGHAM, J. R., HACKETT, A., STRICKLAND, A., MILLER, T. M., LY, C., MITRA, R. D. & MILBRANDT, J. 2022. Disentangling glial diversity in peripheral nerves at single-nuclei resolution. *Nature Neuroscience,* 25**,** 238-251.

YU, X., LIU, H., HAMEL, K. A., MORVAN, M. G., YU, S., LEFF, J., GUAN, Z., BRAZ, J. M. & BASBAUM, A. I. 2020. Dorsal root ganglion macrophages contribute to both the initiation and persistence of neuropathic pain. *Nature Communications,* 11**,** 264.

YU, Y., HUANG, X., DI, Y., QU, L. & FAN, N. 2017. Effect of CXCL12/CXCR4 signaling on neuropathic pain after chronic compression of dorsal root ganglion. *Scientific Reports,* 7**,** 5707.

YUE, L., LIU, F., HU, J., YANG, P., WANG, Y., DONG, J., SHU, W., HUANG, X. & WANG, S. 2023. A guidebook of spatial transcriptomic technologies, data resources and analysis approaches. *Computational and Structural Biotechnology Journal,* 21**,** 940-955.

ZAMPONI, G. W., LEWIS, R. J., TODOROVIC, S. M., ARNERIC, S. P. & SNUTCH, T. P. 2009. Role of voltage-gated calcium channels in ascending pain pathways. *Brain Res Rev,* 60**,** 84-9.

ZHANG, C., LIU, H., TAN, Y., XU, Y., LI, Y., TONG, S., QIU, S., CHEN, Q., SU, Z., TIAN, D., ZHOU, W. & ZHONG, C. 2022a. MS4A6A is a new prognostic biomarker produced by macrophages in glioma patients. *Front Immunol,* 13.

ZHANG, L., JIAO, C., LIU, L., WANG, A., TANG, L., REN, Y., HUANG, P., XU, J., MAO, D. & LIU, L. 2021. NLRC5: A Potential Target for Central Nervous System Disorders. *Frontiers in Immunology,* 12.

ZHANG, W., ZHU, X., LIU, Y., CHEN, M., YAN, S., MAO, X., LIU, Z., WU, W., CHEN, C., XU, X. & WANG, Y. 2015a. Nur77 Was Essential for Neurite Outgrowth and Involved in Schwann Cell Differentiation After Sciatic Nerve Injury. *Journal of Molecular Neuroscience,* 57**,** 38-47.

ZHANG, X., HUANG, J. & MCNAUGHTON, P. A. 2005. NGF rapidly increases membrane expression of TRPV1 heat-gated ion channels. *Embo j,* 24**,** 4211-23.

ZHANG, Y., ZHAO, S., RODRIGUEZ, E., TAKATOH, J., HAN, B. X., ZHOU, X. & WANG, F. 2015b. Identifying local and descending inputs for primary sensory neurons. *J Clin Invest,* 125**,** 3782-94.

ZHANG, Z., LIU, L., ZHANG, H., LI, C. E., CHEN, Y., ZHANG, J., PAN, C., CHENG, S., YANG, X., MENG, P., YAO, Y., JIA, Y., WEN, Y. & ZHANG, F. 2022b. The genetic structure of pain in depression patients: A genome-wide association study and proteome-wide association study. *Journal of Psychiatric Research,* 156**,** 547-556.

ZHAO, L., HUANG, W. & YI, S. 2023. Cellular complexity of the peripheral nervous system: Insights from single-cell resolution. *Frontiers in Neuroscience,* 17.

ZHOU, W., ZHOU, Y., WANG, M., QIAN, C., WANG, C., TANG, J., CAI, Z., DAI, W. & ZHU, X. 2020. Pharmacological inhibition of CXCR2 alleviates neuropathic

pain by inactivating microglia in a rat L5 spinal nerve ligation model. *Am J Transl Res,* 12**,** 3803-3812.

ZHOU, Y., LI, R. J., LI, M., LIU, X., ZHU, H. Y., JU, Z., MIAO, X. & XU, G. Y. 2016. Overexpression of GRK6 attenuates neuropathic pain via suppression of CXCR2 in rat dorsal root ganglion. *Mol Pain,* 12.

ZHU, A., IBRAHIM, J. G. & LOVE, M. I. 2019. Heavy-tailed prior distributions for sequence count data: removing the noise and preserving large differences. *Bioinformatics,* 35**,** 2084-2092.

ZOCHODNE, D. W. 2008. *Neurobiology of Peripheral Nerve Regeneration,* Cambridge, Cambridge University Press.